Beiträge zur Chemie

schwerer Chalkogenidometallate

Kumulative Dissertation

Zur Erlangung des akademischen Grades eines Doktors der Naturwissenschaften (Dr. rer. nat.)

dem Fachbereich Chemie der Philipps-Universität Marburg, Hochschulkennziffer 1180

vorgelegt von

Diplom-Chemiker Günther Thiele

aus Potsdam

Erstgutachterin: Prof. Dr. Stefanie Susanne Dehnen
Zweigutachter: Prof. Dr. Carsten von Hänisch

Termin der Einreichung: 06. Januar 2015
Termin der Prüfung: 06. Februar 2015

Marburg (Lahn) 2015

Erklärung

Ich erkläre, dass eine Promotion noch an keiner anderen Hochschule als der Philipps-Universität Marburg, Fachbereich Chemie, versucht wurde.

Ich versichere, dass ich die vorgelegt Dissertation mit dem Titel „Beiträge zur Chemie schwerer Chalkogenidometallate“ selbst und ohne fremde Hilfe verfasst, nicht andere als die in ihr angegebenen Quellen oder Hilfsmittel benutzt und alle vollständig oder sinngemäß übernommenen Zitate als solche gekennzeichnet habe.

Diese Dissertation wurde in der vorliegenden oder einer ähnlichen Form noch bei keiner anderen in- oder ausländischen Hochschule anlässlich eines Promotionsgesuches oder zu anderen Prüfungszwecken eingereicht.

Marburg, der Unterschrift

Die vorliegende Arbeit entstand in der Zeit von Dezember 2010 bis Januar 2015 unter der Leitung von Prof. Dr. Stefanie Dehnen am Fachbereich Chemie der Philipps-Universität Marburg.

Danksagung

Steffi, für die vielen Jahre, die wir miteinander nun geteilt haben – all die Geduld und die vielen Erklärungen – ob chemisch oder menschlich – die du mir zuteil hast werden lassen. Für die freie Hand in der Bearbeitung dieser Arbeit und die perfekten Arbeitsbedingungen in jeglicher Hinsicht!

Carsten, für die vielen Gedankenanstöße und die fruchtbaren Diskussionen, wissenschaftlich und menschlich.

Ralf, für die geduldige und offene Einführung in die Festkörpertheorie, die Kaffeepausen und Diskussionen im Türrahmen.

Thomas und Marcus, für die fortwährende Unterstützung im Labor, die Organisation der Labore und die synthetische Unterstützung, als auch die kleine Essenz täglichen Wahnsinns. Ebenso ein großer Dank an Fritjof, Uwe und Stephanie für all‘ die Unterstützung.

Allen Mitgliedern des Arbeitskreises für die vielen Diskussionen, Hilfestellungen und geselligen Momente. Basti, Niels, Istemi, Johanna, Sima, Feli, Reza: euch gebührt besonderer Dank!

Radi, Micha, Klaus: ohne eure fortwährende Unterstützung in der Kristallographie hätte diese Arbeit nicht entstehen können. Vielen Dank für die unkomplizierte Vergabe von Messzeit, die ständigen Reparaturen am IDPS I und für die Nachsicht, wenn’s mal wieder etwas stärker „duftete“.

Reuti: ohne dich und dein Einsatz für Hilde, Marc, Erwin, Annemarie und meinen eigenen Rechner hätte ich wohl doppelt so lange benötigt.

Cornelia, Klaus, Gert und Xiulan ein großer Dank für die Unterstützung in allen Fragen zu „seltsamen“ Kernen und die lieben Botschaften am Freitagabend.

Jan und Uwe für die unzähligen Versuche, auch wenn’s dann doch nie funktioniert hat.

Dem C4-Bier-Kern und vorhergehenden und nachfolgenden Vertiefern, sowie Masteranden, Examisten, Bacheloranden, Prakties und Ich-komm-Rum-lern für die abwechslungsreiche Zeit.

Den ProChemlern für die gesellige Zeit ums Labor herum und das gemeinsame Sich-Aufregen.. Vor allem Maddin (ohne Orbs@GOP wär ich erledigt) und Lisa (fsk ohne Schnaps?) sei hier gedankt.

Für eine wundervolle Zeit um die Uni herum sei meinen Freunden in der Hochschulpolitik und Kommilitonen, der Turnermannschaft, den BoNuPs, dem Hugo’s Team, meinen Mitbewohnern und Freunden gedankt.

Für finanzielle Unterstützung sei der Friedrich-Ebert-Stiftung, der Deutschen Forschungsgemeinschaft und dem Bundesministerium für Bildung und Forschung gedankt.

Und – vor allem – der Familie.

Inhaltsverzeichnis

Man schieße mit der Schrotflinte in den Wald und hoffe darauf, dass ein Bär oder zumindest ein Eichhörnchen vom Baume fällt.

J. Heine

1.1 Chalkogenidometallate: Allgemeines

Die Chemie schwerer Chalkogenidometallate ist seit dem Altertum, damals noch im Sinne der Mineralogie und Alchemie, bekannt. Wissenschaftliche Abhandlungen über Struktur und Reaktivität sind besonders in der letzten Hälfte des vorigen Jahrhunderts erschienen. Physikalische Eigenschaften und die damit verbundenen Anwendungsmöglichkeiten von Chalkogenidometallaten sind jedoch erst seit Kurzem ins Zentrum des wissenschaftlichen Interesses gerückt. So wird vor allem aufgrund der großen Bandbreite an bekannten multinären Strukturen Zuversicht in die einstellbaren optoelektronischen Eigenschaften gesetzt. Wegen der hohen Atommassen der in den Verbindungen auftretenden Ionen werden diese auch bezüglich thermoelektrischer Eigenschaften häufig diskutiert.

Generell sind viele Klassen von Metallaten bekannt, von Cyanometallaten, mit dem lange bekannten Berliner Blau,[1,2] bis zu den perowskitischen Halogenidometallaten mit großem Potential in photoelektronischen Anwendungen.[3,4] Diese sollen jedoch nicht Gegenstand dieser Arbeit sein, welche sich auf die Chalkogenidometallate beschränkt. Per Definition sind dies Salze mit formal negativen Chalkogenidliganden an formal positiv geladenen Metallionen. Einige Klassen dieser Metallate wurden bereits intensiv untersucht. Für die große Gruppe der Oxidometallate sind zahlreiche Verbindungen bekannt, deren Strukturen und Eigenschaften bereits ausgiebig in Übersichtartikeln zusammengefasst wurden.[5] Beispielhaft seien die Polyoxidometallate mit ihrer strukturellen Vielfalt und katalytischen Anwendung,[6,7] oder die Silikate, welche im großindustriellen Maßstab zum Beispiel als Trägermaterialien synthetisiert werden, genannt.[8,9]

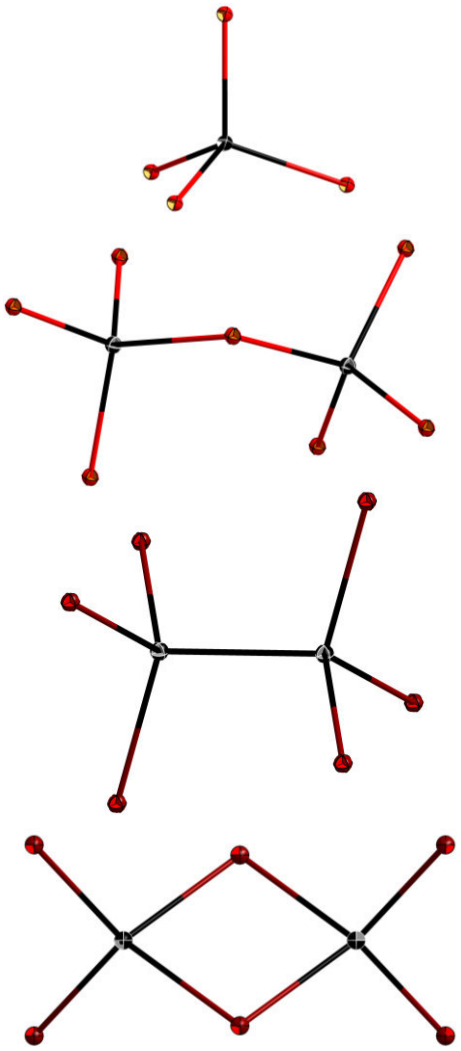

Abbildung 1. Vier Grundbausteine der Chalkogenidotetrelate.[10] Tetrelatome schwarz, Chalkogenidatome rot.

Für die entsprechenden Sulfido-, Selenido- und Telluridometallate hingegen sind verhältnismäßig wenig Studien durchgeführt worden. Als Beiträge zu einer der größten Gruppen der Chalkogenidometallate von Hauptgruppenelementen sind unter anderem die Arbeiten der Arbeitsgruppe Dehnen zu Chalkogenidogermanaten und –stannaten zu nennen,[10] welche jedoch auch auf bereits länger zurückliegenden Untersuchungen aufbauen.[11] Grundbausteine dieser Verbindungen sind vor allem $[MCh_4]^{4-}$-Tetraeder und verschieden kondensierte Aggregate dieser, wie in Abbildung 1 dargestellt.

Über die schwersten nicht-radioaktiven[12] Chalkogenidometallate, also die Selenido- und Telluridometallatanionen des Quecksilbers, Thalliums, Bleis und Bismuts, ist hingegen verhältnismäßig wenig bekannt. Hauptaugenmerk bei den Selenido- und Telluridomerkuraten, -thallaten, -plumbaten und –bismutaten war vornehmlich die Synthese und strukturelle Charakterisierung.

1.2 Synthesemethoden von Chalkogenidometallaten

Synthesechemische Herangehensweisen zur Darstellung von Chalkogenidometallaten sind vor allem die klassischen Festphasenmethoden, namentlich die Hochtemperatursynthese, der reaktive Flux[13,14] oder die Solvothermalsynthese.[15] Hierbei werden vorrangig ausgedehnte Anionenstrukturen erhalten. Sowohl Phasen mit 1D-Substrukturen wie $[HgSnTe_4]^{2-}$,[16] mit 2D-Substrukturen wie $[Hg_3Sn_2S_8]^{2-}$[17] oder auch mit 3D-Substrukturen unterschiedlichster Netzwerktopologien wie der offenen Netzwerkstruktur in $[Zn_4Sn_3Se_{13}]^{6-}$ sind auf diesen Wegen zugänglich.[18] Molekulare Anionen, wie sie in der Reihe der $[M_4T_4S_{17}]^{10-}$-Anionen (M = Mn, Fe, Co, Zn, Cd; T = Ge, Sn) gefunden wurden, sind für diese Synthesemethoden selten.[19]

Die alternative Herangehensweise auf nasschemischem Wege liefert vorrangig molekulare Anionen, wie es für die Anionen $[M_4Sn_4Ch_{17}]^{10-}$ (M = Mn, Co, Zn, Cd, Hg; Ch = S, Se, Te) und $[M_5Sn_5Ch_{20}]^{10-}$ (M = Co, Zn; Ch = S, Se) gezeigt wurde.[20] Obgleich diese aus Lösung erhalten wurden, entstehen nicht alle Verbindungen in Form von Solvaten, wie die nasschemische Synthese von $A_2[MSnE_4]$ zeigte.[21]

Ein großer Vorteil der Synthese in Lösung ist die Möglichkeit, Kryptanden und Kronenether (siehe Abbildung 2) zur Komplexierung der Alkalimetallionen zu verwenden. Dies kann einerseits zur Stabilisierung der Anionen führen, da die Lewis-Basizität der Kationen reduziert wird. Andererseits kann die Kristallisation aufgrund des größeren Kationenradius begünstigt werden.

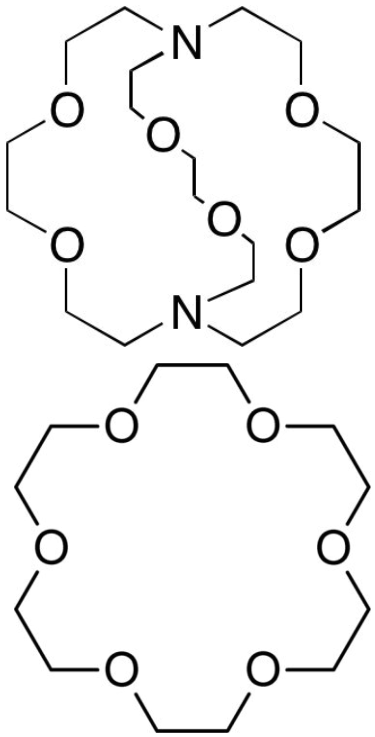

Abbildung 2. Strukturformel des Kryptanden [2.2.2]Krypt (oben) und des Kronenether 18-Krone-6 (unten).

Eine verhältnismäßig neue Methode ist die Synthese in ionischen Flüssigkeiten,[22,23] welche bisher ungekannte Strukturen zugänglich macht.[24,25] Die hierfür angewandten Reaktionsbedingungen ähneln denen der klassischen Reaktionen in Salzschmelzen, finden jedoch bei wesentlich niedrigeren Temperaturen statt. Dies ermöglicht die kinetische Stabilisierung thermodynamisch instabiler oder metastabiler Produkte. Die Produkte solcher Reaktionen enthalten ebenfalls vorrangig ausgedehnte Substrukturen, wie entsprechende Studien der Chalkogenidostannate zeigen. In einem Fall wurde jedoch mit $[Ge_{24}Sn_{36}Se_{132}]^{24-}$ ein sehr großes, molekulares Anion erhalten.[26]

Im Folgenden sollen die kristallographisch charakterisierten Chalkogenidometallate der schwersten nicht-radioaktiven Elemente sowie die Stoffklasse der häufig als Nebenprodukt der Synthesen anfallenden Polychalkogenide kurz vorgestellt werden, die sich tatsächlich oder potentiell als Edukte zur Synthese neuer Verbindungen mit binären oder ternären Chalkogenido-metalltanionen verwenden lassen. Die Chalkogenidometallate der leichteren Elemente wurden bereits ausführlich in Übersichtsartikeln behandelt.[27]

1.3 Strukturen binärer Chalkogenidometallatanionen

Strukturen binärer Merkuratanionen

Für ternäre Merkurate sind vier Grundtypen dominant: A_2HgCh_2,[28] $A_2Hg_3Ch_4$,[29] A_6HgCh_4[30] und $A_2Hg_6Ch_7$[29,31] (A = Alkalimetall, Ch: Chalkogen; siehe Abbildung 3). Daneben wurden Merkurate mit Polychalkogenidliganden[32] oder solche mit organischen oder metallorganischen Kationen, die aus Lösung dargestellt wurden, berichtet.[33] Hierbei liegt das zentrale Quecksilberion in linearer, trigonal-planarer, trigonal-pyramidaler oder tetraedrischer Koordination vor. In allen Fällen handelt es sich formal um Hg^{2+} mit der höchsten erreichbaren Oxidationsstufe am Quecksilberatom. Obgleich Hg_2^{2+}-Ionen in verschiedenen Salzen vorkommen, sind diese – vermutlich aufgrund der energetisch begünstigten Disproportionierung – bisher noch nicht in Metallaten realisiert worden.[34]

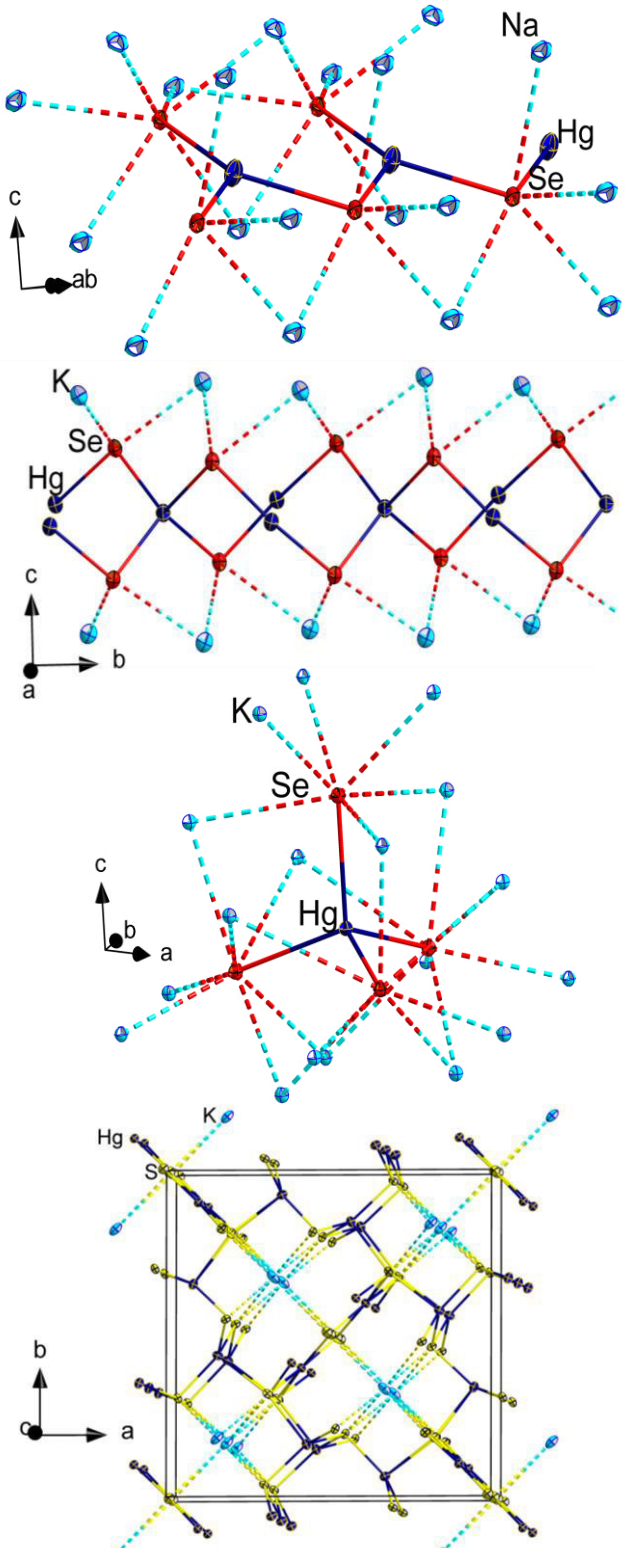

Abbildung 3. Abbildung von Struktur-ausschnitten ausgewählter Merkurate (v.o.n.u.): Na_2HgSe_2,[28] $K_2Hg_3Se_4$,[29] K_6HgSe_4,[30] $K_2Hg_6S_7$.[31]

Stukturen binärer Thallatanionen

Thallium kann in den Oxidationsstufen I und III vorkommen, die beide in Thallaten realisiert wurden. TlSe ist ein gemischtvalentes Thallat, das korrekterweise als $Tl[TlSe_2]$ formuliert werden muss. Das zentrale, von Selenidliganden tetraedrisch koordinierte Ion liegt hier in der formalen Oxidationsstufe +III vor, während Tl(I) als Gegenion dient und isostrukturell mit Kalium oder Natrium ausgetauscht werden kann.[35] Die Anionenstruktur ist hierbei durch *trans*-Kantenverknüpfung der $[TlSe_4]$-Tetraeder eindimensional unendlich ausgedehnt. Analog können Ausschnitte aus dieser Anionenstruktur erhalten werden,[36] wobei auch Verknüpfung[37] oder Termination[38] der Kette durch Polychalkogenidliganden gefunden wurde. $A_5[TlCh_4]$, das einfachste aller denkbaren ternären Chalkogenidothallate – mit isolierten Tetraedern ohne Verknüpfung der Anionen – ist bisher nicht bekannt. Weitere molekularen Aggregate mit Tl(I) Ionen finden sich in binären Anionen: In $[Tl_2Ch_2]^{2-}$ (Ch = Se, Te) mit sogenannter Schmetterlings-geometrie,[39,40] im verzerrten {TlSe}-überkappten Heterocuban-Anion $[Tl_5Se_5]^{3-}$,[41] in verschiedenen Sulfidothallat-,[42] sowie im ternären $[TlPbTe_3]^{3-}$-Anion (siehe Abbildung 4).[43]

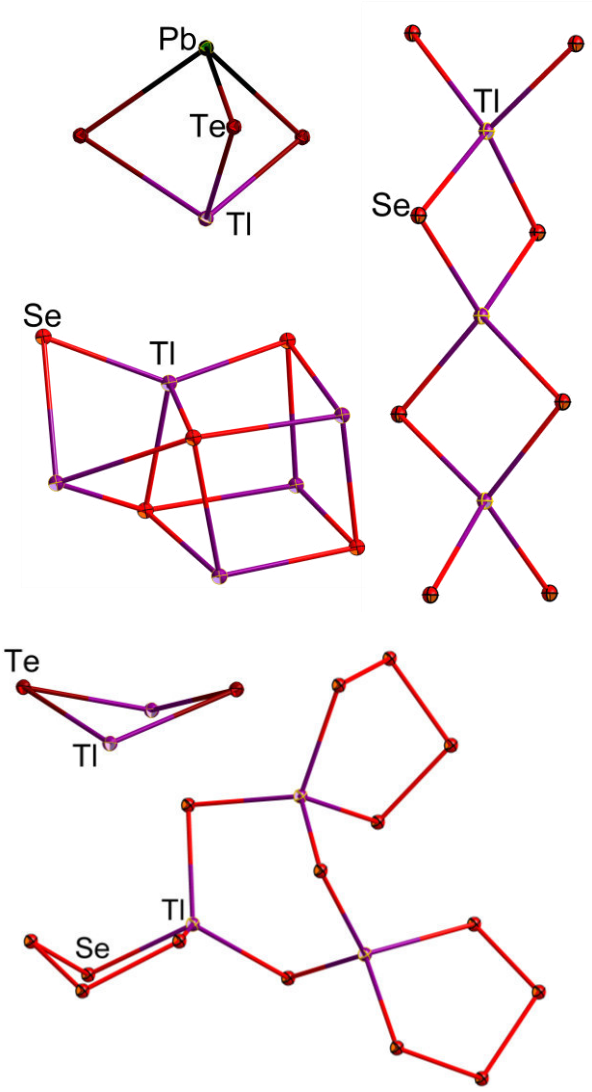

Abbildung 4. Abbildungen ausgewählter Thallatanionen (v.o.n.u. und v.l.n.r.): $[PbTlTe_3]^{3-}$,[43] Ausschnitt aus $[TlSe_2]^{n-}_n$,[35] $[Tl_5Se_5]^{3-}$,[41] $[Tl_2Te_2]^{2-}$,[40] $[Tl_3Se_{15}]^{3-}$.[38]

Strukturen binärer Plumbatanionen

Ternäre Chalkogenidoplumbate wurden bisher ausschließlich in Sauerstoffverbindungen realisiert, wobei $[PbO_4]^{4-}$ und $[PbO_6]^{8-}$ als Strukturmotive in unterschiedlichen Kondensationsgraden vorkommen. In diesen erlangt das zentrale Bleiion die formale Oxidationsstufe IV, was gemäß des Inert-Pair-Effektes nur mit stark elektronegativen Liganden möglich ist. Entsprechende binäre Plumbat(II) Verbindungen konnten hingegen auch mit den schwereren Homologen der Chalkogenide dargestellt werden. Hierfür sind das $[PbTe_3]^{4-}$,[44]

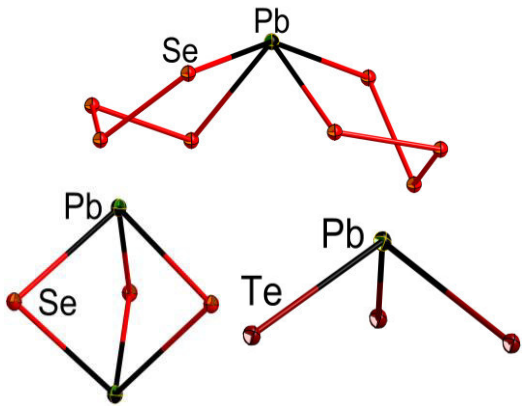

Abbildung 5. Abbildung der Anionen $[Pb(Se_4)_2]^{2-}$ (oben),[46] $[Pb_2Se_3]^{2-}$ (unten links),[45] $[PbTe_3]^{4-}$ (unten rechts).[44]

$[Pb_2Ch_3]^{2-}$,[45] und $[Pb(Se_4)_2]^{2-}$ mit zwei $(Se_4)^{2-}$ Tetraselenidliganden bekannt.[46] Die Koordination ist entsprechend der Oxidationsstufe und eines stereochemisch aktiven, freien Elektronenpaars in erster Näherung trigonal pyramidal für Pb(II) und im Unterschied hierzu tetraedrisch für Pb(IV).

Strukturen binärer Bismutatanionen

Chalkogenidobismutate sind bisher ausschließlich mit der formalen Oxidationsstufe +III am zentralen Bismution bekannt, da eine fünffach positive Ladung am zentralen Bismution eine zu hohe Oxidationskraft für Chalkogenidliganden impliziert. A_3BiCh_3 für Ch = Se, Te[47] und die eckenverknüpften Anionenstränge in $(NEt_4)_n[BiSe_2]_n$[48] oder $A[BiS_2]$[49] wurden daher bisher nur mit Bi(III) realisiert. Das entsprechende $[BiCh_3]^{3-}$-Anion ist in erster Näherung trigonal-planar koordiniert. Daneben ist noch das sulfidische Anion $[(S_7)_2Bi(S_6)Bi(S_7)_2]^{4-}$ bekannt.[50]

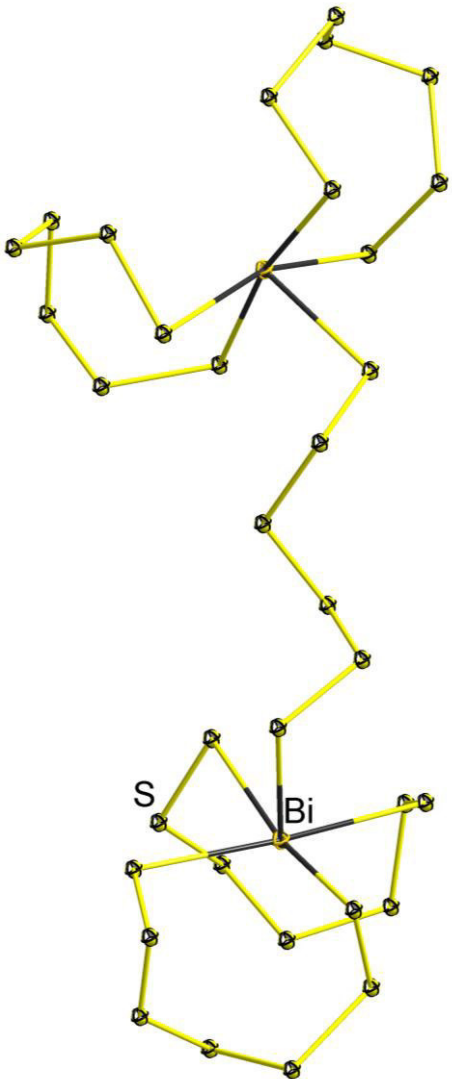

Abbildung 6. Darstellung des $[Bi_2S_{34}]^{4-}$.[50]

1.4 Strukturelemente in Polychalkogeniden

Als häufiges Nebenprodukt der Chalkogenidometallatsynthese ergeben sich viele verschiedene Chalkogenide, die besonders aufgrund der unterschiedlichen Ch...Ch-Wechselwirkungen und ihrer strukturellen Vielfalt von Interesse sind.[51] Klassische Polychalkogenide – also Salze mit kettenförmigen, negativ geladenen Polychalkogenidanionen – sind hierbei von den nicht-klassischen Polychalkogeniden zu unterscheiden. An Polyselenidverbindungen wurden bereits ausführliche spektroskopische,[52] spektrometrische,[53] quantenchemische[54] und elektrochemische Untersuchungen[55] unternommen. Neben den klassischen Polytelluriden[56] sind sowohl die sogenannten tellurreichen Telluriden mit ausgedehnten anionischen Substrukturen,[57] als auch Ring- und Käfigverbindungen,[58] heterometallische, makrozyklische und Carben-analoge Tellurverbindungen bekannt.[59]

1.5 Strukturen multinärer Metallatanionen

Eine große Vielzahl multinärer Chalkogenidometallate, die mittels Synthesemethoden der Festkörperchemie dargestellt wurden, ist bekannt. Vom quarternären $APbBi_3Ch_6$ (A = K..Cs, Ch = S, Se)[60] bis zum multinären $Cs_{0.83}Cu_{0.96}Tl_{0.04}Zn_{0.34}Hg_{4.57}Sb_{0.41}As_{3.59}S_{12}$[61] sind verschiedenste Metallate beschrieben. Als Beispiele ternärer Chalkogenidometallatanionen der

schwersten nicht-radioaktiven Metalle seien (Kation)$_2$[HgSnTe$_4$],[62] (Kation = K, NEt$_4$, PPh$_4$) und K$_2$HgSn$_2$S$_6$[63] mit tetraedrischer Koordination des Quecksilberions, Tl$_2$PbSeS$_4$[64] oder (Me$_4$N)$_2$Rb[Bi(As$_3$S$_6$)$_2$][65] jeweils mit verzerrt oktaedrischen [MS$_6$]-Einheiten genannt. Ternäre Thallatanionen hingegen sind äußerst selten, da Tl(I) in Metallaten vorrangig als Kation vorkommt. Eine der wenigen Verbindungen ist das oben bereits abgebildete [K([2.2.2]Krypt)]$_3$[PbTlSe$_3$].

Die Koordinationsgeometrien der Zentralionen in multinären Verbindungen weichen von jenen in den zuvor beschriebenen binären Anionen nicht ab. Bisher sind keine multinären Metallate dieser Elemente bekannt, die durch Umsetzungen der Chalkogenidomerkurate, -thallate, -plumbate oder –bismutate in Lösung mit Übergangsmetallverbindungen erhalten wurden.

Für deren leichtere Homologe hingegen wurden bereits erfolgreich binäre Chalkogenidometallatanionen für die Synthese von multinären Anionen eingesetzt.

Die Strukturmotive der binären Anionen können innerhalb der multinären Produkte wiedergefunden werden: Beispielhaft genannt seien die Adamantan-artigen [Sn$_4$Ch$_{10}$]$^{4-}$-Anionen, die sowohl isoliert in (Et$_4$N)$_4$[Sn$_4$Se$_{10}$][66] und [K([2.2.2]Krypt)]$_4$[Sn$_4$Se$_{10}$][67] vorkommen, als auch als Baustein der quaternären Verbindung A$_2$[MnSnS$_4$] (A = K, Cs).[63] Durch unterschiedliche Verknüpfungen können so gleiche Bausteine zu verschiedenen Strukturmotiven führen, wie in den Verbindungen der Zusammensetzung (Me$_4$N)$_2$[MGe$_4$S$_{10}$] mit M = Mn, Fe, Cd.[68] Oftmals kann durch die geschickte Substitution einzelner Komponenten solcher quarternärer Anionen zu isostrukturellen oder strukturell verwandten Verbindungen gelangt werden. Realisiert wurde dies in der Synthese von BaHgSnS$_4$,[69] BaCdGeS$_4$,[70] BaCdSnS$_4$[71], BaZnSnS$_4$ und BaMnSnS$_4$,[72] oder auch in der Reihe der Verbindungen SrCu$_2$GeS$_4$, BaCu$_2$GeS$_4$,[73] SrCu$_2$SnS$_4$,[74] BaAg$_2$SnS$_4$,[75] BaCu$_2$SnS$_4$[76] und Ba$_3$CdSn$_2$S$_4$.[77] Im Gegensatz zu diesen vielfältigen Chalkogenidotetrelaten sind zum Beispiel für die multinären Chalkogenidopentelate eine verhältnismäßig geringe Anzahl an Strukturen bisher bekannt. Examplarisch sein Cs$_3$[Ag$_2$Sb$_3$S$_8$][78] mit tetraedrischer Koordination der [SbS$_4$]-Einheiten und (Me$_4$N)[HgAs$_3$S$_6$][79] mit trigonalen [AsS$_3$]-Einheiten. Umfassende Übersichtartikel zu multinären Metallaten[27] und dem schrittweisen Aufbau aus binären Metallatanionen[80] sind publiziert worden.

1.6 Physikalische Eigenschaften

Der Großteil der bisherigen Untersuchungen an Chalkogenidometallaten konzentrierte sich auf multinäre Verbindungen, bei denen durch Variation eines Metallions oder mehrerer Metallionen oder auch im Sinne einer Dotierung verschiedene Eigenschaften zielgenau verändert und durchgestimmt werden konnten. So sind vor allem Verbindungen mit Übergangsmetall-, oder Seltenerdmetallionen[81] bezüglich ihrer magnetischen und optoelektronischen Eigenschaften[82,83,20] oder für Untersuchungen zu deren ionischer und elektronischer Leitfähigkeit von Interesse.[84] Beispielhaft ist die optische Absorption der Stannatanionen [SnSe$_n$Te$_{4-n}$]$^{4-}$ genannt,[85] wobei ein höherer Anteil an Tellurliganden zu einer

bathochromen Verschiebung führt, ein höherer Selenanteil hingegen zu einer Blauverschiebung. Werden diese mit Übergangsmetallsalzen umgesetzt, so können ternäre Stannatanionen erhalten werden, die einen noch größeren Teil des Spektrums abdecken (siehe Abbildung 7).[27c] Somit können optische Eigenschaften durch geeignete Wahl von Übergangsmetallion, Metallation, Ligandatome und Gegenionen wunschgemäß eingestellt werden.

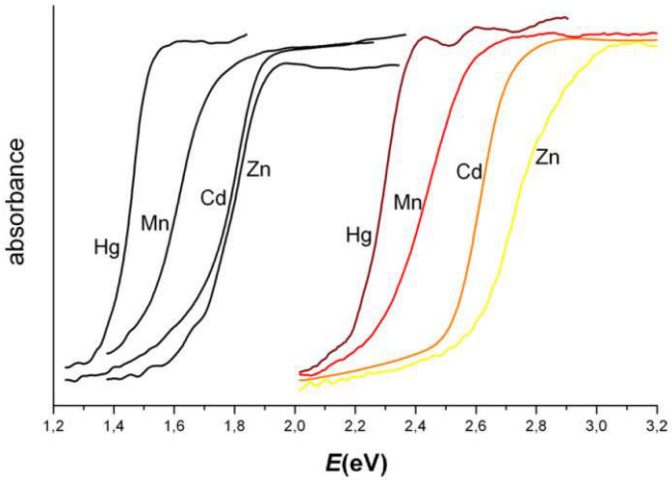

Abbildung 7. UV-Vis Spektren von $[K_{10}(ROH)_n][M_4S(SnCh_4)_4]$ für Ch = Te (links), Se (rechts). M ist im Bild dargestellt.[27c]

Mithilfe solcher Einstellungen können gezielt Materialien für Spezialanwendungen, wie beispielsweise $Cs_2Hg_6S_7$ als Röntgen- und Gamma-strahlendetektormaterial synthetisiert werden.[86]

Vor allem bei Metallaten mit Netzwerktopologien[27d] sind zudem Anwendungen der Gasabsorption, -speicherung, oder -filtertechnik vorgeschlagen worden. Sofern die Verbindungen gegenüber protischen Lösungsmitteln stabil sind, ist ferner der Einsatz als Katalysatormaterialien denkbar.[87]

Schwere Metallate wurden vorrangig bezüglich ihrer thermoelektrischen Eigenschaften untersucht. Hierbei ist der Gütefaktor *ZT* als Produkt aus dem Quadrat des Seebeckkoeffizienten S, der elektrischen Leitfähigkeit σ_{el}, der Temperatur T und dem Reziprok der thermischen Leitfähigkeit σ_{th} gemäß Gleichung 1 gegeben.

$$ZT = \frac{S^2 \cdot \sigma_{el} \cdot T}{\sigma_{th}} \qquad (1)$$

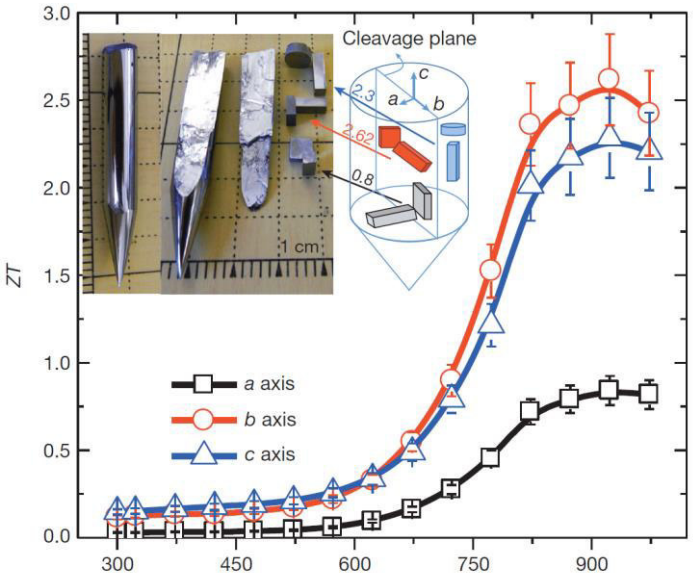

Abbildung 8. Auftragung der gemessenen Gütefaktoren *ZT* gegen die Temperatur für SnSe-Kristalle entlang verschiedener Zellachsen.[88]

Der Seebeckkoeffizient ist eine stoffspezifische Größe, die für jede Verbindung bestimmt werden muss. Die elektrische Leitfähigkeit wird in ionische und elektronische Leitfähigkeit unterteilt, wobei die ionische Leitfähigkeit – neben Gitterschwingungen – auch zur thermischen Leitfähigkeit beiträgt. Entsprechend wird für gute thermoelektrische Materialien eine hohe elektrische und eine geringe thermische Leitfähigkeit angestrebt.

Bei Verbindungen mit bekannten Seebeckkoeffizienten wird daher versucht, durch Dotierung, Korngrenzenvergrößerung oder Fehlstelleneinbau die Leitfähigkeiten zu optimieren. Hohe

thermische Stabilitäten hingegen ermöglichen hohe Arbeitstemperaturen, was zur linearen Steigerung der Gütefaktoren führt. Aktueller Rekordhalter mit einem ZT_{max} von 2.6 ist Zinnselenid (siehe Abbildung 8).[88]

1.7 Toxizität von Schwermetallverbindungen

Untersuchungen an Verbindungen der schweren Metalle, allen voran des Quecksilbers, Thalliums und Bleis, sind häufig aufgrund der potentiellen Giftigkeit unterblieben. Hierbei ist die Angst vor der akuten Toxizität der entsprechenden Organoelementverbindungen prädominant, wobei Dimethylquecksilber im Gebrauch das höchste Gefahrenpotential beinhaltet. Durch die Kombination von hoher Flüchtigkeit, sofortiger Penetration aller gängigen Schutzkleidungen und dem direkten Durchbruch der Blut-Hirn-Schranke *in vivo* mit einer tödlichen Dosis von 100 µL ist diese Verbindung der Spitzenreiter in der Giftigkeit solcher schweren Metallverbindungen.[89]

Abbildung 9. Radiologische Aufnahme nach intravenöser Injektion von 10 mL elementaren Quecksilbers.[90]

Andererseits sind anorganische Verbindungen, besonders Salze dieser Elemente sowie die Elemente in ihrer Reinform, oftmals in ihrer Toxizität überschätzt worden. Einerseits ist die Flüchtigkeit bei solchen Verbindungen nicht mehr gegeben, sodass ihre Inhalation – von Stäuben abgesehen – unwahrscheinlich ist, andererseits muss zwischen chronischen und akuten Vergiftungen unterschieden werden. Letztere ist, wie jüngste Beispiele zeigen, wesentlich unproblematischer als bisher angenommen: Nach versuchtem Suizid durch intravenöse Injektion von 10 mL (135 g) elementarem Quecksilber wurde keine klinische Toxizität festgestellt und eine Neubewertung von akuter und chronischer Effekte vorgeschlagen (siehe Abbildung 9).[90] Weitere Aspekte sind zumeist unzureichend erforscht, was wiederum präparative Arbeiten verhindert und *vice versa*.

Sofern für anorganischen Verbindungen dieser Elemente die gängigen Sicherheitsvorschriften Berücksichtigung finden, ist die synthetische Arbeit unproblematisch. Großindustriellen Einsatz werden diese Verbindungen – nach komplettem Verzicht auf Verbindungen wie Tetraethylblei – voraussichtlich nicht finden. Neben spannender Grundlagenforschung sind diese Verbindungsklassen jedoch für den Spezialeinsatz in solchen Gebieten hochinteressant, in denen nicht auf alternative Materialen ausgewichen werden kann. Als Beispiel wird im Folgenden auf den Einsatz in thermoelektrischen Materialen eingegangen, wohingegen der Autor dieser Dissertation ausdrücklich von der medizinischen Applikation von „Mercurius arsenicosus“, „Mercurius silicicus“ und „Mercurius chloratus natronatus“ abrät.[91]

Im Gegensatz zum Reaktionsverhalten der leichteren Chalkogenidotetrelate $[T_xCh_y]^{q-}$ (T = Ge, Sn; Ch = S, Se, Te) gegenüber Übergangsmetallverbindungen sind entsprechende Reaktionen von Chalkogenidoplumbaten noch nicht beschrieben worden. Auch von Umsetzungen von Chalkogenidometallaten der benachbarten Elemente Quecksilber, Thallium und Bismut mit Übergangsmetallverbindungen gibt es nur wenige Berichte. Das Schließen dieser Wissenslücke durch entsprechende Synthesen und nachfolgende Untersuchungen der Eigenschaften möglicher Produkte war die grundlegende Motivation der vorliegenden Dissertation.

Ausgehend von der literaturbekannten Synthese des Trichalkogenidodiplumbats sollte überprüft werden, ob sich dieses analog der klassischen Chalkogenidostannate unter verschiedenen Reaktionsbedingungen behandeln sowie in Reaktionen mit Übergangsmetallen umsetzen lässt.

Hierfür sollte zunächst eine Syntheseoptimierung durchgeführt werden, die ggf. auf die Verwendung von Kryptand verzichtet und stattdessen Ammonium-, Phosphoniumionen oder Kronenether verwendet. Die optimierten Synthesebedingungen sollten zur Darstellung entsprechender Merkurate, Thallate und Bismutate verwendet werden.

Darauf aufbauend sollten gemäß bekannter Reaktionen der Stannate, Germanate und einiger Pentelate Umsetzungen mit unterschiedlichen Übergangsmetallverbindungen unter verschiedenen Reaktionsbedingungen durchgeführt werden.

Die Produkte aller Umsetzungen sollten bezüglich ihrer optoelektronischen Eigenschaften analysiert und bezüglich potentieller Anwendungen untersucht werden. Wo immer angebracht sollten quantenchemische und weiterführende physikalische Studien helfen, Bindungssituationen innerhalb der Anionen oder im Verband der salzartigen Stoffe zu verstehen.

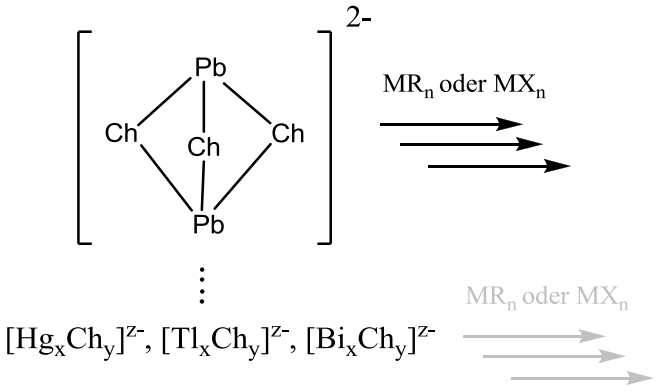

Abbildung 10. Schematische Darstellung der geplanten Umsetzungen.

3.1 $[M_xCh_y]^{q-}$, Synthese und Reaktivität

Ausgehend von der literaturbekannten Synthese des $[K([2.2.2]Krypt)]_2[Pb_2Te_3]$ durch Extraktion einer ternären Phase der nominellen Zusammensetzung „KPbTe“ in Ethylendiamin (*en*) in Gegenwart von [2.2.2]Krypt wurden die in Lösung vorhandenen Nebenprodukte $[Te_2]^{2-}$ und $[Te_3]^{2-}$ identifiziert.[92] Da alle Bemühungen zur Optimierung der Synthese bezüglich der Reinheit oder entsprechender Aufreinigungen fehlschlugen, wurden alternative Synthesen eruiert.

Hierbei erwies sich – in Anlehnung an die von Haushalter präsentierte Reduktion von „$PbTe_2$“ (= PbTe·Te) in flüssigem Ammoniak mit elementarem Kalium – die direkte Reduktion von „$PbCh_2$“ (Ch = Se, Te) mit elementarem Kalium in Ethylendiamin in Gegenwart von 18-Krone-6 oder [2.2.2]Krypt als effektiver Syntheseweg zur Darstellung der Trichalkogenidodiplumbate. Diese Synthesemethode wurde auf die Darstellung der entsprechenden Lithiumverbindungen ausgeweitet, wobei allerdings auf die Gegenwart von Komplexierungsreagenzien verzichtet werden konnte, da in $[Li(en)_x]^+$ die Solvatation durch Ethylendiamin für eine effektive Abschirmung von den Anionen ausreichte, während es bei den schweren Alkalimetallen zur Reaktion mit dem Lösungsmittel kam. Es wurden analoge Reaktionen mit „$BiCh_2$“ (=Bi_2Ch_3·Ch) und elementarem Kalium in Ethylendiamin durchgeführt, wobei erstmals eine Verbindung mit dem Bismutatanion $[BiTe_3]^{3-}$ aus Lösung gewonnen werden konnte. Die Reaktion mit „TlCh“ (=Tl_2Ch·Ch) mit elementarem Kalium in Ethylendiamin ergibt nicht wie erwartet ein $[Tl_2Ch_2]^{2-}$ oder $[Tl_2Ch_3]^{4-}$, sondern führt zur Reaktion mit dem Lösungsmittel, wobei es zur unerwarteten Bildung eines [Te-CN]$^-$-Anions kommt. Entsprechende Ergebnisse sind in Publikation **I** beschrieben.

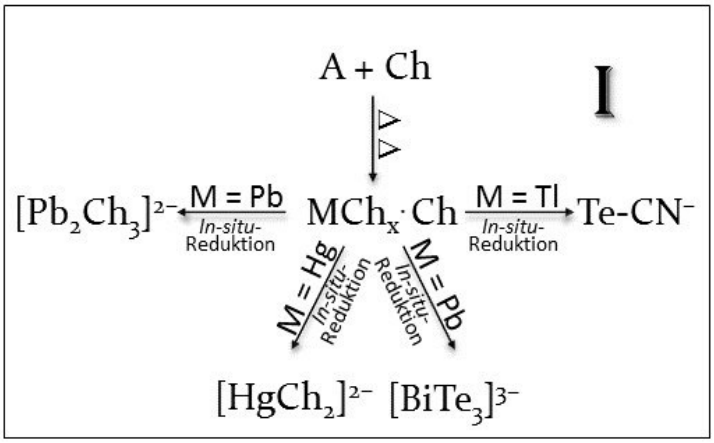

Abbildung 11. Reaktionsschema zu Publikation **I**.

Die Reaktion von „$HgCh_2$“ mit elementaren Alkalimetallen in Ethylendiamin führt in guten Ausbeuten mit hoher Reinheit zur Bildung von Verbindungen mit dem linearen $[HgCh_2]^{2-}$-Anion. Auch Reduktionen zu ternären Anionen der allgemeinen Formel $[MCh^1Ch^2]^{x-}$ waren auf diesem Weg möglich, was jedoch im Rahmen dieser Arbeit nicht besprochen werden

soll. Die Reduktionen von „$PbCh_2$“ mit den Metallocenen $NiCp_2$, $CoCp_2$, $CrCp^*_2$ und weiteren Reduktionsmitteln wie Borhydriden anstelle der elementaren Alkalimetalle, sowie die Verwendung von Erdalkalimetallen und elementarem Europium wurden ebenfalls eruiert, jedoch ergaben sich keine Anzeichen auf eine Bildung des Plumbatanions. Einige der Nebenprodukte dieser Reaktionen – Europiumpolychalkogenide und eine Cobaltocen-Acetonitril-Verbindung – wurden in einer späteren Publikationen beschrieben.

Die auf dem oben beschriebenen Weg erhaltenen Lösungen mit $[Li(en)_x]_2[Pb_2Ch_3]$ und [K(18-Krone-6)]$_2[Pb_2Ch_3]$ wurden daraufhin bezüglich ihrer Reaktivität gegenüber Übergangsmetallverbindungen untersucht. Die hierbei häufig als Oxidationsprodukt auftretenden Polytelluride ließen sich nach dem gleichen Verfahren auch direkt synthetisieren, indem elementares Tellur in Ethylendiamin mit elementarem Lithium oder Kalium (bei letzterem ist erneut die Zugabe von Komplexierungsreagenzien notwendig) in entsprechenden Verhältnissen zur Reaktion gebracht wurde. Die hierbei erhaltenen Verbindungen mit $(Te_x)^{2-}$ Anionen (x = 1-4) wurden strukturell untersucht und bezüglich ihrer NMR-Verschiebungen in Lösung, in Festphase und zudem quantenchemisch untersucht. Entsprechende Ergebnisse und opto-elektronische Untersuchungen werden in Publikation **II** diskutiert.

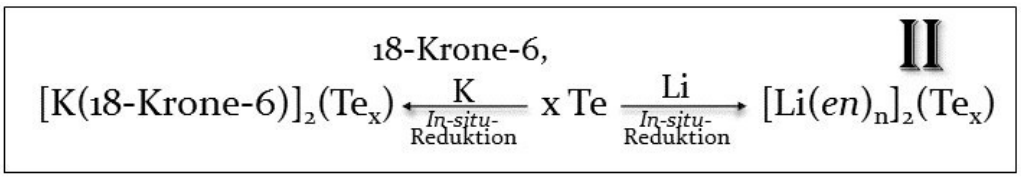

Abbildung 12. Reaktionsschema zu Publikation **II**.

Weitere Reaktivitätsstudien der Trichalkogenidodiplumbate wurden mit $[Rh(PPh_3)_3Cl]$ und $[Pd(PPh_3)_2Cl_2]$ durchgeführt. Hierbei kam es zur Bildung von Verbindungen mit Chevrel-artigen Clustern: $[Rh_6Se_8(PPh_3)_6]\cdot 0.5en$ mit formal vier Rh(II)- und zwei Rh(III)-Ionen, wobei die Oxidation der Rhodiumionen, die im Edukt die formale Oxidationsstufe +I inne hatten, vermutlich mit der Reduktion von Pb(II) zu Pb(0) einherging. Die Verbindung $[Li_4(en)_{10}][Pd_6Te_8]$ kann als kondensiertes Aggregat von sechs quadratisch planaren $[PdTe_4]^{6-}$ aufgefasst werden und beinhaltet formal Pd(II). Die entsprechenden strukturellen Beschreibungen, ausführliche quantenchemische Untersuchungen sowie zyklovoltammographische Experimente sind in Publikation **III** zusammengefasst.

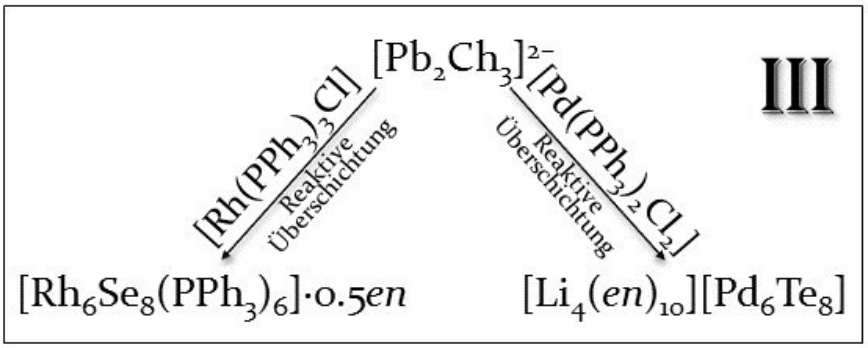

Abbildung 13. Reaktionsschema zu Publikation **III**.

Außerdem konnte in der gleichen Reaktion – in wesentlich geringen Ausbeuten – ein weiteres Produkt erhalten werden: $\{[K(18\text{-Krone-6})][K(en)_2]K[Rh_3Se_2(CN)_2(PPh_3)_4(PbSe)]\}_2 \cdot 1.3en$. Hierbei handelt es sich um eine trigonale Bipyramide mit Rh(I) Ionen in basalen und Se in apikalen Positionen. Neben der Absättigung der Koordinationssphäre der Rhodiumionen durch PPh_3 und CN^- ist eine verbrückende PbSe-Einheit enthalten, welche damit – als schweres Homolog – CO-analog koordiniert. Die Cyanidionen sind möglicherweise aus der Zersetzung des Lösungsmittels in Gegenwart von Rh-Se-Spezies hervorgegangen. Der Versuch einer Syntheseoptimierung mit [2.2.2]Krypt anstelle des Kronenethers ergab das Grundgerüst der Struktur $[K([2.2.2]Krypt)][Se_2(Rh(PPh_3)_2)_3] \cdot 3C_6H_6$ mit vollständig PPh_3-abgesättigten Rhodiumionen und entsprechend ohne PbSe-„Ligand“. Ausführliche Strukturbeschreibungen und detaillierte quantenchemischen Beschreibungen sind in Publikation **IV** zusammengefasst.

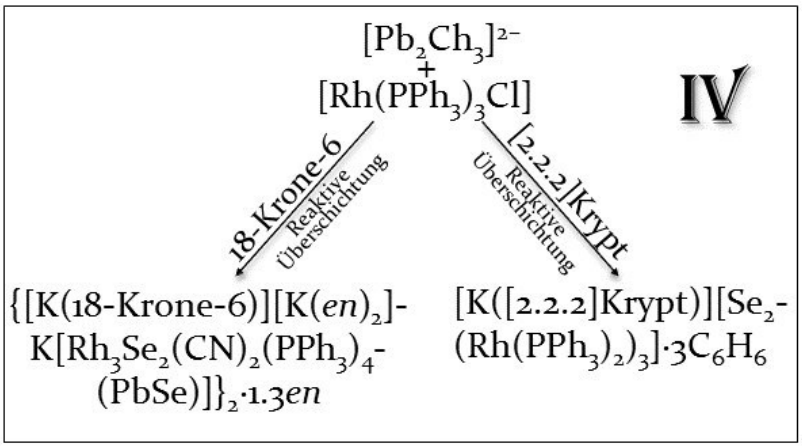

Abbildung 14. Reaktionsschema zu Publikation **IV**.

Weitere Umsetzungen des Trichalkogenidodiplumbats mit Chloriden der Übergangsmetalle in Gegenwart von Ammonium- und Phosphoniumsalzen lieferten eine Reihe von Chloridoplumbaten und –metallaten, die bisher nicht strukturell beschrieben wurden. Umsetzungen mit Dimangandekacarbonyl ergeben eine Reihe neuer chalkogenidverbrückter Mangan(II)carbonyle wie beispielsweise $[K([2.2.2]Krypt)]_2\{Ch_2[Mn(CO)_4]_3\}$ und $[K([2.2.2]Krypt)]_2\{Ch[Mn(CO)_4]\}_2$. Entsprechende Veröffentlichungen stehen noch aus. Weiterhin konnten verschiedene neue Polyselenide erhalten und strukturell aufgeklärt werden, welche in der folgenden Veröffentlichung behandelt werden.

3.2 Solvothermalsynthese von Plumbaten und Merkuraten

Simultan zu der zuvor beschriebenen Darstellung der Trichalkogenidodiplumbate wurde die solvothermale Reaktionsführung eruiert. Da alle Versuche mit tellurhaltigen Phasen oder Edukten zu binären Telluriden (K_2Te_2, K_2Te_3, K_5Te_2, PbTe) oder elementarem Tellur führten, wurde folglich der Fokus auf Selenidoplumbatphasen gelegt. Hierbei wurden sowohl verschiedene Stöchiometrien der Eduktgemische $A_xPb_ySe_z$ permutiert (x, y, z = 1..4), als auch das Lösungsmittel, die Temperatur und Reaktionsdauer. In vielen dieser Reaktionen kam es zur Umwandlung der Eduktphasen zu K_2Se_2 oder K_2Se_3 und PbSe. Unter verschiedenen Reaktionsbedingungen wurden neue Polyselenide erhalten, welche zusammen mit den zuvor

erwähnten, nasschemischen dargestellten Polyseleniden in Veröffentlichung **V** publiziert wurden.

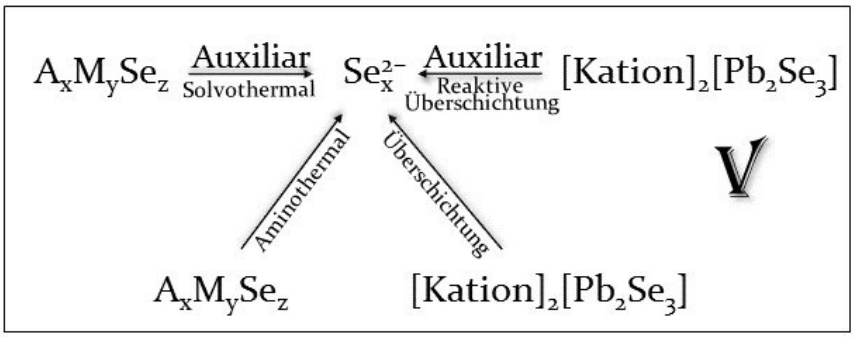

Abbildung 15. Reaktionsschema zu Publikation **V**.

Obgleich Blei nach den meisten dieser solvothermalen Reaktionen nicht im Produkt enthalten war, konnte jedoch unter Verwendung von Ethylendiamin mit einer „K_2PbSe_2“-Phase bei 150°C und einer Reaktionsdauer von einer Woche das neue *ortho*-Plumbat $K_4PbSe_4{\cdot}en{\cdot}NH_3$ erhalten werden. Hierbei muss für eine homogene Eduktlegierung die Reaktionsschmelze für etwa eine halbe Stunde mit dem Sauerstoffbrenner auf Weißglut des Quarzglases gebracht werden. Die Bildung und Isolierung des genannten Plumbats ist insofern überraschend, als es sich um eine Selenverbindung von Blei in der formalen Oxidationsstufe +IV handelt, welches bisher nur mit stark elektronegativen Liganden oder in Form von Organo-Blei-Verbindungen beschrieben worden war. Entsprechende quantenchemische, UV-Vis-spektroskopische und strukturelle Studien sind in Veröffentlichung **VI** aufgeführt.

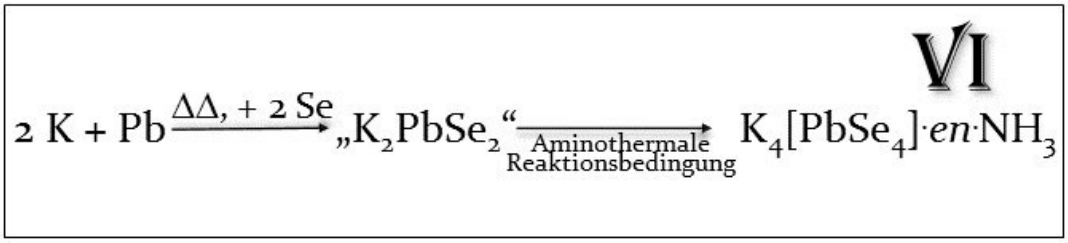

Abbildung 16. Reaktionsschema zu Publikation **VI**.

Weitere Untersuchungen zu den entsprechenden homologen *ortho*-Plumbaten wurden angestellt, jedoch erhält man die für die Synthese des $[PbS_4]^{4-}$ benötigte Eduktphase „K_2PbS_2“ nicht als homogene Schmelze. Es scheint, dass noch höhere Temperaturen vonnöten wären, welche die Quarzampullen jedoch nicht überstehen. Die entsprechende tellurhaltige Phase kann bei bedeutend geringeren Temperaturen erhalten werden. Es kommt bei der anschließenden solvothermalen Reaktion bei Temperaturen über 120°C zur Bildung binärer Produkte (K_2Te_x, PbTe) neben elementarem Tellur. Bei Reaktionstemperaturen unter 120°C ist keine Reaktion sichtbar, die Produkte sind allesamt röntgenamorph und gleichen visuell der eingesetzten Eduktphase.

Weiterhin wurde versucht, ausgehend von der Eduktlegierung „KPbCh“ in Gegenwart von Übergangsmetallsalzen – erneut in verschiedenen Lösungsmitteln – direkt zu quarternären Metallaten mit ternären Plumbatanionen zu gelangen. Unter Verwendung von Acetonitril in Gegenwart von $NiCl_2$ kam es hierbei zur Tetramerisierung des Lösungsmittels, Oxidation des Ni(II) zu Ni(III) und Bildung von $[(C_8H_{12}N_4)NiCl(\mu\text{-}Cl)]_2$. Um den Einfluss der verschiedenen Metallionen zu eruieren, wurden analoge solvothermale Reaktionen ausgehend nur von $NiCl_2$, von $PbCl_2$ und jeweils noch in Gegenwart von LiOH oder K_2Te als Lewis-Base in Acetonitril unternommen. Die Reaktion von $NiCl_2$ und LiOH ergab die Dimerisierung von Acetonitril unter Einschluss eines weiteren Stickstoffatoms und Bildung von $[Ni(C_4N_3H_8)(C_4N_3H_9)]Cl$, wohingegen die Gegenwart von $PbCl_2$ zur Bildung von Imidazol aus Acetonitril führt, welches als Ligand einer eindimensional ausgedehnten $PbCl_2$-Struktur dient. Eine ausführliche Beschreibung der entsprechenden Reaktionen erfolgt in Publikation **VII**.

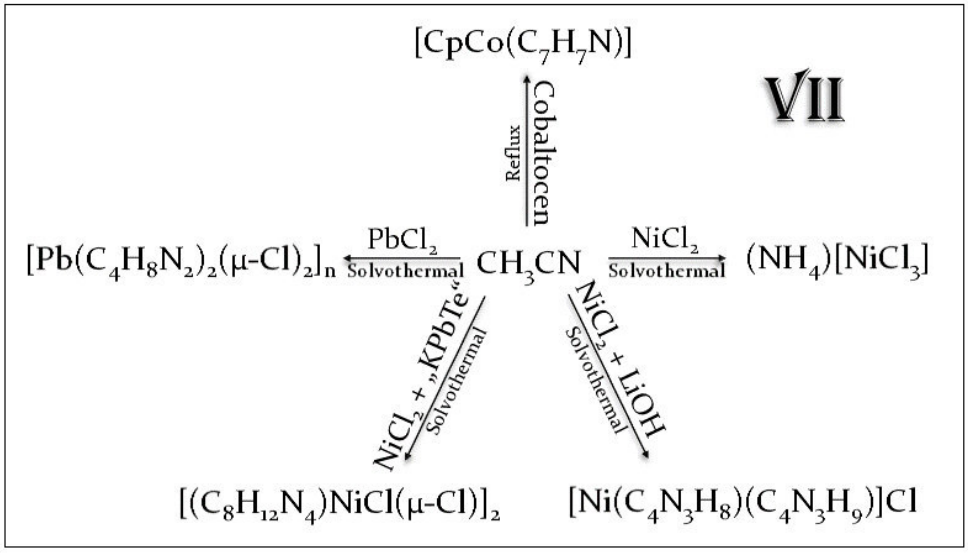

Abbildung 17. Reaktionsschema zu Publikation **VII**.

Die gleichen Reaktionsbedingungen führten unter Verwendung von $HgSO_4$ und „KPbSe“ in verschiedenen Aminen zur Bildung von $K_2Hg_2Se_3$. Synthesechemisch ist der Einsatz einer Plumbatphase allerdings nicht notwendig; durch direkte Festphasensynthese aus den binären Vorläufer K_2Se und HgSe im Verhältnis 1:2 und anschließender solvothermaler Extraktion kann das Selenidomerkurat ebenfalls erhalten werden. Es besitzt eine dreidimensional ausgedehnte Anionensubstruktur, mit Kaliumionen in tunnelförmigen Hohlräumen derselben. Dieses Strukturmotiv ist für Merkurate bisher nicht bekannt und die Verbindung wurde entsprechend bezüglich ihrer photoelektronischen, thermoelektrischen und konduktiven Eigenschaften ausführlich untersucht und mittels quantenchemische Rechnungen mit periodischen Randbedingungen weiterführend studiert. Die Ergebnisse werden in Publikation **VIII** aufgeführt.

Die Synthese des schweren Homologs $K_2Hg_2Te_3$ kann ausgehend von K_2Te und HgTe auf gleichem Wege durchgeführt werden. Thermoelektrische Untersuchungen an diesem Merkurat und die Publikation der Ergebnisse stehen noch aus.

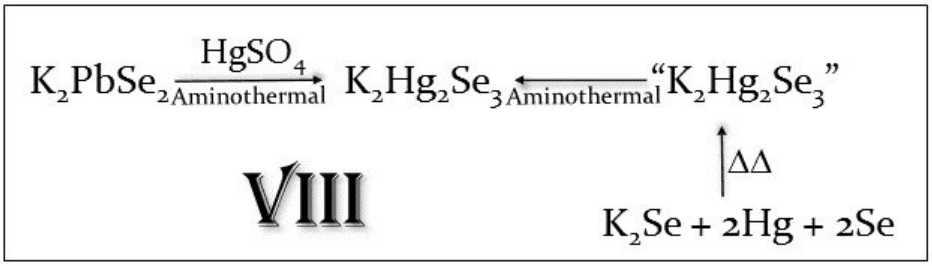

Abbildung 18. Reaktionsschema zu Publikation **VIII**.

Eine analoge solvothermale Behandlung von A_2HgSe_2 oder von A_2Ch und $HgSO_4 \cdot xH_2O$ (A = Na, K; x = 0, 1, 2) führte in verschiedenen Aminen zur Bildung von Na_2HgSe_2 und $K_2HgSe_2 \cdot H2O$ mit bereits für die Oxomerkurate literaturbekannten Strukturmotiven. Auch konnte das *meta*-Merkurat $K_4HgSe_3 \cdot 1H_2O$ als Hydrat hergestellt werden. Da thermoelektrischen Messungen neuer Verbindungen jedoch verhältnismäßig aufwendig sind, und im Falle von $K_2Hg_2Se_3$ eine für entsprechende Applikationen zu geringe Elektronenleitfähigkeit gefunden wurde, sollte zunächst in einem systematischen Ansatz die komplette Reihe der bekannten ternären Merkurate bezüglich ihrer Bandlücken untersucht werden. Strukturelle Beschreibungen, deren Veränderung zwischen den unterschiedlichen Homologen und der Verlauf der Bandstrukturen werden aktuell zur Publikation fertiggestellt.

Mit der gleichen Synthesestrategie konnten auch *ortho*-Chalkogenido-thallate, -stannate, -stibate und vereinzelt deren Hydrate, sowie *meta*-Chalkogenidocadmate und -bismutate dargestellt werden. Letztere sind bereits literaturbekannt, wurden bisher jedoch aufwendig aus Alkalimetallcarbonat und Bismutoxid bei hohen Temperaturen im H_2-Strom dargestellt. Erstmals konnten sie nun zudem mit verschiedenen Chalkogeniden gemäß der generellen Summerformel $K_3[BiTe_xSe_{3-x}]$ dargestellt werden. Entsprechende strukturelle Beschreibungen und Untersuchungen der thermoelektrischen Eigenschaften stehen noch aus.

3.3 Ionothermalsynthesen

Das Verhalten der oben genannten Metallate unter Ionothermalbedingungen wurde eruiert, wobei zunächst kommerziell erwerbliche ionische Flüssigkeiten verwendet wurden. Zur Einstellung der Basizität oder zur (temporären) Koordination wurden verschiedene Amine – vornehmlich Dimethylmorpholin und Ethylendiamin – zugesetzt. Über die Erkenntnisse aus diesen Ansätzen in ionischen Flüssigkeiten und der Vergleich mit dem Verhalten unter solvothermalen Bedingungen, wird zusammen mit einigen der so erhaltenen Strukturen in Publikation **IX** berichtet.

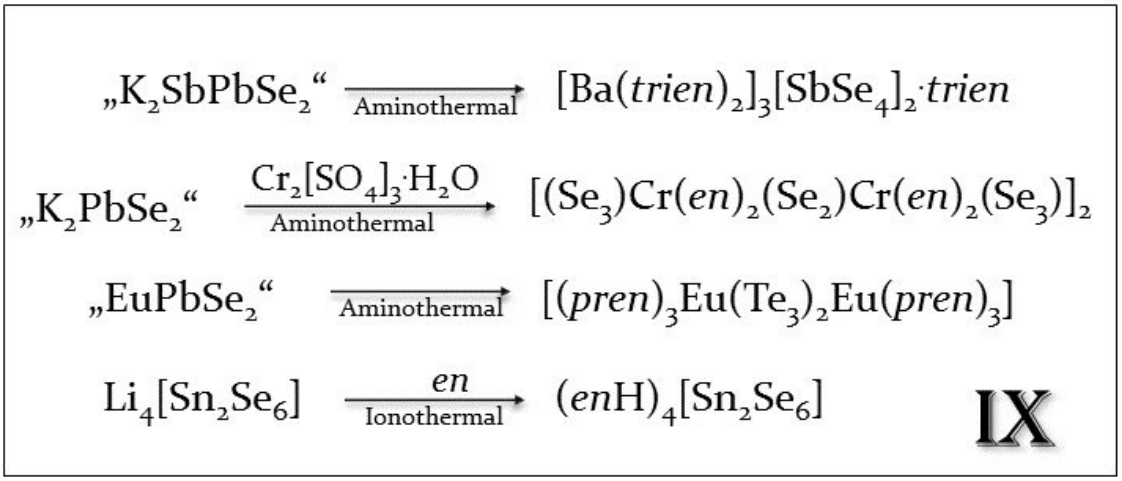

Abbildung 19. Reaktionsschema zu Publikation **IX**.

Die ionothermale Umsetzung von $K_2Hg_2Se_3$ in einer sulfidischen ionischen Flüssigkeit führte zur Bildung der Verbindung $K_2Hg_6Se_7$, deren Struktur für die leichteren Homologe bekannt, jedoch nicht auf klassischen Synthesewegen (Polyselenid-lux, Hochtemperatursynthese, Solvothermale Reaktionsführung) zugänglich ist. Grund hierfür scheinen die durch die ionische Flüssigkeit simulierten Polysulfid-Flux-ähnlichen Bedingungen zu sein. Entsprechende methodische Überlegungen und Strukturbeschreibungen sind in Publikation **X** dargelegt.

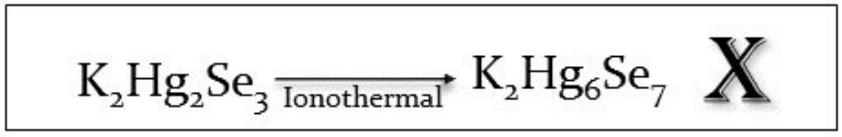

Abbildung 20. Reaktionsschema zu Publikation **X**.

4.1 Themenkomplexe

(**a**) $[M_xCh_y]^{q-}$, Synthese und Reaktivität

(**b**) Solvothermalsynthese von Plumbaten und Merkuraten

(**c**) Ionothermale Umsetzungen

4.2 Übersicht der Artikel

I (a) "About the Syntheses of Chalcogenidometalates by in-situ Reduction with Elemental Alkali Metals"

G. Thiele, L. Vondung, S. Dehnen, *Z. Anorg. Allg. Chem.* **2015**, *im Druck*.

II (a) "Syntheses, Structures and Electronic Properties of a New Series of Tellurides of the Type [Sequestrated Cation]$_2$[Te$_x$] (x = 1-4)"

G. Thiele, N. Lichtenberger, R. Tonner, S. Dehnen, *Z. Anorg. Allg. Chem.* **2013**, *639*, 2809-2815 (*Titelbild*).

III (a) "Molecular CHEVREL-like Clusters $[(RhPPh_3)_6Se_8]$ and $[Pd_6Te_8]^{4-}$"

G. Thiele, Z. You, S. Dehnen, *Inorg. Chem.* **2015**, *in Revision*.

IV (a) "{μ-PbSe}: The Second Heaviest CO Homolog as an Unexpected Ligand"

G. Thiele, S. Dehnen, *Manuskript in Vorbereitung*.

V (b) "Organic Cation and Complex Cation-Stabilized (Poly-)Selenides, [Cation]$_x$(Sey)$_z$: Diversity in Structures and Properties"

G. Thiele, L. Vondung, C. Donsbach, S. Pulz, S. Dehnen, *Z. Anorg. Allg. Chem.* **2014**, *640*, 2684-2700.

VI (b) "$K_4[PbSe_4]\cdot en\cdot NH_3$ – A Non-Oxide, Non-Halide Inorganic Lead(IV) Compound"

G. Thiele, T. Krüger, S. Dehnen, *Angew. Chem.* **2014**, *126*, 4792-4797; *Angew. Chem. Int. Ed.* **2014**, *53*, 4699-4703.

VII (b) "Reactions In and With Acetonitrile"

G. Thiele, S. Dehnen, *Manuskript in Vorbereitung.*

VIII (b) "$K_2Hg_2Se_3$: A novel Selenidomercurate(II) for Photothermoelectric Applications"

G. Thiele, S. Lippert, F. Fahrenbauer, P. Bron, M. Assmann, O. Oeckler, A. Rahimi-Iman, M. Koch, B. Roling, S. Dehnen, *Manuskript in Vorbereitung.*

IX (c) "Solvothermal and Ionothermal Syntheses and Structures Of Amine- and/or (Poly-) Chalcogenide Coordinated Metal Complexes"

G. Thiele, S. Santner, C. Donsbach, M. Assmann, M. Müller, S. Dehnen, *Z. Kristallogr*. **2014**, *229*, 489–495 (*Titelbild*).

X (c) "$K_2Hg_6Se_7$ – A new Mercurate from Ionothermal Synthesis: A Pseudo-Flux Reaction"

G. Thiele, H. Borkowski, L. Finger, J. Sundermeyer, S. Dehnen, *Manuskript in Vorbereitung*.

I About the Syntheses of Chalcogenidometalates by in-situ Reduction with Elemental Alkali Metals

Günther Thiele, Lisa Vondung, Stefanie Dehnen, *Z. Anorg. Allg. Chem.* **2015**, *im Druck*.

Reduction of chalcogen-rich Pb:Ch (1:2) phases in ethane-1,2-diamine (*en*) by elemental alkali metals results in the formation of solutions of $[Pb_2Ch_3]^{2-}$ of high purity and abundance. In contrast, application of the same reaction conditions to a binary Bi:Te (1:2) phase yields the mononuclear $[BiTe_3]^{3-}$ anion. Instead of the expected $[Tl_2Te_3]^{4-}$ or $[Tl_2Te_2]^{2-}$ anions, analogous reactions with a Tl:Te (1:1) phase end up with a C–C-bond cleavage of the solvent *en* under formation of a salt of the telluridocyanate $(N{\equiv}C{-}Te)^-$ anion. Side reactions of *en* and elemental cesium are presented and metalate solutions are investigated with NMR spectroscopy.

Themenkomplex $[M_xCh_y]^{q-}$, Synthese und Reaktivität

Inhalt: Die kristallographisch charakterisierten Chalkogenidometallatanionen des Thalliums, Bleis und Bismuts werden vorgestellt, zusammen mit deren typischer Synthese in flüssigem Ammoniak oder durch Extraktion der durch Festphasenmethoden erhaltenen Feststoffphasen.

In Anlehnung an die Synthese des $K_4PbTe_3{\cdot}2en$ wird die *in-situ*-Reduktion Chalkogen-reicher Phasen „PbSe·Se“, „PbTe·Te“, „Bi_2Te_3·Te“ und „Tl_2Te·Te“ beschrieben. Hierbei können bei Verwendung von Li oder K – bei letzterem in Anwesenheit von 18-Krone-6 oder [2.2.2]Kryptand – in hoher Reinheit und Quantität aus „PbCh·Ch“-Suspensionen die Trichalkogenidodiplumbate erhalten werden. Es werden ^{77}Se-, ^{125}Te- und ^{207}Pb-NMR-spektroskopische Untersuchungen präsentiert, wobei bei den Selenidoplumbaten Se_2^{2-} als Nebenprodukt anfällt. Die NMR-Signale sind durch unvollständige Abschirmung der Alkalimetallionen bei Verwendung von 18-Krone-6 oder elementarem Lithiums äußerst breit und lassen eine Alkalimetallion-Anion-Wechselwirkung vermuten.

Eine Ausweitung der Studien auf Cäsium als Reduktionsmittel wurde durch die Reaktion mit dem Lösungsmittel Ethylendiamin verhindert. Ein stattdessen entstandenes Cäsium-Ethylendiamin-Trimer wird kristallographisch beschrieben. Auch Kalium reagiert auf diese Weise, jedoch viel langsamer. Lithium hingegen zeigt auch nach Wochen in Ethylendiamin keine sichtbare Veränderung.

Das für „Tl_2Te·Te“ erwartete trigonal bipyramidale $[Tl_2Te_3]^{4-}$-Anion, sowie das bereits literaturbekannte $[Tl_2Te_2]^{2-}$-Anion, wurden wird mithilfe quantenchemischer Rechnungen modelliert. Das tatsächlich isolierte Produkt [K(18-Krone-6)][N≡C–Te] wird unter Vergleich mit der Literaturvorschrift für die Darstellung eines Telluridocyanates beschrieben. Als Cyanid-Quelle wird die Zersetzung des Lösungsmittels diskutiert.

$[K(18\text{-Krone-6})]_2[Pb_2Se_3]{\cdot}en$, $[K_2(18\text{-Krone-6})_2(en)K(en)_2][BiTe_3]$, [K(18-Krone-6)](N≡C–Te) werden hinsichtlich ihrer Kristallstruktur und Synthese beschrieben.

Eigener Anteil: Alle Experimente wurden von mir geplant, NMR- und Einkristalldaten wurden von mir aufgenommen und ausgewertet. Quantenchemische Rechnungen und die synthetischen Arbeiten mit Thallium und Bismut wurden von Lisa Vondung unter meiner Aufsicht im Rahmen ihrer Masterarbeit durchgeführt. Vorrausgehende Arbeiten zur *in-situ*-Reduktion mit Lithium wurden von Michael Müller unter meiner Aufsicht im Rahmen eines materialchemischen Masterpraktikums durchgeführt. Niels Lichtenberger konnte im Rahmen seiner Bachelorarbeit unter meiner Anleitung erstmals die Reaktion von Cäsium mit Ethylendiamin nachweisen und ein entsprechendes Produkt kristallisieren. Marcus Müller hat unter meiner Anleitung zu den synthetischen Arbeiten beigetragen. Stefanie Dehnen und ich haben das Manuskript gemeinsam verfasst.

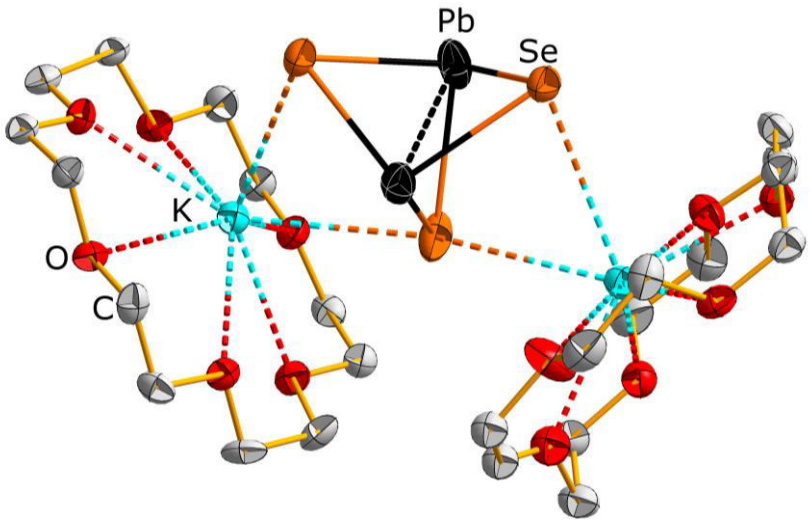

Abbildung 21. Ausschnitt aus der Kristallstruktur von $[K(18\text{-Krone-}6)]_2[Pb_2Se_3]\cdot en$.

ARTICLE

DOI: 10.1002/zaac.200((will be filled in by the editorial staff))

About the Syntheses of Chalcogenidometalates by *in situ* Reduction with Elemental Alkali Metals

Günther Thiele, Lisa Vondung, and Stefanie Dehnen*

Dedicated to Professor Dr. Dr. h.c. mult. Arndt Simon in occasion of his 75th birthday.

Keywords: Chalcogenides, Reduction, Metalates, X-ray diffraction, NMR spectroscopy.

Reduction of chalcogen-rich Pb:Ch (1:2) phases in ethane-1,2-diamine (*en*) by elemental alkali metals results in the formation of solutions of $[Pb_2Ch_3]^{2-}$ of high purity and abundance. In contrast, application of the same reaction conditions to a binary Bi:Te (1:2) phase yields the mononuclear $[BiTe_3]^{3-}$ anion. Instead of the expected $[Tl_2Te_3]^{4-}$ or $[Tl_2Te_2]^{2-}$ anions, analogous reactions with a Tl:Te (1:1) phase end up with a C–C-bond cleavage of the solvent *en* under formation of a salt of the telluridocyanate $(N{\equiv}C–Te)^-$ anion. Side reactions of *en* and elemental cesium are presented and metalate solutions are investigated with NMR spectroscopy.

Introduction

The reduction of main group metals or alloys with elemental alkali metals in liquid ammonia, as was first described by *Joannis*,[1] resulted not only in the characterization of the famous $(Pb_9)^{4-}$ ion,[2] but also in a still growing area of research on a large variety of homoatomic, heteroatomic, intermetalloid or organyl-substituted *Zintl* ions.[3] Our special focus is directed towards the syntheses and characterization of corresponding binary molecular anions of Tl, Pb or Bi besides Se or Te.

The crystallographically determined structures of according chalcogenido metallate anions reported in the literature can be summarized within a few lines: For thallium containing compounds, one knows the butterfly-like anions $[Tl_2Ch_2]^{2-}$ (Ch = Se, Te),[4,5] a distorted and {TlSe}-capped heterocuban-derived anion $[Tl_5Se_5]^{3-}$,[6] $[Tl_4Se_8]^{4-}$ which comprises edge-sharing $[TlSe_4]$ tetrahedra,[7] $[Tl_3Se_{15}]^{3-}$ with $(Se_4)^{2-}$ ligands bound to a $[Tl_3Se_3]$ unit,[8] the tetranuclear Tl^{3+} polyselenide $[Tl_4Se_{16}]^{4-}$,[9] and finally the related, though ternary, trigonal bipyramidal $[TlPbTe_3]^{3-}$ anion.[10] The list of selenido- and telluridoplumbates additionally contains the trigonal bipyramidal $[Pb_2Ch_3]^{2-}$ anions,[10-13] trigonal pyramidal $[PbTe_3]^{4-}$,[14] $[Pb(Se_4)_2]^{2-}$ with two $(Se_4)^{2-}$ tetraselenide ligands,[15] and tetrahedral $[PbSe_4]^{4-}$.[16] For Bi compounds, only the trigonal bipyramid $[BiCh_3]^{3-}$ anions (Ch = Se, Te)[17] and $[(S_7)_2Bi(S_6)Bi(S_7)_2]^{4-}$ [18] have been known so far.

The most common route towards those binary anions is the preparation in liquid ammonia, being – however – quite cumbersome. Therefore, alternative reaction pathways, such as extraction of alloys that were prepared by high-temperature procedures, have been extensively studied, as well as reductions in less volatile solvents – preferably liquid solvents at room temperature, such as ethane-1,2-diamine (*en*). We have previously utilized this *in-situ* reduction technique for the syntheses of polytellurides of *en*-solvated lithium derivatives,[19] and have now extended this study according to *Haushalter's* synthesis of $K_4[PbTe_3]{\cdot}2en$ (see equation 1),[14] towards reduction of heavy main group chalcogenides with lithium or potassium; reactions of potassium were carried out in the presence of cation sequestrating agents. The chalcogen-rich phases are indicated as "PbCh·Ch", "Bi_2Te_3·Te", and "Tl_2Te·Te", as they are anticipated as being mixtures of the common binary chalcogenides with an additional equivalent of elemental chalcogen. This assumption was verified by reactions starting out from separate PbCh and Ch, or Bi_2Te_3 and Te that have been pulverized together at room temperature prior to reaction under otherwise unchanged conditions. All of these reactions afforded the same products in similar abundance. Hence, although the chalcogen-rich phases may be formally viewed as polychalcogenides, the situation in solution is the same, thus formally involving "Ch^{2-}" anions beside "Ch^0". The observation made at dissolving the parent phases contradicts the presence of polychalcogenide anions, as none of the typical colors are obtained.

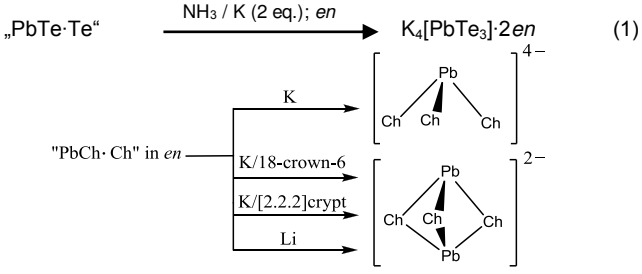

Scheme 1. Reaction pathways for the reduction of "PbCh·Ch".

* Fax: +49 (0)6421 2825653
E-Mail: dehnen@chemie.uni-marburg.de
Philipps-Universität Marburg, Fachbereich Chemie and Wissenschaftliches Zentrum für Materialwissenschaften (WZMW), Hans-Meerwein-Straße 1, 35043 Marburg
Fax: +49 (0)6421 282 5653
E-mail: dehnen@chemie.uni-marburg.de
Homepage: www.uni-marburg.de/fb15/agdehnen

This way, we were able to obtain solutions of the $[Pb_2Ch_3]^{2-}$ anions (Ch = Se, Te)[10] in high abundance and purity, and to isolate single-crystals of $[K(18\text{-crown-}6)]_2[Pb_2Se_3]\cdot en$ (**1**) and $[K(18\text{-crown-}6)_2][Pb_2Te_3]\cdot en$.[20] A corresponding reduction of "$Bi_2Te_3\cdot Te$" yielded the telluridobismuthate $[K_2(18\text{-crown-}6)_2(en)K(en)_2][BiTe_3]$ (**2**). For the analogous reduction of "$Tl_2Te\cdot Te$", we unexpectedly obtained [K(18-crown-6)](N≡C−Te) (**3**) as a side product in high yield.

Results and Discussion

All title compounds were obtained in the course of our current investigations on the synthesis and reactivity of salts of the $[M_xCh_y]^{q-}$ (M = Tl, Pb, Bi; Ch = Se, Te) anions. The literature procedure for the generation of salts of the $[Pb_2Te_3]^{2-}$ anion involves the extraction of an alloy of the nominal composition "KPbTe" with *en* in the presence of [2.2.2]crypt.[12] However, these syntheses always came along with the formation of $[K([2.2.2]crypt)]_2(Te_2)$[19] and $[K([2.2.2]crypt)](Te_3)$[21] as side-products, which was determined via X-ray diffraction of according crystals, beside Te^{2-} and $(HTe)^-$ ions, as observed by ^{127}Te-NMR experiments of the reaction solution (see Supporting Information).

In contrast, after *in-situ* reduction of "PbTe·Te" in *en* with 2.1 equivalents of elemental potassium, in the presence of ≥ 2.1 eq. of [2.2.2]crypt or 18-crown-6, exactly one signal of the desired $[Pb_2Te_3]^{2-}$ anion is observed in the ^{127}Te-NMR spectrum of a concentrated reaction solution. The same result has been obtained for the use of lithium in the absence of a cation sequestrating reagent, due to sufficient cation solvation by the solvent *en* in solution. Scheme 1 provides an overview of the corresponding reaction pathways. However, so far we were not able to obtain the expected "$[Li(en)_2]_2[Pb_2Ch_3]$" as crystals. The *in-situ* reduction with Li or K in *en* can also be applied for the synthesis of the corresponding *selenido*metalates, yet solubilities vary considerably and syntheses usually afford the monoselenide anion as a side product, according to ^{77}Se NMR spectroscopy of the reaction solutions (see Supporting Information).

Exemplarily for the heavier alkali metals, we have also checked the behavior of cesium in this context. However, it is too reactive, and immediately decomposes the solvent *en* to a variety of colorless degradation products (Scheme 2, Figure S1, Table S2), as was described before in part.[22]

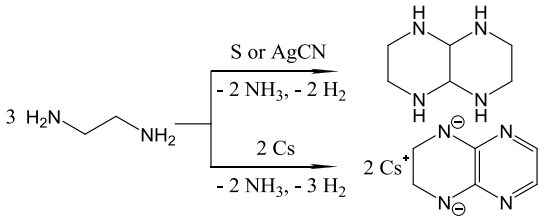

Scheme 2. Reaction pathways for the oligomerization of *en*, as reported[10] or observed herein (see Figure S1 and Table S2).

Also during reductions with elemental potassium, we have observed small quantities of a colorless precipitate, which explains the necessity of a small excess of the alkali metal to compensate for the loss. In the case of reductions with lithium, no such side products were observed; pure lithium/*en* electride solutions are stable for weeks, as deduced from to the unchanged blue color.

The NMR signal obtained from the $[Pb_2Ch_3]^{2-}$ anion in the case of *en*-solvated Li^+ or to a minor degree $[K(18\text{-crown-}6)]^+$ cations is very broad (Figures S2-S7), indicating interactions of the metal cations with the chalcogenide ligands in solution, while the corresponding [2.2.2]crypt complexes are shielded from any electronic affection of the cations, giving rise to sharp signals (see Figures S8, S9) as has been reported before.[19] However, only in the case of cation sequestration or solvation of all cations, the trigonal bipyramidal $[Pb_2Ch_3]^{2-}$ anion can be obtained. As soon as the amount of sequestration agent is lowered to less than one equivalent with respect to the alkali metal ion, no NMR signal can be observed for the $[Pb_2Ch_3]^{2-}$ anion any more.

We note in passing that fusion of precursors like K_2Ch and PbCh or K and PbCh and subsequent extraction of the ternary phases does not yield the $[Pb_2Ch_3]^{2-}$ species in according abundance and purity for PbCh and K_2Ch_x (x = 1…3), which are certainly thermodynamically favoured over the plumbate salts. For the corresponding reactions with Bi, we applied phases that were generated by simply fusing Bi and Ch in a 1:2 ratio. For Tl, we absolutely aimed at the use of a Tl^I species, different from the known, mixed-valence phase TlTe.[23] For this, we started from Tl_2Te,[24] and carefully pulverized it along with 1 eq. of elemental Te.

In the case of an analogous reaction with "$Bi_2Te_3\cdot Te$" and potassium in the presence of 18-crown-6, we obtained an *en*-soluble derivative of *Eisenmann*'s $K_3[BiTe_3]$,[17b] whereas the reduction of "$Tl_2Te\cdot Te$" does not yield the expected butterfly-like $[Tl_2Te_2]^{2-}$ anion, nor the trigonal bipyramidal $[Tl_2Te_3]^{4-}$ aggregate. Both anions represent minima on the energy hypersurface, as studies by means of DFT calculations using the program system Turbomole (see Figure 1 and the Supporting Information).[25] Instead, we isolated [K(18-crown-6)][N≡C−Te] (**3**).

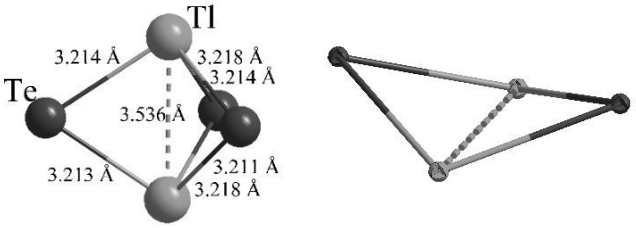

Figure 1. Left: Structure of the $[Tl_2Te_3]^{4-}$ anion upon simultaneous optimization of geometric and electronic structure (in C_1 symmetry) by means of quantum chemistry. Tl–Te–Tl: 66.65°-66.77°; Te–Tl–Te: 92.27°-92.92°.Right: Calculated structure of the $[Tl_2Te_2]^{2-}$ anion, as present in $[K([2.2.2]crypt)]_2[Tl_2Te_2]\cdot en$.[5]

The telluridocyanate anion has been previously synthesized from elemental tellurium and KCN in boiling dimethylsulfoxide.[26] However, within the reaction reported here, C–C, C–H, and N–H bond cleavage must precede the formation of the telluridocyanate, since *en* is the only carbon and nitrogen source within the reaction solution. Whereas we did observed breaking of the *en* C–N bond under comparably harsh conditions (becoming a source for ammonia)[16] no such bond cleavage has been reported under these mild reaction conditions so far. The whereabouts of the hydrogen atoms has

not been clarified so far. We assume hydrogen-richer degradation products, CH_3NH_2 or NH_3 + CH_4, to be more likely than H_2 formation, which is, however, not excluded. An according investigation is underway, but not trivial owing to the given reaction conditions and the aforementioned side-products formed from *en* and elemental potassium.

Apart from compound **3**, which has been obtained in high crystalline yields, all other crown-ether compounds of the above mentioned chalcogenidometalates seem to crystallize rather poorly. Beside low yields all crystals investigated so far have suffered from heavy twinning and disorder. As stated above, for the *en*-solvated lithium salts, we were not yet able to obtain crystalline material, which is probably due to the strong interaction of lithium ions with the anions upon removal of solvent. The crystallization of **3** is accompanied by the precipitation of an amorphous, brownish-black powder that was proven to contain Tl, Te and K – presumably as a mixture of binary tellurides and the elements. The crystallographic information of compounds **1 - 3** is summarized in Table 1. As mentioned above, the crystal structure analysis of $Cs_2(C_6N_4H_6)\cdot 1.5en$ (Scheme 2) is given in the Supporting Information (Figure S1, Table S2).

Crystal Structure of [K(18-crown-6)]$_2$[Pb$_2$Se$_3$]·en (1)

Compound **1** crystallizes in the monoclinic space group $P2_1/c$ with 4 formula units per unit cell. The bond lengths and angles within the trigonal bipyramidal $[Pb_2Se_3]^{2-}$ anion are similar to those in $[K([2.2.2]crypt)]_2[Pb_2Se_3]$[10] (values given in parenthesis): Pb–Pb 3.2194(6) Å (c.f. 3.2260(8) Å), Pb–Se 2.7366(14) - 2.7842(12) Å (c.f. 2.757(11) Å on average). In contrast to the [2.2.2]crypt salt, interactions between K^+ ions and the anion are present (K…Se 3.247(3) - 3.625(2) Å), thereby capping two Se–Se edges of the trigonal bipyramidal anion (Figure 2).

Table 1. Summary of crystallographic and refinement details for **1**-**3** (CCDC 1027982-1027984). Data for $Cs_2(C_6N_4H_6)\cdot 1.5en$ (CCDC 1027985) are given in Table S2.

Compound Formula	**1** **[K(18-crown-6)]$_2$[Pb$_2$Se$_3$]·*en***	**2** **[K$_2$(18-crown-6)$_2$K(en)$_2$][BiTe$_3$]**	**3** **[K(18-crown-6)](N≡C–Te)**
Empirical formula	$C_{26}H_{46}K_2N_2O_{12}Pb_2Se_3$	$C_{56}H_{40}Bi_2K_6N_8O_{24}Te_6$	$C_{13}H_{23}KNO_6Te$
Formula weight /g·mol^{-1}	1308.11	2627.12	456.02
Crystal color and shape	orange stick	red block	colorless block
Crystal size /mm	0.25·0.13·0.06	0.03×0.02×0.01	0.42×0.33×0.10
Crystal system	monoclinic	orthorhombic	monoclinic
Space group / Flack[27]	$P2_1/c$	$Pmc2_1$ / 0.001(5)	$P2_1/n$
a /Å	22.9663(10)	14.4931(4)	8.0125(9)
b /Å	9.3038(3)	14.4538(6)	16.354(2)
c /Å	19.5932(8)	22.7590(11)	14.9103(18)
β /°	91.645(3)		91.953(10)
V /Å^3	4184.8(3)	4767.6(3)	1952.6(4)
Z	4	2	4
ρ_{calc} /g· cm^{-3}	2.076	1.83	1.551
μ(Mo$_{K\alpha}$) /mm^{-1}	10.895	5.809	1.759
2Θ range /°	4-55	3-53	3-51
Abs. corr. T_{min}/T_{max}	0.1931/0.5209	0.9067/0.9757	0.7237/0.8242
Reflections measured	29752	29042	15768
Independent reflections	8830	9850	3475
R(int)	0.0992	0.0663	0.0802
Indep. refl. ($I > 2\sigma(I)$)	6386	6055	2348
Parameters	422	528	199
R_1 ($I > 2\sigma(I)$)	0.0626	0.0322	0.0456
wR_2 (all data)	0.1407	0.0603	0.0788
GooF (all data)	1.059	0.721	0.951
Max. peak/hole /e$^-$·10^{-6}pm^{-3}	1.858 / –2.036	1.107 / –0.592	0.659 / –0.5

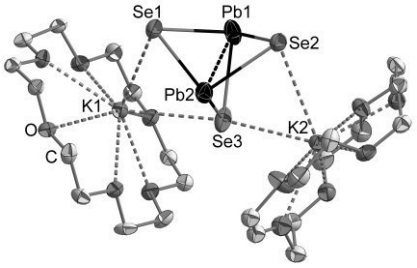

Figure 2. Structure of the $[Pb_2Se_3]^{2-}$ anion and its coordination by $[K(18\text{-crown-6})]^+$ complexes in **1**. Ellipsoids are drawn at 50% probability, hydrogen atoms are omitted for clarity.

Crystal Structure of [K$_2$(18-crown-6)$_2$(en)K(en)$_2$][BiTe$_3$] (2)

Compound **2** crystallizes in orthorhombic space group $Pmc2_1$ with 2 formula units in the unit cell. Each of the trigonal pyramidal $[BiTe_3]^{3-}$ anions is coordinated by three K^+ ions (K…Te 3.471(4) - 3.904(5) Å). Bond lengths for Bi–Te are 2.8474(15) - 2.8558(12) Å, thus slightly shorter than in *Eisenmann's* $K_3[BiTe_3]$ (2.884 Å).[17b] One of the K^+ ions per formula unit (K1) bridges between two adjacent $[BiTe_3]^{3-}$ anions, thereby achieving coordination number (c.n.) 6 through coordination by four Te atoms from the anions and two crown ether oxygen atoms from neighboring cation complexes. The second cation (K2) ion is coordinated by a

18-crown-6 and by the Te atoms of one anion (c.n. 9), like the third K^+ ion (K3), which is additionally coordinated by one (disordered) *en* molecule. The three types of cations alternate along the crystallographic *a* axis, thereby forming a coordination polymer together with the anions, the 18-crown-6 and the *en* molecules (Figure 3, top). As shown in Figure 3 (bottom), the parallel strands are arranged into corrugated layers parallel to the *ac* plane and separated by sheets of further $[K(18\text{-crown-6})(en)_2]^+$ complexes (K4) with highly disordered 18-crown-6 ligands (not indicated in Figure 3 for clarity).

Crystal Structure of [K(18-crown-6)](N≡C−Te) (3)

Compound **3** crystallizes in monoclinic space group $P2_1/n$ with four formula units in the unit cell. The linear $(TeCN)^-$ anion (Te–C–N: 179.2(6)°) is situated between two $[K(18\text{-crown-6})]^+$ fragments with a K…N distance of 2.775(6)Å, a K…Te distance of 3.6249(12)Å and angles of 119.48(16)° (K…Te–C) and 176.3(5)° (K…N–C). Bond lengths within the anion are Te–C 2.015(6)Å and N–C 1.167(7)Å, as expected for a single and a triple bond, respectively, with further interactions of the terminal atoms to adjacent cations. The K^+ ion is coordinated by six O atoms from 18-crown-6 molecules, and additionally by Te and N atoms of the anion. The structure thereby forms a coordination polymer along the [101] direction (Figure 4).

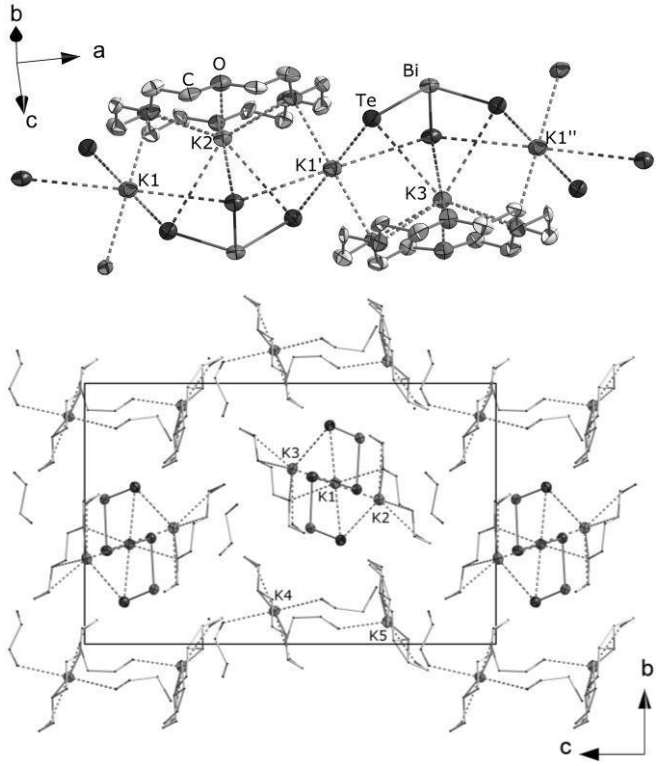

Figure 3. Top: Fragment of the coordination polymer in **2**. Ellipsoids are drawn at 50% probability, hydrogen atoms are omitted for clarity, disorder of *en* is represented by transparent ellipsoids. Bottom: Relative orientation of the strands and further $[K(18\text{-crown-6})(en)_2]^+$ complexes, viewed along [$\bar{1}$00]. Ellipsoids are drawn at 50% probability, C, N, O are drawn as wires; H atoms and disorder of crown ether molecules are omitted for clarity.

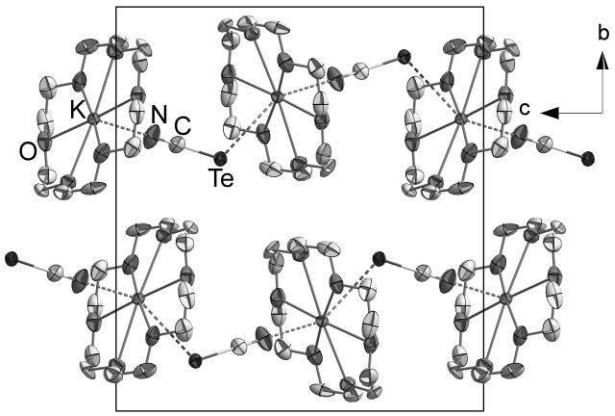

Figure 4. Fragment of the crystal structure of **3**. Ellipsoids are drawn at 50% probability, H atoms are omitted for clarity.

Conclusions

The reduction of crude lead chalcogenide (1:2) phases with elemental alkali metals in *en* is a straightforward route towards solutions containing the $[Pb_2Ch_3]^{2-}$ anion with high abundance and purity. The corresponding treatment of "Bi_2Te_3·Te" produces the first telluridobismutate anion to be obtained from solution. According reactions with "Tl_2Te·Tl" cause C–C-bond cleavage and transfer of protons within solvent *en* molecules under formation of a $[K(18\text{-crown-6})]^+$ salt of the telluridocyanate anion in high yields.

Experimental Section

General: All synthesis steps were performed with strong exclusion of air, moisture (Ar atmosphere at a high-vacuum, double-manifold Schlenk line or in a glove box) and light. Solvents were dried and freshly distilled prior to use. The elements were purchased from Sigma Aldrich (>99%) and used as received. Phases with the nominal composition "PbCh·Ch" or "Bi_2Te_3·Te" were prepared by fusion of the elements in the corresponding ratios in a quartz ampoule under Ar using a Bunsen burner. "Tl_2Te·Te" was prepared by first fusing the elements in a 2:1 ratio, and subsequently adding 1 eqivalent of Te under careful pestling at room temperature to avoid formation of the mixed-valence phase TlTe.

Solutions of the title compounds were generated by suspending 0.5 g of binary compounds that were prepared as mentioned above in 25 mL of *en* (in the case of reduction with K, 2.2 eq of 18-crown-6 with respect to the metal within the phases has been added to the suspension). 2.1 eq of elemental alkali metal was added and the reaction solution was vigorously stirred for at least 12 h. The remaining solid residues were filtered off and the solution volume was reduced to a final volume of 15 mL.

Crystallization of [K(18-crown-6)]$_2$[Pb$_2$Ch$_3$]·en (1)

10 mL of a solution of **1** was carefully layered with 10 mL of toluene and left to stand for 4 weeks. The resulting precipitate was filtered off and the solution was slowly evaporated. **1** crystallizes as yellow-orange plates.

Crystallization of [K$_2$(18-crown-6)$_2$(en)K(en)$_2$][BiTe$_3$] (2)

10 mL of a solution of **2** was carefully layered with 10 mL of toluene. **2** crystallizes within 3 weeks as black blocks.

Synthesis of [K(18-crown-6)](NCTe) (3)

10 mL of a solution of **3** was carefully layered with 10 mL of toluene and left to stand for 4 weeks. The resulting precipitate was filtered off and the solution volume was reduced to 5 mL. **3** crystallizes within one week as colorless sticks in approximately 60% yield with respect to Te.

Single-crystal X-ray diffraction: All measurements have been performed on a Stoe IPDS2 or IPDS2T diffractometer at 100 K (**1**, **2,** $Cs_4(C_6N_4H_6)_2{\cdot}3en$) or at a Stoe IPDS-I diffractometer at 193 K (**3**), using MoK_α radiation and a graphite monochromator (λ = 0.71073 Å). Upon numerical absorption correction, structure solution was performed by direct methods, followed by full-matrix-least-squares refinement against F^2, using SHELXS-97, SHELXL-97 and OLEX2 software.[28] Table 1 summarizes the data of the X-ray diffraction experiments. CCDC 1027982-1027985.

Nuclear magnetic resonance spectroscopy: All NMR-spectra were recorded in *en* on a Bruker DRX 400, with a C_6D_6 capillary for locking. For ^{125}Te experiments with species other than [2.2.2]-crypt salts, short acquisition times (0.2 s) reduced the duration of the experiments and helped avoiding excessive line broadening. Standard experiments applied 15k pulses with short delays (D1 = 1s). ^{77}Se experiments applied standard parameter sets with typically >10k.

Quantum chemical methods: DFT calculations were done with the program system TURBOMOLE[25a] using the RIDFT program[25b,25c] and employing the Becke–Perdew 86 (BP86) functional[25d,25e,25f] with def2-TZVP bases[25g] and respective fitting bases[25h] for the evaluation of the Coulomb matrix. Effective core potentials (ECPs) were used for Tl and Te atoms (ECP-60 and ECP-28, respectively).[25i] Counter ions were modeled by application of COSMO with default parameters.[25j,25k]

Acknowledgements

This work was supported by the Deutsche Forschungsgemeinschaft (DFG) within the framework of SPP1415, and by the Friedrich-Ebert-Stiftung. We thank Marcus Müller, Michael Müller, Steffen Emge and Niels Lichtenberger for their contribution to preliminary work on the subject.

[1] M. Joannis, *C.R. Hebd. Seances Acad. Sci.* **1891**, *113*, 795–798.

[2] J. Campbell, D. A. Dixon, H. P. A. Mercier, G. J. Schrobilgen, *Inorg. Chem.* **1995**, *34*, 5798-5809.

[3] S. Scharfe, F. Kraus, S. Stegmaier, A. Schier, T. F. Fässler, *Angew. Chem.* **2011**, *123*, 3712-3754; *Angew. Chem. Int. Ed.* **2011**, *50*, 3630–3670.

[4] H. Borrmann, J. Campbell, D. A. Dixon, H. P. A. Mercier, A. M. Pirani, G. J. Schrobilgen, *Inorg. Chem.* **1998**, *37*, 1929-1943.

[5] R. C. Burns, J. D. Corbett, *J. Am. Chem. Soc.* **1981**, *103*, 2627-2632.

[6] J. Campbell, H. P. A. Mercier, D. P. Santry, R. J. Suontamo, H. Borrmann, G. J. Schrobilgen, *Inorg. Chem.* **2001**, *40*, 233-254.

[7] A. M. Pirani, H. P. A. Mercier, R. J. Suontamo, G. J. Schrobilgen, D. P. Santry, H. Borrmann, *Inorg. Chem.* **2005**, *44*, 8770-8785.

[8] S. S. Dhingra, M. G. Kanatzidis, *Inorg. Chem.* **1993**, *32*, 1350-1362.

[9] S. Dhingra, F. Liu, M. G. Kanatzidis, *Inorg. Chim. Acta*, **1993**, *210*, 237-239

[10] H. Borrmann, J. Campbell, D. A. Dixon, H. P. A. Mercier, A. M. Pirani, G. J. Schrobilgen, *Inorg. Chem.* **1998**, *37*, 6656-6674.

[11] M. Bjorgvinsson, J. F. Sawyer, G. J. Schrobilgen, *Inorg. Chem.* **1987**, *26*, 741-749.

[12] M. Björgvinsson, J. F. Sawyer, G. J. Schrobilgen, *Inorg. Chem.* **1991**, *30*, 2231-2233. [2.2.2]crypt = 4,7,13,16,21,24-hexaoxa-1,10-diazabicyclo[8.8.8]-hexacosane.

[13] C.-W. Park, R. J. Salm, J. A. Ibers, *Can. J. Chem.* **1995**, *73*, 1148-1156.

[14] C. D. W. Jones, F. J. DiSalvo, R. C. Haushalter, *Inorg. Chem.* **1998**, *37*, 821-823.

[15] R. M. H. Banda, J. Cusick, M. L. Scudder, D. C. Craig, I. G. Dance, *Polyhedron* **1989**, *8*, 1995-1998.

[16] G. Thiele, T. Krüger, S. Dehnen, *Angew. Chem.* **2011**, *126*, 4787-4791; *Angew. Chem. Int. Ed.* **2014**, *53*, 4704-4708.

[17] a) W. Bronger, A. Donike, D. Schmitz, *Z. Anorg. Allg. Chem.* **1996**, *622*, 1003-1005. b) B. Eisenmann, R. Zagler, *Z. Kristallogr.* **1991**, *197*, 257-258.

[18] A. Müller, M. Zimmermann, H. Bögge, *Angew. Chem.* **1986**, *98*, 258-259; *Angew. Chem. Int. Ed.* **1986**, *25*, 272-273.

[19] G. Thiele, N. Lichtenberger, R. Tonner, S. Dehnen, *Z. Anorg. Allg. Chem.* **2013**, *639*, 2809–2815.

[20] The formation of $[K(18\text{-crown-}6)_2]_2[Pb_2Te_3]{\cdot}en$ was unambiguously identified by single-crystal X-ray diffraction and energy dispersive X-ray spectroscopy, as well as via ^{125}Te and ^{207}Pb NMR spectroscopy of the corresponding solution (see Supporting Information). However, we have so far not been able to obtain datasets that are of suitable quality for publication. Cell parameters (space group $P2_1$) at 193 K: a = 10.6029(7) Å, b = 9.0398(4) Å, c = 21.2587(15)Å, β = 98.594(5)°. 18-crown-6 = 1,4,7,10,13,16-hexaoxacyclooctadecane.

[21] A. Cisar, J. D. Corbett, *Inorg. Chem.* **1977**, *16*, 632–635.

[22] G. A. Bowmaker, Effendy, P. C. Junk, B. W. Skelton, A. H. White, *Z. Naturforsch. B* **2004**, *59*, 1277-1292.

[23] E. Cruceanu, S. S. Sladaru, *J. Mater. Sci*. **1969**, *4*, 410-415.

[24] R. Cerny, J.-M. Joubert, Y. Filinchuk, Y. Feutelais, *Acta Crystallogr.* **2002**, *C58*, i63-i65.

[25] a) TURBOMOLE Version 6.4, (c) TURBOMOLE GmbH 2012. TURBOMOLE is a development of University of Karlsruhe and Forschungszentrum Karlsruhe 1989-2007, TURBOMOLE GmbH since 2007; RIDFT: b) K. Eichkorn, O. Treutler, H. Öhm, M. Häser, R. Ahlrichs, *Chem. Phys. Lett.* **1995**, *242*, 652–6600; c) K. Eichkorn, F. Weigend, O. Treutler, R. Ahlrichs, *Theor. Chim. Acta* **1997**, *97*, 119–124; BP-86 functional: d) A. D. Becke, *Phys. Rev. A* **1988**, *38*, 3098-3109; e) S. H. Vosko, L. Wilk, M. Nusair, *Can. J. Phys.* **1980**, *58*, 1200-1205; f) J. P. Perdew, *Phys. Rev. B* **1986**, *33*, 8822–8837; def2-TZVP basis sets: g) F. Weigend, R. Ahlrichs, *Phys. Chem. Chem. Phys.* **2005**, *7*, 3297-3305; auxiliary basis sets: h) F. Weigend, *Phys. Chem. Chem. Phys.* **2006**, *8*, 1057–1065; ECPs: i) B. Metz, H. Stoll, M. Dolg, *J. Chem. Phys*. **2000**, *113*, 2563-2569; COSMO: j) A. Klamt, G. Schürmann, *J. Chem. Soc. Perkin Trans.* **1993**, *5*, 799–805; k) A. Schäfer, A. Klamt, D. Sattel, J. C. W. Lohrenz, F. Eckert, *Phys. Chem. Chem. Phys.* **2000**, *2*, 2187–2193.

[26] C. H. W. Jones, R. D. Sharma, *Organometallics* **1987**, *6*, 1419-1423.

[27] S. Parsons, H. D. Flack, T. Wagner, *Acta Crystallogr. B* **2013**, *69*, 249-259.

[28] a) G. W. Sheldrick, *SHELXTL 5.1*, Bruker AXS Inc. 6300 Enterprise Lane, Madison, WI 53719-1173, USA, **1997**; b) Absorptionskorrektur mit *XPREP V5.1/NT* **1997** Bruker Analytical X-ray Systems c) O. V. Dolomanov, L. J. Bourhis, R. J. Gildea, J. A. K. Howard, H. Puschmann, *J. Appl. Crystallogr.* **2009**, *42*, 339 – 341.

Received: ((will be filled in by the editorial staff))
Published online: ((will be filled in by the editorial staff))

Entry for the Table of Contents

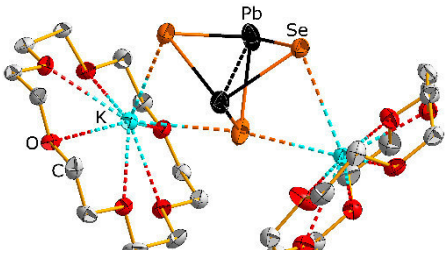

Günther Thiele, Lisa Vondung, and Stefanie Dehnen* **…….. Page No. – Page No.**

About the Syntheses of Chalcogenidometalates by *in situ* Reduction with Elemental Alkali Metals

SUPPORTING INFORMATION

Syntheses of Chalcogenidometalates by *in situ* Reduction with Elemental Alkali Metals

Günther Thiele, Lisa Vondung, and Stefanie Dehnen*

Philipps-Universität Marburg, Fachbereich Chemie and
Wissenschaftliches Zentrum für Materialwissenschaften (WZMW),
Hans-Meerwein-Straße 1, 35043 Marburg.
Fax: +49 (0)6421 282 5653; E-mail: dehnen@chemie.uni-marburg.de

Content:

1. Crystallographic details for $Cs_2(C_6N_4H_6)\cdot 1.5en$

Upon careful addition of elemental Cs to *en* the solution is stirred for half an hour after which the excess *en* is evaporated, yielding $Cs_2(C_6N_4H_6)\cdot 1.5en$ as colorless crystals.

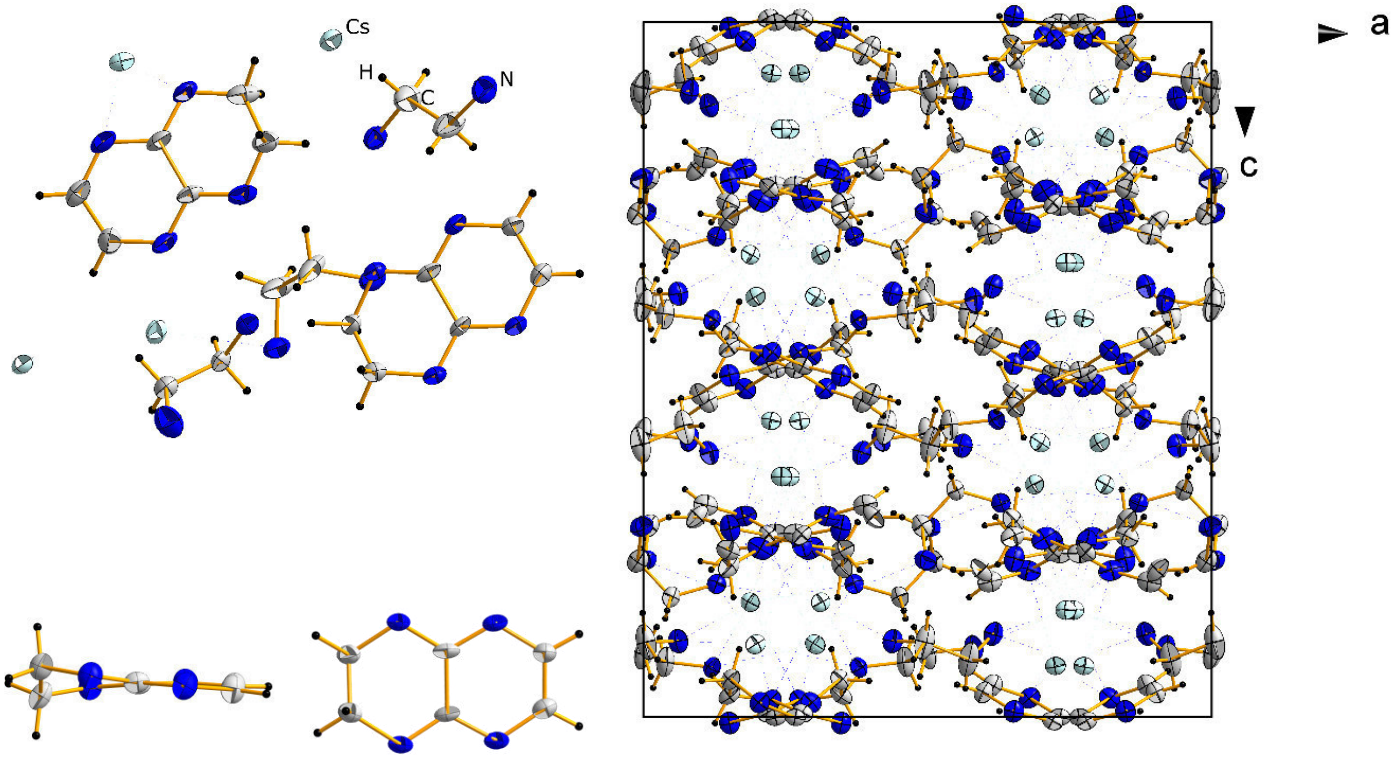

Figure S1. Representation of the asymmetric unit in $Cs_2(C_6N_4H_6)\cdot 1.5en$ (left, top), of the unit cell (right) and the dianionic heterocycle in side and top view (left, bottom). Ellipsoids are drawn at 50% probability.

Table S1. Details of Diffraction experiment and refinement of $Cs_2(C_6N_4H_6)\cdot 1.5en$.

Empirical formula	$C_{18}H_{24}N_{14}Cs_4$
Formula weight	968.15
Temperature/K	100(2)
Crystal system	orthorhombic
Space group	*Pbca*
a/Å	17.5992(10)
b/Å	15.3684(9)
c/Å	21.5057(13)
α/°	90
β/°	90
γ/°	90
Volume/Å^3	5816.7(6)
Z	8
ρ_{calc}mg/mm^3	2.211
m/mm^{-1}	5.009
F(000)	3600.0
Crystal size/mm^3	0.35 × 0.26 × 0.20
Radiation	MoK$_\alpha$ (λ = 0.71073)
2Θ range for data collection	3.996 to 53.488°
Index ranges	$-22 \le h \le 18$, $-16 \le k \le 19$, $-27 \le l \le 23$
Reflections collected	19807
Independent reflections	6137 [R_{int} = 0.0527, R_{sigma} = 0.0491]
Data/restraints/parameters	6137/0/325
Goodness-of-fit on F^2	0.963
Final R indexes [I>=2σ (I)]	R_1 = 0.0371, wR_2 = 0.0877
Final R indexes [all data]	R_1 = 0.0533, wR_2 = 0.0925
Largest diff. peak/hole / e Å^{-3}	1.10/-1.75

2. NMR spectra of the reaction solutions

General approach

a) *Extraction with K:* 2 eq of K and 1eq of Pb were fused in a quartz ampoule with an oxygen/methane burner and 2 eq of Se or Te were added to the melt. The resulting regulus was pestled and extracted for at least 24h with *en* in the presence of at least 2.1 eq of either 18-crown-6 or [2.2.2]crypt.

b) *Extraction with Li:* 1 eq of Pb and 2 eq of Se or Te were fused as in a), followed by pestling, addition of 2.1 eq Li in liquid ammonia and subsequent annealing of the resulting powder for 15min with an oxygen/methane burner. The resulting regulus was pestle and extracted for at least 12 hours with *en*.

c) *In situ reduction:* "MCh_2" (M = Pb; Ch = Se, Te) was prepared as in b), subsequent addition of 2.1 eq of elemental alkali metal in *en* (and in case of K additional 2.2 eq of 18-crown-6 or [2.2.2]crypt) and filtration yielded the solution for NMR characterization upon reduction of the solution volume upon evaporation of the solvent.

All NMR-spectra were recorded in *en* on a Bruker DRX 400, with a C_6D_6 capillary for locking. The quoted chemical shifts were taken from ref. [1] (chalcogenides and polychalcogenides) and ref. [2] (metalates). $\delta(Te^{2-})$ = –1430ppm; $\delta(Te_2^{2-})$ = –1080ppm; $\delta([Pb_2Te_3]^{2-})$ = –927ppm. For the in situ reduction of „$PbSe_2$" with Li in *en* no spectrum of sufficient quality could be obtained due to low solubilty of the $[Pb_2Se_3]^{2-}$ anion (as compared to the $[Pb_2Te_3]^{2-}$) and extremely broad line width.

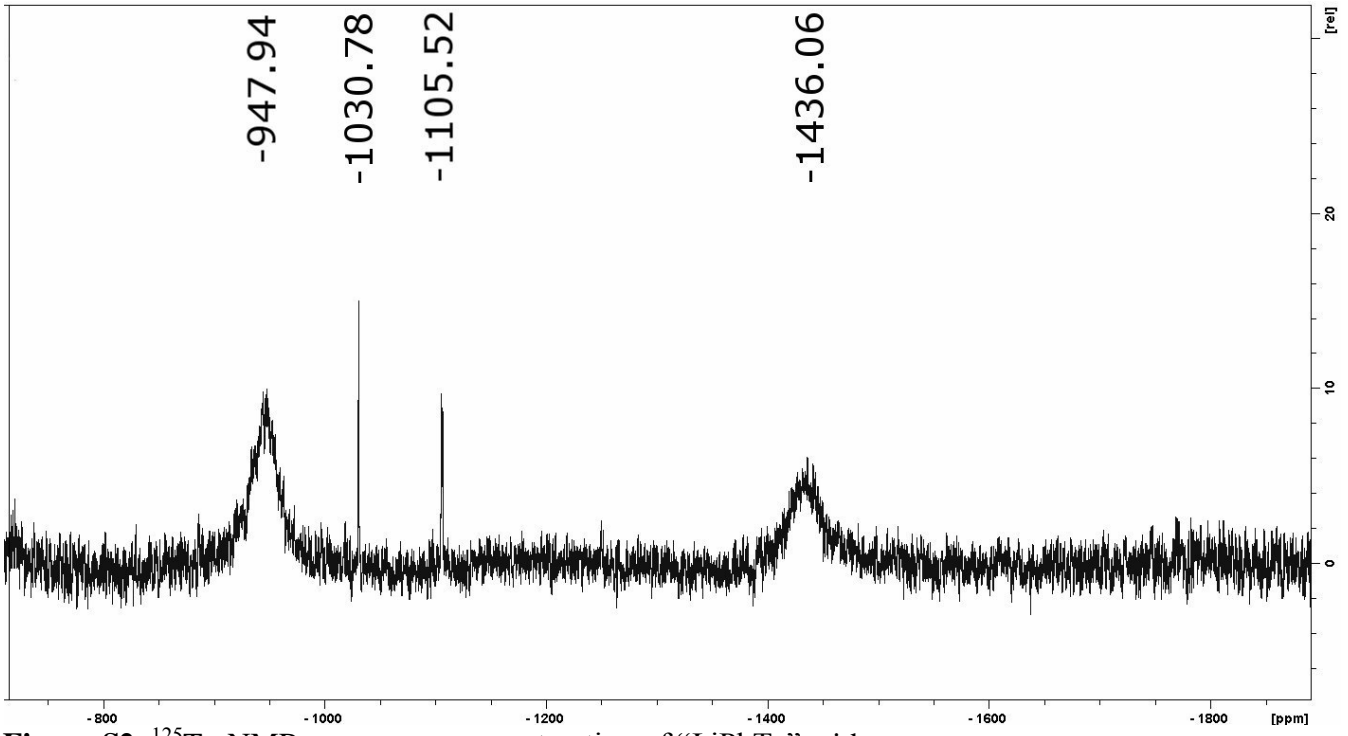

Figure S2. ^{125}Te-NMR spectrum upon extraction of "LiPbTe" with *en*.

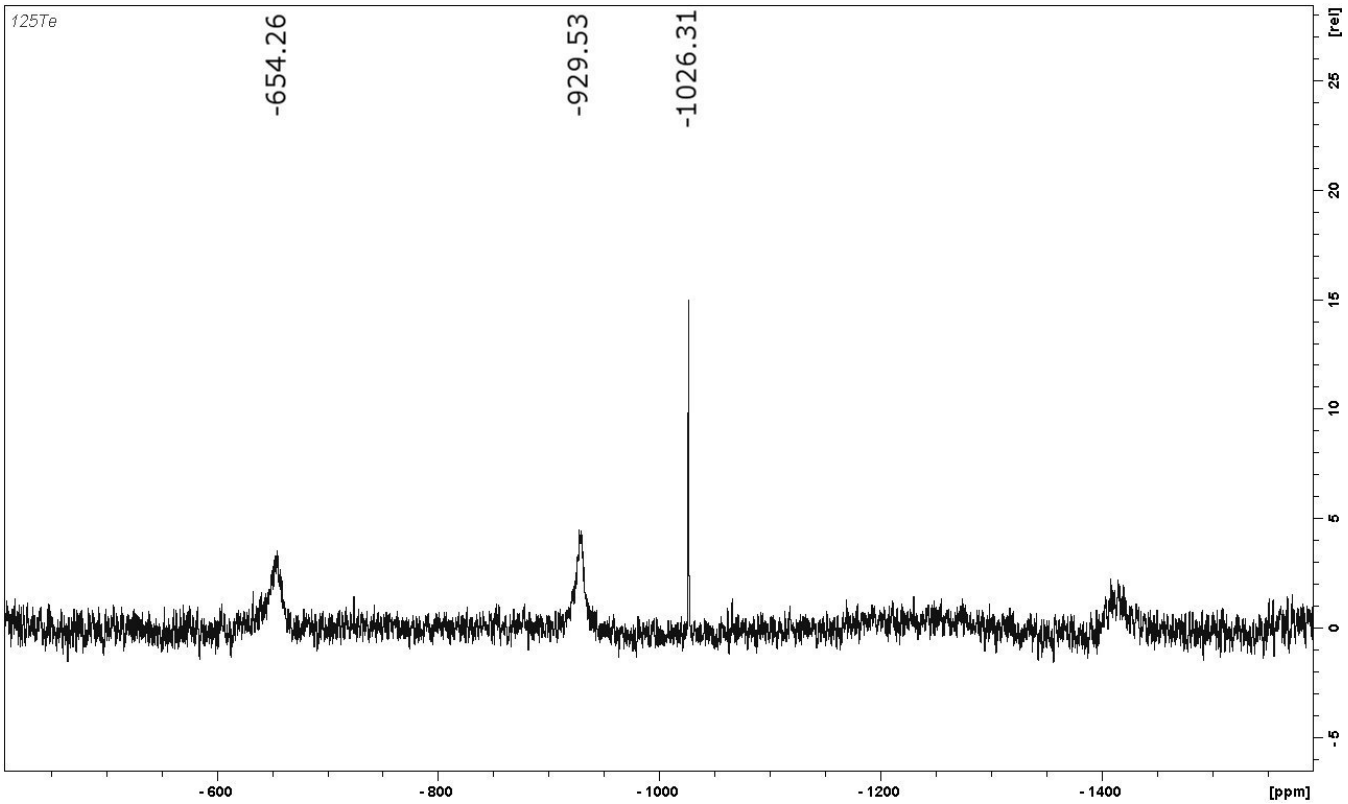

Figure S3. ^{125}Te-NMR spectrum upon extraction of "KPbTe" with *en* in the presence of 18-crown-6.

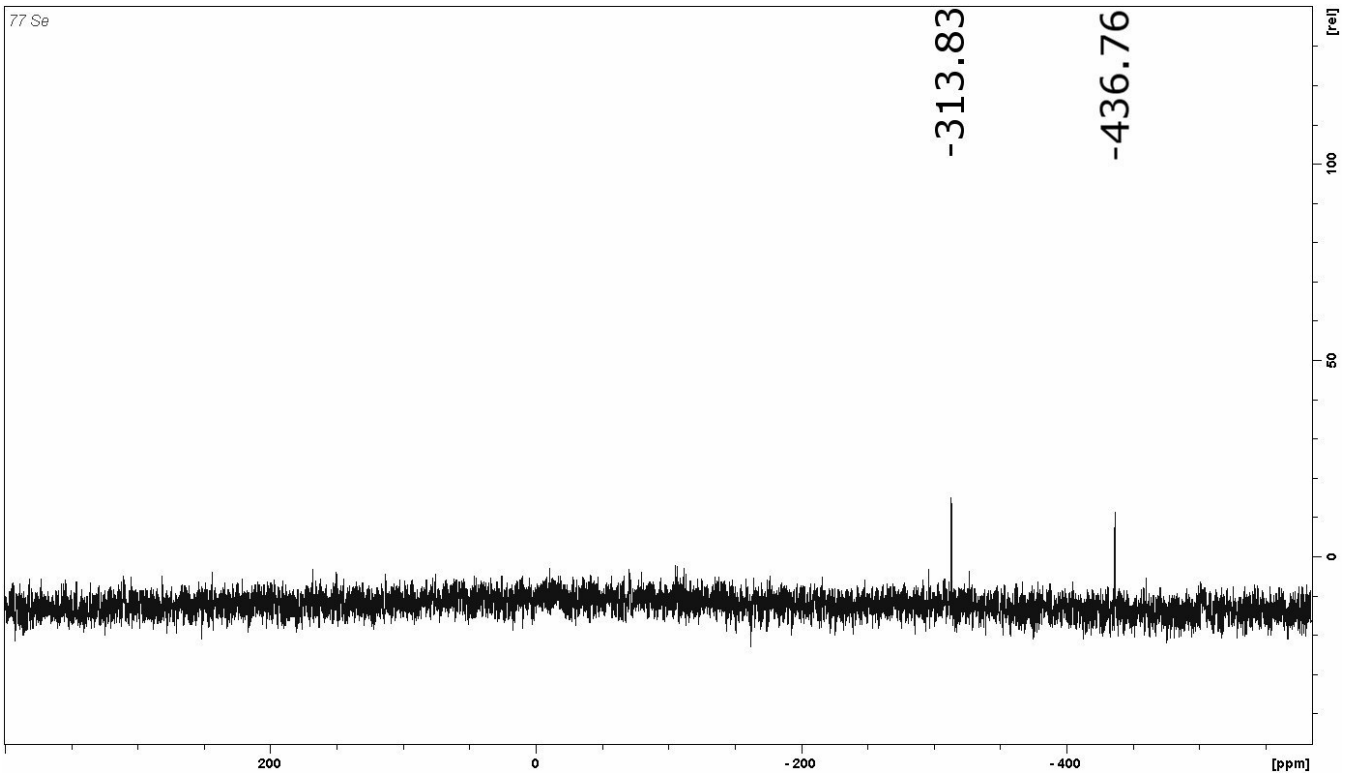

Figure S4. ^{77}Se-NMR spectrum upon extraction of "KPbSe" with *en* in the presence of 18-crown-6.

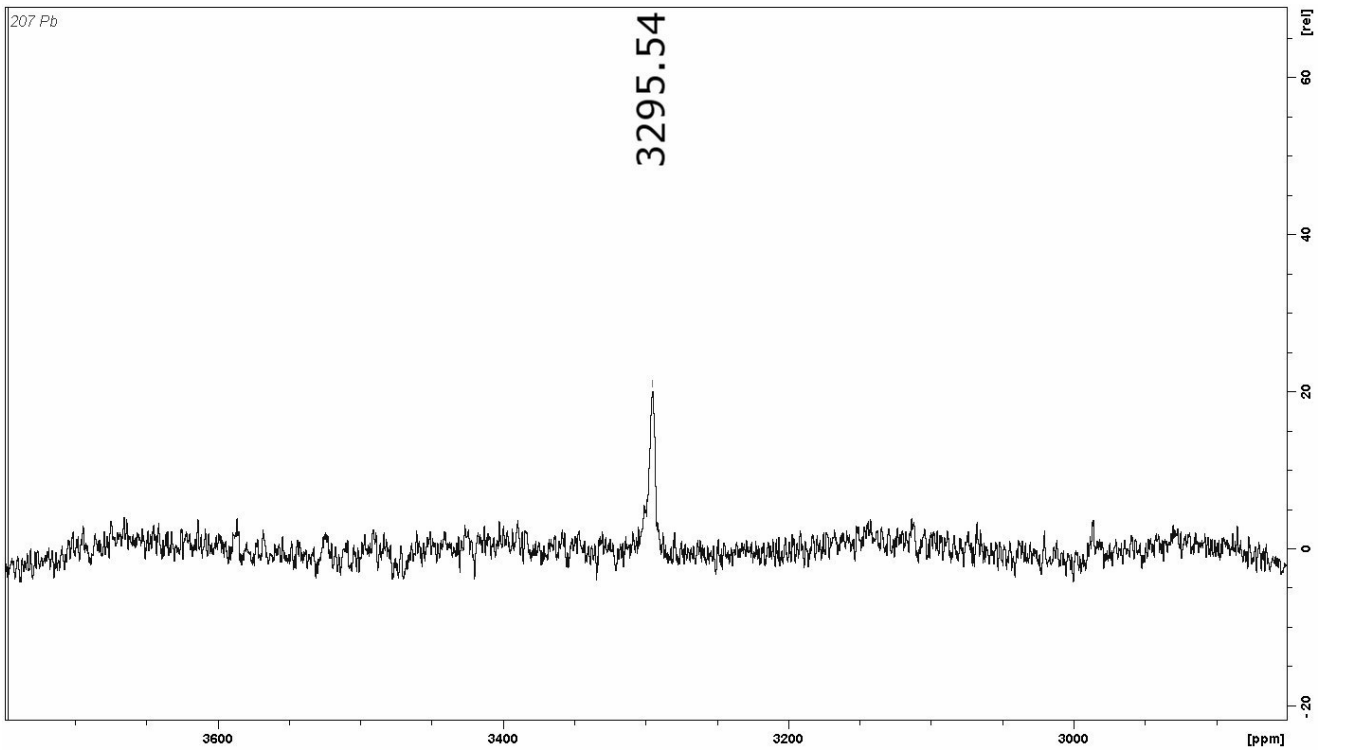

Figure S5. ^{207}Pb-NMR spectrum upon reduction of "PbTe·Te" with K in *en* in the presence of 18-crown-6.

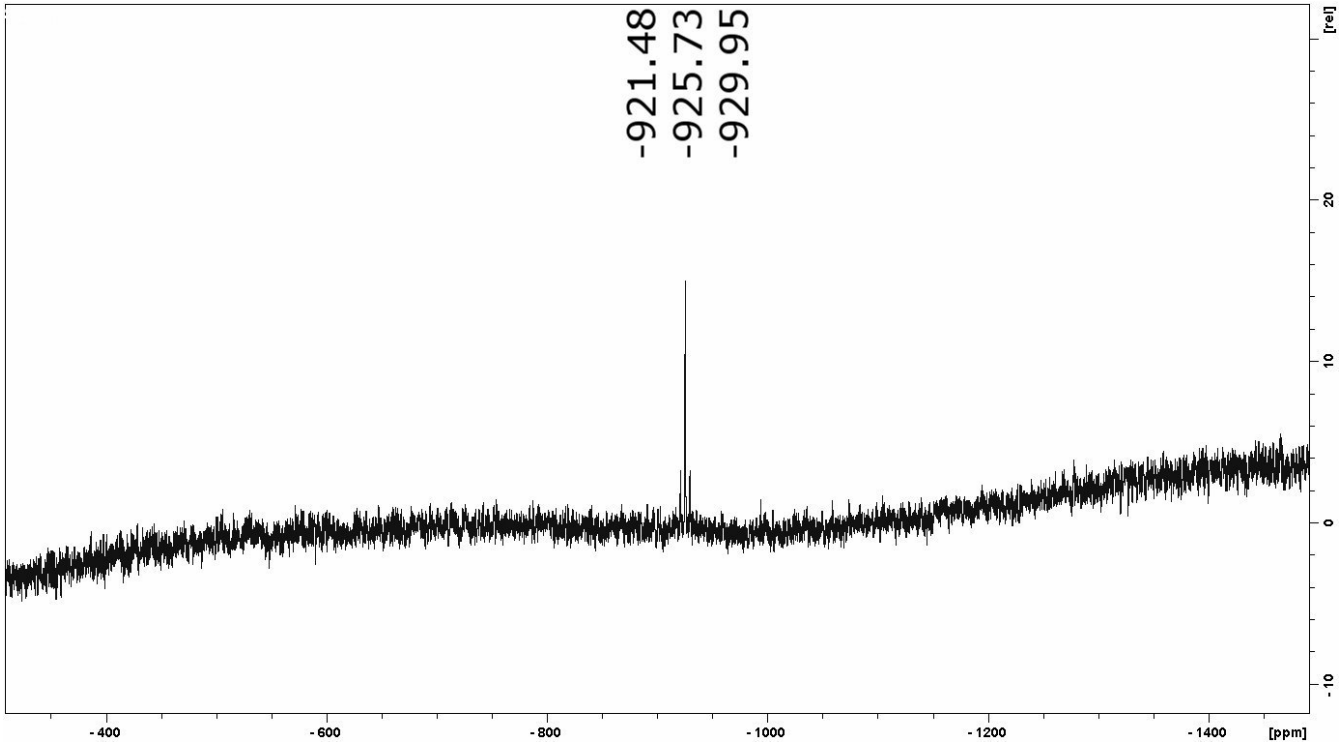

Figure S6. ^{125}Te-NMR spectrum upon reduction of "PbTe·Te" with K in *en* in the presence of 18-crown-6.

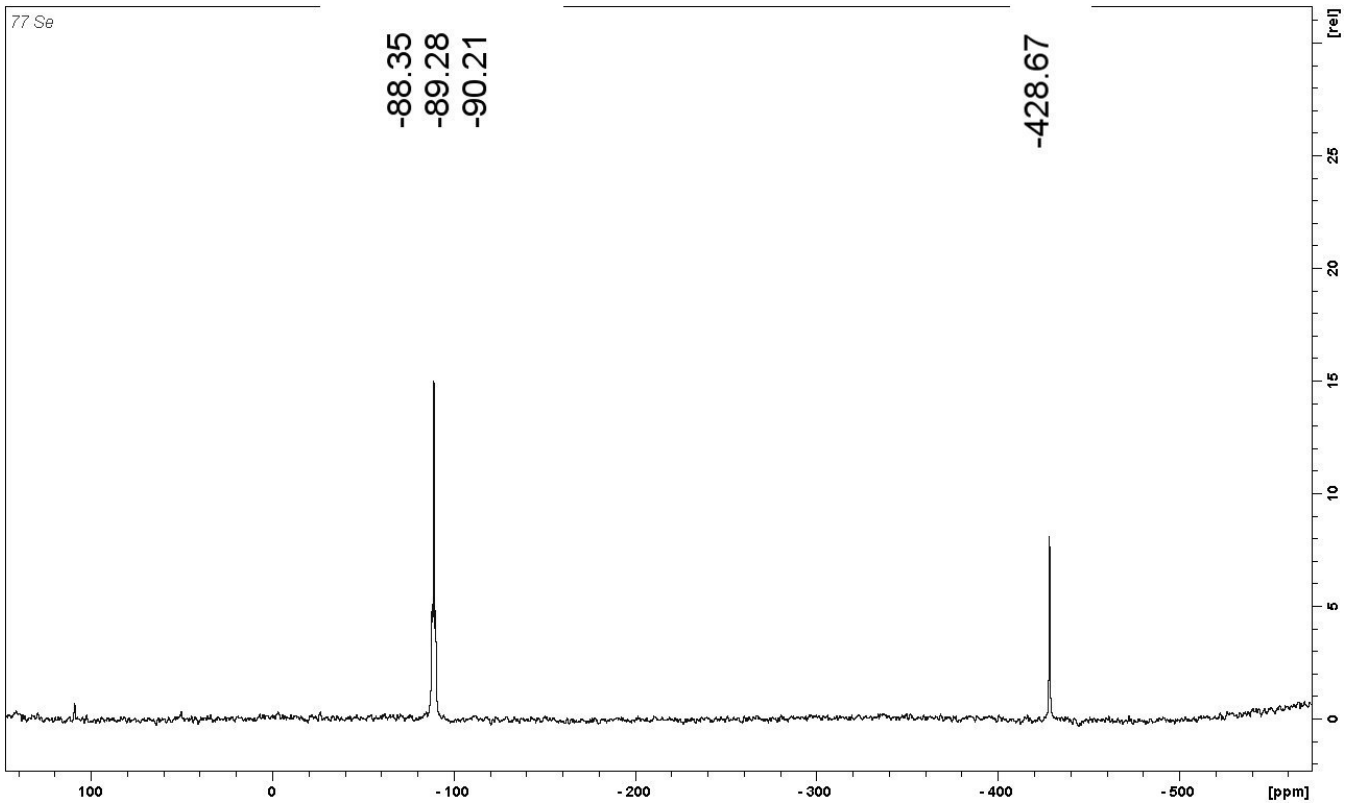

Figure S7. ^{77}Se-NMR spectrum upon reduction of "PbSe·Se" with K in *en* in the presence of 18-crown-6.

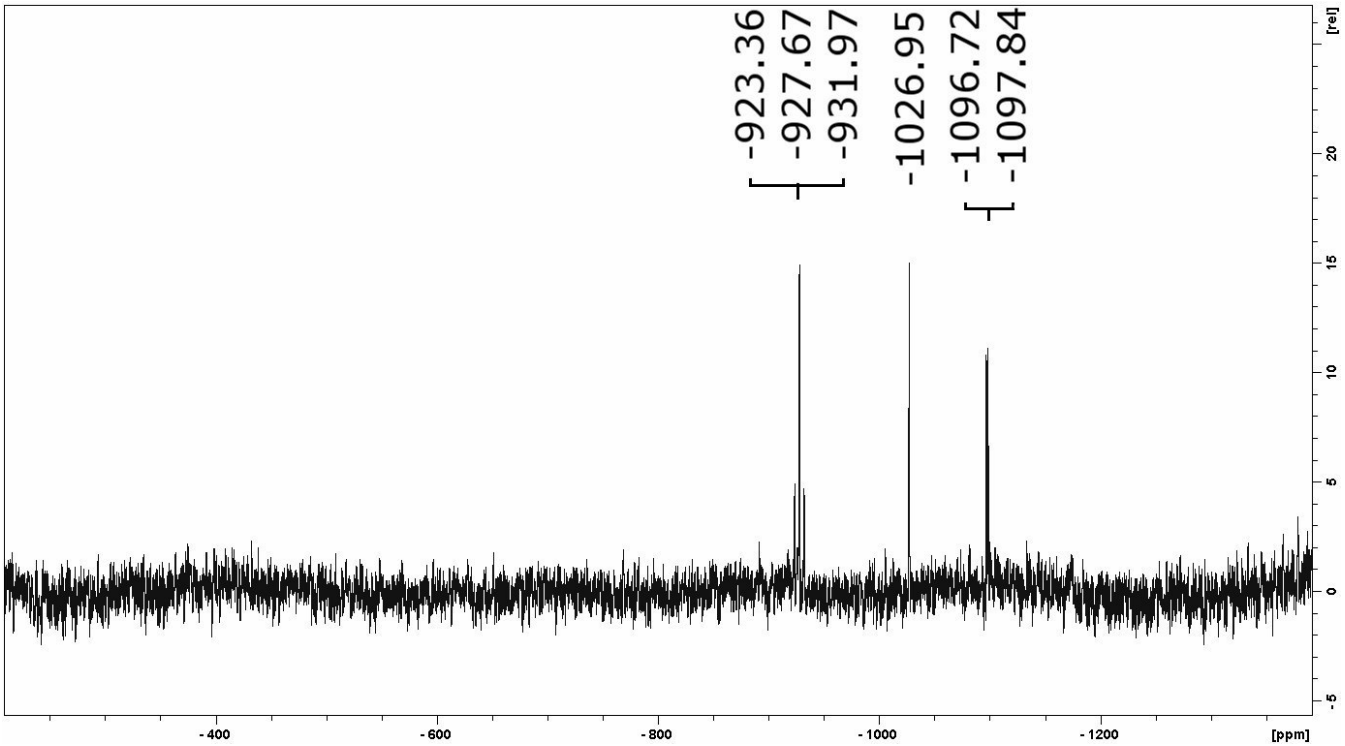

Figure S8. ^{125}Te-NMR spectrum upon extraction of "KPbTe" in *en* in the presence of *[2.2.2]crypt*.

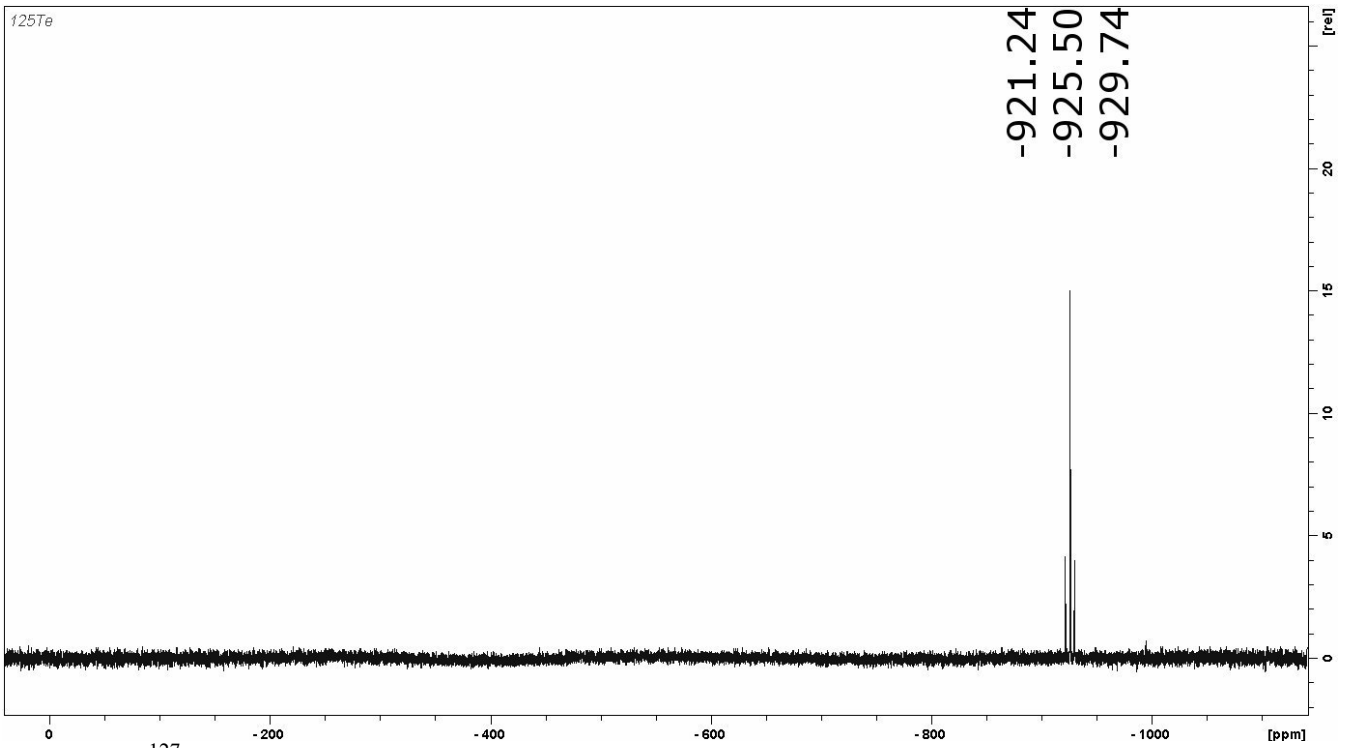

Figure S9. ^{127}Te-NMR spectrum upon reduction of "PbTe·Te" with K in *en* in the presence of [2.2.2]crypt.

2. Quantum chemical calculations on the series $[Tl_2Ch_3]^{4-}$, with Ch = O through Po

DFT calculations were done with the program system TURBOMOLE[3] using the RIDFT program[4] and employing the Becke–Perdew 86 (BP86) functional[5] with def2-TZVP bases[6] and respective fitting

bases[7] for the evaluation of the Coulomb matrix. Effective core potentials (ECPs) were used for Te and Tl, Pb, Bi atoms (ECP-28, and ECP-60, respectively).[8] Counter ions were modelled by application of COSMO with default parameters.[9]

All structures were minima on the potential energy surface as determined from calculating vibrational spectra of the optimized geometries.

Table S2. Structural parameters of the calculated $[Tl_2Ch_3]^{4-}$ anions in c_1 symmetry.

Ch	**d(Tl–Tl) /Å**	**d(Tl–Ch) /Å**	**<(Tl–Ch–Tl) /°**	**<(Ch–Tl–Ch) /°**
O	3.016	2.320-2.321	81.05	82.30-82.39
S	3.310	2.828-2.859	70.98-71.27	89.09-90.14
Se	3.390	2.989-3.004	68.84-69.13	90.32–92.13
Te	3.536	3.211-3.218	66.65-66.78	92.27-92.92
Po	3.558	3.284-3.288	65.52–65.59	93.14-93.67

References for the Supporting Information

[1] M. Björgvinsson, J. F. Sawyer, G. J. Schrobilgen, *Inorg. Chem.* **1991**, *30*, 2231.

[2] M. Björgvinsson, H. P. A. Mercier, K. M. Mitchell, G. J. Schrobilgen, G. Strohe, *Inorg. Chem.* **1993**, *32*, 6046.

[3] TURBOMOLE Version 6.4, (c) TURBOMOLE GmbH 2012. TURBOMOLE is a development of University of Karlsruhe and Forschungszentrum Karlsruhe 1989-2007, TURBOMOLE GmbH since 2007.

[4] a) K. Eichkorn, O. Treutler, H. Öhm, M. Häser, R. Ahlrichs, *Chem. Phys. Lett.* **1995**, *242*, 652–660; b) K. Eichkorn, F. Weigend, O. Treutler, R. Ahlrichs, *Theor. Chim. Acta* **1997**, *97*, 119–124.

[5] a) A. D. Becke, *Phys. Rev. A* **1988**, *38*, 3098-3109; b) S. H. Vosko, L. Wilk, M. Nusair, *Can. J. Phys.* **1980**, *58*, 1200-1205; c) J. P. Perdew, *Phys. Rev. B* **1986**, *33*, 8822–8837.

[6] F. Weigend, R. Ahlrichs, *Phys. Chem. Chem. Phys.* **2005**, *7*, 3297-3305.

[7] F. Weigend, *Phys. Chem. Chem. Phys.* **2006**, *8*, 1057–1065.

[8] B. Metz, H. Stoll, M. Dolg, *J. Chem. Phys*. **2000**, *113*, 2563-2569.

[9] a) A. Klamt, G. Schürmann, *J. Chem. Soc. Perkin Trans.* **1993**, *5*, 799–805; b) A. Schäfer, A. Klamt, D. Sattel, J. C. W. Lohrenz, F. Eckert, *Phys. Chem. Chem. Phys.* **2000**, *2*, 2187–2193.

II Syntheses, Structures and Electronic Properties of a New Series of Tellurides of the Type [Sequestrated Cation]$_2$[Te$_x$] (x = 1-4)

Günther Thiele, Niels Lichtenberger, Ralf Tonner, Stefanie Dehnen, *Z. Anorg. Allg. Chem.* **2013**, *639*, 2809-2815. (Titelbild)

The list of "classical" tellurides with organic cations was expanded by the synthesis of single-crystalline salts [Li$_2$(*en*)$_n$](Te$_x$) (*en* = ethylenediamine) with n = 4, x = 1 (**1**), n = 4, x = 2 (**2**), or n = 5, x = 3 (**3**), [K(*18c6*)]$_2$(Te$_x$) (*18c6* = 1,4,7,10,13,16-hexaoxacycloocta-decane) with, x = 2 (**4**), 4 (**5**), [K([2.2.2]crypt)]$_2$(Te$_2$) ([2.2.2]crypt = 4,7,13,16,21,24-hexaoxa-1,10-diazabicyclo[8.8.8]-hexacosane, **6**) and [K(*18c6*)]$_2$[K(*en*)]$_2$(Te$_2$)$_2$ (**7**). Electronic structure calculations on free molecules and periodic approaches are discussed and compared with experimental UV-visible spectra, providing a correlation of the band gaps with the telluride chain length, and a possibility for affecting the gap by according choice of the counterions. Additionally, ^{125}Te NMR chemical shifts of the presented series of *en* solvated lithium tellurides are presented.

Themenkomplex: [M$_x$Ch$_y$]$^{q-}$, Synthese und Reaktivität

Inhalt: Es wird eine Übersicht über die bekannten Telluride gemäß der Klassifizierung nach Ibers gegeben. Kristallographisch charakterisierte Alkali- und Erdalkalitelluride in Form von Solvaten, Kronenether- oder Kryptandkomplexen werden zusammengetragen.

Die unterschiedliche Komplexierungsstärke von Kronenethern, Kryptanden und organischen Aminen wird in Verbindung mit der Breite der NMR-spektroskopischen Signale der Telluridspezies diskutiert. Die NMR-chemische Verschiebung wird anhand der experimentellen Werte im Vergleich mit Gasphasenrechnungen, Rechnungen mit periodischen Randbedingungen und in der Literatur beschriebenen Daten verglichen und erörtert.

Experimentelle UV-Vis-Spektren in Kombination mit molekularen und periodischen quantenchemischen Rechnungen belegen einen starken Einfluss der Kationen auf die optischen Bandlücken.

Die kristallographischen Strukturen und Synthesen von [Li$_2$(*en*)$_4$]Te, [Li$_2$(*en*)$_4$](Te$_2$), [Li$_2$(*en*)$_5$](Te$_3$), [K(18-Krone-6)]$_2$(Te$_2$), [K(18-Krone-6)]$_2$(Te$_4$), [K(18-Krone-6)$_2$]$_2$[K(*en*)]$_2$(Te$_2$)$_2$ und [K([2.2.2]Krypt)]$_2$(Te$_2$) werden beschrieben.

Eigener Anteil: Alle Experimente wurden von mir geplant. Radostan Riedel half bei der kristallographischen Datensammlung. Klaus Harms, Małgorzata Hołyńska und Johanna Heine halfen bei der Analyse der kristallographischen Daten. Eberhard Matern und Klaus Pützer halfen bei der Aufnahme der NMR-Spektren. Alexander von Tesmar führte die quantenchemischen NMR-Rechnungen der molekularen Spezies unter meiner Anleitung im Rahmen eines materialchemischen Praktikums durch. Ralf Tonner führte alle Rechnungen mit

periodischen Randbedingungen durch und schrieb die entsprechenden Teile des Manuskripts. Niels Lichtenberger führte Teile der experimentellen Arbeiten und Analysen der NMR-Daten im Rahmen seiner Bachelorarbeit unter meiner Anleitung durch und entwarf die Strukturdarstellungen für das Manuskript. Thomas Krüger führte Teile der experimentellen Arbeiten unter meiner Anleitung durch. Das Manuskript wurde von Stefanie Dehnen und mir zusammen verfasst.

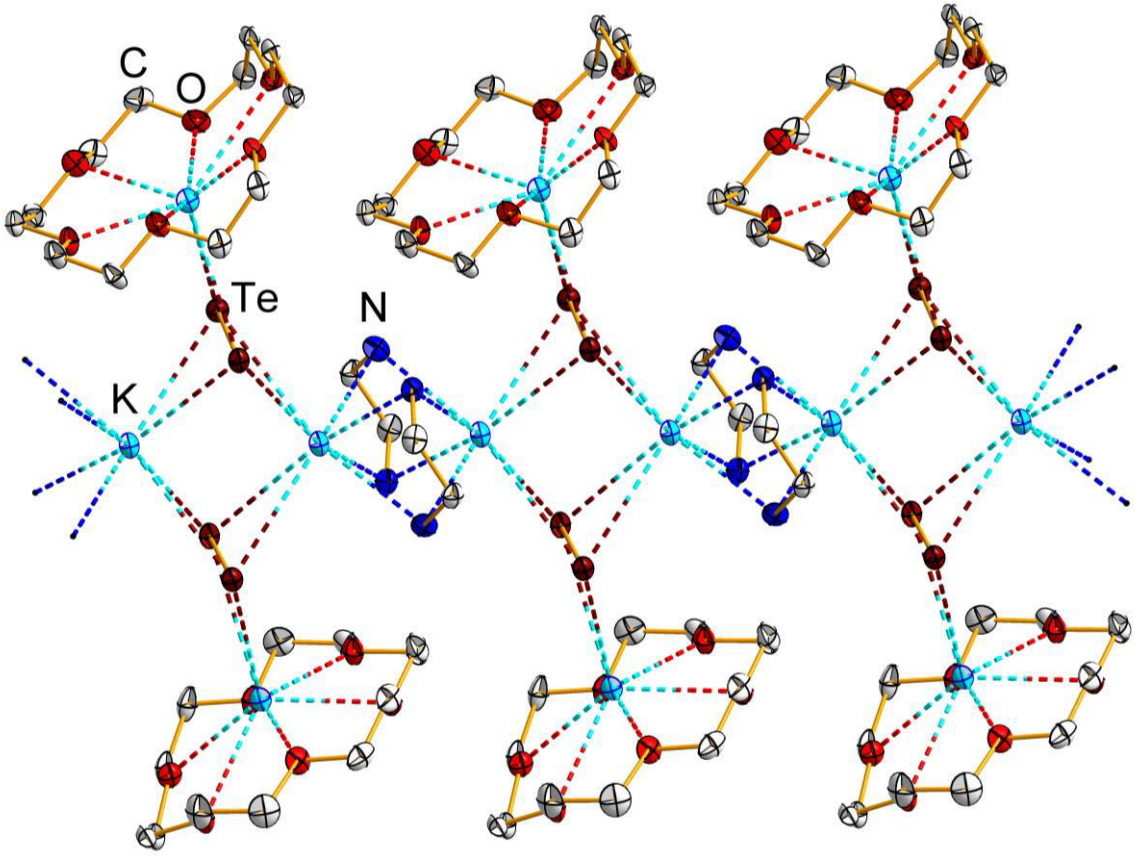

Abbildung 22. Ausschnitt aus der Kristallstruktur von $[K(18\text{-Krone-}6)_2]_2[K(\textit{en})]_2(Te_2)_2$.

DOI: 10.1002/zaac.201300303

Syntheses, Structures, and Electronic Properties of a New Series of Tellurides of the Type [Sequestered Cation]$_2$(Te$_x$) (x = 1–4)

Günther Thiele,[a] Niels Lichtenberger,[a] Ralf Tonner,[a] and Stefanie Dehnen*[a]

Dedicated to Professor Wolfgang Bensch on the Occasion of His 60th Birthday

Keywords: (Poly-)tellurides; Solvation effects; Electronic structure calculation; Plane wave calculation; X-ray diffraction; ^{125}Te NMR spectroscopy

Abstract. The list of "classical" tellurides with organic cations was expanded by the synthesis of single-crystalline salts [Li$_2$(*en*)$_n$](Te$_x$) (*en* = ethylenediamine) with n = 4, x = 1 (**1**), n = 4, x = 2 (**2**), and n = 5, x = 3 (**3**), [K(*18c6*)]$_2$(Te$_x$) (*18c6* = 1,4,7,10,13,16-hexaoxacyclooctadecane) with x = 2 (**4**), 4 (**5**), [K(*18c6*)]$_2$[K(*en*)]$_2$(Te$_2$)$_2$ (**6**), and [K([2.2.2]*crypt*)]$_2$(Te$_2$) (**7**) ([2.2.2]*crypt* = 4,7,13,16,21,24-hexaoxa-1,10-diazabicyclo[8.8.8]-hexacosane). Electronic structure calculations on free molecules and periodic approaches are discussed and compared with experimental UV/Vis spectra, providing a correlation of the bandgaps with the telluride chain length, and a possibility for affecting the gap by according choice of the counterions. Additionally, ^{125}Te NMR chemical shifts of the presented series of *en* solvated lithium tellurides are presented.

Introduction

Since the synthesis of the first single crystalline polytelluride[1] the interest in tellurides and tellurium compounds has been constantly growing – due to interesting structural properties and a variety of different types of Te–Te-interactions.[2] The latter is especially valid for tellurium-rich tellurides – in contrast to classical tellurides, which comprise exclusively well separated chains with an overall charge of –2. In 2000, *Smith* and *Ibers* elaborately reviewed all tellurides known until then and classified those into (a) alkali metal/ alkaline-earth metal cation and (b) organic cation tellurides, respectively.[3] The latter included solvated telluride salts. Since then, a large progress has been made in the area of non-classical tellurides, including one, two and three-dimensional telluride architectures,[2f,4a,4b] rings and cage formations,[4c] heterometallic, macrocyclic and carbene analogeous tellurium compounds[4d,4e,4f,4g] as well as the syntheses of a large variety of telluronium, tellurolate,[4h,4i] and polycationic tellurium salts.[4j,4k,4l,4m] Nevertheless, the total number of so-called "organic cation" tellurides, which contain either alkali metal or alkaline-earth metal cations in solvent, crown ether or cryptand complexes, or ammonium or phosphonium ions, is still small. Apart from some arsonium tellurides,[5a] and ammoniates[5b] it has not been increased since this last review.

* Prof. Dr. S. Dehnen
Fax: +49-6421-2825653
E-Mail: dehnen@chemie.uni-marburg.de
[a] Philipps-Universität Marburg
Fachbereich Chemie and Wissenschaftliches Zentrum für Materialwissenschaften (WZMW)
Hans-Meerwein-Straße 1
35043 Marburg, Germany

Table 1 summarizes the classical "organic cation" tellurides with solvated alkali or alkaline earth metal cations currently known, including our contribution of solvated lithium polytellurides, [Li$_2$(*en*)$_4$](Te$_2$) (**2**) and [Li$_2$(*en*)$_5$](Te$_3$) (**3**), and sequestered potassium polytellurides, [K(*18c6*)]$_2$(Te$_2$) (**4**), [K(*18c6*)]$_2$(Te$_4$) (**5**), [K(*18c6*)$_2$]$_2$[K(*en*)]$_2$(Te$_2$)$_2$ (**6**), and [K([2.2.2]*crypt*)]$_2$(Te$_2$) (**7**), that were obtained beside the lithium monotelluride [Li$_2$(*en*)$_4$]Te (**1**).

Results and Discussion

The title compounds were obtained during our current attempts to extend and optimize the synthesis of salts of the [Pb$_2$Te$_3$]$^{2-}$ anion, which we use as starting material in reactions with transition metal compounds. According to literature procedures,[7a] the syntheses always afford **7** and [K([2.2.2]*crypt*)]$_2$(Te$_3$)[1] as side-products. We intended to achieve a crown ether complexation of potassium ions, as well as synthesis with lithium as reducing agent. For the lithium derivatives, we expected a stronger solvation by ethylenediamine (*en*) and were interested to investigate the effect of an exchange of K$^+$ with Li$^+$ in the planned ^{125}Te NMR experiments to identify products as well as side-products. Thus, **1–7** were isolated as so far unknown side-products during the experiments described above. Additionally, we have performed straightforward: direct syntheses of the lithium compounds **1–3** from the elements in *en* (see Experimental Section). All of the title compounds represent so far missing species in the well-established class of telluride salts. **1–7** were structurally characterized by means of single-crystal X-ray diffraction. The crystallographic data and refinement details are given in Table 2.

Dedicated Issue

Table 1. Summary of structurally determined alkali metal/alkaline-earth metal polytellurides with solvated or sequestered cations.[1,6]

$(Te_x)^{2-}$	$(Te_2)^{2-}$	$(Te_3)^{2-}$	$(Te_4)^{2-}$
A^+ or EA^{2+} in solvate complexes	Na, Li (**2**)	Ba, Li (**3**)	Ca
A^+ or EA^{2+} in crown ether complexes	K (**4**), (**6**)	a)	Sr, Ba, Na, K (**5**)
A^+ or EA^{2+} in cryptand complexes	K (**7**)	K	Na

a) A compound with the nominal composition $[K(18c6)]_2(Te_3)$ was obtained as single-crystals; however, the quality of the data sets were too low so far for publication.

Table 2. Crystallographic data and refinement details of **1**–**7**.

	$[Li_2(en)_4]Te$ (**1**)	$[Li_2(en)_4](Te_2)$ (**2**)	$[Li_2(en)_5](Te_3)$ (**3**)	$[K(18c6)]_2(Te_2)$ (**4**)	$[K(18c6)]_2(Te_4)$ (**5**)	$[K(18c6)_2]_2$-$[K(en)]_2(Te_2)_2$ (**6**)	$[K([2.2.2]crypt]_2(Te_2)$ (**7**)
Empirical formula	$C_8H_{32}Li_2N_8Te$	$C_8H_{32}Li_2N_8Te_2$	$C_9H_{18}Li_2N_9Te_3$	$C_{24}H_{48}K_2O_{12}Te_2$	$C_{24}H_{48}K_2O_{12}Te_4$	$C_{28}H_{56}K_4N_4O_{12}Te_4$	$C_{36}H_{72}K_2N_4O_{12}Te_2$
Formula weight /g·mol^{-1}	381.90	509.50	649.00	862.02	1117.22	1307.57	1086.38
Crystal color and shape	colorless block	black block	black block	blue block	black block	purple stick	purple plate
Crystal size /mm	$0.17\times0.41\times0.14$	$0.36\times0.79\times0.47$	$0.17\times0.37\times0.14$	$0.15\times0.17\times0.22$	$0.10\times0.06\times0.06$	$0.51\times0.11\times0.06$	$0.14\times0.27\times0.06$
Crystal system	monoclinic	monoclinic	monoclinic	monoclinic	monoclinic	monoclinic	trigonal
Space group	$P2_1/c$	$P2_1/n$	$C2/c$	$C2/c$	$P2_1/c$	$P2_1/c$	$R\bar{3}$
a / Å	9.2326(4)	11.1617(15)	32.520(4)	22.7116(9)	20.5835(9)	7.5835(2)	11.8966(4)
b / Å	19.5608(9)	14.6234(16)	9.0526(10)	8.5340(2)	11.1976(4)	17.3171(6)	28.1868(18)
c / Å	9.7818(4)	12.4530(16)	17.1476(19)	19.5794(9)	18.1348(7)	36.4663(11)	
β /°	94.494(4)	94.413(10)	103.599(10)	112.779(3)	113.370(3)	95.930(2)	
V /Å^3	1761.13(13)	2026.6(4)	4906.6(10)	3498.9(2)	3836.9(3)	4763.3(3)	3454.8(3)
Z	4	4	8	4	4	4	3
ρ_{calc} /g·cm^{-3}	1.440	1.670	1.757	1.636	1.934	1.823	1.566
$\mu(Mo_{K\alpha})$ /mm^{-1}	1.688	2.880	3.550	1.957	3.280	2.827	1.506
2Θ range /°	4–55	4–51	5–51	4–54	4–54	2–55	10–53
Abs. corr. T_{min}/T_{max}	0.6136 /0.8015	0.0202/0.0539	0.4811 /0.6382	0.6172 /0.7802	0.8454/0.8940	0.3678/0.8376	0.7042/0.9471
Reflections measured	8548	18627	11517	51182	21054	23230	5470
Independent reflections	3729	3729	4334	3714	8082	10617	1616
R(int)	0.0239	0.0902	0.0811	0.0345	0.0749	0.0719	0.0473
Indep. refl. [$I > 2\sigma(I)$]	2937	2777	4334	3055	4867	6544	1282
Parameters	300	183	248	277	379	469	86
R_1 [$I > 2\sigma(I)$]	0.0166	0.0736	0.0329	0.0288	0.0397	0.0422	0.0409
wR_2 (all data)	0.0379	0.2731	0.1057	0.0850	0.0971	0.1290	0.1035
GooF (all data)	0.854	1.115	0.667	0.670	0.689	0.568	0.909
Max. peak/hole /e$^-$·10^{-6} pm^{-3}	0.559/–0.550	2.130/–0.822	0.572/–0.554	0.651/–1.461	1.716/–0.838	1.759/–2.772	1.207/–0.795
CCDC No.	954799	954800	954801	954802	954803	954805	954804

Inspired by the work of *Seifert-Lorenz* and *Hafner*,[7b] we performed quantum chemical calculations of molecular anionic species $(Te_x)^{2-}$ (x = 1–4) and of solid-state structures. The latter served to evaluate differences in the electronic structure as a function of both the anion chain lengths and the different cations. The results were compared with experimental UV/Vis and ^{125}Te NMR spectra. All reactions were monitored by NMR spectroscopy, and compared with the chemical shifts reported already by *Schrobilgen* and co-worker.[7c]

Crystal Structures of $[Li_2(en)_4]Te$ (1), $[Li_2(en)_4](Te_2)$ (2), and $[Li_2(en)_5](Te_3)$ (3)

Compounds **1**–**3** crystallize in monoclinic space groups. Unlike the heavier congeners, the coordination number (c.n.) of Li^+ ions is restricted to c.n. = 4. The coordination of Li^+ cations by *en* molecules leads to the formation of 2D (**1**, **2**) or 1D (**3**) arrangements.

In **1** (Figure 1), the Li^+ ions are arranged into double-layers parallel to the crystallographic *ac* plane upon bridging by *en* ligands. All *en* molecules bridge between different cations, thus, there is no chelating ligand present. Three of the four coordination sites per Li^+ ion are involved in bridges within one layer, with the fourth *en* ligand acting as bridge to the second layer. The telluride anions are located within the double-layers. The six nearest Te···Li distances (4.60–5.93 Å) form a distorted octahedron. Four of the Te···Li contacts are situated within one layer, a fifth one involves a Li^+ ion of the second layer, and the remaining Te···Li contact involves a Li^+ ion of the next double-layer, which is not connected to the respective double-layer by *en* bridges. The octahedra share corners and edges, thereby forming a complicated 3D network.

Compound **2** (Figure 2) comprises single layers of solvated lithium ions that are folded in zigzag fashion and extend parallel to the *ac* plane. Herein, the Li^+ ions form a folded tetragonal net with bridging *en* molecules along all of the Li···Li edges. Every second tetragonal loop accommodates one of the $(Te_2)^{2-}$ dumbbells [Te–Te 2.774(2) Å], which are orientated perpendicular to the mean planes of the loops. Six closest Li^+ ions form distorted octahedra (4.38–5.46 Å) around the Te–Te

Zeitschrift für anorganische und allgemeine Chemie ZAAC Journal of Inorganic and General Chemistry

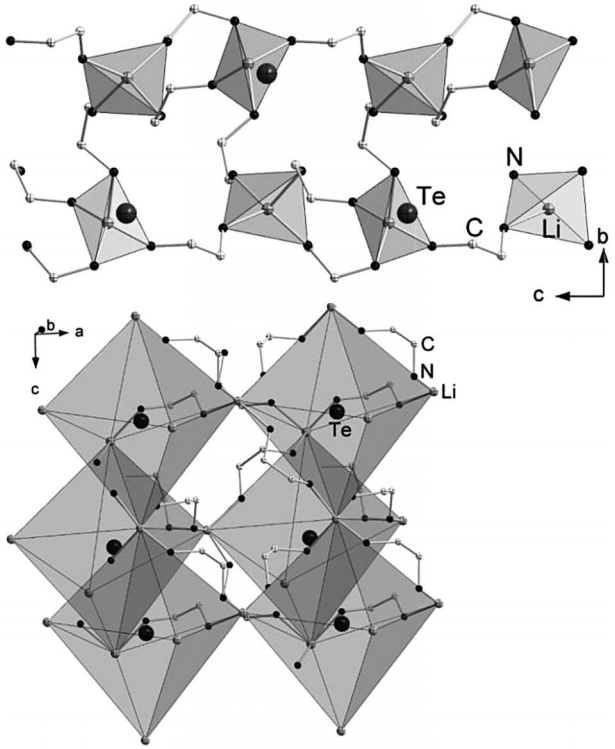

Figure 1. Crystal structure of **1**. Side view of one double-layer of *en*-bridged Li^+ ions (top) and distorted octahedral coordination environment of the Te^{2-} ions (bottom). Hydrogen atoms are omitted for clarity.

dumbbells. Four of the six Li^+ ions belong to the same zigzag net, the remaining two Li^+ ions above and below belong to adjacent Li^+/*en* layers. The octahedra are corner-sharing within one Li^+/*en* layer, and corner-sharing as well as edge-sharing between adjacent layers to form a 3D network.

The 1D arrangement of Li^+ ions and *en* molecules in **3** (Figure 3) instead of a network of higher dimensionality results from a different coordination mode of the *en* ligands with respect to the all-bridging mode observed in **1** or **2**. Here, the Li^+ ions are linked to two (Li2) or three (Li1) adjacent Li^+ ions by *en* ligands, while the remaining coordination sites are occupied by non-bridging *en* molecules: a chelating one (Li2) or a terminal one (Li1). The Li^+ ions within the strands form rectangular, six-membered loops that are connected by joining two opposite Li···Li edges along the long rectangular edges per ring. The $(Te_3)^{2-}$ anions [Te–Te 2.722(1) and 2.719(1) Å; Te–Te–Te 109.41(3)°] are situated between the Li^+/*en* strands within the crystal.

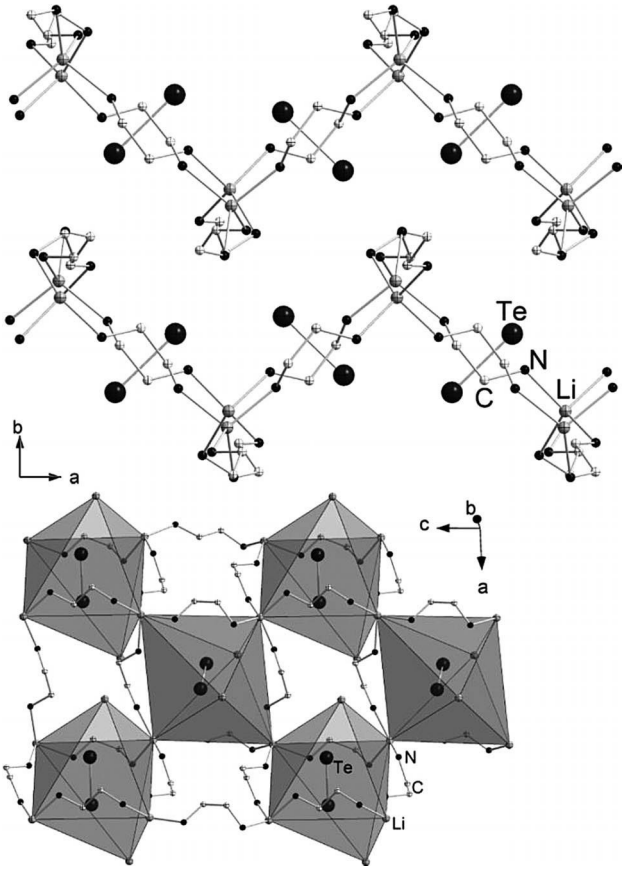

Figure 2. Crystal structure of **2**. Side view of the 2D network (top) and distorted octahedral coordination of the $(Te_2)^{2-}$ dumbbells within one Li^+/*en* layer (bottom). Hydrogen atoms are omitted for clarity.

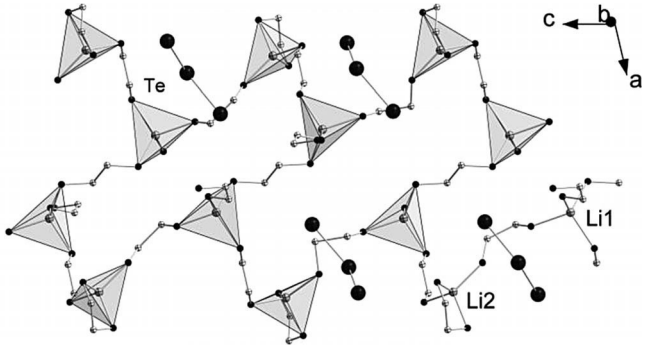

Figure 3. Crystal structure of **3**. Fragment of one Li^+/*en* strand, emphasizing the peculiar coordination modes at Li1 and Li2. Hydrogen atoms and disorder of two e*n* molecules are omitted for clarity.

Crystal Structures of [K(18c6)]$_2$(Te$_2$) (4), [K(18c6)]$_2$(Te$_4$) (5), and [K(18c6)$_2$]$_2$[K(en)]$_2$(Te$_2$)$_2$ (6)

Although all reactions with potassium as reducing agent were carried out in *en*, only compound **6** actually incorporates *en* within the crystal structure. Potassium ions in **4**, **5**, and **6** have c.n. of 8 or higher, including the coordination by *18c6*. Again, all compounds crystallize in monoclinic space groups. Te–Te distances amount to 2.7842(4) Å (**4**) and 2.7807(6), 2.7823(6) Å (**6**) in the ditellurides. The tetratelluride Te–Te bonds in **5** differ in lengths with 2.7121(7), 2.7095(7) (Te1–Te2, Te3–Te4) and 2.7438(6) Å (Te2–Te3). This is similar to the values observed in related structures.[3] Bond angles are 107.46(2) and 108.07(2)°, the torsion angle amounts to 100.52(3)°.

Within **4** (Figure 4) the $(Te_2)^{2-}$ dumbbells bridge two $[K(18c6)]^+$ cations in a bent side-on mode [K–(Te$_2$ bond center)–K angle 114.94°], resulting in c.n. 8 for the K^+ ions; the mean planes spanned by the crown ether oxygen atoms are

Dedicated Issue

tilted toward each other by 101.75°. The barycenters of these complexes form a strongly distorted cubic closed pack lattice with next barycenter-to-barycenter distances of 8.53–12.13 Å.

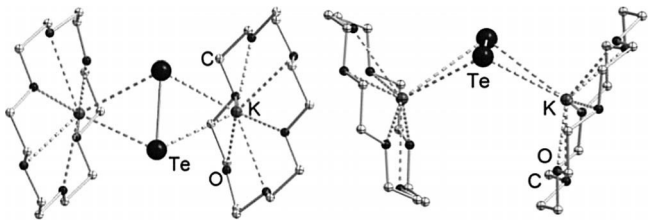

Figure 4. $[K(18c6)]_2(Te_2)$ aggregate in **4** in top view (left) and side view (right). Hydrogen atoms are omitted for clarity.

The structural motif of polytelluride-bridged $[K(18c6)]^+$ cations is also present in **5** (Figure 5). However, the $(Te_4)^{2-}$ units bridge in end-on mode between two cations, and the whole ensemble forms a dimer by self-complementary $[K\cdots O]_2$ aggregation of two cation complexes; accordingly, K^+ ions achieve coordination numbers of c.n. = 7 or 8. The complexes have a total extension of 28.1 Å (outmost C···C) and form stacks in crystallographic *a* and *b* directions.

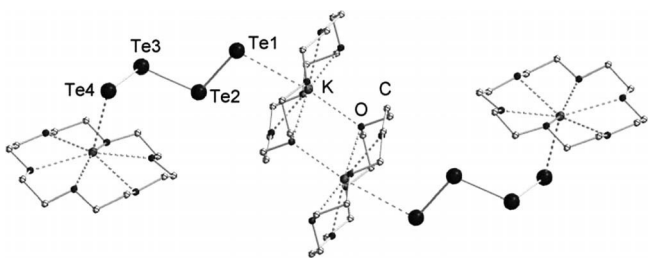

Figure 5. $[K(18c6)]_4(Te_4)_2$ aggregate in **5**. Hydrogen atoms are omitted for clarity.

Two of four independent potassium ions in **6** (K1, K3) have c.n. of 8, resulting from a side-on coordination by the ditelluride anions beside the crown ether coordination. K2 and K4 exhibit another coordination mode, involving two *en* molecules each instead of the crown ether ligands, and two $(Te_2)^{2-}$ anions, each bridging in side-on mode. This way, infinite coordination strands are formed extending parallel to the crystallographic *a* axis (Figure 6). The ditelluride units [Te–Te 2.781(1) Å] are surrounded by three K^+ ions each, and are stacked along the *a* axis.

Crystal Structure of [K([2.2.2]crypt)]$_2$(Te$_2$) (7)

Compound **7** crystallizes in the trigonal space group $R\bar{3}$. The $(Te_2)^{2-}$ dumbbells [Te–Te 2.764(1) Å] are aligned parallel to the crystallographic *c* axis, and their barycenters occupy the positions of a hexagonal close packing topology. Potassium ions are captured by [2.2.2]*crypt* molecules revealing accordingly c.n. = 8, and therefore have only weak interactions with the ditelluride anions. Each $[K([2.2.2]crypt)]^+$ cation complex is surrounded by three $(Te_2)^{2-}$ anions (K···Te distances 6.89, 7.24 Å) with the Te–Te dumbbells orientated "side-on", nearly parallel to the O···O edges of the trigonal prism formed by the six [2.2.2]*crypt* oxygen atoms (Figure 7). A fourth $(Te_2)^{2-}$

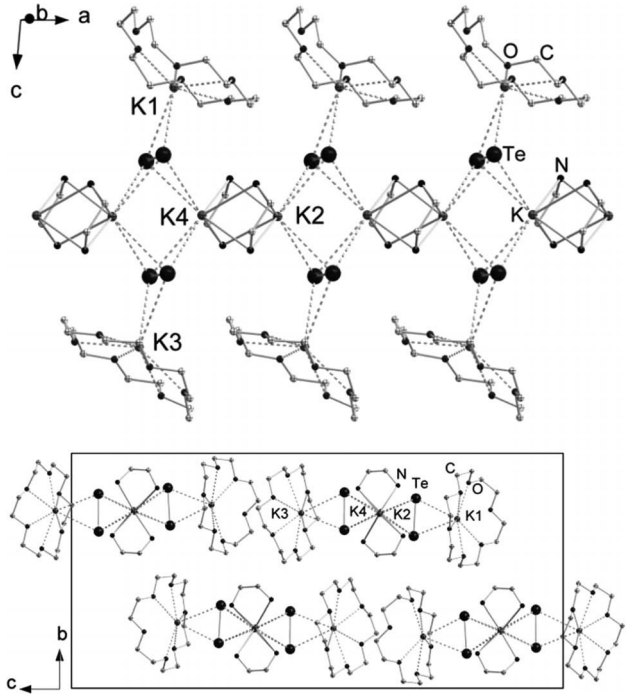

Figure 6. Crystal structure of **6**. One-dimensional strands along the crystallographic *a* axis, including $(Te_2)^{2-}$ dumbbells in side-on coordination mode (top) and arrangement of the strands within the crystal (bottom). Hydrogen atoms are omitted for clarity.

anion is found "end-on" 7.12 Å apart the K^+ ions, in the direction of one of the K···N contacts. The $(Te_2)^{2-}$ anions, in turn, have eight K^+ "neighbors", six within the *ab* plane, and two in *c* direction.

Experimental and Computational ^{125}Te NMR Studies

In terms of reaction monitoring we performed ^{125}Te NMR experiments and were able to identify the potassium sequestered tellurides according to *Schrobilgen's* compilation of chalcogenide shift tables.[7c] Changing to lithium tellurides, the telluride anion of **1** and monohydrogentelluride were also detected as reported [$\delta(Te^{2-})$ = –1430 ppm, $\delta(HTe^-)$ = –1100 ppm], while lithium polytellurides produce different chemical shifts.

Table 3 compares ^{125}Te chemical shifts of the terminal tellurium atoms of polytellurides as measured from solutions of lithium solvated or potassium sequestered polytellurides, respectively. In the case of lithium salts, the terminal tellurides do not undergo an upfield shift with increasing chain length, which might be due to a higher Lewis acidity of the (solvated) lithium ions compared to sequestered potassium salts. Further indications for a direct interaction of polytellurides with lithium cations are given by relatively broad signals with line widths of up to 6402 Hz. These indicate a dynamic equilibrium of solvated and free lithium cations, facilitating a direct impact of the latter on the electronic structure of the terminal tellurium atom. Bridging tellurium atoms are not affected that much, since the negative charge is not delocalized over them to a

Zeitschrift für anorganische und allgemeine Chemie ZAAC Journal of Inorganic and General Chemistry

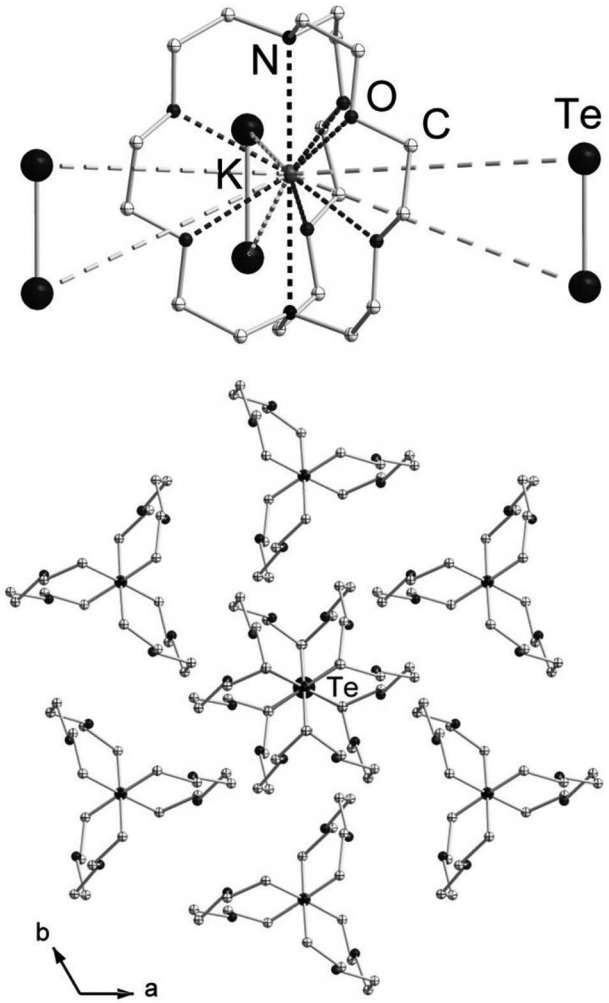

Figure 7. Crystal structure of **7**. Coordination environment and three of four next $(Te_2)^{2-}$ dumbbells around K^+ ions within [2.2.2]*crypt* ligands (top). Embedding of a $(Te_2)^{2-}$ dumbbell within eight $[K([2.2.2]crypt)]^+$ cation complexes (bottom, K···O, and K···N contacts not drawn). Hydrogen atoms are omitted for clarity.

significant extent. Solutions of potassium tellurides in the absence of complexation agents do not produce any detectable signals at all, since the interaction of the (softer) potassium ions with the tellurium atoms is even stronger, and the solvation tendency by *en* is lower than for Li^+ – according to the HSAB principle.[8] The broadening of the NMR signals is strong enough to make them disappear in the noise. Solid state NMR investigations did not yield any valuable information, since line broadening even exceeds the overall shift range of polytelluride anions.

Quantum chemical calculations of ^{125}Te NMR shifts were performed for the different anions $(Te_x)^{2-}$ (x = 1–4) (Table 3), including a full relativistic treatment and an all electron basis set. Due to problems when treating anions in chemical shift calculations, the absolute numbers differ considerably. However, they confirm the trend of an upfield shift of terminal telluride atoms with increasing chain length, which was reported for non-interacting (sequestered) telluride salts.[7c]

Table 3. ^{125}Te NMR chemical shifts of the terminal tellurium atoms of different (poly)telluride anions. Values for bridging tellurium atoms in parentheses; values for K^+-sequestered anions taken from Ref. [7c].

$\delta(^{125}Te)$ /ppm	K^+-sequestered	Li^+-solvated	Calculated[a)]
$(Te)^{2-}$	–1430	–1441	–2901
$(Te_2)^{2-}$	–1080	–1022	–1519
$(Te_3)^{2-}$	–298 (–372)	–1509 (–323)[b)]	–380 (80)
$(Te_4)^{2-}$	19 (19)	–1229 (–47)[c)]	–199 (844)

a) For free dianions, see Experimental Section. b) The NMR spectrum recorded on an *en* solution of **3** is identical with the NMR spectra recorded on a solution that was obtained upon reduction of three equivalents of elemental tellurium with two equivalents of metallic lithium in situ. c) Since no lithium salt of the $(Te_4)^{2-}$ anion is known, the NMR spectrum was recorded on a solution that was obtained upon reduction of four equivalents of elemental tellurium with two equivalents of metallic lithium in situ.

Electronic Structure Calculations and Experimental UV/Vis Spectroscopy

While the monotellurides are colorless and electronic insulators, the classical polytellurides $(Te_x)^{2-}$ with x = 2–4 should exhibit smaller – that is semiconducting – bandgaps, as indicated by a variety of colors.

The continuous reduction of the bandgap with growing chain length was examined and confirmed on the examples reported herein by several approaches: (i) TD-DFT (energy of HOMO–LUMO singlet excitations, S) for the molecular anions, (ii) periodic DFT calculations (fundamental bandgap, bg) considering the periodic arrangement in the crystal and the corresponding cations (Li^+, Na^+ or K^+), and (iii) UV/Vis spectroscopic measurements for our series of lithium solvated tellurides (exp).

Table 4 documents the bandgap narrowing for the series of $(Te_x)^{2-}$ with x = 1–4 by all methods applied. As expected due to the large impact of charge compensation for a single atom, single molecule calculations (S) fail to correctly describe the isolated monotelluride ion in comparison to periodic calculations and the experiment, but strongly overestimate the gap. Additionally, the trend from $(Te_3)^{2-}$ to $(Te_4)^{2-}$ is not correctly described by this method. In contrast, the calculations taking into account the full periodic arrangement in the crystal including counterions deliver bandgaps in good agreement with the measured data, both regarding the trend and the absolute values. This might, however, incorporate some error compensa-

Table 4. Calculated first singlet excitation energies (S), fundamental bandgaps (bg), and experimental onset of absorption (exp) for $(Te_x)^{2-}$, x = 1–4. All values in eV.

Anion	S (TD-DFT)	bg (periodic DFT)[a)]	Exp (UV/Vis)
Te^{2-}	6.66	2.13	[c)]
$(Te_2)^{2-}$	1.50	1.55 / *1.74*	1.34
$(Te_3)^{2-}$	1.16	[b)]	1.05
$(Te_4)^{2-}$	1.27	1.27	[d)]

a) bg calculated for **1**–**3** and $[Na([2.2.2]crypt)]_2(Te_4)$;[6c] value for $[K([2.2.2]crypt)]_2(Te_2)$ (**7**) in italics. b) Convergence not achieved. c) The samples decompose during the measurement due to extreme air-sensitivity. d) Due to the co-crystallization of K_2Te_3 (see Exp. Sect.), a value for the $(Te_4)^{2-}$ salt was not available.

tion since the DFT methods used are known to underestimate bandgaps of semiconductors.[9]

For the $(Te_2)^{2-}$ dianion, periodic DFT values are given for both Li^+ and K^+ as counterions. The calculated values indicate that the counterion does affect the bandgaps, such as suggested from the NMR measurements.

Conclusions

A variety of new polytelluride salts were synthesized and characterized by means of single-crystal X-ray diffraction and NMR spectroscopy. The continuous decrease of the bandgap was demonstrated using a combination of quantum chemical calculations and UV/Vis spectroscopy. Computational approaches taking the full crystal environment into account are needed for accurate results. Additionally, spectroscopic as well as periodic quantum chemical methods revealed a notable influence of the very counterion present on electronic structures of the $(Te_x)^{2-}$ chain.

Experimental Section

General: All synthesis steps were performed with strong exclusion of air, moisture (argon atmosphere at a high-vacuum, double-manifold Schlenk line or in a glove box) and light. Solvents were dried and freshly distilled prior to use. The elements were purchased from Sigma Aldrich (>99 %) and used as received. *Crypto*fix© was purchased from Merck. A phase with the nominal composition KPbTe was prepared by fusion of the elements in 1:1:1 ratio in a quartz ampoule in an argon atmosphere using a Bunsen burner.

Synthesis of $[Li(en)_x]_2(Te_y)$ (y = 1–3) (1–3): Lithium (300 mg) and the according equivalents of tellurium were suspended in *en* (60 mL). The reaction mixture was stirred for 2 d and filtered to remove possible solid residues. The solution (40 mL) was taken and carefully layered with toluene (40 mL). Compounds **1**–**3** crystallize within 2 weeks as colorless (**1**) or black blocks (**2**, **3**). Yields: 48 % (**1**), 91 % (**2**), 94 % (**3**).

Crystallization of $[K(18c6)]_2(Te_2)$ (4): A phase with the nominal composition KPbTe (500 mg), *18c6* (500 mg), and *en* (10 mL) were stirred for 2 d, filtered, and carefully layered with toluene (10 mL). After 2 weeks, compound **4** crystallized as black blocks. Yield approx. 10 %.

Crystallization of $[K(18c6)]_2(Te_4)$ (5): A phase with the nominal composition KPbTe (250 mg), *18c6* (250 mg), and *en* (2 mL) were heated in an autoclave for 7 d at 150 °C. **5** was picked manually from the reaction mixture as black blocks beside black blocks of K_2Te_3.[10]

Crystallization of $[K(18c6)]_2[K(en)]_2(Te_2)_2$ (6): A phase with the nominal composition KPbTe (330 mg) and *18c6* (400 mg) were stirred with en (25 mL) for 2 d, filtered and allowed to stand for one week. Crystallization was realized by layering of the reaction solution (10 mL) with toluene (15 mL). **6** crystallized after 5 d as long purple sticks in approx. 15 % yield.

Crystallization of $[K([2.2.2]crypt)]_2(Te_2)$ (7): A phase with the nominal composition KPbTe (330 mg) and cryptofix© (400 mg) were stirred with *en* (25 mL) for 2 d, filtered and allowed to stand for one week. **7** crystallized as purple plates with approx. 15 % yield.

Single crystal X-ray Diffraction: All measurements were performed at a Stoe IPDS-II or a Stoe IPDS-IIT diffractometer at 100 K (**1**, **4**–**7**) or at an Stoe IPDS-I diffractometer at 193 K (**2**, **3**), using Mo-K_α radiation (λ = 0.71073 Å) and a graphite monochromator. Upon numerical absorption correction, the structure solution was performed by direct methods, followed by full-matrix-least-squares refinement against F^2, using SHELXS-97, SHELXL-97, and OLEX2 software.[11] Table 2 summarizes the data of the X-ray diffraction experiments.

Crystallographic data (excluding structure factors) for the structures in this paper have been deposited with the Cambridge Crystallographic Data Centre, CCDC, 12 Union Road, Cambridge CB21EZ, UK. Copies of the data can be obtained free of charge on quoting the depository numbers CCDC-954799, -954800, -954801, -954802, -954803, -954804, and -954805 for **1**–**7** (Fax: +44-1223-336-033; E-Mail: deposit@ccdc.cam.ac.uk, http://www.ccdc.cam.ac.uk)

UV/Vis Spectroscopy: Optical absorption spectra were recorded with a Varian Cary 5000 spectrometer. Single-crystalline samples were pulverized in nujol oil between two quartz plates (Figure 8).

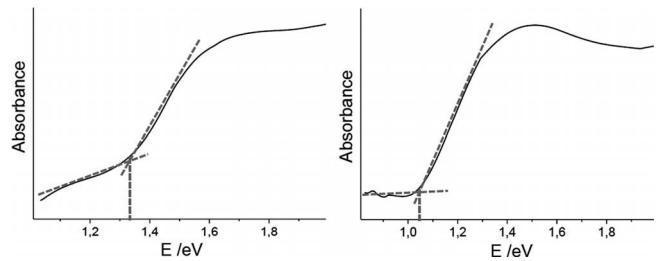

Figure 8. Optical absorption spectra of $(Te_2)^{2-}$ (left hand side) and $(Te_3)^{2-}$ (right hand side) units, such as observed in compounds **2** and **3**, recorded as suspension of single crystals in nujol oil.

Nuclear Magnetic Resonance Spectroscopy: All ^{125}Te NMR spectra were recorded with a BRUKER DRX 400 in *en* with a C_6D_6 capillary for locking. The use of short acquisition times (0.2 s) reduced the duration of the experiments and avoided excessive line broadening parameters (15Hz). Standard experiments applied 15k pulses with a delay (D1) of 1 s.

Methods of the Quantum Chemical Investigations: All molecular electronic structure calculations were carried out with the Turbomole program package V6.2.[12] As proven reasonable for many of our previous investigations of main group element anions,[13] the COSMO model was used for the compensation of negative charges.[14] Structure optimizations were undertaken by employment of the RIDFT program, using the BP86 functional[15] and def2-TZVP basis sets with an effective core potential at the Te atoms (ECP-28-mdf-TZVP).[16] Nuclear magnetic resonance properties were calculated using ADF V2010.02b,[17] with the GIAO Ansatz[18] and all electron basis sets (QZ4P). For the TD-DFT calculations, all geometries were optimized using the BP86 functional and def2-TZVP basis sets. Calculations at crystal structure geometries do change the absolute values, yet the tendencies are the same. Solid state calculations were carried out using DFT methodology with periodic boundary conditions applying the exchange-correlation functional proposed by *Perdew*, *Burke* and *Ernzerhof* (PBE)[19] in combination with a plane-wave basis set. The projector-augmented wave (PAW) method[20] was used and enabled a truncation of the plane-wave basis set at a kinetic energy of 350 eV. The Brillouin zone was sampled at the Γ-point and the experimental crystal structures used. Convergence tests for the basis set (400 eV), a larger k-mesh (spacing of 0.1 $Å^{-1}$ between k-points) and optimization of ionic

positions changed the values by < 0.05 eV. The energy during SCF cycles was converged to 10^{-5} eV. The VASP code was used.[21]

Acknowledgements

This work was supported by the Deutsche Forschungsgemeinschaft (DFG, SPP 1415, GRK 1782) and the Friedrich-Ebert-Stiftung (FES). We thank *R. Riedel*, *Dr. K. Harms*, *Dr. M. Holynska*, and *Dr. J. Heine* for their help with the X-ray diffraction analyses. We are indebted to *Dr. E. Matern* and *K. Pützer* for help with the NMR spectroscopy. We also thank *A. von Tesmar* for his contributions to the NMR calculations.

References

[1] A. Cisar, J. D. Corbett, *Inorg. Chem.* **1977**, *16*, 632.
[2] a) M. A. Ansari, J. M. McConnachie, J. A. Ibers, *Acc. Chem. Res.* **1993**, *26*, 574; b) L. C. Roof, J. W. Kolis, *Chem. Rev.* **1993**, *93*, 1037; c) A. K. Singh, S. Sharma, *Coord. Chem. Rev.* **2000**, *209*, 49; d) W. S. Sheldrick in *Handbook of Chalcogen Chemistry* (Ed.: F. Devillanova), The Royal Society of Chemistry **2007**, 43; e) C. Graf, A. Assoud, O. Mayasree, H. Kleinke, *Molecules* **2009**, *14*, 3115; f) J. Beck, *Angew. Chem.* **1994**, *106*, 172.
[3] D. M. Smith, J. A. Ibers, *Coord. Chem. Rev.* **2000**, *200–202*, 187.
[4] a) K. Stöwe, S. Appel, *Angew. Chem.* **2002**, *114*, 2849; *Angew. Chem. Int. Ed.* **2002**, *41*, 2725; b) C. Feldmann, A. Okrut, *Z. Anorg. Allg. Chem.* **2009**, *635*, 1807; c) Q. Zhang, C. D. Malliakas, M. G. Kanatzidis, *Inorg. Chem.* **2009**, *48*, 10910; d) A. Günther, A. Isaeva, A. I. Baranov, M. Ruck, *Chem. Eur. J.* **2011**, *17*, 6382; e) A. Panda, *Coord. Chem. Rev.* **2009**, *253*, 1947; f) E. R. Clark, R. L. Melen, J. M. Rawson, *Annu. Rep. Prog. Chem. Sect. A* **2010**, *106*, 119; g) C. D. Martin, P. J. Ragogna, *Annu. Rep. Prog. Chem. Sect. A* **2011**, *107*, 110; h) S. S. dos Santos, E. S. Lang, G. M. de Oliveira, *J. Organomet. Chem.* **2007**, *692*, 3081; i) H. T. M. Fischer, D. Naumann, W. Tyrra, *Chem. Eur. J.* **2006**, *12*, 2515; j) E. Ahmed, M. Ruck, *Coord. Chem. Rev.* **2011**, *255*, 2892; k) J. Beck, F. Steden, A. Reich, H. Fölsing, *Z. Anorg. Allg. Chem.* **2003**, *629*, 1073; l) M. Lindsjö, L. Kloo, *Acta Crystallogr. Sect. E* **2005**, *61*, i18; m) E. Ahmed, E. Ahrens, M. Heise, M. Ruck, *Z. Anorg. Allg. Chem.* **2010**, *636*, 2602.
[5] a) E. Ruzin, W. Massa, S. Dehnen, *Eur. J. Inorg. Chem.* **2007**, 4429; b) B. Osterrath, Diploma Thesis, Rheinische Friedrich-Wilhelms-Universität Bonn, **2005**.
[6] a) J. C. Huffmann, R. C. Haushalter, *Z. Anorg. Allg. Chem.* **1984**, *518*, 203; b) L. A. Devereux, G. J. Schrobilgen, *Acta Crystallogr., Sect. C* **1985**, *41*, 1730; c) R. Zagler, B. Eisenmann, H. Schäfer, *Z. Naturforsch. B* **1987**, *42*, 151; d) H. Wolkers, B. Schreiner, R. Staffel, U. Müller, K. Dehnicke, *Z. Naturforsch. B* **1991**, *46*, 1015; e) R. J. Batchelor, F. W. B. Einstein, I. D. Gay, C. H. W. Jones, R. D. Sharma, *Inorg. Chem.* **1993**, *32*, 4378; f) K.-H. Thiele, A. Steinicke, U. Dümichen, B. Neumüller, *Z. Anorg. Allg. Chem.* **1996**, *622*, 231; g) B. Schreiner, B. Neumüller, K. Dehnicke, *Chem. Ztg.* **1991**, *115*, 326.
[7] a) M. Björgvinsson, J. F. Sawyer, G. J. Schrobilgen, *Inorg. Chem.* **1991**, *30*, 2231; b) K. Seifert-Lorenz, J. Hafner, *Phys. Rev. B* **2002**, *66*, 094105; c) M. Björgvinsson, G. J. Schrobilgen, *Inorg. Chem.* **1991**, *30*, 2540.
[8] R. G. Pearson, *J. Am. Chem. Soc.* **1963**, *85,* 3533.
[9] G. Onida, L. Reining, A. Rubio, *Rev. Mod. Phys.* **2002**, *74*, 601.
[10] B. Eisenmann, H. Schäfer, *Angew. Chem.* **1978**, *90*, 731; *Angew. Chem. Int. Ed. Engl.* **1978**, *17*, 684.
[11] a) G. M. Sheldrick, *SHELXL97*, Program for the Refinement of Crystal Structures, Universität Göttingen, **1997**; b) O. V. Dolomanov, L. J. Bourhis, R. J. Gildea, J. A. K. Howard, H. Puschmann, *J. Appl. Crystallogr.* **2009**, *42*, 339.
[12] *TURBOMOLE v6.2*, TURBOMOLE GmbH 2011. TURBOMOLE is a development of University of Karlsruhe and Forschungszentrum Karlsruhe **1989–2007**, TURBOMOLE GmbH since 2007.
[13] a) S. Dehnen, M. K. Brandmayer, *J. Am. Chem. Soc.* **2003**, *125*, 6618–6619; b) M. K. Brandmayer, R. Clérac, F. Weigend, S. Dehnen, *Chem. Eur. J.* **2004**, *10*, 5147–5157; c) C. Zimmermann, C. E. Anson, F. Weigend, R. Clérac, S. Dehnen, *Inorg. Chem.* **2005**, *44*, 5686–5695; d) E. Ruzin, A. Fuchs, S. Dehnen, *Chem. Commun.* **2006**, 4796–4798; e) E. Ruzin, E. Zent, E. Matern, W. Massa, S. Dehnen, *Chem. Eur. J.* **2009**, *15*, 5230–5244; f) F. Lips, S. Dehnen, *Angew. Chem.* **2009**, *121*, 6557; *Angew. Chem. Int. Ed.* **2009**, *48*, 6435; g) F. Lips, S. Dehnen, *Angew. Chem.* **2011**, *123*, 986; *Angew. Chem. Int. Ed.* **2011**, *50*, 955; h) F. Lips, R. Clérac, S. Dehnen, *Angew. Chem.* **2011**, *123*, 991; *Angew. Chem. Int. Ed.* **2011**, *50*, 960; i) F. Lips, R. Clérac, S. Dehnen, *J. Am. Chem. Soc.* **2011**, *133*, 14168; j) F. Lips, I. Schellenberg, R. Pöttgen, S. Dehnen, *Chem. Eur. J.* **2009**, *15*, 12968; k) F. Lips, M. Holynska, R. Clérac, U. Linne, I. Schellenberg, R. Pöttgen, F. Weigend, S. Dehnen, *J. Am. Chem. Soc.* **2012**, *134*, 1181; l) B. Weinert, F. Weigend, S. Dehnen, *Chem. Eur. J.* **2012**, *18*, 13589.
[14] A. Klamt, G. Schürmann, *J. Chem. Soc. Perkin Trans. 2* **1993**, 799.
[15] a) A. D. Becke, *Phys. Rev. A* **1988**, *38*, 3098; b) J. P. Perdew, *Phys. Rev. B* **1996**, *33*, 8822.
[16] F. Weigend, R. Ahlrichs, *Phys. Chem. Chem. Phys.* **2005**, *7*, 3297.
[17] ADF2010, SCM, Theoretical Chemistry, Vrije Universiteit, Amsterdam, The Netherlands, **2010**,http://www.scm.com.
[18] G. Schreckenbach, T. Ziegler, *J. Phys. Chem.* **1995**, *99*, 606.
[19] J. P. Perdew, K. Burke, M. Ernzerhof, *Phys. Rev. Lett.* **1996**, *77*, 3865.
[20] a) P. E. Blöchl, *Phys. Rev. B* **1994**, *50*, 17953; b) G. Kresse, D. Joubert, *Phys. Rev. B* **1999**, *59*, 1758.
[21] a) J. Hafner, *J. Comput. Chem.* **2008**, *29*, 2044; b) G. Kresse, J. Furthmüller, *Phys. Rev. B* **1996**, *54*, 11169.

Received: June 25, 2013
Published Online: September 4, 2013

III

Molecular CHEVREL-like Clusters $[(RhPPh_3)_6Se_8]$ and $[Pd_6Te_8]^{4-}$

Günther Thiele, Zhiliang You, Stefanie Dehnen, *Inorg. Chem.* **2015**, *in Revision*.

$[(RhPPh_3)_6(\mu_3\text{-}Se)_8]\cdot 0.5en$ (**1**; *en* = ethane-1,2-diamine), obtained by reaction of $[Pb_2Se_3]^{2-}$ anions with $[Rh(PPh_3)_3Cl]$ in *en*, represents the first compound comprising a molecular $[Rh_6]$ octahedron with all faces capped by Se atoms. Analogous treatment of $[Pb_2Te_3]^{2-}$ with $[Pd(PPh_3)_2Cl_2]$ yielded $[Li_4(en)_{10}][Pd_6(\mu_3\text{-}Te)_8]$ (**2**), the first compound exhibiting a molecular, chalcogen-capped $[Pd_6]$ aggregate. Besides syntheses and structures of the title compounds, we report quantum chemical calculations and cyclic voltammetry to understand the electronic properties of these molecular CHEVREL-like complexes.

Themenkomplex $[M_xCh_y]^{q-}$, Synthese und Reaktivität

Inhalt: Die beiden Verbindungen $[(RhPPh_3)_6(\mu_3\text{-}Se)_8]\cdot 0.5en$ und $[Li_4(en)_{10}][Pd_6(\mu_3\text{-}Te)_8]$ werden als Reaktionsprodukte von $[Pb_2Ch_3]^{2-}$-Lösungen in Ethylendiamin mit $[Rh(PPh_3)_3Cl]$ und $[Pd(PPh_3)_2Cl_2]$ vorgestellt, die Kristallstrukturen werden diskutiert und mit verwandten Verbindungen verglichen.

Quantenchemische Rechnungen ergeben für die Rhodiumverbindung eine gemischtvalente Situation mit formal zwei Rh(II) und vier Rh(III) Ionen, wobei die Oxidation vermutlich mit einer Reduktion des Plumbates einherging. Anhand der Kristallstruktur können keine unterschiedlichen Oxidationszustände der Rhodiumatome zugeordnet werden, so dass von einer gleichmäßigen Verteilung der Ladungen über alle Atome ausgegangen werden muss. Mithilfe von Differentialpulsvoltammogrammen konnte allerdings ein klarer Hinweis auf die gemischtvalente Situation in der Rhodiumverbindung erhalten werden, wobei zwei separierte Oxidationssignale auftreten.

Die Palladiumverbindung enthält wie im Edukt Pd(II) und kann als Kondensationsprodukt von sechs, über Te-Atome Ecken-verknüpften „$[PdTe_4]^{6-}$“-Einheiten angesehen werden.

Eigener Anteil: Alle Synthesen wurden von mir geplant und durchgeführt. Die röntgenographischen Daten wurden von mir aufgenommen und ausgewertet. Alle quantenchemischen Untersuchungen wurden von mir durchgeführt und zusammen mit Stefanie Dehnen ausgewertet. Thomas Krüger hat die EDX-Analysen durchgeführt. Zhiliang You hat die elektrochemischen Untersuchungen durchgeführt, ausgewertet und den entsprechenden Teil des Manuskriptes erstellt. Das Manuskript wurde von Stefanie Dehnen und mir zusammen verfasst.

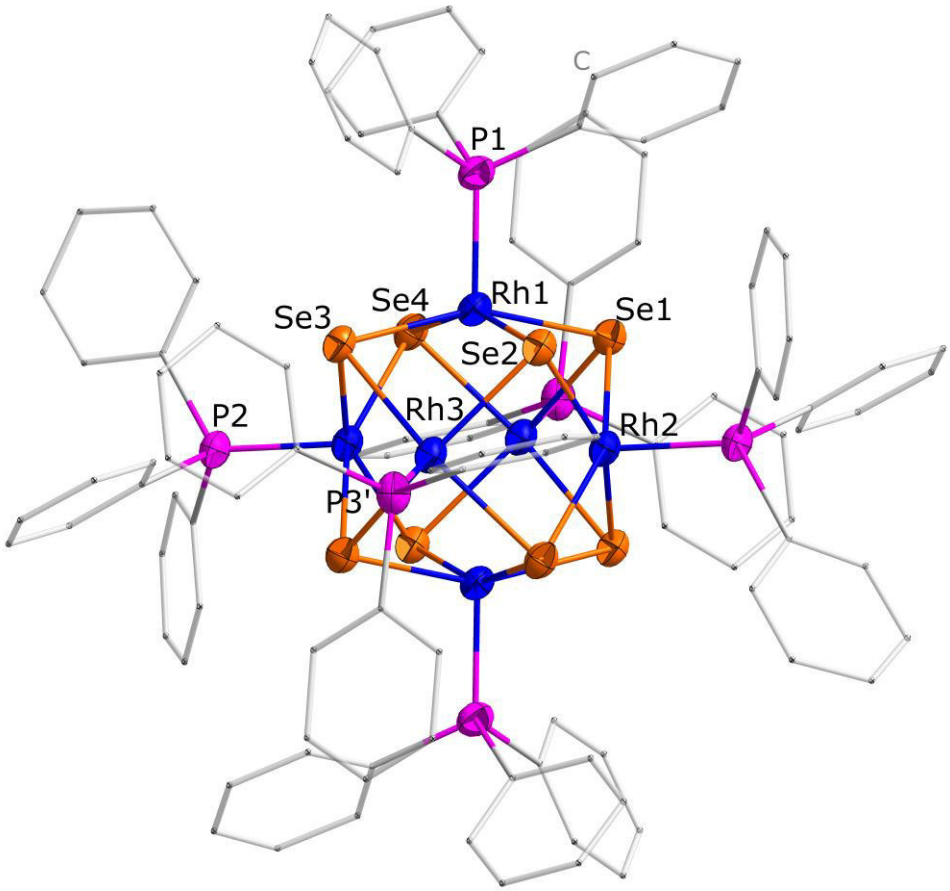

Abbildung 23. Molekülstruktur von $[(RhPPh_3)_6(\mu_3\text{-}Se)_8]$.

Molecular CHEVREL-like clusters $[(RhPPh_3)_6(\mu_3\text{-}Se)_8]$ and $[Pd_6(\mu_3\text{-}Te)_8]^{4-}$

Günther Thiele, Zhiliang You, and Stefanie Dehnen*

Fachbereich Chemie and Wissenschaftliches Zentrum für Materialwissenschaften, Hans-Meerwein-Straße, 35043 Marburg, Germany

Rhodium Palladium Chalcogenide, Molecular Chevrel Compound, Density Functional Theory

SupportingInformation Placeholder

ABSTRACT: $[(RhPPh_3)_6(\mu_3\text{-}Se)_8]\cdot 0.5en$ (**1**; en = ethane-1,2-diamine), obtained by reaction of $[Pb_2Se_3]^{2-}$ anions with $[Rh(PPh_3)_3Cl]$ in en, represents the first compound comprising a molecular $[Rh_6]$ octahedron with all faces capped by Se atoms. Analogous treatment of $[Pb_2Te_3]^{2-}$ with $[Pd(PPh_3)_2Cl_2]$ yielded $[Li_4(en)_{10}][Pd_6(\mu_3\text{-}Te)_8]$ (**2**), the first compound exhibiting a molecular, chalcogen-capped $[Pd_6]$ aggregate. Besides syntheses and structures of the title compounds, we report quantum chemical calculations and cyclic voltammetry to understand the electronic properties of these molecular CHEVREL-like complexes.

For many years, rhodium and palladium compounds have attracted great interest in inorganic, organometallic and organic chemistry due to their properties in various catalytic reactions, such as *Grubbs*' $[RuCl_2(=CHR')(PR_3)_2]$ for alkene metathesis[1] and *Wilkinson*'s $[RhCl(PPh_3)_3]$ for hydrogenation of olefins and acetylenes.[2]

Polynuclear rhodium complexes incorporating an $[Rh_6]$ octrahedron, such as the hexadecacarbonyl-hexarhodium $[Rh_6(CO)_{16}]$,[3] with its unique properties as redox catalyst,[4] have been extensively investigated, as well. A large diversity of according Rh clusters with terminal, bridging and/or capping carbonyl groups have been known, including condensed clusters with up to 33 Rh atoms,[5] amine and phosphine ligated derivatives,[6] as well as the corresponding hydride clusters, such as $[Rh_6H_{12}(PCy_3)_6][B(C_8H_3F_6)_4]_2$[7] or $[Rh_6H_{12}(P^iPr_3)_6]$,[8] and a "pure" $[Rh_6]$ octahedron[9] with potential in syngas conversion.[10] Compounds that contain $[Pd]_6$ aggregates, in contrast, have been far less represented in the literature. Apart from $[Pd_6(CO)_4(PMe_3)_7]$,[11] only higher aggregates such as the $[Pd_{33}Ni_9(CO)_{41}(PPh_3)]^{4-}$ cluster anion,[12] or $[Pd_{37}(CO)_{28}\{P(p\text{-Tolyl})_3\}_{12}$ were reported.[13]

Corresponding molecular $[M_6]$ octahedra with face-bridging by chalcogenide ligands have been only known for transition metals of groups V-VIII,[14] and Co[15] to date. These represent molecular analogs of the fundamental building units of CHEVREL phases $A^{II}Mo_6Ch_8$ (A = Ca, Sr, Ba, Sn, Pb, Au, Ln; Ch = chalcogen), which have triggered large interest due to their thermoelectric and/or superconducting potentials.[16]

In the course of our investigations on the reactivity of $[Pb_2Ch_3]^{2-}$ anions[17] towards transition metal complexes, a solution resulting from an extraction of a binary Pb:Se phase (1:2) with 2.2 eq. of *18c6* and 2.1 eq. of K (*18c6* = 1,4,7,10,13,16-hexaoxacyclooctadecane) was treated with a stoichiometric amount of $[Rh(PPh_3)Cl]$ in *en* (*en* = ethan-1,2-diamine), which resulted in the formation of $[(RhPPh_3)_6(\mu_3\text{-}Se)_8]\cdot 0.5en$ (**1**) upon slow removal of the solvent. In a corresponding reaction of a solution resulting from an extraction of a binary Pb:Te phase (1:2) with 2.1 eq. of Li with $[Pd(PPh_3)_2Cl_2]$, we obtained the related compound $[Li_4(en)_{10}][Pd_6(\mu_3\text{-}Te)_8]$ (**2**). For synthesis and characterization details see the Supporting Information. Both product compounds, **1** and **2**, are based on octahedral $[M_6]$ aggregates. They represent the first octahedral clusters in Rh or Pd chemistry to be capped by chalcogen atoms, in the style of molecular CHEVREL-like complexes.

Compound **1** crystallizes in the triclinic space group $P\bar{1}$ with one formula unit of the C_i-symmetric cluster and one additional, heavily disordered solvent molecule of *en* in the unit cell. All deltahedral faces are μ_3-capped by Se atoms, and each of the Rh atoms is additionally coordinated by one PPh_3 ligand (Figure 1).

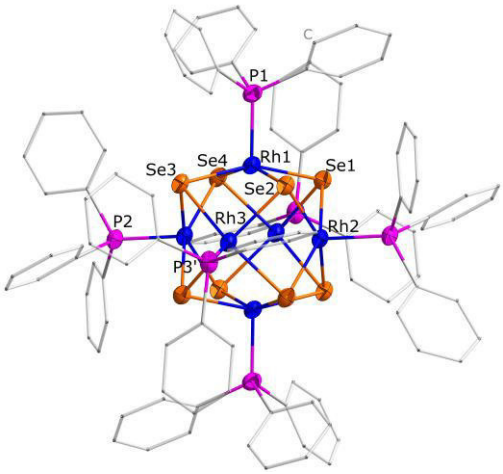

Figure 1. Molecular structure of the cluster in compound **1**. Ellipsoids are drawn at 50% probability, C atoms are drawn as wires, H atoms and split positions of disordered Ph rings are omitted for clarity. Selected structural parameters [pm, °]: Rh…Rh 310.69(6)-313.26(7), Se–Rh 243.63(7)-249.90(7), Rh–P 220.44(15)-221.18(16), Se…Se 339.64(9)-343.83(10); Rh…Rh…Rh(mer) 89.768(16)-90.230(16)°, R…Rh…Rh(fac) 59.639(14)-60.445(14)°, Se–Rh–Se(mer) 156.20(3)-157.24(2)°, Se-Rh-Se(fac) 87.01(2)-88.28(2)°, Se–Rh–P 90.17(4)-112.58(4)°, Rh–Se–Rh 77.45(2)-79.60(2)°.

Different from the carbonyl complex $[Rh_6(CO)_{16}]$,[3] the electronic structure of compound **1** cannot be depicted by using electron counting rules according to Wade and Mingos.[19] The $[Rh_6]$ cluster core is comprised of 98 valence electrons, with the μ_3-Se ligands counted as 4 electron donors and the phosphine ligands as 2 electron donors – much more than the number of 86 electrons expected for an octahedral *closo* cluster. This is well reflected by the different Rh...Rh distances

(310.69(6)-313.26(7) pm), which are much longer than in $[Rh_6(CO)_{16}]$ (277.6 pm),[3] $[Rh_6(CO)_{10}(dpm)_3]$ (dpm = bis(diphenylphosphino)methane; 278.3 pm),[18] $[Rh_6H_{12}(P^iPr_3)_6]$ (271.8-305.9 pm),[8] or in $[(Cp^*Rh)_3(\mu_3\text{-}Se)_2][PF_6]_2$ (288.0(1), 288.79(8) pm),[20a] but similar to the values observed in $[NMe_4][Rh_3(\mu_3\text{-}Se)_2(CO)_6]$ (308.6(1), 315.9(1) pm).[20b] Still, there is a slight electron deficit (each of the Rh atoms possesses $16^1/_3$ electrons without metal-metal bonding). Although an 18 electron situation for the Rh atoms is not urgently expected as the cluster is not an organometallic compound, we explored whether the Rh atoms would gain the missing $1^2/_3$ electrons each from Rh...Rh interactions, or not.

Quantum chemical calculations applying density function theory methods,[21] with a subsequent population analysis of the DFT wave function based on occupation numbers (PABOON),[22] suggest a very weak interaction of the Rh atoms. A total shared electron number (SEN) of 1.7 e^- was calculated for twelve 2-center and eight 3-center Rh...Rh interactions (that can be summarized as eight (Rh_3) interactions à 0.2 e^-). As compared with a total of 11.1 e^- for 24 Rh–(μ_3-Se) interactions (that can be summarized as eight (Rh_3)–(μ_3-Se) interactions à 1.4 e^-), the Rh...Rh interactions amount to about 14% of the strength of the Rh–Se covalent bonds that are mainly responsible for tethering of the atoms within the complex. Inspection of the molecular orbitals (MOs) and localized MOs (LMO) confirms the absence of significant Rh...Rh bonding interactions (see Figures S5 and S6), but indeed reveals an LMO that indicates some interaction of the Rh atoms (Figure 2, left), and is based on the highest energy MOs.

Formally, the Rh atoms exhibits different oxidation states, $Rh(II)_2Rh(III)_4$. Actually, it is not possible to clearly assign such charges based on the crystal structure, as the Rh_6Se_8 core deviates only very slightly from octahedral symmetry (Rh_{ap}–Rh_{eq} 311.53(6)-313.26(7) pm, Rh_{eq}–Rh_{eq} 310.69(6)-312.83(5) pm, Rh_{ap}–Se 245.77(7)-247.98(6) pm, Rh_{eq}–Se 243.63(7)-249.90(7) pm). It is possible to discriminate the metal atoms by Mulliken population analysis[23] of the DFT wave function, if the calculations are based on the crystal structure geometry (Figure 2, right). However, simultaneous optimization of the geometric and electronic structure leads to an equalization of both the cluster core symmetry and the atomic charges. Thus, we conclude that (a) the slight deviations from octahedral symmetry may be put down to packing effects and that (b) the respective electrons are delocalized over all Rh atoms.

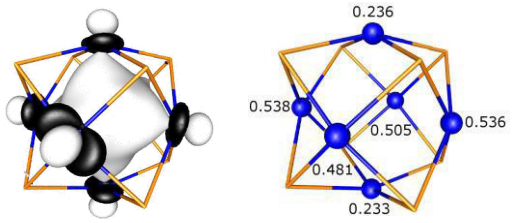

Figure 2. Left: Representation of the LMO representing (very) weak Rh…Rh interactions in **1**. Further LMOs and the valence MOs are given in the Supporting Informations. Phenyl rings are omitted for clarity. Amplitudes are drawn at ±0.05 a.u.. Right: Charges at Rh atoms (blue) according to a Mulliken analysis of the DFT wave function calculated for the complex structure in **1** as determined by X-ray crystallography. Se atoms (orange wires) possess Mulliken charges of –0.493 to –0.587. PPh_3 fragments are omitted for clarity. Note that the charges do not reflect formal oxidations states, but are a measure for it.

To confirm the assumption of a mixed-valence situation in **1**, we examined its electrochemical properties by means of cyclic and differential pulse voltammetry (CV and DPV). Initially, the investigations were carried out on a CH_2Cl_2 solution of **1** (about 1.20 mM), in the presence of tetra-*n*-butylammonium hexafluorophosphate (TBFP; 0.1 M) at 25 °C (Figure S9). However, these studies failed due to the oxidation of CH_2Cl_2 itself, occurring prior to the oxidation of **1** (see Supporting Information for further details). Thus, we changed the electrolyte/solvent combination (TBFP/MeCN), and repeated the measurement under otherwise unchanged conditions (Figure S10). Although the solubility of **1** in MeCN is not high, two well separated oxidation steps were observed (Figure 3). The nearly equal intensities of the two peaks, with half-wave potentials ($E_{1/2}$) at 1.11 V and 1.39 V, respectively, suggest that each of the two oxidation processes should involve the same number of electrons, which is in agreement with two successive oxidations of the cluster core in **1**.

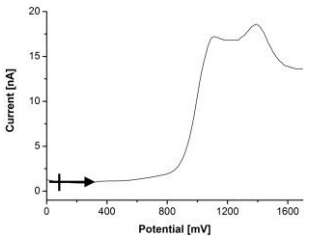

Figure 3. Differential pulse voltammogram (DPV) of a MeCN solution of **1**, recorded at a platinum electrode in the presence of TBFP (0.1 M). Scan range and rate: 0 to +1700 mV, 10 mV/s. Pulse amplitude 50 mV.

The mixed-valence character of **1** might be made responsible for the failure of a straight forward syntheses *via* reaction of $[K(18c6)]_2Se$ with $Rh(PPh_3)_3Cl$; we assume that the Pb atoms in $[Pb_2Se_3]^{2-}$ most likely acted as oxidizing agent, such as observed in our earlier work on according chalcogenidostannate salts, beside their role as chalcogen source.[24] The uncommon reaction pathway also rationalizes the relatively low yield of **1**; however, the use of $[K(18c6)]_2Se$ along with alternative oxidants is not easily feasible, since Se^{2-} is sensitive to oxidation itself, yielding polyselenides as highly favorable reaction products.

Compound **2** crystallizes in the monoclinic space group $P2_1/n$, and the cluster possesses crystallographic C_i symmetry. The Pd...Pd distances within the $[Pd_6]$ aggregate (> 320 pm) are even longer than the Rh...Rh distances in **1**. All faces are μ_3-capped by Te atoms (Figure 4). In contrast to the complex in **1**, no phosphine groups are attached to the Pd-Te core, which remains anionic. Instead, the complexes are embedded in an extended $\{[Li_4(en)_{10}]^{4+}\}_n$ network that forms sheets of double layers parallel to the $(10\bar{1})$ plane (Figure 5).

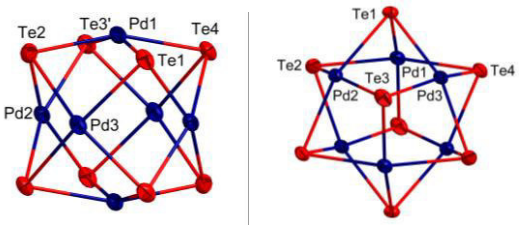

Figure 4. Molecular structure of the anion in compound **2**. Ellipsoids are drawn at 50% probability, Selected structural parameters [pm, °]: Selected structural parameters [pm, °]: Pd…Pd 320.64(16)-324.90(16), Pd–Te 260.43(13)-264.21(16). Te…Te 357.20(14)-408.05(13) pm; Pd…Pd…Pd(mer) 89.79(4)-90.21(4)°, Pd..Pd..Pd(fac) 59.34(3)-61.10(4)°, Te–Pd–Te(mer) 157.97(6)-161.37(6)°, Te-Pd-Te(fac) 86.05(5)-90.31(5)°, Pd–Te–Pd 74.84(4)-78.03(4)°.

In contrast to the situation in **1**, the $[Pd_6Te_8]^{4-}$ anion comprises formal Pd^{II} throughout, which is consistent with the corre-

sponding Mulliken charges in the range of 0.170 to 0.172. The charges at the Te atoms are in the range of −0.703 to −0.546, thus indicate a slightly higher accumulation of electron density at the Te atoms in comparison with the situation at the Se atoms in **1** in agreement with the lower formal oxidation state on average. By considering only Pd–μ_3-Te bonds, the Pd atoms possess 16 electrons each if the total charge of the anion is equally smeared over all atoms. Thus, the cluster can be viewed as an aggregate of six "$[Pd^{II}Te_4]^{6-}$" complexes that are linked by sharing of μ_3-Te^{2-} ligands to reduce the overall charge. The absence of Pd...Pd interactions is clearly shown by negligible SEN values (<0.1 for both 2-center and 3-center bonds) and the analyses of canonical as well as localized molecular orbitals and localized molecular orbitals (Figures S7 and S8) that show no notable Pd...Pd bonding interactions.

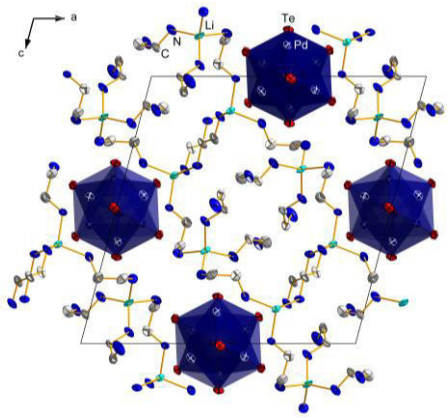

Figure 5. View of the $[Li_4(en)_{10}]^{4+}$ network in **2** that embeds the CHEVREL-like $[Pd_6Te_8]^{4+}$ clusters, viewing down the crystallographic *b* axis. The anions are highlighted by polyhedral representation. Ellipsoids are drawn at 50% probability, H atoms are omitted for clarity. Selected structural parameters [pm]: Li…N 203(3)-214(3), Te…N 268.24(14), Pd…N 370.26(14)-391.37(14).

In conclusion, two transition metal chalcogenide complexes with CHEVREL-like topologies were obtained by reaction of $[Pb_2Ch_3]^{2-}$ anions with $[Rh(PPh_3)_3Cl]$ (Ch = Se) or $[Pd(PPh_3)_2Cl_2]$ (Ch = Te). In both cases, the $[Pb_2Ch_2]^{2-}$ anion acted as chalcogen source, in the first case, it was also active as an oxidant to produce a mixed-valence Rh^{II}/Rh^{III} complex, as confirmed by quantum chemistry and electrochemical studies. The second compound can be viewed as six μ_3-Te-sharing, square planar "$[Pd^{II}Te_4]^{6-}$" complexes that aggregate to reduce the overall charge. While both compounds differ in that the Rh-Se cluster possesses a PPh_3 ligand shell and the Pd-Te cluster is a binary anion, both compounds comprise the first molecular $[M_6Ch_8]$ aggregates with the respective elemental combinations.

ASSOCIATED CONTENT

Supporting Information

Crystal structure refinement details, energy dispersive X-Ray analysis results, cyclovoltammetric measurement results and experimental details. This material is available free of charge via the Internet at http://pubs.acs.org

AUTHOR INFORMATION

Corresponding Author

Prof. Dr. S. Dehnen, dehnen@chemie.uni-marburg.de

ACKNOWLEDGMENT

Financial support by the Friedrich-Ebert-Stiftung and the Deutsche Forschungsgemeinschaft (DFG, SPP 1415) is gratefully acknowledged.

Notes

The authors declare no competing financial interests.

REFERENCES

(1) Schwab, P.; Grubbs, R. H.; Ziller, J. W. *J. Am. Chem. Soc.* **1996**, *118*, 100.
(2) Osborn, J. A.; Jardine, F. H.; Young, J. F.; Wilkinson, G. *J. Chem. Soc. A.* **1966**, 1711.
(3) Corey, E. R.; Dahl, L. F.; Beck, W. *J. Am. Chem. Soc.* **1963**, *85*, 1202.
(4) Uribe-Godínez, J.; Hernández-Castellanos, R.; Jiménez-Sandoval, O. *J. Power Sources* **2010**, *195*, 7243.
(5) Dolzhnikov, D. S.; Iapalucci, M. C.; Longoni, G.; Tiozzo, C.; Zacchini, S.; Femoni, C. *Inorg. Chem.* **2012**, *51*, 11214.
(6) (a) Tunik, S. P.; Koshevoy, I. O.; Poë, A. J.; Farrar, D. H.; Nordlander, E.; Haukkad, M.; Pakkanend, T. A. *Dalton Trans.* **2003**, 2457. (b) Hiney, R. M.; Chaplin, A. B.; Harmer, J.; Green, J. C.; Weller, A. S. *Dalton Trans.* **2010**, *39*, 1726.
(7) Brayshaw, S. K.; Ingleson, M. J.; Green, J. C.; Raithby, R. R.; Kociok-Köhn, G.; McIndoe, J. S.; Weller, A. S. *Angew. Chem. Int. Ed. Engl.* **2005**, *44*, 6875.
(8) Ingleson, M. J.; Mahon, M. F.; Raithby, P. R.; Weller, A. S. *J. Am. Chem. Soc.* **2004**, *126*, 4784.
(9) (a) Goellner, J. F.; Gates, B. C. *J. Phys. Chem. B* **2001**, *105*, 3269. (b) Aguilera-Granja1, F.; Rodríguez-López, J. L.; Michaelian, K.; Berlanga-Ramírez, E. O.; Vega, A. *Phys. Rev. B* **2002**, *66*, 224410.
(10) Shetty, S.; van Santen, R. A.; Stevens, P. A.; Raman, S. *J. Mol. Cat. A: Chem.* **2010**, *330*, 73.
(11) Klein, H.-F.; Mager, M.; Flörke, U.; Haupt, H.-J. *Organometallics* **1992**, *11*, 3915.
(12) Kawano, M.; Bacon, J. W.; Campana, C. F.; Winger, B. E.; Dudek, J. D.; Sirchio, S. A.; Scruggs, S. L.; Geiser, U.; Dahl, L. F. *Inorg. Chem.* **2001**, *40*, 2554.
(13) Mednikov, E. G.; Dahl, L. F. *J. Am. Chem. Soc.* **2008**, *130*, 14813.
(14) See for example: (a) Cecconi, F.; Ghilardi, C. A.; Midollini, S. *J. Chem. Soc., Chem. Commun.* **1981**, 640. (b) Eckermann, A. L.; Wunder, M.; Fenske, D.; Rauchfuss, T. B.; Wilson, S. R. *Inorg. Chem.* **2002**, *41*, 2004.
(15) See for example: (a) Fenske, D.; Ohmer, J.; Hachgenei, J. *Angew. Chem. Int. Ed. Engl.* **1985**, *24*, 993. (b) Hong, M.; Huang, Z.; Lei, X.; Wei, G.; Kang, B.; Liu, H. *Polyhedron* **1991**, *10*, 927.
(16) Zheng, Z.; Long, J. R.; Holm, R. H. *J. Am. Chem. Soc.* **1997**, *119*, 2163.
(17) The anions have been identified by their respective NMR shifts, see Schrobilgen $[Pb_2Ch_3]^{2-}$: (a) Borrmann, H.; Campbell, J.; Dixon, D. A.; Mercier, H. P. A.; Pirani, A. M.; Schrobilgen, G. J. *Inorg. Chem.* **1998**, *37*, 6656. (b) Björgvinsson, M.; Sawyer, J. F.; Schrobilgen, G. J. *Inorg. Chem.* **1987**, *26*, 741. (c) Björgvinsson, M.; Sawyer, J. F.; Schrobilgen, G. J. *Inorg. Chem.* **1991**, *30*, 2231.
(18) Ceriotti, A.; Ciani, G.; Garlaschelli, L.; Sartorelli, U.; Sironi, A. *J. Organomet. Chem.* **1982**, *229*, C9.
(19) (a) Wade, K. *Adv. Inorg. Chem. Radiochem.* **1976**, *18*, 1; (b) Mingos, D. M. P. *Acc. Chem. Res.* **1984**, *17*, 311.
(20) (a) Seino, H,: Mizobe, Y.; Hidai, M. *Organometallics* **2000**, *19*, 3631. (b) Galli, D.; Garlaschelli, L.; Ciani, G.; Fumagalli, A.; Martinengo, S.; Sironi, A. *J. Chem. Soc., Dalton Trans.* **1984**, 55.
(21) (a) TURBOMOLE Version 6.4, © TURBOMOLE GmbH 2012. TURBOMOLE is a development of University of Karlsruhe and Forschungszentrum Karlsruhe 1989-2007, TURBOMOLE GmbH since 2007. BP-86 functional: (b) Becke, A. D. *Phys. Rev. A* **1988**, *38*, 3098. (c) Perdew, J. P. *Phys. Rev. B* **1996**, *33*, 8822. Basis sets: (d) Weigend, F.; Ahlrichs, R. *Phys. Chem. Chem. Phys.* **2005**, *7*, 3297. (e) Weigend, F. *Phys. Chem. Chem. Phys.* **2006**, *8*, 1057. ECPs: (f) Dolg, M.; Stoll, H.; Savin, A.; Preuss, H. *Theor. Chim. Acta* **1989**, *75*, 173. (g) Stoll, H.; Metz, B.; Dolg, M. *J. Comput. Chem.* **2002**, *23*, 767. COSMO: (h) Klamt, A.; Schüürmann, G. *J. Chem. Soc. Perkin Trans.* **1993**, *2*, 799.
(22) Ehrhardt, C.; Ahlrichs, R. *Theor. Chim. Acta* **1985**, *68*, 231.
(23) Mulliken, R. S. *J. Chem. Phys.* **1955**, *23*, 1833.
(24) (a) Dehnen, S.; Zimmermann, C. *Chem. Eur. J.* **2000**, *6*, 2256. (b) Dehnen, S.; Zimmermann, C. *Eur. J. Inorg. Chem.* **2000**, 1471. (c) Zimmermann, C.; Anson, C. E.; Eckermann, A. L.; Wunder, M.; Fischer, G.; Keilhauer, I.; Herrling, E.; Pilawa, B.; Hampe, O.; Weigend, F.; Dehnen, S. *Inorg. Chem.* **2004**, *43*, 4595.

SYNOPSIS TOC: $[(RhPPh_3)_6(\mu_3\text{-}Se)_8]$ and $[Pd_6(\mu_3\text{-}Te)_8]^{4-}$, two complexes with $[M_6]$ octahedra capped by eight μ_3-Ch ligands (Ch = Se or Te), were obtained by treatment of $[Pb_2Ch_3]^{2-}$ anions with $[Rh(PPh_3)_3Cl]$ or $[Pd(PPh_3)_2Cl_2]$, respectively, in en. Both compounds comprise the first molecular $[M_6(\mu_3\text{-}Ch)_8]$ aggregates with the respective elemental combinations. Besides syntheses and structures of the title compounds, we report quantum chemical calculations and cyclic voltammetry to understand the electronic properties of these molecular CHEVREL-like complexes.

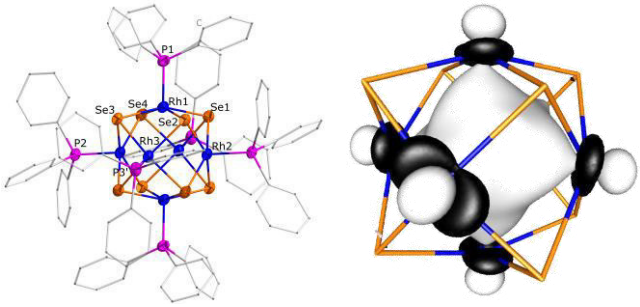

Supporting Information

Molecular CHEVREL-like clusters $[(RhPPh_3)_6(\mu_3\text{-}Se)_8]$ and $[Pd_6(\mu_3\text{-}Te)_8]^{4-}$

Günther Thiele, Zhiliang You, and Stefanie Dehnen*

Fachbereich Chemie and Wissenschaftliches Zentrum für Materialwissenschaften, Hans-Meerwein-Straße, 35043 Marburg, Germany

Contents

1. Synthesis Details

1.1 General

All manipulations were performed under strict exclusion of air and moisture using standard Schlenk and glovebox techniques. Solvents were freshly distilled prior to use. 18-crown-6 was evacuated for at least 24h at $p < 1 \cdot 10^{-3}$ mbar prior use. All elements and complexes (Sigma Aldrich) were transferred into a glovebox and used as received. Potassium was freshly cut prior to use.

1.2 Synthesis of **1**:

5 g (0.024 mol, 1 eq) of Pb and 3.81 g (0.048 mol, 2 eq) of Se are placed in a quartz ampule and heated for 5 min with an oxygen/methane burner. The homogenous melt is allowed to cool before being thoroughly grinded. 500 mg (1.369 mmol, 1 eq) of the resulting powder and 760 mg (2.875 mmol, 2.1 eq) of 18-crown-6 are vigorously stirred in 50 mL en while 112 mg (2.875 mmol, 2.1 eq) of K is added. The solution is stirred for 48 h, filtered and 10 mL of the resulting solution is carefully layered with 10 mL of a saturated THF solution of $[Rh(PPh_3)_3Cl]$. The resulting reaction mixture is allowed to stand for 2 weeks, filtered and the solution slowly evaporated to dryness. **1** crystallizes as black sticks in approx. 16% yield (with respect to Rh) along with an amorphous powder.

Synthesis of **2**:

5 g (0.024 mol, 1 eq) of Pb and 6.16 g (0.048 mol, 2 eq) of Te are placed in a quartz ampule and heated for 5 min with an oxygen/methane burner. The homogenous melt is allowed to cool before being thoroughly grinded. 500 mg (1.081 mmol, 1 eq) of the resulting powder is vigorously stirred in 50 mL en while 16 mg (2.3 mmol, 2.1 eq) of Li is added. The solution is stirred for 48 h, filtered and 10 mL of the resulting solution is carefully layered with 10 mL of a saturated THF solution of $[Pd(PPh_3)_2Cl_2]$. **2** crystallizes after 5 weeks as black blocks in approx. 12% yield (with respect to Pd) along with an amorphous powder.

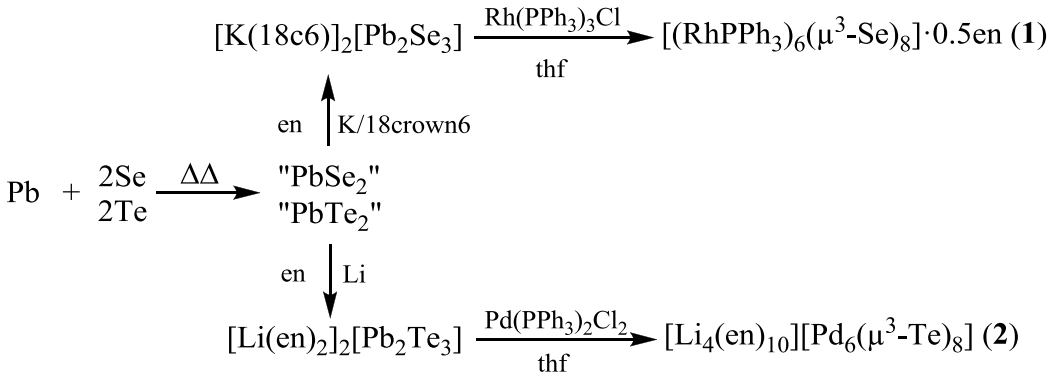

Figure S1. Reaction scheme towards **1** and **2**.

2. Crystal structure refinement details

Single-crystal X-ray data were collected on a Stoe IPDS-II (**1**) or a Stoe IPDS (**2**) diffractometer at 100 K (**1**) or 193 K (**2**), respectively with Mo-K_α radiation and a graphite monochromator (λ = 0.71073 Å). Upon numerical absorption correction (Stoe X-AREA), the structure solution was performed by direct methods, followed by full-matrix-least-squares refinement against F^2, using SHELXS-97, SHELXL-97, and OLEX2 software.[1] A summary of crystallographic and refinement details is given in Table S1. Figure S2 provides additional views of the $[Li_4(en)_{10}]^{4+}$ coordination network around the anionic $[Pd_6Te_8]^{4-}$ clusters observed in **2**.

Table S1. Crystal data and structure refinement details for **1** and **2**.

Identification code	$[(RhPPh_3)_6(\mu^3\text{-}Se)_8]\cdot en$ (**1**)	$[Li_4(en)_{10}][Pd_6(\mu^3\text{-}Te)_8]$ (**2**)
Empirical formula	$C_{109}H_{94}NP_6Rh_6Se_8$	$C_{10}H_{40}Li_2N_{10}Pd_3Te_4$
Formula weight	2852.92	1144.04
Radiation	MoK_α (λ = 0.71073)	MoK_α (λ = 0.71073)
Diffractometer type	STOE IPDS II	STOE IPDS
Temperature/K	100(2)	193(2)
Crystal system	triclinic	monoclinic
Space group	P-1	$P2_1/n$
a/Å	14.1332(6)	16.9445(19)
b/Å	14.5044(6)	10.3190(10)
c/Å	15.4160(7)	16.9561(18)
α/°	64.416(3)	90
β/°	67.409(3)	104.894(9)
γ/°	62.898(3)	90
Volume/Å^3	2467.3(2)	2865.2(5)
Z	1	4
ρ_{calc}mg/mm^3	1.9200	2.6520
μ/mm^{-1}	4.077	5.87
F(000)	1380.7	2070.0
Crystal size/mm^3	0.17 × 0.11 × 0.08	0.12 × 0.1 × 0.08
2Θ range for data collection/°	3.32 to 53.48	3.94 to 50.89
Reflections collected	31827	31974
Independent reflections	10392 [R_{int} = 0.0974]	5281 [R_{int} = 0.1639]
Absorption correction T_{min} / T_{max}	0.4622_/ 0.8080	0.4417 / 0.5695
Data/restraints/parameters	10392/106/633	5281/60/263
Goodness-of-fit on F^2	0.9532	0.9830
Final R indexes [$I>=2\sigma(I)$]	R_1 = 0.0417, wR_2 = 0.1016	R_1 = 0.0544, wR_2 = 0.1221
Final R indexes [all data]	R_1 = 0.0637, wR_2 = 0.1098	R_1 = 0.0624, wR_2 = 0.1262
Largest diff. peak/hole / e$^-$ Å^{-3}	3.0885/-1.1757	1.5454/-2.0356

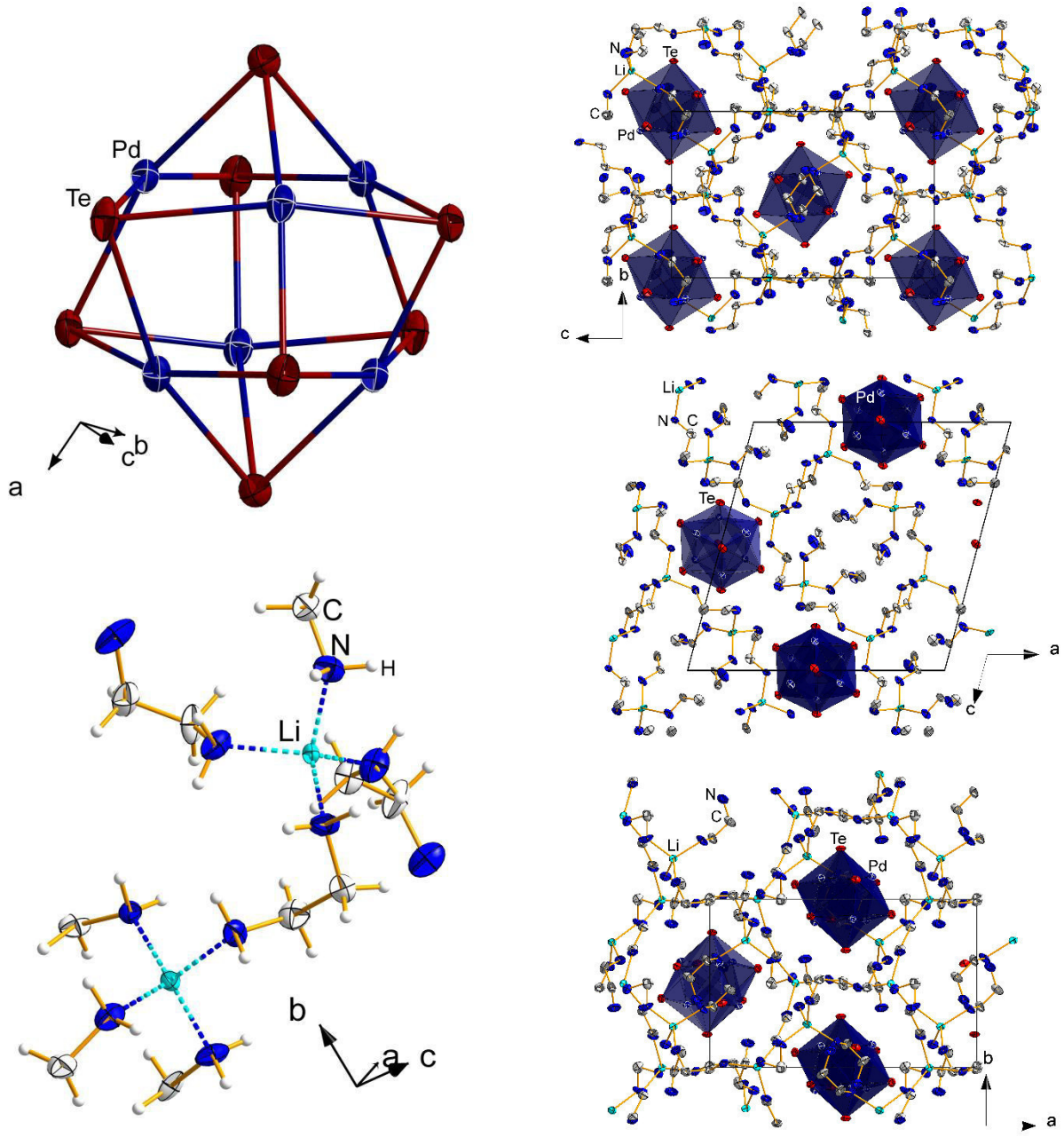

Figure S2. Left: Thermal ellipsoid diagram of the cluster in **2** and detailed representation of the coordination sphere at the Li^+ cations. Right: Three different views of the $[Li_4(en)_{10}]^{4+}$ network that embeds the CHEVREL-like $[Pd_6Te_8]^{4-}$ clusters in **2**, viewing down the crystallographic axes *a, b*, or c, respectively. The anions are highlighted by polyhedral representation. Ellipsoids are drawn at 50% probability, H atoms are omitted for clarity.

3. Energy dispersive X-Ray analysis results

EDX analyses were carried out using an EDX-device Voyager 4.0 of Noran Instruments coupled with an electron microscope CamScan CS 4DV. Data acquisition was performed with an acceleration voltage of 20 kV and 100 s accumulation time. The data were collected on various crystals and at multiple sites of the respective sample. Figures S3-S4 show representative spectra; Tables S2-S3 list mean values that were averaged over all values collected for each sample. Slight differences in observed and calculated atomic composition is caused by inhomogenous decomposition of the sample due to short contact with air and moisture during sample preparation.

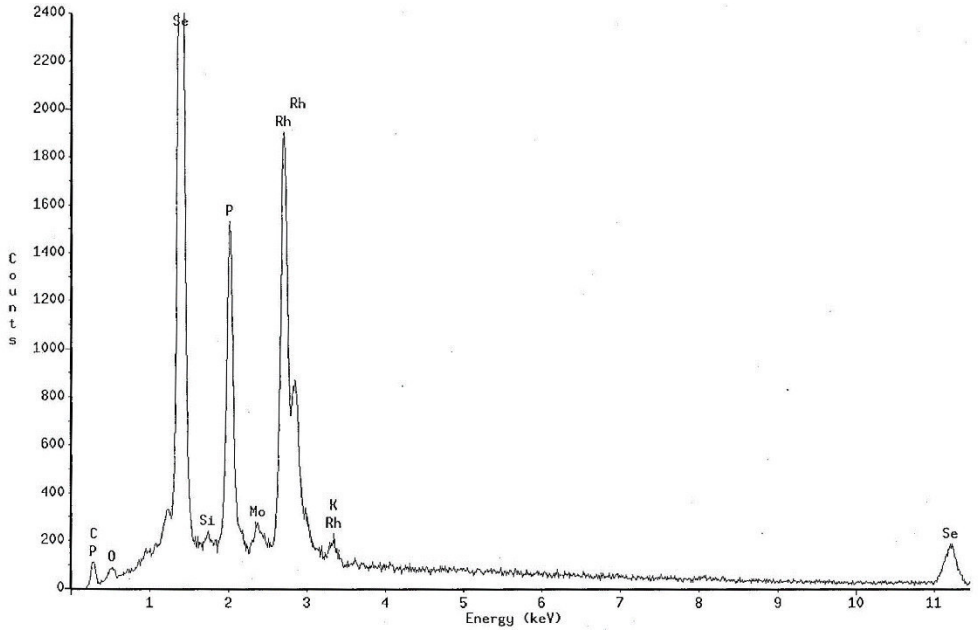

Figure S3. EDX spectrum of **1**.

Table S2. EDX results for **1**.

Element	k-ratio (calc.)	ZAF	Atom % (calc)	Element Wt %	Wt % Err. (1-Sigma)
Se-K	0.3796	0.989	43.93 (42)	37.55	+/- 2.34
Rh-L	0.5135	1.216	56.07 (57)	62.45	+/- 1.17
Total			100 (100)	100	

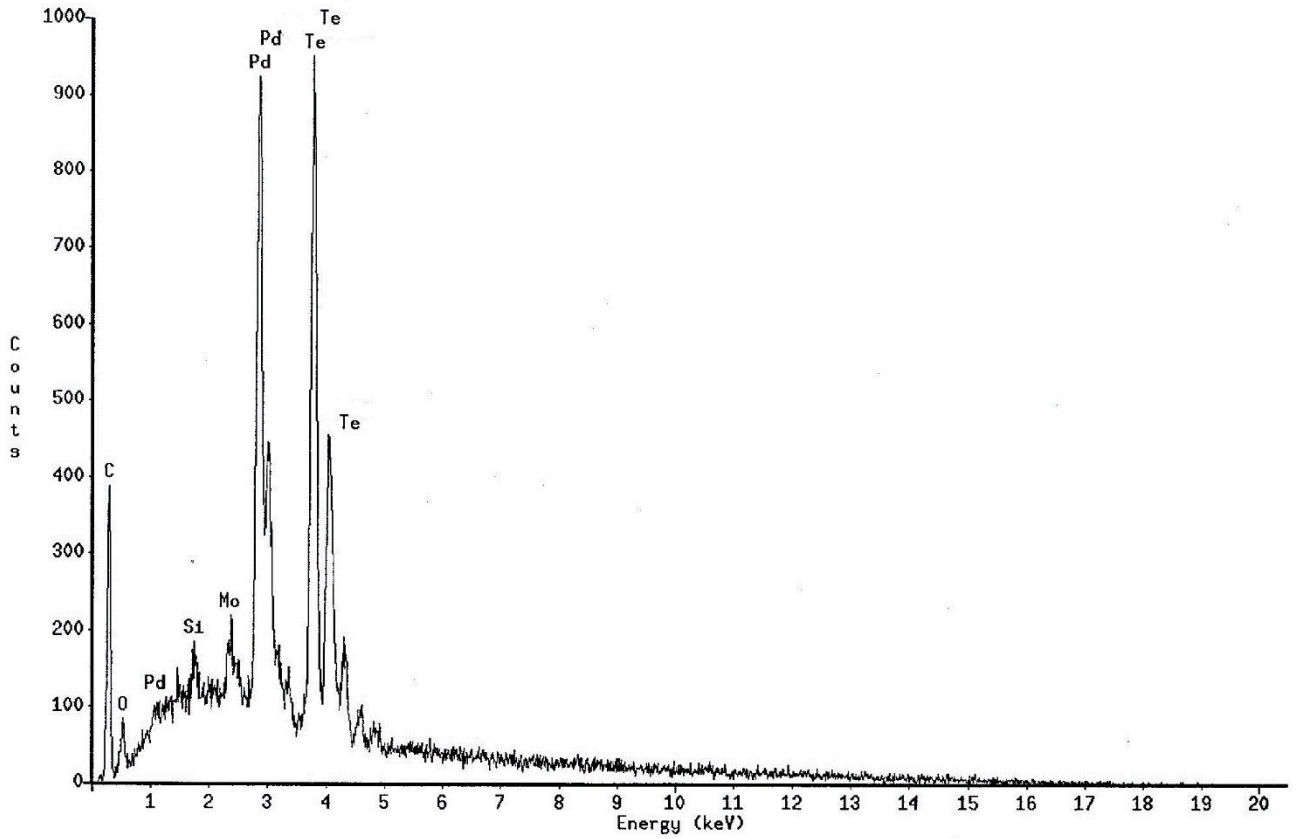

Figure S4. EDX spectrum of **2.**

Table S3. EDX results of **2.**

Element	k-ratio (calc.)	ZAF	Atom %	Element Wt %	Wt % Err. (1-Sigma)
Te-L	0.3998	1.002	44.50 (42)	40.07	+/- 2.95
Pd-L	0.5046	1.188	55.50 (48)	59.93	+/- 5.44
Total			100 (100)	100	

4. Quantum chemical calculations

4.1 Methods

DFT calculations were carried out with the program system TURBOMOLE[2] using the BP86 Functional[3] with def2-ECPs[4] and def2-TZVP basis sets[5] as well as respective auxiliary basis sets.[6] The COSMO solvation model[7] was applied to compensate molecular charges. Population analyses were applied via Mulliken analysis[8] with and without localization or via SEN.[9] Applied symmetry: C_1 (**1**), O_h (**2**).

Canonical molecular orbital diagrams for the clusters in **1** and **2** are shown in Figures S5 and S7. Localized molecular orbital diagrams are given in Figures S6 and S8, respectively. SEN values are summarized in Tables S4-S5 for **1** and in Table S6 for **2**.

Due to C_1 symmetry in **1**, which is caused by the relative orientation of phenyl rings of (PPh_3) ligands, no degeneracy occurred. Nevertheless, orbitals of similar energy and shape (yet different orientation) can be summarized (namely 600a/599a; 589a/597a/596a; 595a/594a/593a; g89a/588a and 585a/584a) and only one of them is shown in Figure S5 as a representative example.

For localized molecular orbitals, the corresponding orbital shapes for even more orbitals are alike: 601a, 600a-595a, 594a-580a. Therefore only few representatives are shown without consideration of respective energies.

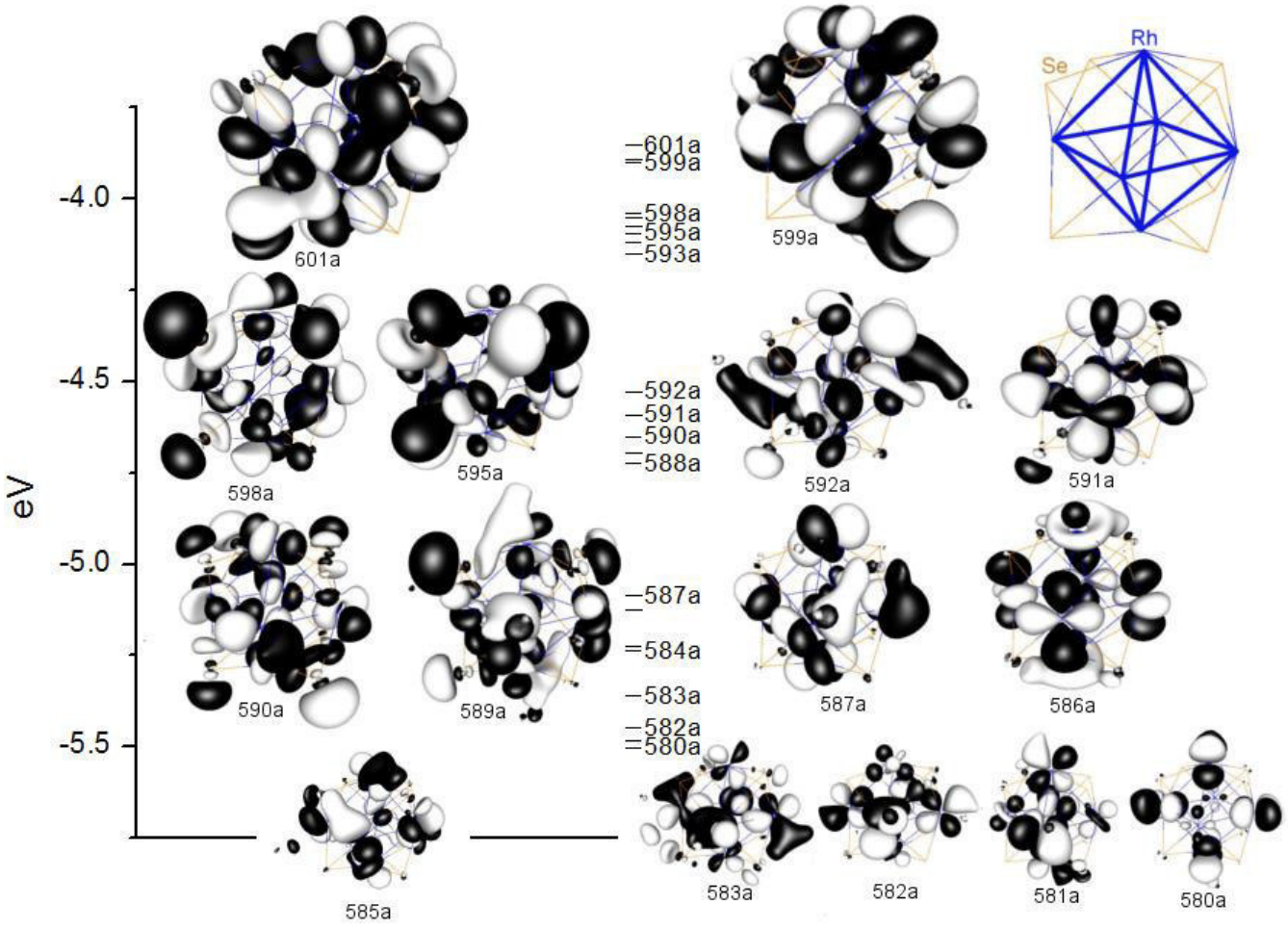

Figure S5. Molecular orbital diagram of **1**. (PPh_3) groups and minor contributions to orbitals are omitted for clarity. Threshold for orbital plotting set to +/−0.033 a.u.

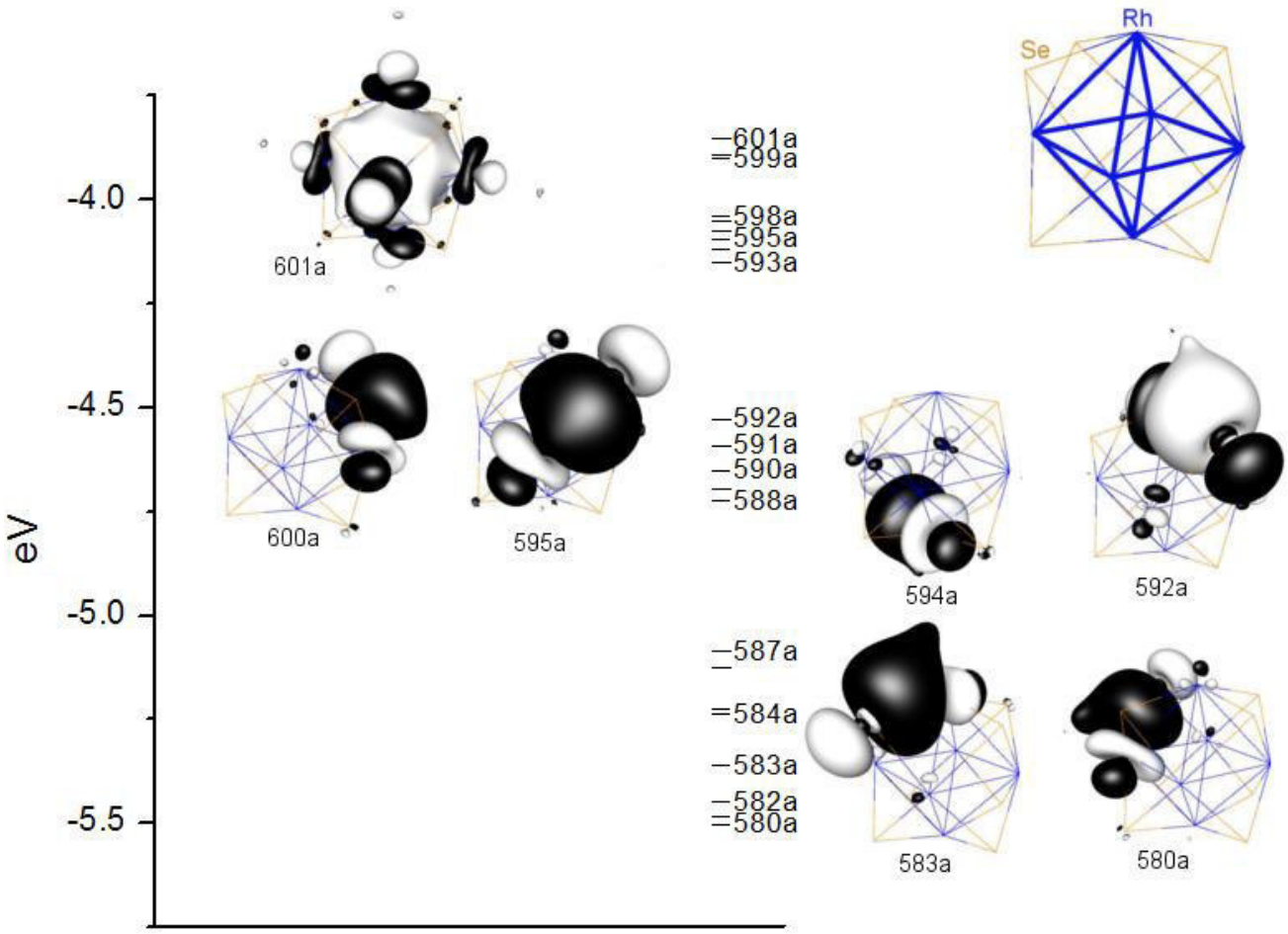

Figure S6. Localized molecular orbital diagram of **1**. (PPh_3) groups are omitted for clarity. Threshold for orbital plotting set to +/−0.033 a.u.. Mind that the energies can only be taken as a guide to the eye as they are lost during the localization procedure and artificially added thereupon.

Table S4. Two center shared electron numbers in **1** (restricted to Rh/Se).

14 Rh – 15 Se	0.4839	25 Rh – 73 Se	0.0355	15 Se – 52 Se	0.0942
14 Rh – 33 Se	0.0525	25 Rh – 74 Se	0.0526	15 Se – 72 Se	0.0947
14 Rh – 42 Se	0.0373	34 Rh – 15 Se	0.0373	15 Se – 74 Se	0.0906
14 Rh – 51 Se	0.0528	34 Rh – 33 Se	0.3963	33 Se – 42 Se	0.0905
14 Rh – 52 Se	0.0346	34 Rh – 42 Se	0.0528	33 Se – 51 Se	0.0945
14 Rh – 72 Se	0.4165	34 Rh – 51 Se	0.4758	33 Se – 73 Se	0.0941
14 Rh – 73 Se	0.4086	34 Rh – 52 Se	0.0356	42 Se – 52 Se	0.0932
14 Rh – 74 Se	0.3686	34 Rh – 72 Se	0.0576	42 Se – 72 Se	0.0882
16 Rh – 15 Se	0.3700	34 Rh – 73 Se	0.3917	51 Se – 52 Se	0.0945
16 Rh – 33 Se	0.0395	34 Rh – 74 Se	0.4481	51 Se – 74 Se	0.0881
16 Rh – 42 Se	0.0520	43 Rh – 15 Se	0.0395	72 Se – 73 Se	0.0945
16 Rh – 51 Se	0.3060	43 Rh – 33 Se	0.3700	73 Se – 73 Se	0.0932
16 Rh – 52 Se	0.4320	43 Rh – 42 Se	0.5097	Total Se – Se	1.1103
16 Rh – 72 Se	0.0529	14 Rh – 16 Rh	0.0616		
16 Rh – 73 Se	0.0360	14 Rh – 24 Rh	0.0899		
16 Rh – 74 Se	0.5092	14 Rh – 25 Rh	0.0561		
24 Rh – 15 Se	0.0523	14 Rh – 34 Rh	0.1616		
24 Rh – 33 Se	0.4821	14 Rh – 43 Rh	0.1193		
24 Rh – 42 Se	0.3698	16 Rh – 24 Rh	0.1195		
24 Rh – 51 Se	0.4157	16 Rh – 25 Rh	0.2162		
24 Rh – 52 Se	0.4084	16 Rh – 34 Rh	0.0606		
24 Rh – 72 Se	0.0526	16 Rh – 43 Rh	0.1050		
24 Rh – 73 Se	0.0347	24 Rh – 25 Rh	0.1603		
24 Rh – 74 Se	0.0371	24 Rh – 34 Rh	0.0576		
25 Rh – 15 Se	0.3952	24 Rh – 43 Rh	0.0615		
25 Rh – 33 Se	0.0374	25 Rh – 34 Rh	0.0953		
25 Rh – 42 Se	0.4455	25 Rh – 43 Rh	0.0606		
25 Rh – 51 Se	0.0576	34 Rh – 43 Rh	0.2168		
25 Rh – 52 Se	0.3932	Total Rh - Rh	1.6419		
25 Rh – 72 Se	0.4779				
43 Rh – 51 Se	0.0530				
43 Rh – 52 Se	0.0360				
43 Rh – 72 Se	0.3062				
43 Rh – 73 Se	0.4316				
43 Rh – 74 Se	0.0521				
Total Rh - Se	11.0933				

Table S5. Three center shared electron numbers in **1** (restricted to Rh/Se).

14Rh 15Se 16Rh	0.0708	14Rh 15Se 74Se	0.0114	14Rh 16Rh 24Rh	0.0553
14Rh 15Se 24Rh	0.0339	14Rh 33Se 51Se	0.0132	14Rh 16Rh 25Rh	0.0393
14Rh 15Se 25Rh	0.0508	14Rh 51Se 74Se	0.0106	14Rh 16Rh 34Rh	0.0516
14Rh 16Rh 33Se	0.0129	15Se 24Rh 72Se	0.0131	14Rh 16Rh 43Rh	0.053
14Rh 15Se 34Rh	0.0251	15Se 43Rh 72Se	0.0115	14Rh 24Rh 43Rh	0.0553
14Rh 16Rh 42Se	0.0137	16Rh 33Se 51Se	0.0115	14Rh 25Rh 34Rh	0.0611
14Rh 16Rh 74Se	0.0981	16Rh 42Se 72Se	0.0124	14Rh 25Rh 43Rh	0.0508
14Rh 24Rh 33Se	0.0338	24Rh 33Se 42Se	0.0113	14Rh 34Rh 43Rh	0.1152
14Rh 24Rh 51Se	0.0331	24Rh 42Se 72Se	0.0103	16Rh 25Rh 43Rh	0.0507
14Rh 24Rh 72Se	0.0329	25Rh 51Se 74Se	0.0123	16Rh 34Rh 43Rh	0.051
14Rh 25Rh 33Se	0.0145	34Rh 42Se 72Se	0.0123	24Rh 25Rh 34Rh	0.0608
14Rh 25Rh 51Se	0.0207	43Rh 51Se 74Se	0.0125	24Rh 25Rh 43Rh	0.0507
14Rh 25Rh 72Se	0.0779	Total Rh Se Se	0.1424	24Rh 34Rh 43Rh	0.0396
14Rh 34Rh 42Se	0.0209			Total Rh Rh Rh	0.7344
14Rh 34Rh 52Se	0.0163				
14Rh 34Rh 72Se	0.0332				
14Rh 34Rh 73Se	0.0443				
14Rh 34Rh 74Se	0.051				
14Rh 43Rh 51Se	0.0313				
14Rh 43Rh 52Se	0.0148				
14Rh 43Rh 72Se	0.0426				
14Rh 43Rh 73Se	0.1395	24Rh 25Rh 74Se	0.0208		
15Se 16Rh 25Rh	0.1416	24Rh 33Se 34Rh	0.051		
15Se 24Rh 34Rh	0.0144	24Rh 33Se 43Rh	0.0715		
15Se 24Rh 43Rh	0.0129	24Rh 34Rh 51Se	0.0779		
16Rh 25Rh 52Se	0.1344	24Rh 34Rh 72Se	0.0206		
16Rh 25Rh 74Se	0.0102	24Rh 42Se 43Rh	0.0981		
16Rh 34Rh 42Se	0.0238	24Rh 43Rh 74Se	0.0137		
16Rh 34Rh 51Se	0.0657	25Rh 34Rh 42Se	0.0303		
16Rh 34Rh 72Se	0.0227	25Rh 34Rh 51Se	0.0362		
16Rh 34Rh 74Se	0.084	25Rh 34Rh 72Se	0.0361		
16Rh 42Se 43Rh	0.0272	25Rh 34Rh 74Se	0.0301		
16Rh 43Rh 51Se	0.0382	25Rh 42Se 43Rh	0.0843		
16Rh 43Rh 72Se	0.0382	25Rh 43Rh 51Se	0.0227		
16Rh 43Rh 74Se	0.0272	25Rh 43Rh 72Se	0.0651		
24Rh 25Rh 33Se	0.0258	25Rh 43Rh 74Se	0.0237		
24Rh 25Rh 42Se	0.0492	33Se 34Rh 43Rh	0.1414		
24Rh 25Rh 51Se	0.034	34Rh 42Se 43Rh	0.0104		
24Rh 25Rh 52Se	0.044	34Rh 43Rh 73Se	0.1344		
24Rh 25Rh 73Se	0.0162	Total Rh Rh Se	2.6901		

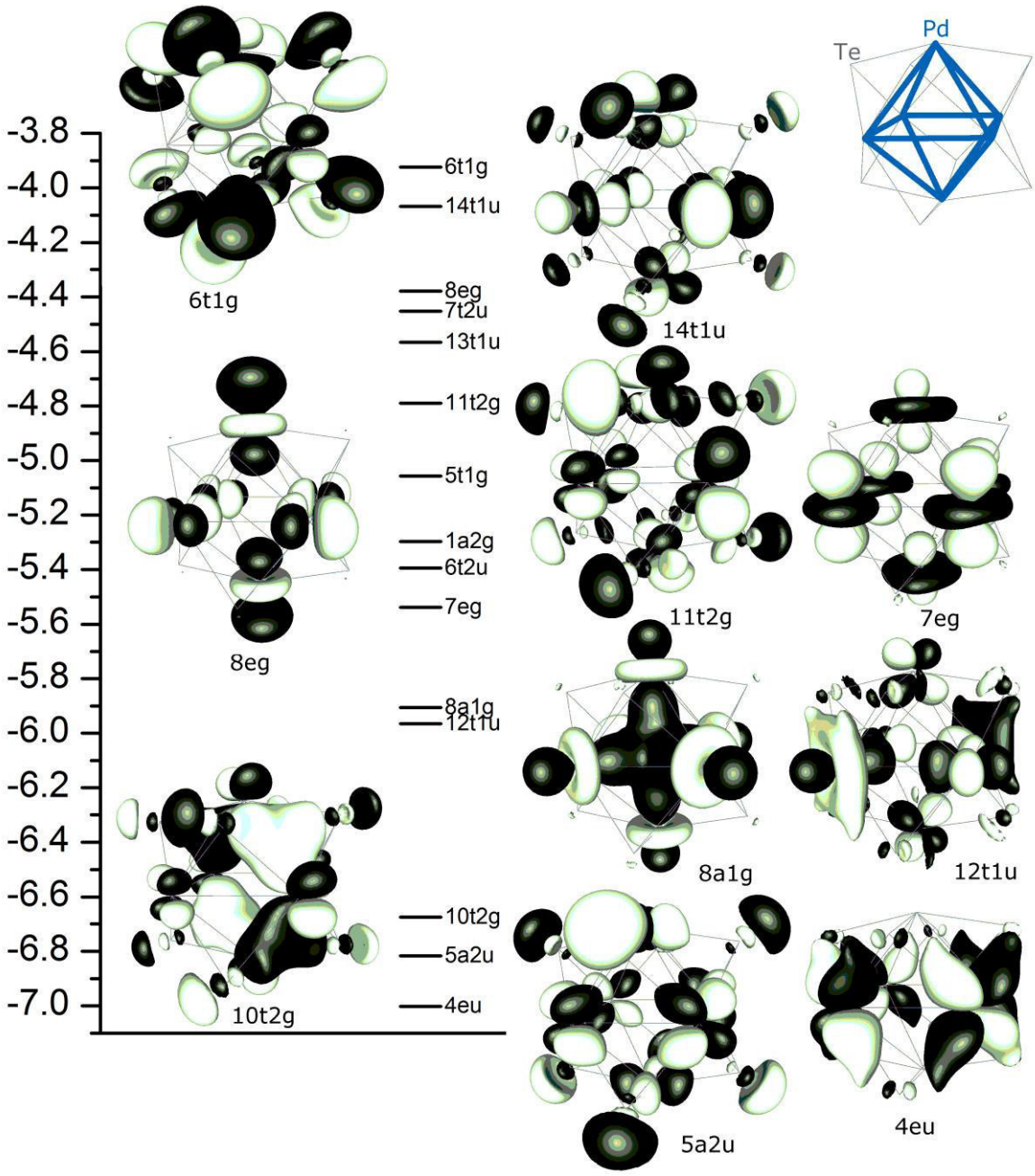

Figure S7. Molecular orbital diagram of **2**. Threshold for orbital plotting set to +/−0.033 a.u.

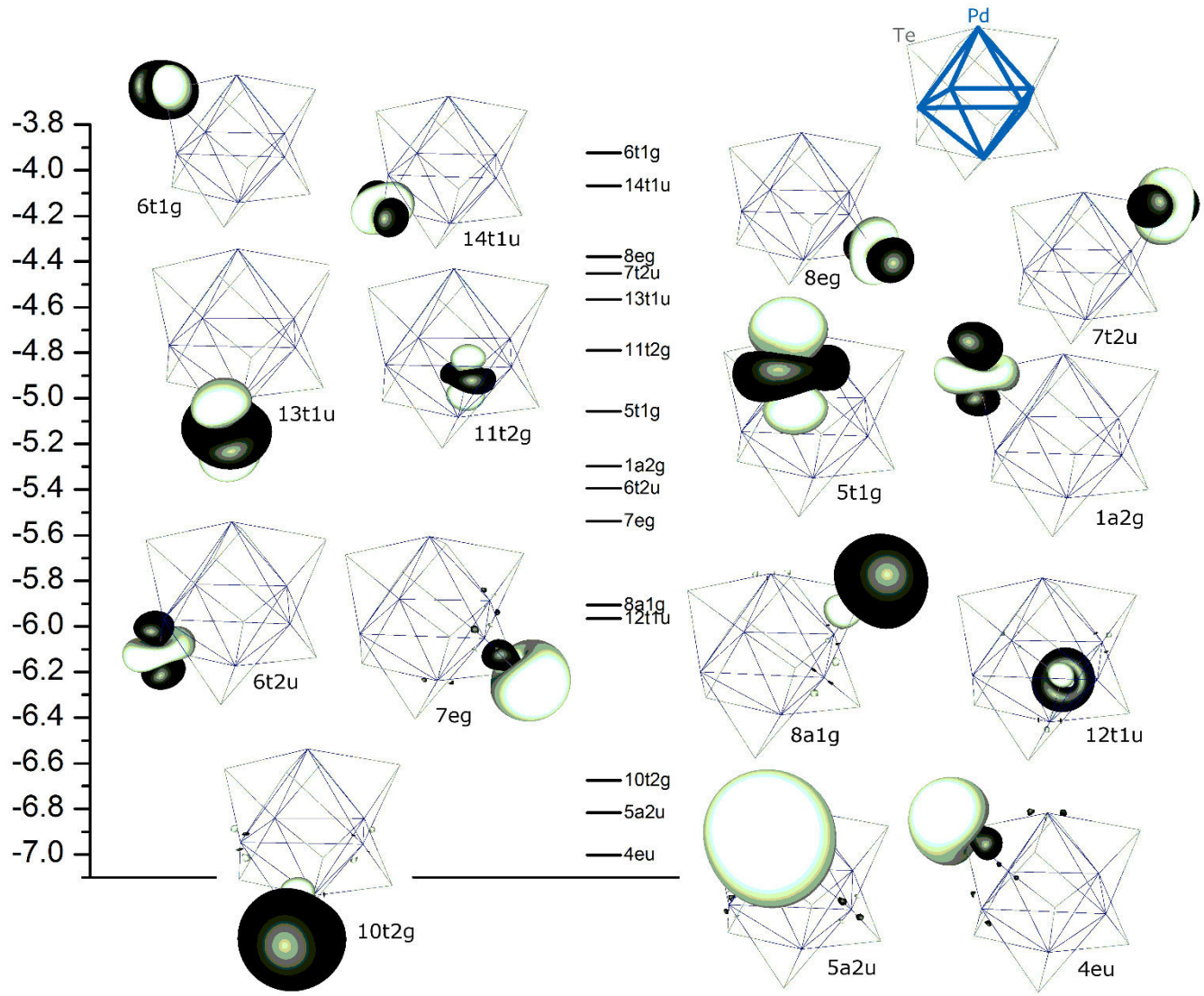

Figure S8. Localized molecular orbital diagram of **2**. Threshold for orbital plotting set to +/−0.033 a.u.. Mind that the energies can only be taken as a guide to the eye as they are lost during the localization procedure and artificially added thereupon.

Table S6. Shared electron numbers in **2**.

Two center SEN	Te – Pd	0.3756
	Te – Te	0.1399
Three center SEN	Te – Pd - Te	0.0453
	Te – Pd - Te	-0.2603

5. Cyclovoltammetric measurement results

The cyclovoltammetric measurements (Figures S9-S10) were done under Ar atmosphere at 25 °C, using 0.1 mol/L [nBu$_4$N][PF$_6$] (TBFP) as the supporting electrolyte. Working and counter electrodes: Pt; scan rate: 50 mV/s.

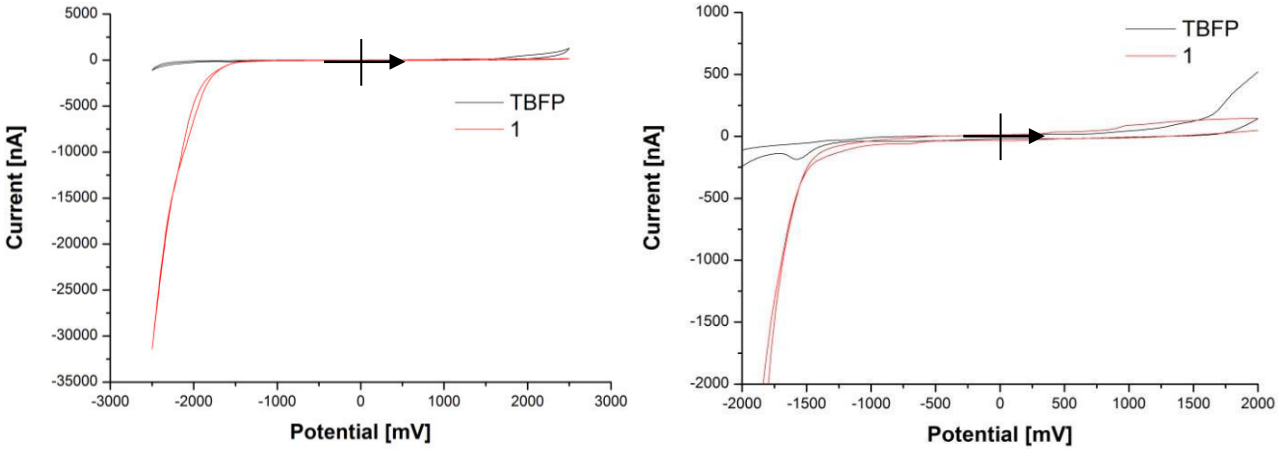

Figure S9. Left: Cyclic voltammogram of **1** (red), recorded at platinum electrode in a CH_2Cl_2 solution (1.20 mM), in the presence of TBFP (0.1 M). Also shown for comparison is voltammogram of a 0.1 mM TBFP/DCM solution (black). Scan ranges and rates: –2.5 to +2.5 V, 50mV/s. Right: Zoom into the oxidation side of the peak.

Instead of two discrete oxidation processes that are expected from the twofold $Rh^{II} \rightarrow Rh^{III}$ oxidations in CH_2Cl_2, a remarkable, very large negative peak potential in the cathodic scan has been observed, indicating $Rh^{III} \rightarrow Rh^{II}$ reduction. Previous studies by cathodic stripping voltammetry (CSV) analysis to selectively detect redox processes in selenium compounds indicated that accumulation of M^{n+} selenides on the electrode surfaces, which occurred upon reduction of $M^{(n+1)+}$ selenides (M = Cu, Hg, Rh, for instance), led to respective chemical responses – in an extraordinarily strong manner in the case of rhodium.[10] We therefore assume decomposition of the cluster during the twofold oxidation such that the reduction peak monitors the reduction of Rh(III)Se. This may additionally explain the lack of any steps on the reduction side. In contrast to the strong reduction signal, an $Rh^{II} \rightarrow Rh^{III}$ oxidation could not be clearly observed. Beside the high oxidation potential of $Rh^{II} \rightarrow Rh^{III}$, this is probably due to the accumulation of rhodium selenide on the electrode that inhibits the diffusion of material to the electrodes and thus reduces the oxidation current. The very combination of electrolyte and solvent additionally limits the experimental resolution, as the background current increases with increasing potentials owing of the oxidation of the electrolyte and/or solvent. In the current system, this obviously caused an overlap of the latter with the $Rh^{II} \rightarrow Rh^{III}$ peak.

However, by performing the measurements in CH_3CN, it was possible to detect a stepwise two-electron oxidation (prior to decomposition, see above) both in the CV and the DPV experiment (see Figure S10 and Figure 3 in the main text), in accordance with the proposed composition of the cluster.

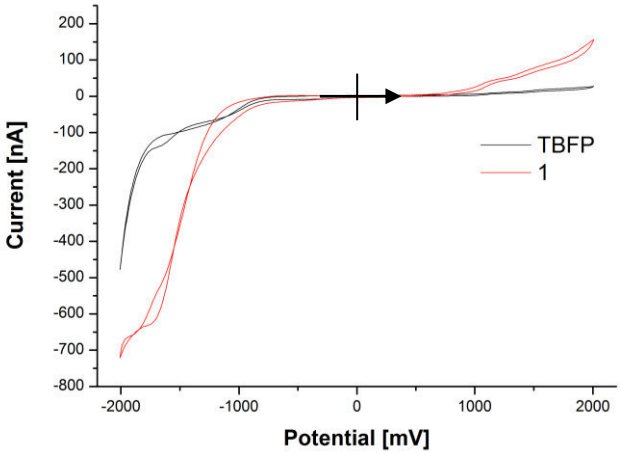

Figure S10. Cyclic voltammogram of **1** (red), recorded at platinum electrode in a MeCN solution in the presence of TBFP (0.1 M). Also shown for comparison is the voltammogram of a 0.1 mM TBFP/MeCN solution (black). Scan ranges and rates: –2 to +2 V, 50mV/s.

6. References for the Supporting Information

[1] (a) Sheldrick, G. M. SHELXL97, Program for the Refinement of Crystal Structures, Universität Göttingen, 1997. (b) Dolomanov, O. V.; Bourhis, L. J.; Gildea, R. J.; Howard, J. A. K.; Puschmann, H. *J. Appl. Crystallogr.* **2009**, *42*, 339.

[2] TURBOMOLE V6.4 2012, a development of University of Karlsruhe and Forschungszentrum Karlsruhe GmbH, 1989-2007, TURBOMOLE GmbH, since 2007; available from http://www.turbomole.com.

[3] (a) Becke, A. D. *Phys. Rev. A* **1988**, *38*, 3098. (b) Perdew, J. P. *Phys. Rev. B* **1986**, *33*, 8822.

[4] (a) Metz, B.; Stoll, H.; Dolg, M. *J. Chem. Phys.* **2000**, *113*, 2563. (b) Peterson, K. A.; Figgen, D.; Dolg, M.; Stoll, H. *J. Chem. Phys.* **2007**, *126*, 124101.

[5] Weigend, F.; Baldes, A. *J. Chem. Phys.* **2010**, *133*, 174102.

[6] Weigend, F. *Phys. Chem. Chem. Phys.* **2006,** *8*,1057.

[7] Klamt, A.; Schürmann, G. *J. Chem. Soc. Perkin Trans.* **1993**, *5*, 799.

[8] Mulliken, R. S. *J. Chem. Phys.* **1955**, *23*, 1833.

[9] Ehrhardt, C.; Ahlrichs, R. *Theor. Chim. Acta*, **1985**, *68*, 231.

[10] (a) Lange, B.; van den Berg, C. M. G. *Anal. Chim. Acta.* **2000**, *418*, 33. (b) Wang, J.; Lu, J. M. *Anal. Chim. Acta.* **1993**, *274*, 219.

IV

{μ-PbSe}: The Second Heaviest CO Homolog as an Unexpected Ligand

G. Thiele, S. Dehnen, Manuskript in Vorbereitung.

The reaction of a solution containing $[Pb_2Se_3]^{2-}$ anions with $[Rh(PPh_3)_3Cl]$ yields Rh-Se cluster compounds with a μ-PbSe Ligand. Quantum chemical investigations reveal a strongly ionic Pb–Se double bond and an analogy to the bonding as found in CO complexes.

Themenkomplex $[M_xCh_y]^{q-}$, Synthese und Reaktivität

Inhalt: Die Verbindungen $\{[K(18\text{-Krone-}6)][K(en)_2]K[Rh_3Se_2(CN)_2(PPh_3)_4(PbSe)]\}_2 \cdot 1.3en$ und $[K([2.2.2]Krypt)][(\mu^3\text{-}Se)_2(\mu\text{-}Rh(PPh_3)_2)_3] \cdot 3C_6H_6$ werden als Produkte der Reaktionen von Ethylendiamin-Lösungen des $[Pb_2Se_3]^{2-}$-Anions mit $[Rh(PPh_3)_3Cl]$ in Gegenwart unterschiedlicher Sequestrierungsreagenzien erhalten und bezüglich ihrer Kristallstruktur diskutiert.

Beide Anionen wurden quantenchemischen Analysen unterzogen. In Kombination mit Rechnungen an den (hypothetischen) Fragmenten PbSe, PPh_3 und CN^- wird auf eine exoenergetische Bildungsreaktion des ersteren aus letzterem geschlossen. Ein hypothetischer, CO-verbrückter Cluster wird ebenfalls quantenchemisch simuliert, und die sehr unterschiedlichen Bindungssituationen in beiden Verbindungen werden ausgiebig beleuchtet.

Eigener Anteil: Alle Experimente wurden von mir geplant. Die experimentelle Durchführung wurde unter meiner Anleitung durch Maximilian Fritz, Maximilian Jost und Maximilian Biermeier im Rahmen von Vertiefungspraktika und auch von Marcus Müller durchgeführt. Die quantenchemischen Untersuchungen wurden von mir durchgeführt und zusammen mit Stefanie Dehnen ausgewertet. EDX-Analysen wurden von Thomas Krüger durchgeführt. Das Manuskript wird derzeit von Stefanie Dehnen und mir gemeinsam verfasst.

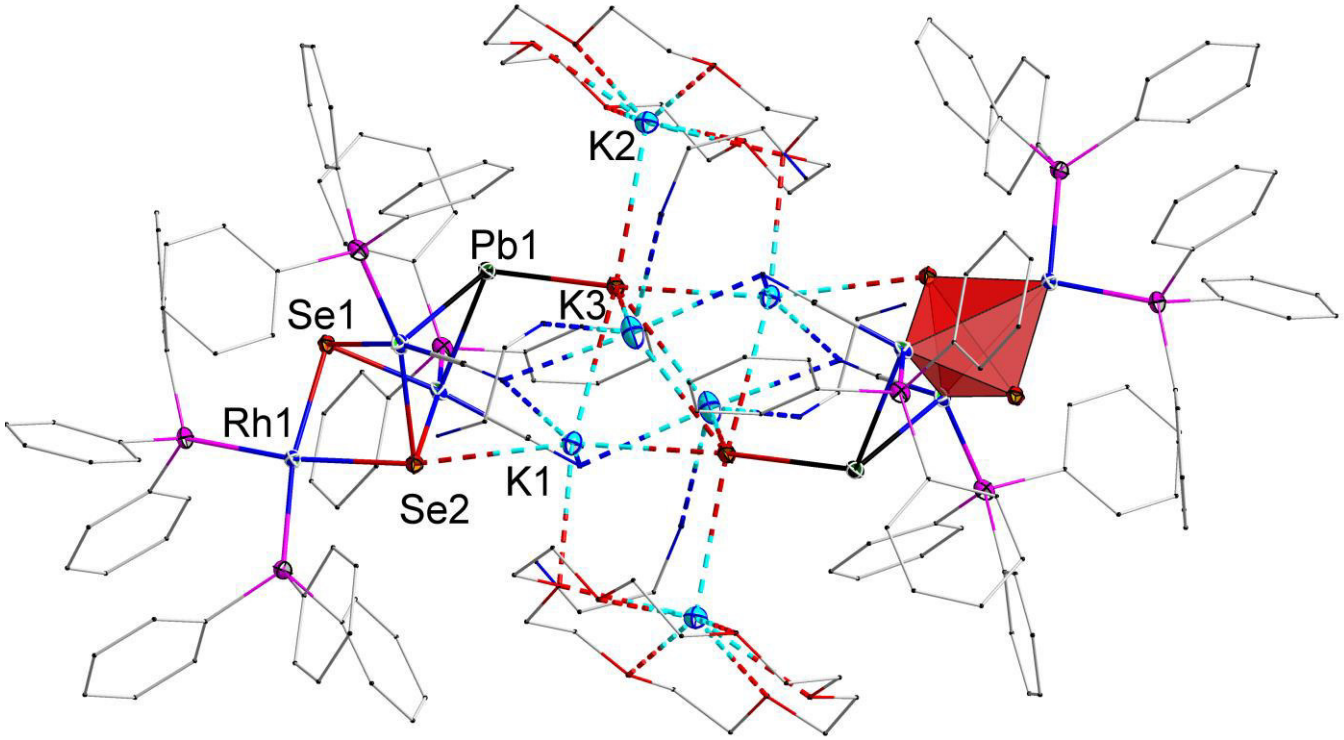

Abbildung 24. Ausschnitt aus der Kristallstruktur von $\{[K(18\text{-Krone-}6)][K(en)_2]K[Rh_3Se_2(CN)_2(PPh_3)_4(PbSe)]\}_2 \cdot 1.3en$.

{μ-PbSe}: The Second Heaviest CO Homolog as an Unexpected Ligand

Günther Thiele and Stefanie Dehnen*

Abstract: Reactions of $[K(18\text{-}crown\text{-}6)]_2[Pb_2Se_3]$ or $[K([2.2.2]crypt)]_2[Pb_2Se_3]$ with $[Rh(PPh_3)_3Cl]$[22] in *en* (ethane-1,2-diamine) afforded ionic compounds with $[Rh_3(PPh_3)_6(\mu_3\text{-}Se)_2]^-$ and $[Rh_3(CN)_2(PPh_3)_4(\mu_3\text{-}Se)_2(\mu\text{-}PbSe)]^{3-}$ anions, respectively. The latter comprises a PbSe ligand, thus a very uncommon homolog of C≡O, that acts as μ-bridge between two Rh atoms.

The meaningfulness of C≡O, both as ligand or reactant, can hardly be overestimated. Publication of a total of 43 reviews in *Angewandte Chemie*, 41 in *Chemical Reviews* and more than 50 in *Coordination Chemistry Reviews* within the last decade reflects the huge diversity of synthesis and catalytic applications of carbon monoxide and its compounds.

In contrast, apart from matrix isolation experiments,[1] the corresponding (coordination) chemistry of the heavier homologs of CO, thus the neutral molecular tetrel monochalcogenides TCh (T = C…Pb; Ch = O…Te), is restricted to complexes with chalcogenocarbonyls CS, CSe and CTe.[2] All others were only discussed in the course of spectroscopic[3-7] and theoretical[4-17] studies of intermediate species, such as molecular PbO that was obtained under single-collision conditions from atomic Pb and O_3.[18]

The reason for the obvious difference between the chemistry of C≡O and that of its higher homologs has been put down to the distinctly lower bond strength of the corresponding "triple" bond with increasing atomic number, and therefore a higher tendency towards aggregation – ultimately yielding the corresponding minerals, such as litharge or massicot in the case of PbO.[19] Nevertheless, according to periodic calculations on PbO and PbS minerals, the nature and role of the lone pair at the Pb atom is reported to be strongly influenced by the corresponding chalcogenide, ranging from small contributions (due to the possibility of state mixing) in PbO to rather high electron density in the lone pair region of PbS.[8] Following this trend, a high electron density on the tetrel atom, as in C≡O, is expected within the heavier homologs of the Pb≡Ch (Ch = Se, Te) series, which will be discussed herein.

At the synthesis of the mixed-valence compound $[(RhPPh_3)_6(\mu_3\text{-}Se)_8]$[20] (**A**) from solutions of $[K(18\text{-}crown\text{-}6)]_2[Pb_2Se_3]$[21] and $[Rh(PPh_3)_3Cl]$[22] in *en* (ethane-1,2-diamine), we detected small amounts of $\{[K(18\text{-}crown\text{-}6)][K(en)_2]K[Rh_3(CN)_2(PPh_3)_4(\mu_3\text{-}Se)_2(\mu\text{-}PbSe)]\}_2 \cdot 1.3en$ (**1**, approx.. XX%; Figure 1), as a well-reproducible side-product.

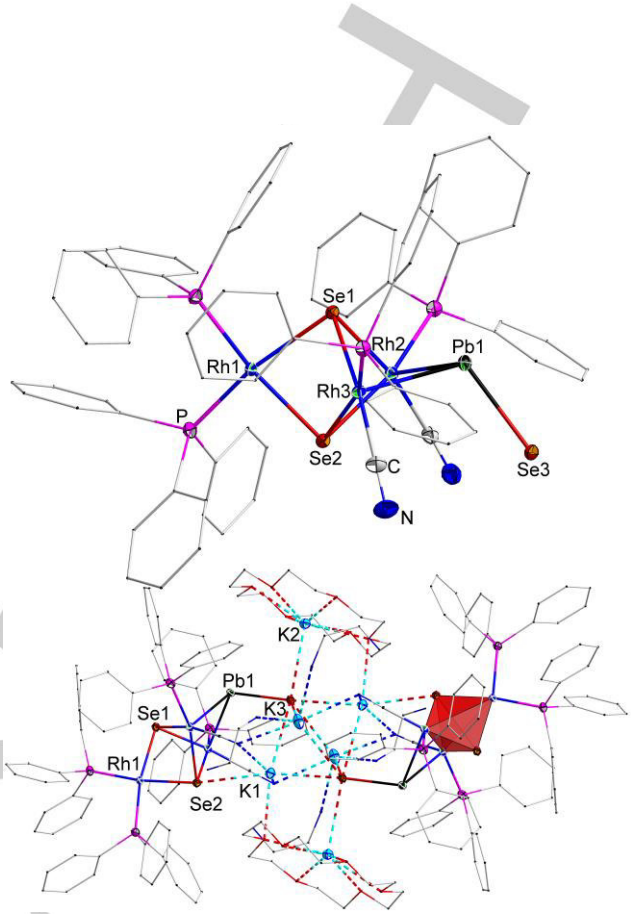

Figure 1. Top: Molecular structure of the anion in **1**. Ellipsoids are drawn at 50% probability. Disorder of Se3 atom (see Figure S1) and H atoms are omitted for clarity. Phenyl groups are drawn as wires. Selected structural parameters [Å/°]: Rh–Se 2.4563(4)-2.4868(5), Rh–Pb 2.7542(3)-2.7576(3), Pb–Se 2.647(4) and 2.7105(6) (disorder), Rh(1,2)…Rh3 XXX-XXX, Rh1…Rh2 XXX-XXX, K…Se2 3.2331(9) Å, K…Se3 3.165(5)-3.593(2); Rh–Pb–Rh 64.972(9), Se–Pb–Rh 106.54(10)-119-09(8), Se–Rh–Pb 83.691(12)-83.773(12) and 103.701(13)-103.959(13), Se–Rh–Se 79.333(14)-80.273(14), Pb–Rh–P 92.34(3)-94.06(3). Bottom: Dimeric unit in **1** with one $[Rh_3Se_2]$ polyhedron highlighted. Organic groups are drawn as wires. Non-coordinating solvent molecules are omitted for clarity.

The anion in **1** (Figure 1, top) is based on an $[Rh_2Se_3]$ trigonal bipyramid, with two μ_3-Se bridges (Se1, Se2) in apical and three Rh atoms (Rh1-Rh3) in basal positions. At first glance, the Rh atoms adopt an approximately square planar coordination by two Se atoms (cis) and two further ligands: two PPh_3 groups at Rh1, or one PPh_3 and one CN^- ligand at Rh2 and Rh3. However, the bonding environment of the latter is extended towards a (distorted) square pyramid by a μ-bridging Pb atom (Pb1) that is bonded to an Se atom (Se3). Pb1, in turn, forms three bonds (Pb1–Rh2, Pb1–Rh3, and Pb1–Se3) in a trigonal pyramidal manner, which is in accordance with the expectation for a formal Pb^{II} atom.

Two complexes are ever interconnected by a total of six K^+ ions around an inversion center of the unit cell. While Se1 does not show significant interactions with the K^+ couterions, and Se2 has only one notable Se…K^+ contact (3.2331(9) Å), Se3 coordinates

[a] Dipl.-Chem. G. Thiele, Prof. Dr. S. Dehnen
Fachbereich Chemie und Wissenschaftliches Zentrum für Materialwissenschaften, Philipps-Universität Marburg
Hans-Meerwein-Straße 4, D-35032 Marburg (Germany)
Fax: (+49) 6421-282-5653
E-mail: dehnen@chemie.uni-marburg.de

Supporting information for this article is available on the WWW under http://dx.doi.org/10.1002/anie.xxx.

to five K^+ ions, thus adopting a near octahedral μ_6-bridging mode in the sum. One of the K^+ ions (K2) is additionally coordinated by a 18-crown-6 molecule, the others show a multiple ligand situation including one further O atom per crown ether molecule, both N atoms of the CN^- ligands and N atoms form solvent *en* molecules besides one (K2, K3) or two (K1) Se neighbors.

The list of crystallographically determined compounds that comprise a Pb–Se interactions of any kind can be classified into three groups, (a) inorganic solid state phases, ranging from binary PbSe (clausthalite[23] or two high pressure modifications[24,25]) and $PbSe_2$[26] to multinary phases such as $Cd(In_{0.4}Bi_{0.6})PbBi_3(Se_{0.05}S_{0.95})_8$,[27] (b) (element-)organic compounds without any further Pb–M or Se–M bonds (M ≠ Pb), such as $Ph_3Pb(\mu\text{-}Se)P(OEt)_2Se$[28] or $(AsPh_4)[Pb(SePh)_3]$,[29] and (c) a total of three complexes with further Se–M (but no Pb–M) bonds, namely $[(Pt(PPh_3)_2)_2(PbSe_2)]NO_3{\cdot}CH_2Cl_2$,[30] $(PPh_4)_4[Pb_2W_4Se_{16}]$,[31] and $[Eu\{Pb(SePh)_3\}(thf)]$.[32] In the latter three cases, coordination to further metal ions is always achieved *via* Se, and Pb ions are at least bound to two Se atoms. Thus, apart from **1**, none of the compounds known to date comprise a PbSe fragment with a coordination behavior reminding of that of of CO, i.e., *via* the Pb atom.

The origin of the CN^- ions is likely a result of C–N bond cleavage occurring to the solvent *en* – as the only C/N source within the reaction solution (possibly under assistance of the $[Rh(PPh_3)_3Cl]$ complex or an intermediate Rh species, and/or Se),[ref] see equation (1). Intentional addition of KCN to the reaction solution increases the reaction yield of single-crystals of **1** by a factor of three.

$$H_2N\text{–}CH_2\text{–}CH_2\text{–}NH_2 \xrightarrow{\text{<Rh/Se>}} 2\ CN^- + 2\ H^+ + 3\ H_2 \qquad (1)$$

Further attempts to increase the yield by variation of the solvent only afforded solvent isomers of **1**,[33] while the exchange of 18-crown-6 with [2.2.2]crypt by utilization of $[K([2.2.2]crypt)]_2[Pb_2Se_3]$[34] as the starting material leads to the formation of $[K([2.2.2]crypt)[Rh_3(PPh_3)_6(\mu_3\text{-}Se)_2]{\cdot}3C_6H_6$ (**2**). The latter is also based on an $[Rh_3Se_2]$ trigonal bipyramid, but unlike the situation in **1**, all Rh atoms exhibit an approximately square planar coordination by two selenium atoms and two PPh_3 ligands (see Figure 2).

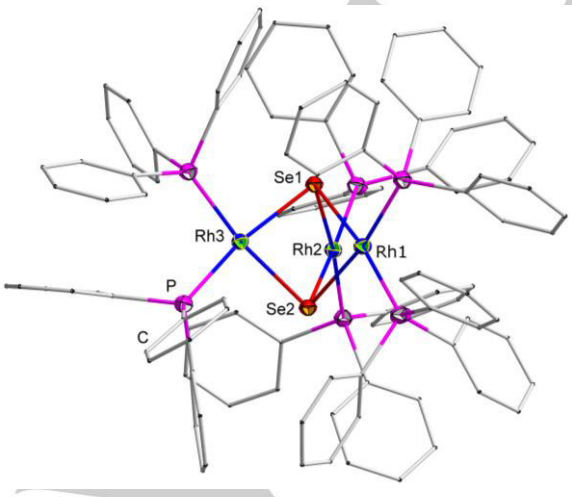

Figure 2. Molecular structure of the $\{[(Ph_3P)_2Rh]_3(\mu_3\text{-}Se)_2\}^-$ anion in **2**. Ellipsoids are drawn at 50% probability, H atoms are omitted, C atoms are drawn as wires. Selected structural parameters [Å/°]: Rh–P 2.2307(7)-2.2372(7), Rh–Se 2.4619(3)-2.4701(3), Rh(1,2)…Rh3 XXX-XXX, Rh1…Rh2 XXX-XXX; Se–Rh–Se 79.493(10)-79.598(10), Rh–Se–Rh 81.802(10)-85.775(10), P–Rh–P 98.89(3)-101.18(3), P–Rh–Se 88.76(2)-91.743(19).

To further investigate the properties of the highly uncommon and unexpected PbSe ligand, its similarities with or differences from the CO homolog, and its μ-bridging interaction with the Rh/Se cluster, comprehensive quantum chemical calculations were performed using density functional theory methods implemented in the program system TURBOMOLE.[35-45] The calculations served to answer the following questions: (1) Can the anion in **1** form from that in **2** and how are the energetics for a hypothetical CO-bridged homolog? (2) What are the differences between molecular PbSe and CO and how does this affect the bonding in the anion in **1** and the hypothetical CO homolog?

To answer the first question, we simultaneously optimized the electronic and geometric structures of the anions in **1** and **2** (maximum deviations of bond lengths: ±XXX pm in **1**, ±XXX pm in **2**), as well as those of all further reactants along a formal reaction pathway from the latter to the first, i.e., PPh_3, $(CN)^-$, and PbSe, For comparison, the CO homolog of the anion in **1** and CO itself were calculated by the same methods. Scheme 1 summarizes the results.

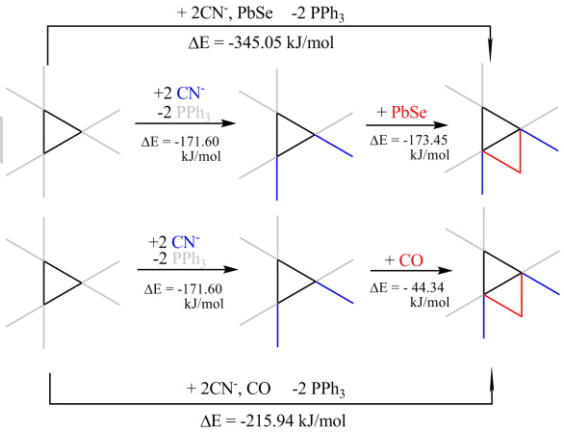

Scheme 1. Calculated reaction pathway from the anion in **2** to the anion in **1** (top) or to a hypothetical CO homolog (bottom). Black triangles represents the $[Rh_2Se_2]$ unit, grey terminal lines denote PPh_3 ligands, black terminal lines denote $(CN)^-$ ligands. Total energies of all species are provided in Table SX.

As shown in Scheme 1, both the formation of the anion in **1** and its hypothetical CO-bridged homolog, from the anion in **2** are exoenergetic, with a distinctly larger energy difference in the case of the PbSe-bridged cluster. This indicates that the Rh–(μ-PbSe)–Rh interaction is not only efficient, but even stronger than a corresponding CO bridge. For that, to answer the second question, we inspected the bonding situation into detail, starting out from a comparison of the molecular orbital (MO) schemes of isolated CO and PbSe molecules (Figure 3).

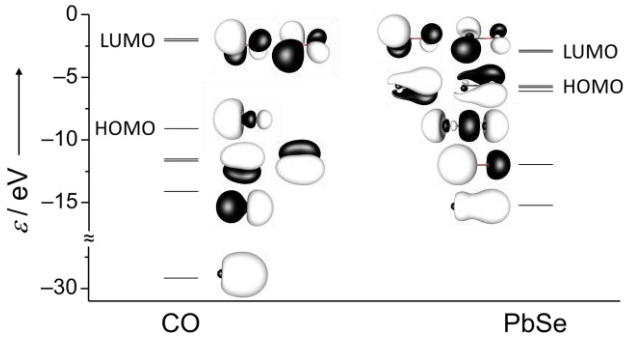

Figure 3. MO scheme of the frontier MO region of CO (left) and PbSe (right). Amplitudes are plotted at ±0.033 a.u..

The MO schemes of CO and PbSe differ significantly. (a) The large HOMO-LUMO gap in CO (5.7 eV) is reduced to 2.9 eV in PbSe, (b) rather similar energy differences between HOMO and HOMO–1 and HOMO–1 and HOMO–2 in CO (ca. 2.6 and ca. 2.4 eV, respectively), are replaced by very unequal differences in PbSe (ca. 1.2 and ca. 7.1 eV, respectively), (c) the two highest occupied MOs (e and a) show an inverse energetic order, and (d) all MOs differ in the distribution of the electron density over the molecule. Whereas the HOMO of CO contributes to the $2p_C$-$2p_O$ σ-bond with a much larger MO coefficient at the (σ-donor) C atom, the HOMO in PbSe represents a weak $6p_{Pb}$–$3p_{Se}$ π-bond with a somewhat larger contribution of the Se 3p-AO. A σ-donor activity of PbSe is hence to be realized via HOMO–1; however, as in HOMO, the electron density is shifted slightly toward the Se atom here. HOMO–2 is largely non-bonding $6s_{Pb}$-AO in PbSe with a negligible $3p_{Se}$ contribution, whereas in CO, it represents a rather balanced $2s_C$-$2p_O$ σ-interaction with somewhat larger contribution of the $2p_O$ AO. In sum, the MO schemes indicate a rather ionic situation in the PbSe molecule, which is better represented by $^{+}\overline{Pb}$–$\underline{\overline{Se}}|^{-}$ than by $^{-}|Pb{\equiv}Se|^{+}$.

A a consequence of this difference, also the MO schemes of the anion in **1** and that of the corresponding CO homolog differ markedly. One might imagine the formation of the anions as shown in Scheme 1, thus starting out from the anion in **2**.

For the (PPh_3)-decorated complex in **2**, the molecular orbital (MO) diagram reveals a mixture of Rh-centered lone pairs with some contribution of (i.e. bonding interactions with) Se atoms for HOMO and all lower-energy MOs down to HOMO-16. On replacing two PPh_3 ligands with $(CN)^{-}$, the situation does not change dramatically – a minor contribution of the $(CN)^{-}$ ligands is recogniced ad HOMO-11 and HOMO-12.

The MO diagram of **1**, in contrast, does not show any lone pairs centered at the Rh atoms. The HOMO (378a) represents the σ-type bonding interaction between Pb and Se, followed, in the order of decreasing energy by, six MOs that represent the Rh–Se interactions (377a…372a). Three lower-energy MOs are mostly centered at the Se atoms of the Pb–Se fragment (371a, 370a, 363a), but possess some contributions from Pb atoms (0.03, 0.12, and 0.06, respectively, according to Mulliken analyses[42]). According with these numbers, 370a might be considered a weak π-bonding interaction – or at least a polarization of the corresponding Se p orbital towards the Pb atom. Based on this picture, the Pb–Se bond should be considered essentially as XXX, which is surprising for the fact, that isolated PbSe in comparison to CO does not obtain such double bonding contributions (see Figure 5, left). Further down on the energy scale within the MO diagram of **1** are orbitals for Rh–P interactions (369a, 366a…364a), Rh–CN interactions (362a, 361a) and lone pairs of the N atoms at the CN ligands (368a, 367a).

We conclude that the PbSe fragment has a (weak) double-bond character, thus behaves qualitatively like μ-bridging CO. A comparison of shared electron numbers (SEN)[45] for Rh–Pb and Pb–Se in comparison to e.g. Rh–P or the Rh–Se bonds (see Figure 5, left) indicates strong Rh–Pb interactions. Evtl diskutieren Rh3Se2-Cluster mit μPbSe versus Rh3PbSe3-Cluster. On replacing the Pb–Se unit with a C–O molecule, the bonding situation remains qualitatively similar, but naturally, the order of the energy levels is different. Rh-centered localized orbitals (357a-353a, see Figure S5) are highest in energy again, followed by Rh/Se centered (352a, 351a) and Rh/CO(/P) centered orbitals (350a-345a) with decreasing energy. This energetic shift is in agreement with the energies of the frontier molecular orbital in PbSe and CO, respectively (Figure 5, left): upon coordination with PbSe, the bonding orbitals would be expected at similar energies as HOMO and HOMO–1 in isolated PbSe, while the corresponding orbitals from CO ligands would be lower in energy. The 350a orbital for the calculated CO-ligated cluster represents the well-known textbook example of a π-backdonation from the Rh-atoms into the anti-bonding orbital of the CO bond. The corresponding σ-bonds are far below in energy (e.g. Rh–CN and C–N: 317a, 315a, 313a, 311a).

Therefore no direct isolobal relationship in terms of the bonding situation between CO and PbSe can be concluded, yet coordination mode and double bond character exhibit strong similarities and an unexpected new ligand.

Experimental Section

General: All manipulations and reactions were performed under an Ar atmosphere using standard Schlenk or glove box techniques. All manipulations with Pb-species were performed under exclusion of light. Solutions of $[K(18\text{-crown-6})]_2[Pb_2Se_3]$ and $[K([2.2.2]crypt)]_2[Pb_2Se_3]$ have been prepared according to literature procedures.[21] THF, toluene and benzene were freshly distilled from NaK alloys prior use. $[Rh(PPh_3)_3Cl]$ (Sigma Aldrich) was dried at dynamic vacuum ($p < 1{\cdot}10^{-4}$ mbar) for at least 12h.

Syntheses: **1**: 10 mL of an *en* solution of $[K(18\text{-crown-6})]_2[Pb_2Se_3]$ was carefully layered with 10 mL of a saturated THF solution of $[Rh(PPh_3)_3Cl]$. **1** crystallizes after 4 weeks alongside of $[Rh_6Se_8(PPh_3)_6]$[20] as black blocks. **2**: 10 mL of an *en* solution of $[K([2.2.2]crypt)]_2[Pb_2Se_3]$ was carefully layered with 10 mL of a saturated THF solution of $[Rh(PPh_3)_3Cl]$. **2** crystallizes after 1 week as black blocks in approx. 25% yield.

Single-crystal X-ray diffraction: Data collection was performed using a Bruker Quest (1) or Stoe IPDS2/T diffractometer at 100 K with $Mo_{K\alpha}$ radiation and graphite monochromatization (λ=0.71073). Structure solution was realized by direct methods, refinement with full-matrix-least-squares against F^2 using SHELXS-97, SHELXL-97, and Olex2 software.[46,47] Crystal data for $C_{182.33}H_{176}K_6N_{13.67}O_{12}P_8Pb_2Rh_6Se_6$ (**1**, M_W = 4738.65 g/mol): a = 17.4936(5) Å, b = 24.6283(7) Å, c = 22.2850(5) Å, β = 91.7940(10)°; $C_{144}H_{136}KN_2O_6P_6Rh_3Se_2$ (**2**, M_W = 2682.11 g/mol): a = 15.7285(4) Å, b = 33.0820(7) Å, c = 24.6448(7) Å, β = 106.220(2)°. CCDC XXX (**1**) and XXX (**2**) contain the supplementary crystallographic data for this paper. These data can be obtained free of charge from The Cambridge Crystallographic Data Centre via www.ccdc.cam.ac.uk/data_request/cif.

Quantum chemical methods: DFT calculations were performed with the program system TURMOMOLE[35] using the RIDFT program[36] and employing the Becke-Perdew 86 (BP86) functional[37] with def2-TZVP bases[38] and respective fitting bases[39] for the evaluation of the Coulomb matrix. Effective core potentials (ECPs) were used for Pb atoms (ECP-

60).[40] Counterions were modelled by application of COSMO with default parameters.[41] Mulliken population analyses[42] served to evaluate atomic orbital contributions to the molecular orbitals. Population analysis based on occupation numbers (PABOON) are given as shared electron numbers (SEN).[43] MO plots were generated using the visualization tool gOpenMol.[44]

Acknowledgements

We are indepted to R. Riedel for his sorrowful attempts on X-ray crystallography and for financial support from the Deutsche Forschungsgemeinschaft (DFG, SPP 1415) and the Friedrich-Ebert-Stiftung (FES). We thank Maximilian Fritz, Maximilian Jost and Maximilian Biermeier for antecedent experimental studies.

Keywords: keyword 1 • keyword 2 • keyword 3 • keyword 4 • keyword 5

[1] B. Meyer, J. J. Smith, K. Spitzer, J. Chem. Phys. 1970, 53, 3616-3620.
[2] For CCh (Ch=O…Te) Review see: Y. Mutoh, N. Kozono, K. Ikenaga, Y. Ishii, Coord. Chem. Rev. 2012, 256, 589-605 and references therein.
[3] K. P. Huber, G. Herzberg, in Molecular Structure and Molecular Spectra IV. Constants of Diatomic Molecules (Van Nostrand Reinhold, New York, 1979).
[4] J. Drowart, R. Colin, G. Exsteen, Trans. Faraday Soc. 1965, 61, 1376.
[5] C. Linton, H. P. Broida, J. Mol. Spectrosc. 1976, 62, 396-415.
[6] B. M. Giuliano, L. Bizzocchi, J.-U. Grabow, J. Mol. Spectrosc. 2008, 251, 261-267.
[7] B. M. Giuliano, L. Bizzocchi, R. Sanchez, P. Villanueva, V. Cortijo, M. E. Sanz, J.-U. Grabow, J. Chem. Phys., 2011, 135, 084303 and references therein.
[8] Z. J. Wu, Chem. Phys. Lett. 2003, 370, 39-43. And References therein.
[9] J.-M. Raulot, G. Baldinozzi, R. Seshadri, P. Cortona, Solid State Sci., 2002, 4, 467-474.
[10] D. Zagorac, K. Doll, J. C. Schön, M. Jansen, Chem. Eur. J., 2012, 18, 10929-10936.
[11] F. Demiray, S. Berber, Phys. Scr. 2013, 88, 015603-015603.
[12] see e.g. P. Canepa, P. Ugliengo, M. Alfredsson, J. Phys. Chem. C, 2012, 116, 21514-21522 and references therein.
[13] K. G. Dyall, J. Chem. Phys. 1993, 98, 2191-2197.
[14] S. Chattopadhyaya, A. Chattopadhyay, K. K. Das, J. Phys. Chem. A, 2002, 106, 833-841.(in 24)
[15 D. Shi, W. Xing, X. Zhang, J. Sun, Z. Zhu, Y. Liu, Comput. Theor. Chem., 2011, 969, 17-26. And references therein.
[16] S. Chattopadhyaya, K. K. Das, Chem. Phys. Lett, 2003, 382, 249-257 and references therein.
[17] A. F. Jalbout, X.-H. Li, H. Abou-Rachid, Int. J. Quantum Chem. 2007, 107, 522-539. And references therein.
[18] R. C. Oldenborg, C. R. Dickson, R. N. Zare, J. Mol. Spectrosc. 1975, 58, 283-300.
[19] E. S. Larsen, American Mineralogist 1917, 2, 18-19.
[20] G. Thiele, Z. You, S. Dehnen, submitted.
[21] G. Thiele, L. Vondung, S. Dehnen, submitted.
[22] Eine Chemikalie referenzieren?
[23] L. S. Ramsdell, Am. Mineral., 1925, 10, 281-304.
[24] A. N. Mariano, K. L. Chopra, Appl. Phys. Lett. 1967, 10, 282-284.
[25] T. K. Chattopadhyay, H. G. von Schnering, W. A. Grosshans, W. B. Holzapfel, Physica B+C, 1986, 139/140, 356-360.
[26] M. Bremholm, Y. S. Hor, R. J. Cava, Solid State Sci. 2011, 13, 38-41.
[27] T. B. Zunic, E. Makovicky, Can. Mineral., 2007, 45, 437-443.
[28] C. W. Liu, T. S. Lobana, J.-L. Xiao, H.-Y. Liu, B.-J. Liaw, C.-M. Hung, Z. Lin, Organometallics, 2005, 24, 4072.
[29] P. A. W. Dean, J. J. Vittal, N. C. Payne, Inorg. Chem. 1984, 23, 4232.
[30] J. S. L. Yeo, J. J. Vittal, W. Henderson, T. S. A. Hor, J. Chem. SOc., Dalton Trans., 2002, 328.
[31] Y.-J. Lu, J. A. Ibers, Acta Crystallogr., Sect. C: Cryst. Struct. Commun., 1991, 47, 1600.
[32] J. Lee, T. J. Emge, J. G. Brennan, Inorg. Chem., 1997, 36, 5064.
[33] Benzene solvent isomer of **1**: a = 18.0335(13) Å, b = 23.8399(16) Å, c = 25.7552(19) Å, β = 106.032(2)°, V=10642.0(13)Å³; Space group $P2_1$. Due to heavy disorder of 2-4 solvent benzene molecule at approx. 8 positions, disorder of 2-3 solvent *en* molecules at approx. 6 positions and further disorder of coordinating crown ether and *en* molecules, no dataset of sufficient quality for publication could be refined.
[35] TURBOMOLE Version 6.4, TURBOMOLE GmbH 2012. TURBOMOLE is a development of University of Karlsruhe and Forschungszentrum Karlsruhe 1989–2007, TURBOMOLE GmbH since 2007.
[36] a) K. Eichkorn, O. Treutler, H. Öhm, M. Häser, R. Ahlrichs, Chem. Phys. Lett. 1995, 242, 652 – 660; b) K. Eichkorn, F. Weigend, O. Treutler, R. Ahlrichs, Theor. Chim. Acta 1997, 97, 119 – 124.
[37] a) A. D. Becke, Phys. Rev. A 1988, 38, 3098 – 3109; b) S. H. Vosko, L. Wilk, M. Nusair, Can. J. Phys. 1980, 58, 1200 – 1205; c) J. P. Perdew, Phys. Rev. B 1986, 33, 8822 – 8837.
[38] F.Weigend, R. Ahlrichs, Phys. Chem. Chem. Phys. 2005, 7, 3297 – 3305.
[39] F. Weigend, Phys. Chem. Chem. Phys. 2006, 8, 1057 – 1065.
[40] B. Metz, H. Stoll, M. Dolg, J. Chem. Phys. 2000, 113, 2563 – 2569.
[41] a) A. Klamt, G. Schüürmann, J. Chem. Soc. Perkin Trans. 1993, 799 – 805; b) A. Schaefer, A. Klamt, D. Sattel, J. C. W. Lohrenz, F. Eckert, Phys. Chem. Chem. Phys. 2000, 2, 2187 – 2193.
[42] R. S. Mulliken, J. Chem. Phys. 1955, 23, 1833 – 1840.
[43] Ehrhardt, C.; Ahlrichs, R. Theor. Chim. Acta 1985, 68, 231-245.
[44] gOpenMol, Leif Laaksonen, Center for Scientific Computing, Espoo, Finland, Version 3.0, 2005: D. L. Bergman, L. Laaksonen, A. Laaksonen, J. Mol. Graphics Modell. 1997, 15, 301 – 306.

Supporting Information

{μ-PbSe}: The Second Heaviest CO Homolog as an Unexpected Ligand

*Günther Thiele and Stefanie Dehnen**

1 Experimental details

1.1 General

All manipulations were performed under strict exclusion of air and moisture using standard Schlenk and glovebox techniques. Solvents were freshly distilled prior to use.

1.2 Synthesis of 1:

5 g (0.024 mol, 1 eq) of Pb and 3.81 g (0.048 mol, 2 eq) of Se are placed in a quartz ampule and heated for 5 min with an oxygen/methane burner. The homogenous melt is allowed to cool and thoroughly grinded. 500 mg (1.369 mmol, 1 eq) of the resulting powder and 760 mg (2.875 mmol, 2.1 eq) of 18-crown-6 are vigorously stirred in 50 mL en while 112 mg (2.875 mmol, 2.1 eq) of K is added. The solution is stirred for 48 h, filtered and 10 mL of the resulting solution is carefully layered with 10 mL of a saturated THF solution of $Rh(PPh_3)_3Cl$. **1** crystallizes as black blocks after 4 weeks.

Synthesis of 2:

According to the synthesis of **1** but with 18-crown-6 replaced by [2.2.2]crypt. **3** crystallizes as black blocks after **1** week in approx. 25% yield.

Figure S1. Reaction scheme towards **1,** and **2.**

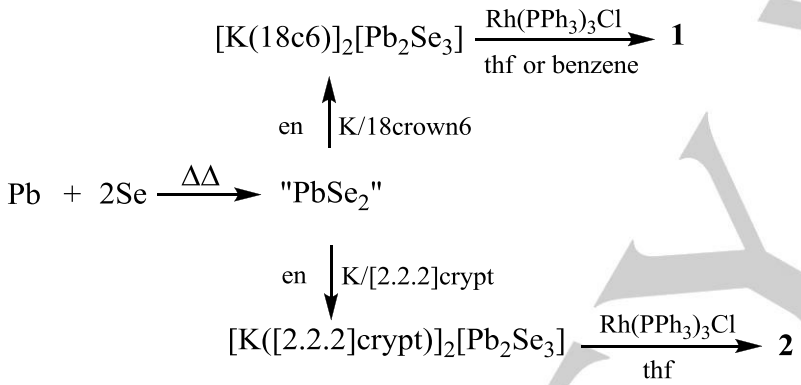

2 Single crystal X-Ray structure and refinement details

Crystallographic data (excluding structure factors) for the structures reported in this paper have been deposited with the Cambridge Crystallographic Data Center as supplementary publication no. CCDC-XXX (**1**), and CCDC-XXX (**2**).

Table S1. Crystal data and structure refinement.		
Identification code	1	2
Empirical formula	$C_{182.33}H_{176}K_6N_{13.67}O_{12}P_8Pb_2Rh_6Se_6$	$C_{144}H_{136}KN_2O_6P_6Rh_3Se_2$
Formula weight	4738.65	2682.11
Temperature/K	100(2)	100(2)
Crystal system	monoclinic	Monoclinic
Space group	$P2_1/n$	$P2_1/c$
a/Å	17.4936(5)	15.7285(4)
b/Å	24.6283(7)	33.0820(7)
c/Å	22.2850(5)	24.6448(7)
β/°	91.7940(10)	106.220(2)
Volume/Å^3	9596.5(4)	12313.0(6)
Z	2	4
ρ_{calc}mg/mm^3	1.640	1.447
Crystal size/mm^3	0.22 × 0.21 × 0.19	0.12 x 0.10 x 0.09
Radiation	MoK_α (λ = 0.71073)	MoK_α (λ = 0.71073)
2Θ range for data collection	4.04 to 56.75°	2.46 to 53.65°
Diffractometer type	Bruker Quest	STOE IPDS2/T
Reflections collected	224485	161527
Independent reflections	23969	26033
Data/restraints/parameters	20670/0/1095	21435/0/1474
Goodness-of-fit on F^2	1.087	1.106
Final R indexes [I>=2σ (I)]	R_1 = 0.0339, wR_2 = 0.0821	R_1 = 0.0416, wR_2 = 0.0844
Final R indexes [all data]	R_1 = 0.0456, wR_2 = 0.0913	R_1 = 0.0587, wR_2 = 0.0906
Largest diff. peak/hole / e Å^{-3}	2.231/-1.278	0.692/-0.791

Hier müssen zusätzliche X-Ray-Bilder rein. Zum einen die Fehlordnung in **1** als Figure S1 (siehe Caption of Figure 1) und anderen Zellplots aller Verbindungen.

3 Energy dispersive X-Ray spectroscopy results

EDX analyses were carried out using an EDX-device Voyager 4.0 of Noran Instruments coupled with an electron microscope CamScan CS 4DV. Data acquisition was performed with an acceleration voltage of 20 kV and 100 s accumulation time. Variations in the different observed and calculated atomic composition is caused by extreme sensitivity of the single crystals and an inhomogenous decomposition due to contact with air and moisture during sample preparation.

Figure S2. EDX spectrum of **1**.

Table S2. EDX results for **1**.

Element	k-ratio (calc.)	ZAF	Atom %	Element Wt %	Wt % Err. (1-Sigma)
Se-K					
Rh-L					
Total			100	100	

4 Quantum chemical details

4.1 Methods

DFT calculations were carried out with the program system TURBOMOLE[1] using the BP86 Functional[2] with def2-ECPs[3] and def2-TZVP basis sets[4] as well as respective auxiliary basis sets.[5] COSMO[6] was applied to compensate molecular charges. Population analyses were applied via Mulliken analysis[7] with and without localization or via SEN.[8] Applied symmetry: C_1 in all cases.

EIN KOMMENTAR ZUR GENAUIGKEIT fehlt: maximale Abweichung von Bindungslängen/Winkeln für jede Sorte von Bindungen/Winkeln muss noch her – z.B. als Tabelle für die beiden Moleküle.

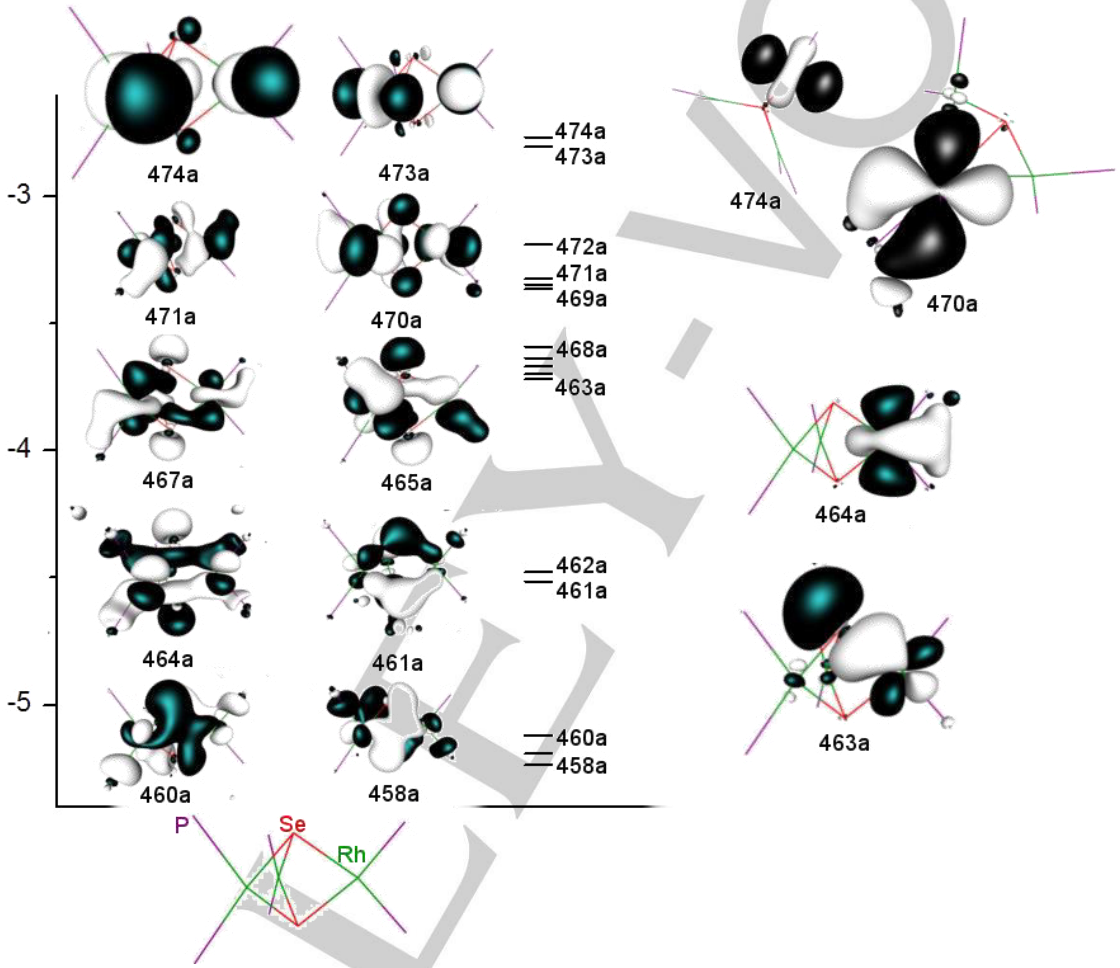

Figure S3. Molecular orbital diagram of the anion in **3** (left) and selected localized orbitals of **3** (right). Phenyl groups and their minor contributions to the shown orbitals are omitted for clarity. Amplitudes are plotted at ±0.033 a.u.

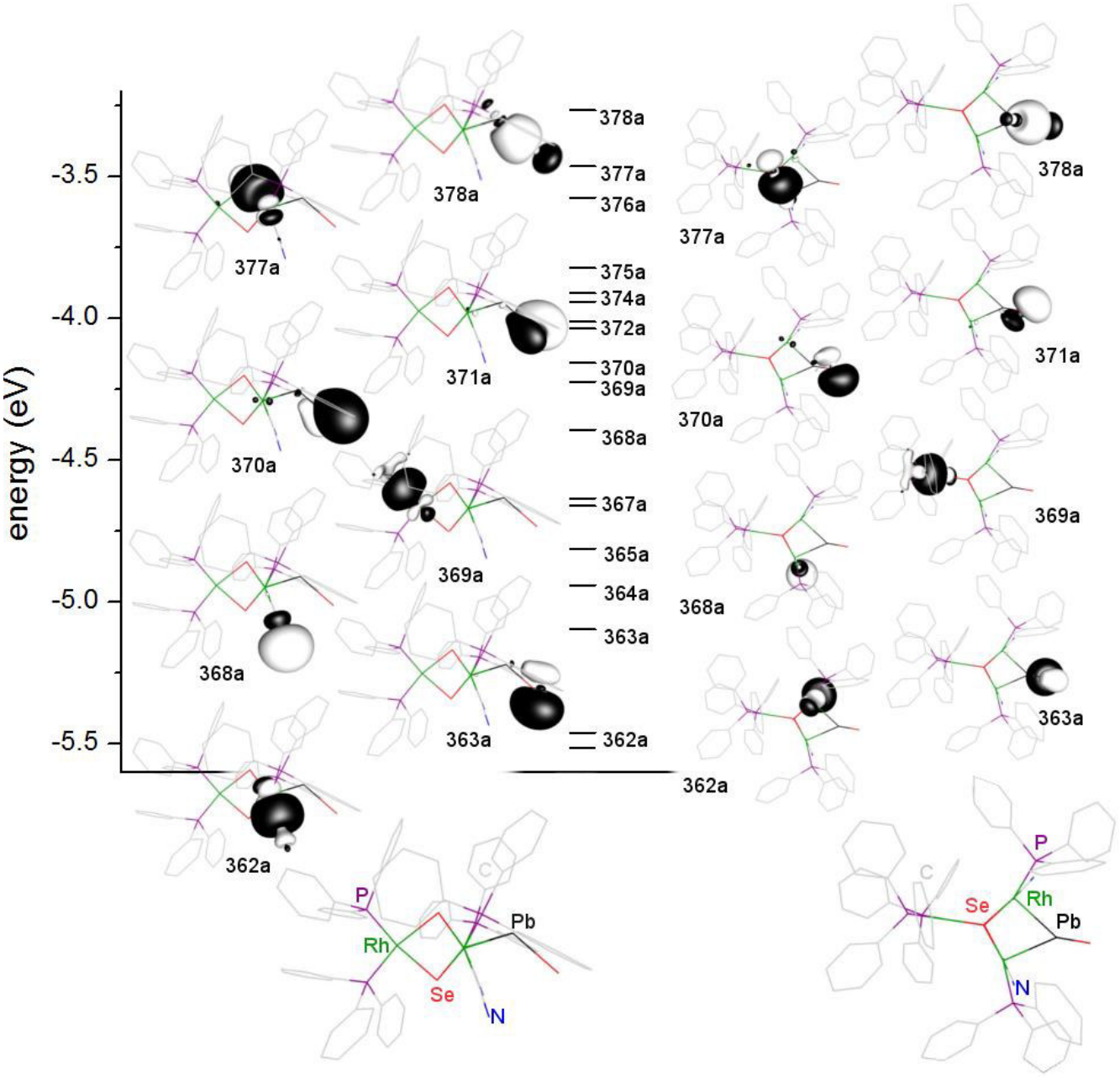

Figure S4. Localized MO diagram for the $[Rh_3Se_2(PPh_3)_4(CN)_2(\mathbf{PbSe})]^{3-}$ fragment in **1**. Amplitudes are plotted at ±0.033 a.u.. View along Rh…Rh (left) and along Se…Se axis (right).

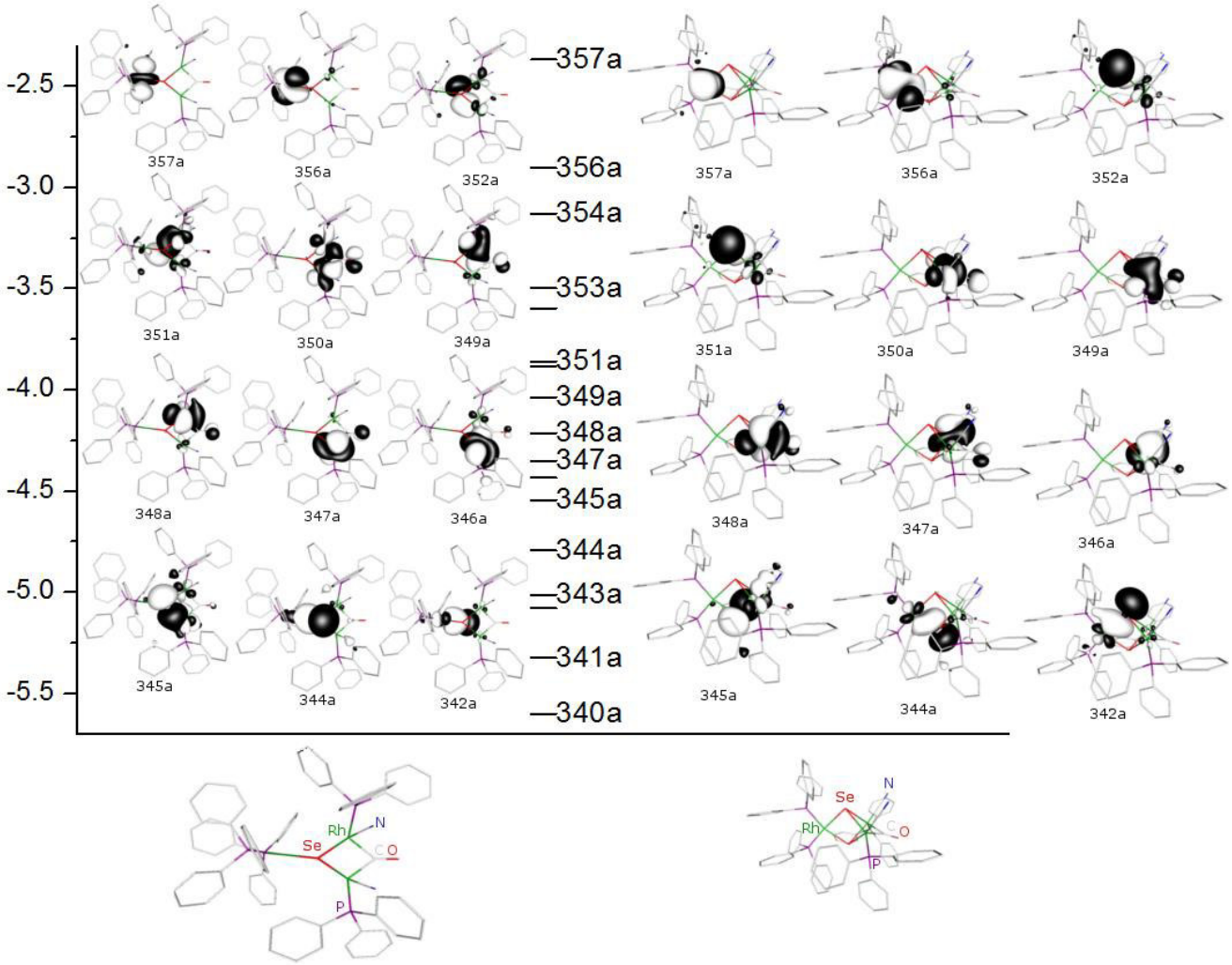

Figure S5. Localized MO diagram for the CO analogue of the anion in **1,** $[Rh_3Se_2(PPh_3)_4(CN)_2(\mathbf{CO})]^{3-}$. Threshold for orbital plotting set to +/- 0.033 a.u. View along Se–Se axis (left) and along Rh–Rh axis (right).

V

Organic Cation and Complex Cation-Stabilized (Poly-)Selenides, $[Cation]_x(Se_y)_z$: Diversity in Structures and Properties

Günther Thiele, Lisa Vondung, Carsten Donsbach, Susanne Pulz, Stefanie Dehnen, *Z. Anorg. Allg. Chem.* **2014**, *640*, 2684-2700.

Based on the synthesis and characterization of a series of new (poly-)selenide salts, a classification of anionic (poly-)selenide-containing compounds is proposed. The new compounds have been categorized according to these classes. Synthetic approaches of organic cation-stabilized (poly-) selenide compounds that have been already known from literature are reviewed, along with the crystal structures of new compounds and some spectroscopic data, and an experimental and theoretical approach towards dichroism observed in some of the triselenides.

Themenkomplex Solvothermalsynthese von Plumbaten und Merkuraten

Inhalt: Die Vielfältigkeit von Seleniden wird anhand auswählter Beispiele verdeutlicht und die Vorteile phasenreiner, kristalliner Substanzen hervorgehoben.

Eine Klassifizierung der (Poly-)Selenide analog der von Ibers für Telluride aufgestellten Kategorien wird vorgestellt: Solvatfreie (Poly-)Selenide der Alkali- und Erdalkalimetalle, (Poly-)Selenidometallate, (Poly-)Selenide mit organischen Kationen, koordinierten Metallkationen und Solvate der (Poly-)Selenide sowie selenreiche Polyselenide.

Es wird eine Übersicht über die synthetischen Herangehensweisen zur Darstellung von Seleniden und Polyseleniden gegeben, und es erfolgt eine ausführliche Auflistung aller (Poly-)Selenide mit organischen oder komplexierten Kation bzw. derer Solvate.

Eine Zusammenfassung der literaturbekannten spektroskopischen Methoden für elektrochemische, UV-Vis, Raman, massenspektrometrische und NMR-spektroskopische Untersuchungen wird dargelegt.

Die Arbeit berichtet über die Synthesen und Kristallstrukturen der Verbindungen $[Li_2(H_2O)_7](Se)$, $[K(H_2O)_4]_2(Se)$, $[K_4(H_2O)_{10}](Se_2)(Se)$, $[Ba(H_2O)_x]_3[Ba(OH)_2(H_2O)_{x-2}](Se)_3$, $(enH)_2(Se_2)$, $[Li(en)_3]_2(Se_2)$, $[K_2(H_2O)](Se_2)$, $[K_2(NH_3)](Se_2)$, $[K(18\text{-Krone-6})]_2(Se_2)\cdot en$, $[\{K(18\text{-Krone-6})\}\{K(NH_3)\}(Se_2)]$, $Cs_4(Se_2)(Se_3)\cdot en$, $(NMe_4)_2(Se_2)$, $[K(18\text{-Krone-6})]_2(Se_3)\cdot H_2O$, $[K(18\text{-Krone-6})]_2(Se_3)\cdot H_2O$, $[\{K(18\text{-Krone-6})\}_2(H_2O)_3](Se_3)\cdot 2H_2O$, $[K([2.2.2]Krypt)]_2(Se_3)\cdot H_2O$, $[M(en)_3](Se_3)$ (M = Fe, Cd), $[K_2(H_2O)](Se_4)$, $[K_2(H_2O)_2](Se_4)$, $[K_2(NH_3)](Se_4)$, $[K([2.2.2]Krypt)]_2(Se_4)$, $[Ba(H_2O)_6](Se_4)$, $[K(18\text{-Krone-6})]_2(Se_6)\cdot(18\text{-Krone-6})\cdot H_2O$, $[K(18\text{-Krone-6})]_2(Se_6)\cdot(18\text{-Krone-6})\cdot 2NH_3$ und $(enH)_2(Se_6)$.

Dichroismus wurde an Verbindungen mit Triselenidionen beobachtet und mithilfe quantenchemischer Rechnungen und UV-Vis-spektroskopischer Messungen studiert. Voraussagen zu neuen Konformationen konnten mithilfe quantenchemischer Rechnungen getroffen werden.

Eigener Anteil: Alle Experimente wurden von mir konzipiert. Die Aufnahme und Auswertung der analytischen Daten und der quantenchemischen Untersuchungen wurden von mir durchgeführt. Die folgenden Personen haben unter meiner Anleitung Teile der Synthesen durchgeführt: Lisa Vondung im Rahmen ihrer Masterarbeit, Susanne Pulz im Rahmen einer Vertiefung, Carsten Donsbach im Rahmen seiner Examensarbeit, Stephan Krisch im Rahmen seiner Bachelorarbeit und Marcus Müller. Carsten Donsbach hat die Tabellen S8-S13 zusammengetragen. Stefanie Dehnen und ich haben das Manuskript zusammen geschrieben. Susanne Pulz, Lisa Vondung und Carsten Donsbach lasen das Manuskript Korrektur.

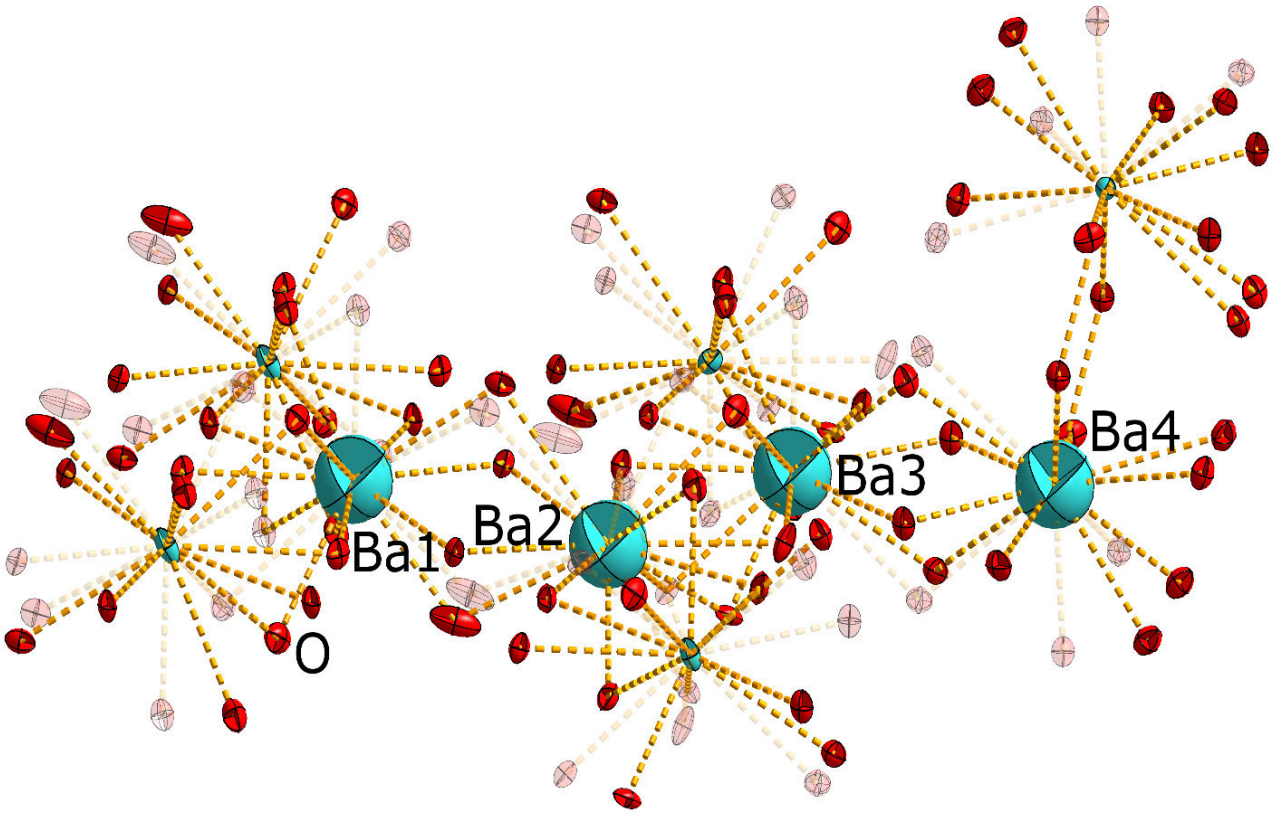

Abbildung 25. Illustration der Fehlordnung von Solvenzmolekülen in $[Ba(H_2O)_x]_3[Ba(OH)_2(H_2O)_{x-2}](Se)_3$.

DOI: 10.1002/zaac.201400457

Organic Cation and Complex Cation-Stabilized (Poly-)Selenides, $[Cation]_x(Se_y)_z$: Diversity in Structures and Properties

Günther Thiele,[a] Lisa Vondung,[a] Carsten Donsbach,[a] Susanne Pulz,[a] and Stefanie Dehnen*[a]

Dedicated to Professor Martin Jansen on the Occasion of His 70th Birthday

Keywords: Polyselenides; Selenium; Organic cations; Complex cations; Crystal structure

Abstract. Based on the synthesis and characterization of a series of new (poly-)selenide salts, a classification of anionic (poly-)selenide-containing compounds is proposed. The new compounds were categorized according to these classes. Synthetic approaches of organic cation-stabilized (poly-)selenide compounds that have been already known from literature are reviewed, along with the crystal structures of new compounds and some spectroscopic data, and an experimental and theoretical approach towards dichroism observed in some of the triselenides.

Introduction

Selenides in general are a huge class of compounds, many of which show exciting properties, leading to vivid discussions on various applications as well as already established applications – mainly in semi-conductor technologies – ranging from photovoltaic devices of $CuInSe_2$[1] to the tunable optoelectronic series of $[M_4Sn_4Se_{17-x}Te_x]^{10-}$ with M = Mn, Zn.[2] Within this exciting class of compounds especially solid state (poly-)selenides and selenidometalates have been regularly reviewed.[3] In contrast, organic cation-stabilized selenides – that is, salts of well separated (poly-)selenide anions $(Se_x)^{2-}$ besides purely organic cations or solvated / coordinated metal ions, respectively – have been lesser focused on, although their solubility in both aqueous and organic solvents makes them ideal for processing[4] or further reactions towards new materials. As an alternative to the usage of *in situ*-generated polyselenides, where the corresponding reagents serve as both precursor and reducing agent at the same time[5] [see, for example, Equation (1) and Equation (2); *N*-MeIm = *N*-methylimidazole], or preformed polyselenides with varying and undetermined chain lengths,[6] the application of crystalline polyselenides as well defined starting materials can additionally help understanding basic reaction mechanisms, for instance towards complicated metalates with different chain lengths of polyselenide ligands.

$$2\,Fe(CO)_5 + Se_8 + 6\,N\text{-MeIm} \rightarrow [Fe(N\text{-MeIm})_6][Fe(Se_4)_2(CO)_2] + 8\,CO \quad (1)$$

$$2\,Zn + Se_8 + 4\,N\text{-MeIm} \rightarrow 2\,[Zn(Se_4)(N\text{-MeIm})_2] \quad (2)$$

Polyselenides have also been discussed to be of use for electrolyte modifications in photoelectrochemical solar cells.[7] Examples for the advantages are enhanced solubilities of organic cation-stabilized selenides in new types of electrolytes like ionic liquids, or a fully determined electronic situation, providing easy to observe markers to monitor the various (photo-) redox processes.

Additionally desired properties can be introduced by changing the cation from pure organic or solvated alkali(ne earth) metal ions to homo- or heteroleptic transition metal complexes.

Therefore, a unique combination of semiconducting properties on the one hand, and excellent solubilities and diverse crystalline structures on the other hand, render organic cation-stabilized (poly-)selenides promising synthons, which shall be the focus of this work. Besides (poly-)selenide salts with purely organic cations, this report comprises also compounds with solvated or otherwise coordinated metal cations and solvates due to similar solubilities, which usually differ from the solvent-free salts.

Classification

In the style of *Ibers*' review on polytelluride anions,[8] we would first of all like to assign anionic (poly-)selenide compounds to the following four predominant categories (*M* being any metal atom):

(a) (Poly-)selenides of the general formula $M_x(Se_y)_z$, with well separated anions and no solvation of metal cations or solvate molecules within the crystal structure. Furthermore

* Prof. Dr. S. Dehnen
Fax: +49-6421-2825653
E-Mail: dehnen@chemie.uni-marburg.de
[a] Fachbereich Chemie und
Wissenschaftliches Zentrum für Materialwissenschaften
Hans-Meerwein-Straße 4
35043 Marburg, Germany

Supporting information for this article is available on the WWW under **http://dx.doi.org/10.1002/zaac.201400457** or from the author.

Zeitschrift für anorganische und allgemeine Chemie ZAAC Journal of Inorganic and General Chemistry

hydrogenselenide anions of the general formulae $M_x(HSe_y)_z$, such as Na(HSe),[9] again without molecules of solvation.

(b) (Poly-)selenidometalates $A_x[M(Se_y)_z]$, with any cation A^{n+}, incorporating at least one covalent *M*–Se bond.

(c) Organic cation-stabilized (poly-)selenides $[OrgCat]_x(Se_y)_z$, including solvated and sequestered metal cation-stabilized (poly-)selenides of the general formula $[M(solv)_w]_x(Se_y)_z$, again with well separated anions.

(d) Selenium-rich selenides with extended anionic structures, or with selenium in formal oxidations states other than –II…0 and/or other than two-bonding, yet without direct *M*–Se interactions. Alternatively those compounds can be described as a special case of (b) with selenium acting as central ion and ligand at the same time.[10]

Radical species, such as $(Se_x)^{\bullet-}$, or hyper-coordinated species, such as $(Ph_4P)_2[Se(Se_5)_2]$,[11] might be assigned to (a), to (c), or to (d) in accordance with the involved cations and bonding situations. The same concept can easily be applied to heterochalcogenides, such as $[NEt_4]_2[Te_3Se_6]$.[12] Concerning organo-substituted (poly-)selenides,[13] an additional categorization according to the number of organic substituents (1–3) is conceivable, but shall not be part of this work. This holds also for cationic[14] or neutral[15] (poly-)selenium species.

To the best of our knowledge, there is no example described in literature so far that cannot clearly be accommodated within these classes of compounds. $Rb_2[Pd(Se_4)_2]\cdot(Se_8)$,[16] for example, would be reasonably classified as a metalate (b), in agreement with direct *M*–Se bonding within the $[Pd(Se_4)_2]$ subunit; this seems to be justified since the influence of the Pd–Se bonds on physical and chemical properties will certainly dominate over the presence of Se–Se bonds. Cs_2Se_{22}[17] as a second example, is a selenium-rich selenide (d), since an extended $^3_\infty[(Se_6)^{3-}]$ anionic network is present instead of well-separated, molecular anions.

A problem remains where the interatomic distances do not allow for a clear discrimination of a covalent Se–*M* bond from a rather ionic interaction, such that it becomes difficult to assign the compounds to categories (a) or (b). This holds especially for lanthanide compounds. $[La_2(en)_8(Se_2)]^{4+}$ (*en* = ethane-1,2-diamine),[18] for instance, comprises a La–Se distance of 3.143(2) Å, which is significantly longer than the Hg–Se bond in $[Hg(Se_4)_2]^{2-}$ [2.65(2) Å].[19]

However, since the lanthanide–selenium interactions will affect physical properties, we will categorize those examples into the metalate group (b). Exceptions are made if the involved lanthanide – or equally: transition metal – ions are entirely solvated. Since the properties of alkali(ne earth) metal (poly-)selenides are usually widely unaffected by eventual metal–selenium interactions, such compounds will always be assigned to the organic cation-stabilized selenides (c), if any solvation or sequestration is present within the crystal structure.

Syntheses of (Poly-)selenides

Selenides and polyselenides that are assigned a number in the following refer to new compounds. Salts that comprise two or more types of (poly-)selenide anions with different chain lengths are listed with other compounds of the respective shortest chain length. Below, completeness of reported data is claimed only for compounds of category (c). Examples from other categories are only given for comparison and clarification and have been reviewed elsewhere.[3]

Synthetic Approaches

The most straight forward method for the generation of polyselenides is the oxidation[20] of H_2Se or alkali (poly)selenide salts or, *vice versa*, the reduction of elemental selenium.[21] Oxidation can be achieved with H_2O_2, elemental iodine or via electrolysis. Reducing agents range from borohydrides and N_2H_4 to elemental alkali metals.[22]

A combination of both methods leads to comproportionation reactions, for instance between elemental selenium and selenide salts, or between two selenide salts with different selenide chain lengths. Catalytic amounts of iodine serve as redox mediator when starting from selenide salts,[23] aqueous carbonate solutions are employed, when the reactions start out from H_2Se.

Further methods usually comprise solvothermal experiments or solvent-based extractions of binary or ternary selenides that have been gained from high-temperature solid state syntheses.[3] Especially for *in situ* generation of selenides, which are immediately consumed by subsequent reactions, a broad variety of methods has been used, such as ultrasound-induced electrochemical synthesis,[24] pulse radiolysis in saturated aqueous N_2O solutions, which resulted in the interim formation of $(Se_2)^{2-}$ and the formation of short-lived HSe, Se^-, probably $(Se_3)^-$ and "fairly stable" $(Se_2)^-$, as well as $(H_2Se_2)^-$ and $(HSe_2)^{2-}$.[25]

Salts of Monoselenide or Hydrogenselenide Anions Se^{2-} and $(HSe)^-$

$[(Me_2NH_2P)_2N]_2Se$ (c) was obtained from decomposition reactions of selenophosphazane heterocycles,[26] $[Mn(cyen)_3]_2[H_2cyen](Se_2Te)_2Se$ (c) (*cyen* = *trans*-cyclohexane-1,2-diamine),[27] $[Ph_2P(NH_2)_2]_2Se$ (c),[28] the H_2O/MeOH solvated double salt of $K_{10}[Zn_4Sn_4Se_{13}Te_4]\cdot 4K_2Se$ (c) with the Se^{2-} anions aggregating to a dodecahedral substructure,[29] $(NMe_4)(HSe)$ (c),[30] and $Na_2Se\cdot xH_2O$ with $x = 5$[31] or 9[32] (c) are reported in the literature. Our own contributions include the formation and characterization of $[Li_2(H_2O)_7]Se$ (**1**) (c), $[K(H_2O)_4]_2Se$ (**2**) (c), $[K_4(H_2O)_{10}](Se_2)Se$ (**3**) (c), and $[Ba(H_2O)_x]_3[Ba(OH)_2(H_2O)_{x-2}]Se_3$ (**4**) ($x \approx 13$) (c).

Salts of the Diselenide Anion $(Se_2)^{2-}$

$[Li_4(THF)_5](SeP(NPh)_3)]_2(Se_2)$ (b) has been the only known organic cation-stabilized diselenide so far, yet with Li–Se distances as short as 2.561 Å, hence shorter than the sum of Li(+I) and Se(–II) ionic radii (2.57 Å).[33] In combination with an only threefold coordination of the Li^+ ion, this compound would probably be classified as a selenidolithiate.[34] We were

able to generate and isolate the following diselenides, including two double salts with monoselenide or triselenide anions: (*en*H)$_2$(Se$_2$) (**5**) (c) [Li(*en*)$_3$]$_2$(Se$_2$) (**6**) (c), [K$_2$(H$_2$O)](Se$_2$) (**7**) (c), [K$_2$(NH$_3$)](Se$_2$) (**8**) (c), [K(18-*crown*-6)]$_2$(Se$_2$)·*en* (**9**) (c) (18-*crown*-6 = 1,4,7,10,13,16-hexaoxacyclooctadecane), $^1_\infty$[{K(18-*crown*-6)}{K(NH$_3$)}(Se$_2$)] (**10**) (c), Cs$_4$(Se$_2$)(Se$_3$)·*en* (**11**) (a), and (NMe$_4$)$_2$(Se$_2$) (**12**) (c). A summary of Se–Se bond lengths alongside with Se–Se–Se angles of the known category (c) polyselenides are presented in the Supporting Information (Tables S8–S13).

Salts of the Triselenide Anion (Se$_3$)$^{2-}$

The formula of [Eu$_8$(*dmf*)$_{13}$(μ^4-O)(μ^3-OH)$_{12}$(Se$_3$)(Se$_4$)$_2$(Se$_5$)$_2$] (*dmf* = *N*,*N*-dimethylformamide) might suggest the presence of fully solvated Eu^{3+} ions besides well-separated tri-, tetra-, and pentaselenide chains; yet, as stated by the authors,[35] polyselenide fragments serve as bridging and chelating ligands to the Eu^{3+} ions, therefore classification would lead to category (b), hence as a selenidoeuropate. In contrast, [Sr$_2$Sn(OH)$_6$(H$_2$O)$_5$](Se$_3$)·H$_2$O[36] (c), [Mn(NH$_3$)$_6$](Se$_3$)[37] (c), [Ni(*tren*)$_2$](Se$_3$) (c) (*tren* = diethylene triamine),[38] [Mn(*en*)$_3$](Se$_3$)[39] (c), and the two ammoniates Li(NH$_3$)$_4$Rb(Se$_3$) and Na(NH$_3$)$_5$Rb(Se$_3$)·3NH$_3$,[40] (c) incorporate well separated (Se$_3$)$^{2-}$ anions. This is also the case for [*ct*NMe$_3$]$_2$(Se$_3$) (c) [*ct* = cetyl, (CH$_2$)$_{15}$CH$_3$],[23] which was determined by means of CHN analysis only, owing to large cell constants that hampered a proper crystal structure analysis at the time of publication. We characterized a variety of triselenides, namely [K(18-*crown*-6)]$_2$(Se$_3$) (**13**) (c), [K(18-*crown*-6)]$_2$(Se$_3$)·H$_2$O (**14**) (c), [{K(18-*crown*-6)}$_2$(H$_2$O)$_3$](Se$_3$)·2H$_2$O (**15**) (c), and [K([2.2.2]*crypt*)]$_2$(Se$_3$)·H$_2$O (**16**) (c) ([2.2.2]*crypt* = 4,7,13,16,21,24-hexaoxa-1,10-diazabicyclo[8.8.8]-hexacosane), as well as the solvated transition metal cation-stabilized triselenides [*M*(*en*)$_3$](Se$_3$) [*M* = Fe, Cd (**17**, **18**)] (c).

Salts of the Tetraselenide Anion (Se$_4$)$^{2-}$

[Sr$_2$Sn(OH)$_6$(H$_2$O)$_6$](Se$_4$) (c),[36] [Ba$_2$(OH)$_2$(H$_2$O)$_{10}$]$_2$(Se)$_4$ (c),[41] [Ba([2.2.2]*crypt*)](Se$_4$)·*en* (c),[42] [Ba(*en*)$_4$](Se$_4$)·*en* (c),[43] and [Ca(*en*)$_4$](Se$_4$)[44] (c) clearly belong to organic cation-stabilized selenides, although *Fässler* and *Menezes* discuss a 3D network due to interconnecting hydrogen bridges. Dimorpholine and dipiperidine tetraselanes should be excluded from this list, although they are sometimes quoted in literature as (NC$_4$H$_8$O)$_2$(Se$_4$), (NC$_5$H$_{10}$)$_2$(Se$_4$).[45] However, as the authors correctly state, these organoselenium compounds with Se–N bond lengths of 1.836 Å and 1.824 Å respectively, do not comprise salt like ion separation. [Ph$_3$PNPPh$_3$]$_2$(Se$_4$)·4MeCN[46] (c) and [Mn(MeNH$_2$)$_6$](Se$_4$)[37] (c) are further prominent examples of selenides of category (c), whereas [Li(*tmeda*)$_2$]$_2$(Se$_4$) (*tmeda* = *N*,*N*,*N*′,*N*′-tetramethylethane-1,2-diamine), with Li–Se distances of 2.589 Å to 2.661 Å,[47] belong rather to the metalate group (b). We hereby add [K$_2$(H$_2$O)](Se$_4$) (**19**) (c), [K$_2$(H$_2$O)$_2$](Se$_4$) (**20**) (c), [K$_2$(NH$_3$)](Se$_4$) (**21**) (c), [K([2.2.2]*crypt*)]$_2$(Se$_4$) (**22**) (c), and [Ba(H$_2$O)$_6$](Se$_4$) (**23**) (c) to the list of known tetraselenides.

Salts of the Pentaselenide Anion (Se$_5$)$^{2-}$

[Cs(18-*crown*-6)]$_2$(Se$_5$)·DMF[48] (c) and [Cs(18-*crown*-6)]$_2$(Se$_5$)·MeCN[46] (c) have been reported with well separated anions, as well as (NEt$_4$)$_2$(Se$_5$)·(Se$_7$)·(Se$_6$) (c) that contains (Se$_5$)$^{2-}$ chains and associated six- and seven-membered (Se$_6$)^0 and (Se$_7$)^0 rings.[49] The structural deviations due to this association are small – for instance, the mean Se–Se bond length is 2.325 Å as compared to 2.339 Å in (PPh$_4$)$_2$(Se$_5$) (c);[50] therefore the classification is done alongside with (NMe$_4$)$_2$(Se$_5$) (c),[51] [Na(15-*crown*-5)]$_2$(Se$_5$) (c) (15-*crown*-5 = 1,4,7,10,13-pentaoxacyclopentadecane),[52] [*td*NMe$_3$]$_2$(Se$_5$) (c) [*td* = tetradecyl = (CH$_2$)$_{13}$CH$_3$],[23] again, the latter only characterized by means of elementary analysis, and [Mn(NH$_2$CH$_3$)$_6$](Se$_5$) (c).[53] [Li$_2$(Se$_5$)$_2$(*pmeta*)$_2$] (b)[54] (*pmeta* = pentamethyldiethylenetriamine) exhibits mean Se–Li distances of 2.59 Å that are close to the sum of ionic radii, and further elongations of the terminal Se–Se bond also indicate a strong Li–Se interaction. The authors exclude lattice effects to be the reason for the short Se–Li distances; hence this compound should be viewed as a lithiate (b).

Salts of the Hexaselenide Anion (Se$_6$)$^{2-}$

(PPh$_4$)$_2$(Se$_6$) (c) was synthesized in an uncommon way by oxidation of K$_2$Se$_2$ with K$_3$[Mn(CN)$_6$].[55] [Ba(15-*crown*-5)$_2$](Se$_6$)·DMF (c) and [Rb([2.2.2]crypt)]$_2$(Se$_6$) (c) were also obtained from K$_2$Se$_2$, however, with an excess of elemental selenium.[48] Only elementary analyses were reported for [NEt$_4$]$_2$(Se$_6$) (c),[23] whereas [NMe$_4$]$_2$(Se$_6$) (c),[51] and (NBu$_4$)$_2$(Se$_6$) (c)[56] could be characterized by means of single-crystal X-ray diffraction. Isostructural [*M*(NH$_3$)$_6$](Se$_6$) (*M* = Mn, Fe)[37] (c) and [Mn(*cyen*)$_3$](Se$_6$)[27] (c) exhibit pseudo-layers and weak hydrogen bonding, with intermolecular Se–Se distances of at least 3.618 Å, which are significantly larger than all intramolecular bonds (terminal: 2.313 Å, intra-chain: 2.360 Å). [Mg$_6$(μ^4-OH)$_2$(μ^3-MeO)$_4$(MeO)$_4$(MeOH)$_{12}$](Se$_6$)·2MeOH,[57] with six Mg ions and six bridging ligands in a face-sharing cubic arrangement that stabilize the (Se$_6$)$^{2-}$ unit, is further known besides [(*td*)NMe$_3$]$_2$(Se$_6$) (c).[23] We additionally present the compounds [K(18-*crown*-6)]$_2$(Se$_6$)·(18-*crown*-6)·H$_2$O (**24**) (c), [K(18-*crown*-6)]$_2$(Se$_6$)·(18-*crown*-6)·2NH$_3$ (**25**) (c), and (*en*H)$_2$(Se$_6$) (**26**).

Salts of Polyselenide Anions (Se$_x$)$^{2-}$ with $x > 6$

Generally, selenides show a large tendency to form aggregates with five-membered or six-membered rings. This can even lead to situations that apparently contradict the formal charge assignment, such as observed in [Sr(15-*crown*-5)$_2$](Se$_9$) (c) (see Figure 1).[58] Here, the formation of a six-membered ring would lead to a formally monocationic, 3-connected selenium atom besides the monoanionic terminal one, thus producing an overall neutral species. However, the third interaction of the respective bridgehead selenium atom is a rather weak, secondary interaction (2.954 Å); thus seven of the nine selenium atoms are two-bonded and formally neutral, besides

Dedicated Cluster

Zeitschrift für anorganische und allgemeine Chemie ZAAC Journal of Inorganic and General Chemistry

the two terminal, monoanionic ones – in agreement with the total charge. The bridgehead atoms found in $[Ph_3PNPPh_3]_2[Se_2(Se_4)_2]$·DMF (d)[59] or $(Ph_4P)_2[Se(Se_5)_2]$ (d),[11] in contrast, possess formal oxidation states of +I and +II, respectively.

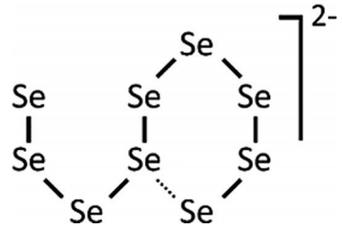

Figure 1. Proposed *Lewis* diagram of the nonaselenide dianion in $[Sr(15\text{-}crown\text{-}5)_2](Se_9)$.[58]

$[Na(12\text{-}crown\text{-}4)_2]_2(Se_7)$ (c)[48] and $[K([2.2.2]crypt)]_2(Se_7)$·$H_2O$ (c)[60] are structurally unambiguously determined, whereas the compounds $[(ct)NMe_3]_2(Se_x)$ (x = 7–9) (c) were published based on elementary analysis only, and discussed in analogy with the corresponding crystal structure of the hexaselenide compound $[(ct)NMe_3]_2(Se_6)$ (c).[23] $[Na(12\text{-}crown\text{-}4)_2]_2[Se_8$·$(Se_6,Se_7)]$ (d), which was synthesized in the presence of $CeCl_3$, forms strongly associated layers parallel to (100).[61] The usual finding of short terminal Se–Se bonds within the chain anions and comparably long internal Se–Se bonds are not found in this species. Unfortunately heavy disorder hampered further interpretations.[61]

Chalcogenidoselenides [Cat](Ch$_x$Se$_y$)

$[Mn(MeNH_2)_6(S_5)_{0.15}(S_{1.57}Se_{2.43})_{0.85}$ (c) and $[Mn(NH_3)_6](S_{2.71}Se_{2.29})$[37] (c) can unbiased be associated to group (c) selenides, whereas $[M(NH_3)_4](TeSe_3)$ (b) (M = Zn, Mn)[62] do not belong to this group, since the central tellurium atom exhibits a formal +II oxidation state; therefore it rather belongs to the group of metalates. $[Mn(en)_3](Se_2Te)$[39] (c) that is isostructural to its $(Se_3)^{2-}$ congener, $[Mn(cyen)_3]_2[H_2cyen](Se_2Te)_2(Se)$ (c),[27] $(NBu_4)_2(Se_3SSe_2)$ (c),[63] $[K([2.2.2]crypt)]_2[SeTeSe]$·*en* (c) and $[K([2.2.2]crypt]_2[Te_{0.9}Se_{3.4}]$·*en* (c) were reported, though the latter suffered from disorder and the co-crystallization of an anion of the same composition but with trigonal pyramidal structure (b).[64] The latter structural arrangement would again be a metalate-type one, whereas those mentioned before all belong to the group of organic cation selenides.

Spectroscopic Data and Properties

The first experiments on physical properties of (poly-)selenides date back to the original works by *Zintl*, who performed potentiometric titrations in liquid ammonia.[65] Much effort has been put into the understanding of the multifaceted species that exist in solution.

Electrochemical Investigations

Lyons and *Young* discussed spectrophotometric, titrimetric, ESR, and NMR studies of soluble selenium species and determined various redox potentials in a 1 mol·dm^{-3} KOH solution.[66] Further spectroelectrochemical data were published by *Paris* and *Ahrika*.[67] With a combination of *in situ* synchrotron diffraction, K-edge absorption, X-ray photoelectron, and electrochemical impedance spectroscopy, Li/SeS_x (x = 0–7) as promising phases for secondary lithium cells, were investigated regarding (de)lithiation mechanisms.[68]

UV/Vis and Raman Spectroscopy

Following *Hugot's* examples,[69] sodium polyselenides were synthesized in liquid ammonia and studied by UV/Vis spectroscopy. As a result, equilibrium constants between polyselenides with adjacent chain lengths were determined, and the nonexistence of $(Se_2)^{2-}$ and $(Se_5)^{2-}$ within these solutions was shown.[70] Interestingly, no ammoniates such as $[Na(NH_3)_4]_2(Se_x)$ have been crystallographically determined to date. Further UV/Vis spectroscopic characteristics were recorded for H_2Se, HSe^- and $(Se_x)^{2-}$ (x = 1–4) in aqueous solutions, and their equilibria were investigated by *Licht* and *Forouzan*.[71] Complementary Raman spectroscopy and *ab initio* molecular orbital calculations led to the observation of an $(Se_2)^-$ radical anion by *Saboungi* and co-workers.[20] Pressing these Raman results further, the same group succeeded in incorporating selenium species in zeolites; they reported a subsequent, photoinduced decomposition of the original chains,[72] and generated an air-stable selenium/zeolite nanocomposite.[73]

Mass Spectometry

The existence of a $(Se_5)^{2-}$ species in solution was determined by electrospray ionization mass spectroscopy (ESI-MS) and further studies on pH dependencies and the impact of different counterions were elucidated by *Dorhout* and coworkers.[74] However, further mass spectrometric data have not been reported to date.

^{77}Se NMR Spectroscopy

Björgvinsson and *Schrobilgen* started a compilation of various homo- and hetero-(poly)chalcogenides in *en* and/or liquid NH_3[21] and on the $(HSe)^-$ anion in the solid state,[30] which were complemented by *Cusick* and *Dance* in other solvents.[75] Both groups could not observe an $(Se_2)^{2-}$ in solution, which seems to disproportionate. *Kanatzidis* and co-workers carried out complementary studies in the solid state and reported ^{77}Se experiments on $(NMe_4)_2Se_x$ with x = 5, 6.[51] Computational NMR studies so far focused on different methods, functionals and basis sets,[76] or on special treatment of relativistic effects.[77]

Crystal Structures

Crystallographic data and refinement details for compounds **1–26** are summarized in Tables S1–S7 (Supporting Infor-

Dedicated Cluster

mation). A summary of selected structural parameters of all known (poly-)selenide compounds with cations according to category (c) is provided in Tables S8–S13, including closest distances between selenium atoms and adjacent atoms from solvent molecules or cations. The crystal structures of all new compounds will be provided in the following, in comparison with known data.

[$Li_2(H_2O)_7$]Se (1)

The structure is composed of dimeric $[Li_2(H_2O)_7]^{2+}$ cations with two corner sharing tetrahedral $[Li(OH_2)_4]^+$ units [Li···O 1.910(8)–1.998(7) Å]. Although hydrogen atoms could not be located crystallographically during the structure determination, it is anticipated that Se^{2-} ions and water molecules are connected to each other by hydrogen bridges [Se···O 3.303(3)–3.444(4) Å]. Selenium ions are situated at the barycenter of distorted, gyroelongated square bipyramids that are formed by oxygen atoms of the cations [Se···O 3.303(3)–3.444(3) Å, see Figure 2].

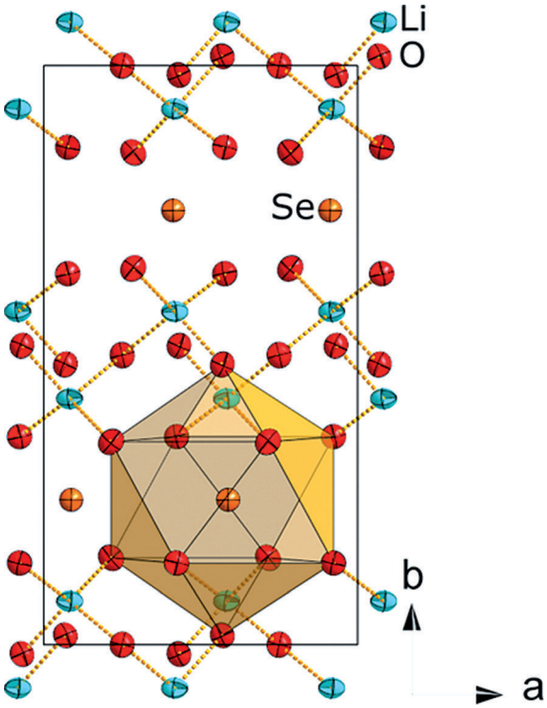

Figure 2. Fragment of the crystal structure of **1** and selenide anion embedding polyhedra of oxygen atoms. Thermal ellipsoids are drawn at 50% probability.

[$K(H_2O)_4]_2Se$ (2)

The cationic substructure represents distorted $[K(H_2O)_6]^+$ octahedra with K···O distances of 2.754(2)–2.954(3) Å, which form 1D strands by *trans*-face-sharing. The strands extend along [120] or [–110], being stacked into sheets parallel to (004) (Figure 3). Both orientations alternate along the crystallographic [001] axis. Selenide anions are located within the almost ideal icosahedral voids that are built by oxygen atoms from four adjacent anionic strands. Even though no hydrogen atoms could be crystallographically determined, the interaction is anticipated to be realized via hydrogen bonds. Accordingly, Se···O-distances for the icosahedral assembly are 3.391(2), 3.417(2), and 3.462(2) Å.

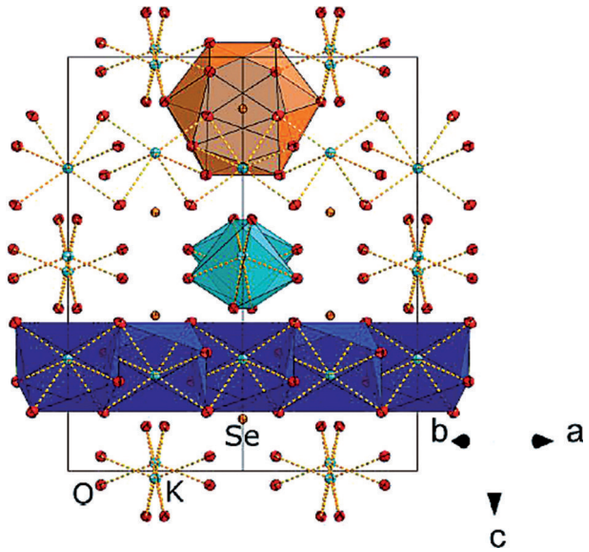

Figure 3. Fragment of the crystal structure of **2**, highlighting the polyhedra discussed in the text: strands of edge-sharing $[K(OH_2)_6]^+$ units along [120] (light blue) or [–110] (dark blue), and icosahedral selenide anion embedding polyhedron (orange). Thermal ellipsoids are drawn at 50% probability.

[$K_4(H_2O)_{10}$](Se_2)Se (3)

The cation substructure is constructed from two different potassium cation coordination spheres. The first polyhedron is based on a $[K(H_2O)_6]^+$ pentagonal pyramid with an additional coordination of a diselenide fragment opposite the apical water oxygen ligand (see Figure 4, top right). The second polyhedron, $[K(H_2O)_7(Se_2)]^-$, possesses an equatorial hexangular coordination by four neighboring oxygen atoms of water ligands and one diselenide unit, capped on one side by one further water molecules, and on the opposite side by two oxygen atoms from water (see Figure 4, bottom right). The two coordination polyhedra are interconnected in such a way, that a 3D network is formed with channels parallel to [001] (at 0,0,z or ½,½,z, Figure 4) that comprise the monoselenide anions. The diselenide dumbbells are located close to ½,0,¼, ½,0,¾ and 0,½,¼, 0,½,¾, aligned parallel to [001] and coordinating to four potassium ions [K···Se 3.3689(15)–3.4668(14) Å] orthogonal to and centered around the Se–Se bond [2.4468(16) Å]. Alternatively, this arrangement can be described as an $[K_4Se_2]$ square pyramid with selenium on the apical and potassium on the equatorial positions. The monoselenide ions are again embedded within icosahedra of water oxygen atoms.

[$Ba(H_2O)_x]_3[Ba(OH)_2(H_2O)_{x-2}]Se_3$ ($x \approx 13$) (4)

The asymmetric unit contains four barium cations and 14.75 oxygen atoms from solvent water, coordinating water mol-

Dedicated Cluster

Zeitschrift für anorganische und allgemeine Chemie ZAAC Journal of Inorganic and General Chemistry

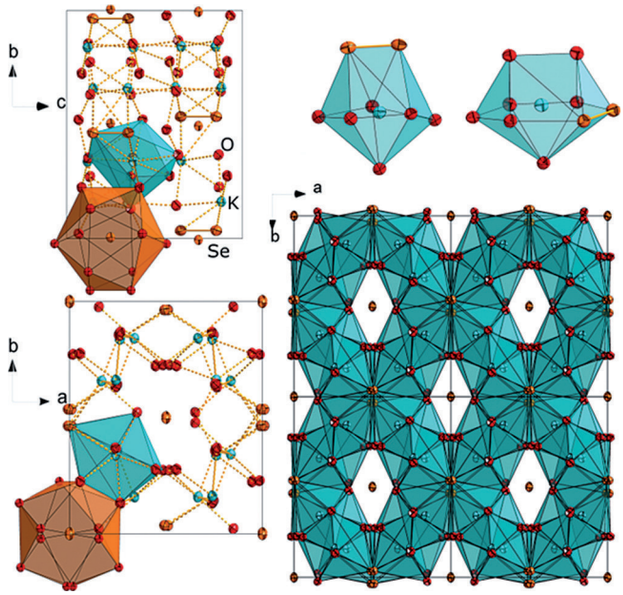

Figure 4. Crystal structure of **3** with coordination polyhedron of monoselenide and potassium ion with c.n. 9 along [110] (top left) and [001] (bottom left) axis. Coordination polyhedron of potassium ions (top right) and super cell with resulting channels comprising monoselenide ions (bottom right). Thermal ellipsoids are drawn at 50 % probability.

ecules or coordinating hydroxide anions. Most of the oxygen atoms are disordered with occupation numbers of 0.25 or 0.5. Reasonable coordination models taking into account the disorder due to diverse positions of the water ligands result in occupation numbers of 8 to 10 for the cations. Figure 5 (top) emphasizes one possible model that will be described in the following: A threefold face-sharing of the coordination polyhedra of Ba1, Ba2, and Ba3 within the same plane results in 2D layers parallel to the (201). The Ba4 coordination polyhedron in contrast is face-sharing with the coordination polyhedron of Ba3 within the Ba1/2/3 plane and edge-sharing with its symmetry equivalent out of the Ba1/2/3 plane, thereby forming a step of the cationic substructure as can be depicted in Figure 5. The whole arrangement results in cavity channels along [001] that are occupied by additional solvent water and monoselenide anions. The latter are situated in between the aforementioned layers.

(enH)$_2$(Se$_2$) (5)

Diselenide anions are aligned parallel to [110] with Se–Se distances of 2.3917(5) Å. *En*-onium cations form dimers by hydrogen bridges [N···N 2.822(4)–2.910(3) Å, see Figure 6] and coordinate diselenide anions by hydrogen bridges [N···Se 3.350(2)–3.580(3) Å].

[Li(en)$_3$]$_2$(Se$_2$) (6)

All lithium ions possess a distorted tetrahedral coordination by three amine groups of three different *en* molecules and one

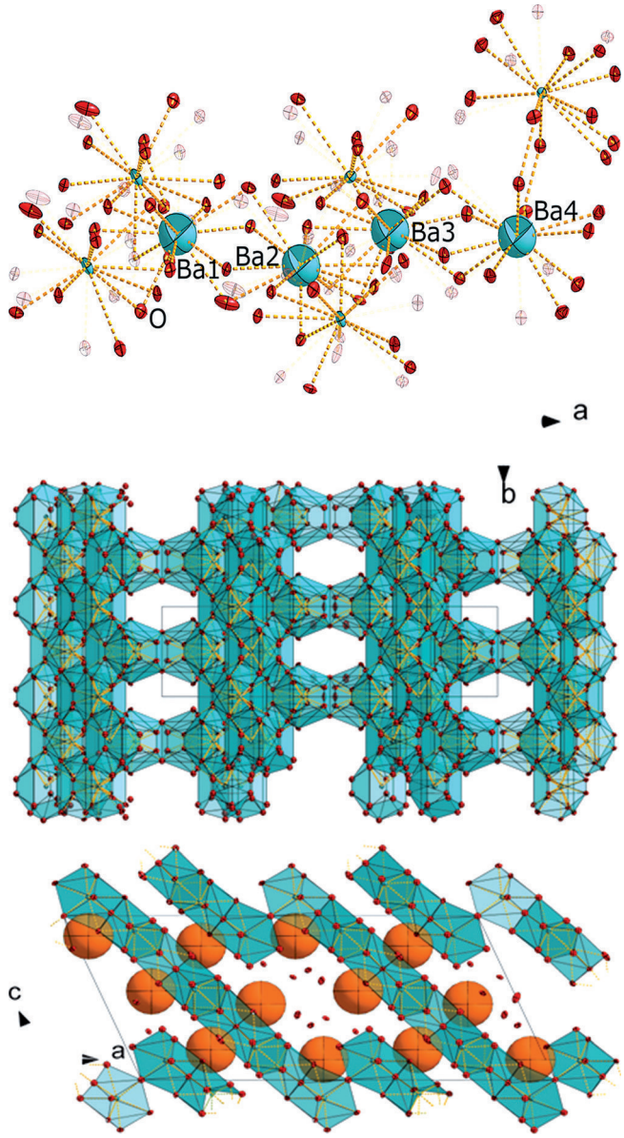

Figure 5. Crystal structure of **4**: Coordination of disordered water molecules to barium ions. Four barium ions of the asymmetric unit are drawn in balls/stick mode, one arrangement of disordered water molecules is drawn opaque (top). Resulting accumulated disorder network of barium hydrate/hydroxide substructure with cavity channels (middle), and monoselenide packing between the cation layers with selenide ions drawn in size-filling mode (bottom). Thermal ellipsoids are drawn at 50 % probability.

terminal selenium atom of a diselenide unit. In turn, all *en* molecules and the diselenide anions act as *trans* end-on μ-η^1:η^1-bridges between two lithium ions each, which results in the formation of two interpenetrated diamondoid coordination networks (Figure 7).[79] The Se–Se bond length is 2.3911(7) Å, the Li···Se distance amounts to 2.648(6) Å, Li···N distances are 2.055(6), 2.057(6), and 2.065(6) Å.

[K$_2$(H$_2$O)](Se$_2$) (7)

Potassium ions are coordinated in a pseudo-octahedral manner by two oxygen atoms of water molecules, three selenium

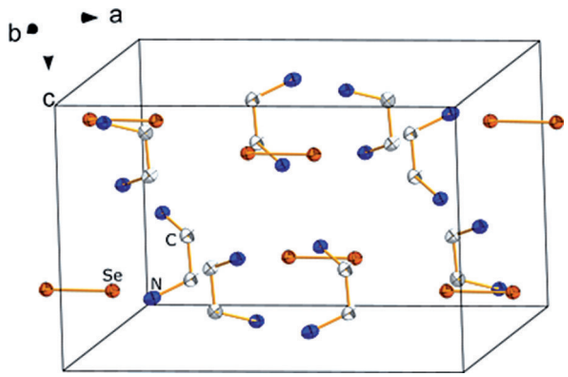

Figure 6. Crystal structure of **5**. Thermal ellipsoids are drawn at 50% probability, hydrogen atoms are omitted for clarity.

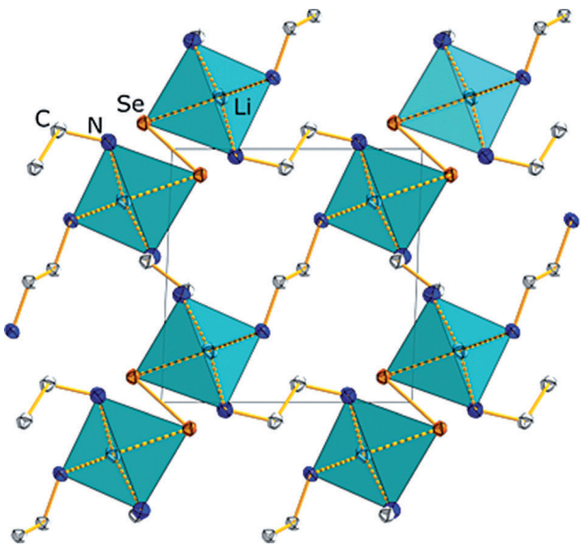

Figure 7. Crystal structure of **6**, highlighting the coordination polyhedra around lithium cations. Only one of the interpenetrating diamondoid nets is shown. Thermal ellipsoids are drawn at 50% probability, hydrogen atoms are omitted for clarity.

atoms of three different diselenide units, and two selenium atoms of one diselenide anion, if the barycenter of the latter is counted as one coordination site. According to their position within the coordination polyhedron, the two water ligands have very different distances to the potassium ions: 2.818(6) and 3.3201(16) Å. K···Se distances amount to 3.3588(15) and 3.4136(19) Å. The oxygen atoms bridge between two potassium cations each; closest selenium atoms are 3.3492(31) Å apart. Diselenide dumbbells are located within a coordination polyhedron, which is best described as two rectangular face-sharing trigonal prisms, built from eight potassium cations (Figure 8).

[K$_2$(NH$_3$)](Se$_2$) (8)

Compound **8** crystallizes isotypically to **7**, with slight variations of the lattice parameter (see Table S4, Supporting Information). Selected bond length are Se–Se 2.405(3) Å and K···N 2.835(14) Å.

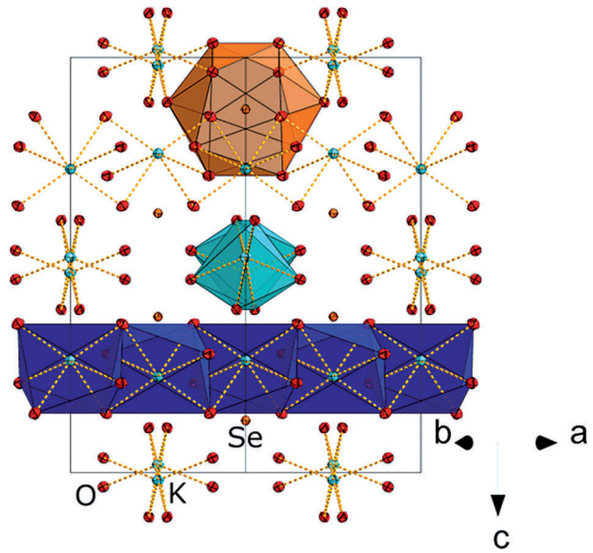

Figure 8. Crystal structure of **7** with diselenide containing (top) and potassium containing (bottom) coordination polyhedron. Thermal ellipsoids are drawn at 50% probability.

[K(18-crown-6)]$_2$(Se$_2$)·en (9)

Potassium ions are coordinated by six oxygen atoms of the crown ether molecules [K···O 2.8143(15)–3.0541(16) Å], two selenide atoms of one side-on μ-η^2:η^2-bridging diselenide dumbbell [Se–Se 2.4063(4) Å, K···Se 3.1868(5) and 3.2995(5) Å], and one amine group of a *trans* end-on μ-η^1:η^1-bridging *en* molecule [K···N 3.462(2) Å]. The two crown ether molecules show an inclined orientation to each other, including a mean plane angle of approximately 33°, owing to the lone pairs at the selenium atoms of the bridging (Se–Se)$^{2-}$ anion. The arrangement forms a 1D strand along [001]. Two neighboring strands are shifted against each other, such that crown ether molecules step into the voids that the smaller (Se–Se) units produce along the chains (Figure 9).

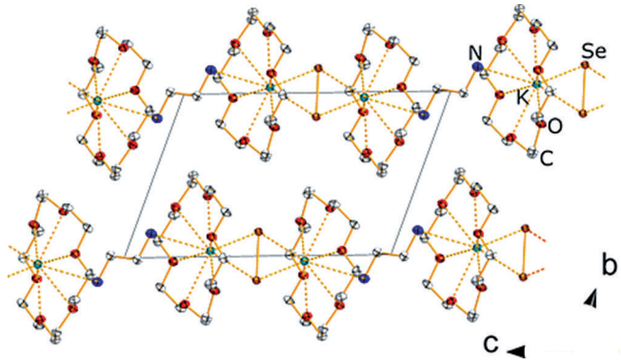

Figure 9. Crystal structure of **9**. Thermal ellipsoids are drawn at 50% probability. Hydrogen atoms are omitted for clarity.

Zeitschrift für anorganische und allgemeine Chemie ZAAC Journal of Inorganic and General Chemistry

$^{1}_{\infty}$[{K(18-crown-6)}{K(NH$_3$)}(Se$_2$)] (10)

The essential structural motif is a $^{1}_{\infty}$[{μ^3-η^2:η^2:η^2-Se_2)K]$^-$} zigzag strand along [001]. Besides coordination to two diselenide anions [Se–Se 2.4182(6) Å, K···Se 3.2877(10), 3.2969(12) Å], each potassium cation within the strand is coordinated by one molecule of ammonia [K···N 3.063(5) Å] and one oxygen atom from an adjacent crown ether complex [K···O 2.977(4) Å], to receive a distorted sixfold coordination. The crown ether embeds a second potassium ion [K···O 2.846(3)–2.925(4) Å], which is not part of the zigzag strand. This second potassium ion is further coordinated by the diselenide unit within the strand [K···Se 3.2877(10) Å, Figure 10] to obtain c.n. = 8. As in **9**, the different strands within the crystal structure are shifted against each other to enable best packing.

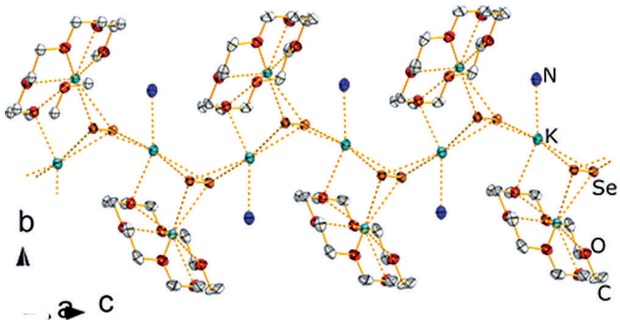

Figure 10. Fragment of the crystal structure of **10**. Thermal ellipsoids are drawn at 50 % probability. Hydrogen atoms are omitted for clarity.

Cs$_4$(Se$_2$)(Se$_3$)·en (11)

Within the structure, one observes twelve crystallographically independent cesium atoms with ten different types of coordination (see Figure 11) that are realized by various combinations of every possible hapticity of $(Se_2)^{2-}$, $(Se_3)^{2-}$ and *en* moieties (Table 1). The most frequent c.n. is 8, yet 7 (Cs6, Cs9) and 9 (Cs1, Cs2, Cs11) is also realized. By interconnection of these coordination polyhedra, a complicated 3D network is produced. The polyselenide anions show different cationic environments, as well, and come up with different structural parameters: Se–Se distances within the four crystallographically independent diselenide anions are very similar, 2.394(3), 2.401(3), 2.403(3), and 2.404(3) Å. The two crystallographically independent triselenide anions show a slightly larger range of Se–Se distances, with or without intramolecular differences [2.305(4) and 2.358(3) Å or 2.342(3) Å and 2.349(3) Å, respectively]. Se–Se–Se angles are 108.27(15) and 107.85(14)°.

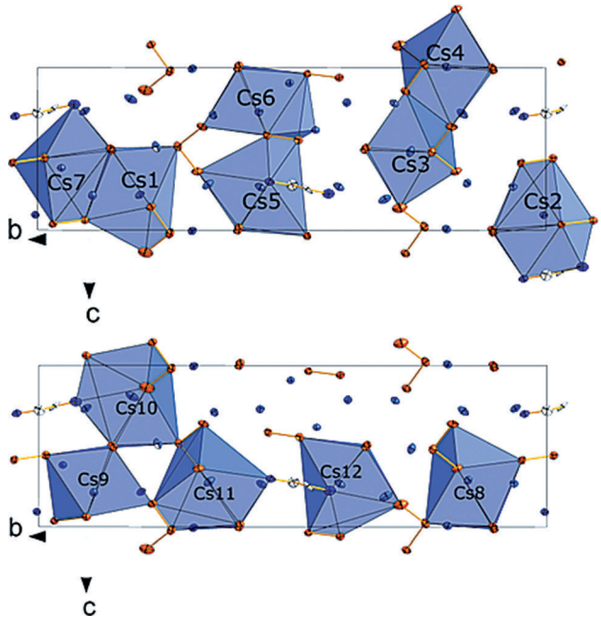

Figure 11. Crystal structure of **11** with coordination polyhedron of Cs1 through Cs7 (top) and Cs8 through Cs12 (bottom). Thermal ellipsoids are drawn at 50 % probability. Hydrogen atoms are omitted for clarity.

(NMe$_4$)$_2$(Se$_2$) (12)

The barycenters of diselenide dumbbells [Se···Se 2.3888(3) Å] occupy corners and face centers of the cubic cell, being tilted by 66.007(17)°. The $(NMe_4)^+$ cations are situated in the tetrahedral holes (Figure 12) and interact with the Se_2 units via hydrogen bridges.

[K(18-crown-6)]$_2$(Se$_3$) (13)

Potassium cations are coordinated by six oxygen atoms from crown ether ligands [K···O 2.839(2)–3.150(2) Å] and by two or three selenium atoms, respectively (depending on the disorder

Table 1. Coordination environment of different Cs atoms within **11**. Asterisks indicate terminal and bridging Se atom of different $(Se_3)^{2-}$ subunits responsible for coordination.

	$(\eta^1\text{-}Se_2)^{2-}$	$(\eta^2\text{-}Se_2)^{2-}$	$(\eta^1\text{-}Se_3)^{2-}$	$(\eta^2\text{-}Se_3)^{2-}$	$(\eta^3\text{-}Se_3)^{2-}$	η^1-en	η^2-en	c.n.
Cs1	1	1	1	1	1			9
Cs2	1	3					1	9
Cs3, Cs4	2		2	2				8
Cs5, Cs12	3	1	1			1		8
Cs6, Cs9	4	1	1					7
Cs7	1	3				1		8
Cs8	1	1	2*		1			7
Cs10		1	2*		1	1		8
Cs11		1	1	1	1	1		9

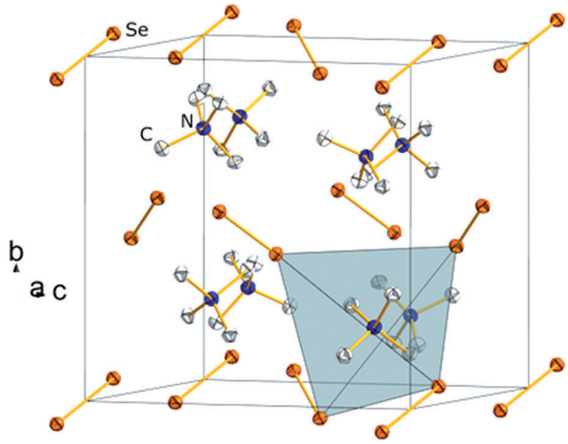

Figure 12. Crystal structure of **12**, highlighting the tetrahedral coordination sphere of one of the $(NMe_4)^+$ cations. Thermal ellipsoids are drawn at 50% probability. Hydrogen atoms are omitted for clarity.

situation), from triselenide anions [K···Se 3.2969(13)–3.8584(13) Å, see Figure 13]. The triselenide anion, in turn, is a μ-η2:η3-bridge between two $[K(18\text{-}crown\text{-}6)]^+$ fragments [Se–Se 2.2486(10)–2.4892(11) Å]. The central selenium atom is statistically disordered over two positions [0.7953(11) Å apart from each other], which includes an uncertainty in the absolute Se positions and explains the relatively short Se–Se distance. The crown ether complexes are tilted against each other by approximately 85°.

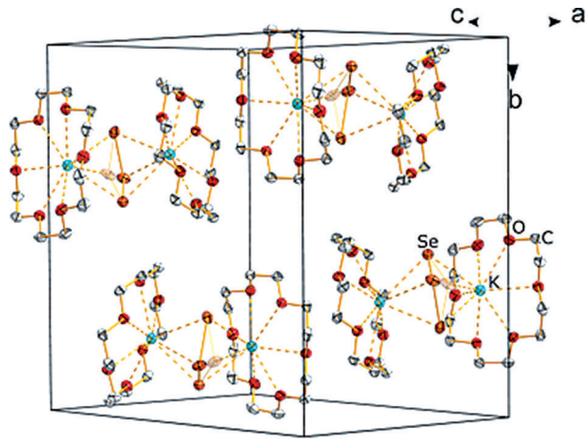

Figure 13. Crystal structure of **13**. Thermal ellipsoids are drawn at 50% probability, disorder is shown via opaque atoms. Hydrogen atoms are omitted for clarity.

[K(18-crown-6)]$_2$(Se$_3$)·H$_2$O (14)

Potassium cations show coordination by six oxygen atoms from crown ether ligands, by three selenium atoms of the triselenide anion [K···Se 3.3952(13)–3.7946(12) Å] and – statistically – half an oxygen atom from water [see below; K···O 2.940(7) Å]. The triselenide anion is situated in a side-on μ-η^2:η^2-bridging position between two $[K(18\text{-}crown\text{-}6)]^+$ complexes. The central Se atom (Se2) is disordered over two positions with according half site occupation. Se–Se bond lengths are 2.2927(11) and 2.6110(13) Å. The disorder of the triselenide unit comes along with a disorder of the coordinating water molecule, which is also disordered over two positions, such that only one of the two potassium ions per dinuclear complex comprises an additional water ligand on average.

Taking the disorder into account, the resulting complex $[K(18\text{-}crown\text{-}6)](OH_2)(\mu\text{-}\eta^2\text{:}\eta^2\text{-}Se_3)[K(18\text{-}crown\text{-}6)]$ shows crystallographic inversion symmetry. The corresponding barycenters are positioned on the centers of the four unit cell edges parallel to the *b* axis (0,½,0; 0,½,1; 1,½,0; 1,½,1) and on the centers of the two faces parallel to the *ac* plane (½,0, ½; ½,1, ½). The imaginary K···K axes of both positions are inclined against each other by 139.534(65)° (Figure 14).

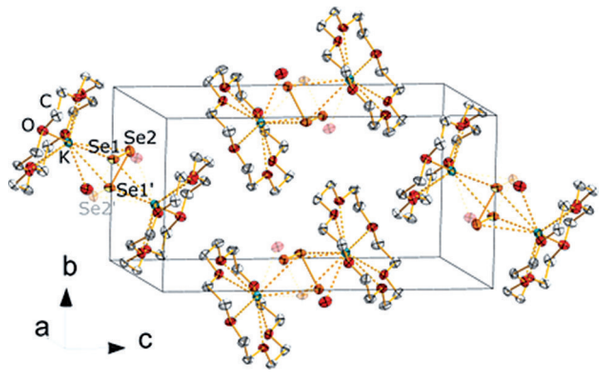

Figure 14. Crystal structure of **14**. Dinuclear complexes that are centered around 0,½,0 or 1,½,1 (see text) are not drawn for clarity. Thermal ellipsoids are drawn at 50% probability. Hydrogen atoms are omitted for clarity.

[{K(18-crown-6)}$_2$(H$_2$O)$_3$](Se$_3$)·2H$_2$O (15)

Potassium cations are coordinated by six oxygen atoms from the crown ether. Further coordination sites are either occupied by two adjacent selenium atoms from the triselenide unit and one oxygen atom from coordinating water [K···Se 3.4029(11) and 3.5839(11) Å, K···O 2.991(3) Å], or by two oxygen atoms [K···O 2.871(4) and 2.784(3) Å]. The triselenide can be regarded as a *trans* end-on-side-on μ-η^1:η^2-bridging by Se···(H)O···K [Se···O: 3.286(3) Å] ligand [Se–Se 2.3610(6) and 2.3687(7) Å] between two $[K(18\text{-}crown\text{-}6)]^+$ complexes. Besides those water molecules that are involved in coordination, two further solvent water molecules are found within the crystal structure (Figure 15). A pair of dinuclear complexes $[K(18\text{-}crown\text{-}6)](OH_2)_2(\mu\text{-}\eta^1\text{:}\eta^2\text{-}Se_3)(H_2O)[K(18\text{-}crown\text{-}6)]$, which enclose an inversion center between them, is located on each of the faces parallel to (002) and (020).

[K([2.2.2]crypt)]$_2$(Se$_3$)·H$_2$O (16)

The potassium ions are entirely encapsulated by the cryptand molecules, thus coordinated by six oxygen and two nitrogen atoms. As observed in **14**, the central Se atom of the triselenide anion shows twofold disorder. Again, a statistically dis-

Dedicated Cluster

Zeitschrift für anorganische und allgemeine Chemie ZAAC Journal of Inorganic and General Chemistry

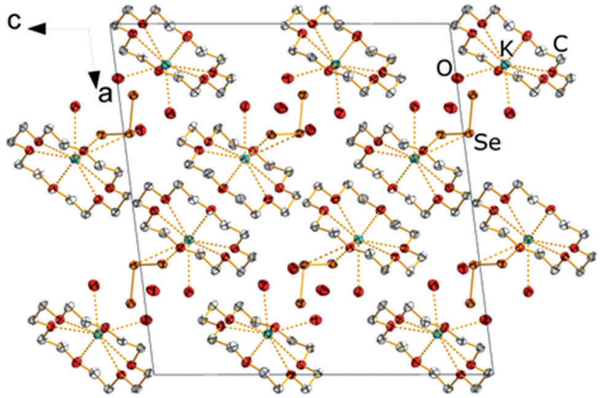

Figure 15. Crystal structure of **15**. Thermal ellipsoids are drawn at 50 % probability. Hydrogen atoms are omitted for clarity.

ordered solvent water molecule is nearby, with site occupation factors of 0.5 for the four split positions of Se and O atoms (Figure 16). Se–Se bonds are 2.3474(8) Å and 2.4224(8) Å, enclosing an Se–Se–Se angle of 111.59(3)°. The barycenter of the disordered triselenide *pseudo*-four-membered rings occupy corners and faces of the (002) plane at $c = 0$ and 0.5, with the arrangements in both positions being inclined against each other by 65.785(33)°. Eight $[K([2.2.2]crypt)]^+$ cations per unit cell are located within the polyselenide anions such that they have five nearest polyselenide units within 6.957–9.413 Å (K···"Se–$(Se_{0.5})_2$–Se" centroid).

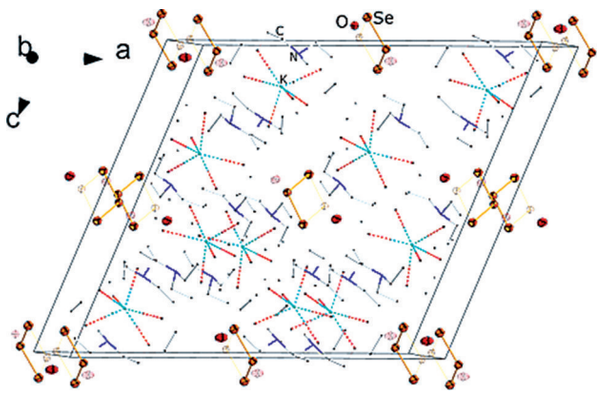

Figure 16. Crystal structure of **16**. Thermal ellipsoids are drawn at 50 % probability. $[K([2.2.2]crypt)]^+$ units are drawn as wireframes and hydrogen atoms are omitted for clarity, disorder is represented by opaque drawing.

$[M(en)_3](Se_3)$ with M = Fe, Cd (17, 18)

The structure of **17** comprises distorted octahedral $[Fe(en)_3]^{2+}$ complexes and triselenide anions. Fe–N distances range from 2.20(5) to 2.235(5) Å. N–Fe–N angles are 78.6(3)–97.68(18)°. The triselenide units are almost coplanar within (004) and (004–), with a Se–Se bond lengths of 2.3489(6) Å and an Se–Se–Se angle of 103.63(4)°.

18 crystallizes in the monoclinic space group *C*2/*c* with four formula units per unit cell and $[Cd(en)]^{2+}$ replacing the iron complexes of the latter compound. The *en* ligands show twofold disorder, which was modeled by according split positions. Selected structural parameters are Cd–N 2.354(16)–2.400(14) Å, Se–Se 2.3411(14) Å, Se–Se–Se 104.70(8)° (Figure 17).

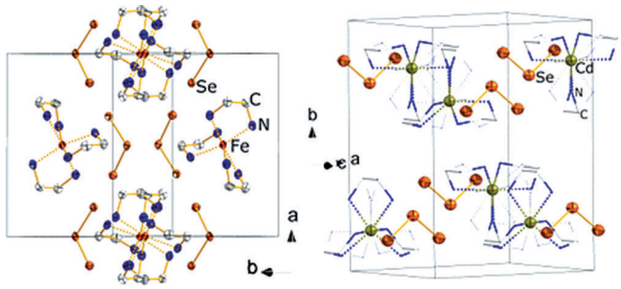

Figure 17. Crystal structures of **17** (left) and **18** (right). Thermal ellipsoids are drawn at 50 % probability. Disorder is shown by opaque representation and hydrogen atoms are omitted for clarity.

$[K_2(H_2O)](Se_4)$ (19)

Potassium cations exhibit two different coordination polyhedra, both with c.n. 10. One of them comprises two tetraselenide anions in a η^2-(1,2) coordination mode [K···Se 3.287(2)–3.990 (2) Å], and two additional oxygen atoms from water ligands [K···O 2.830(8)–3.398(8) Å]. The second coordination polyhedron is realized by twofold η^1 coordination of terminal selenium atoms of tetraselenide units, two tetraselenide ligands in η^2-(1,3) coordination, one η^2-(2,3) coordination, besides two further oxygen atoms with η^1 coordination (Figure 18). The shortest K···Se distance is obtained for terminal coordination [3.295(2) Å], the longest occurs for bridging selenium atom in the η^2-(1,3)-coordination mode [3.940(2) Å]. The tetraselenide anion is not disordered; it exhibits Se–Se bond lengths of 2.3622(15) Å (Se1–Se2), 2.3618(13) Å (Se2–Se3), and

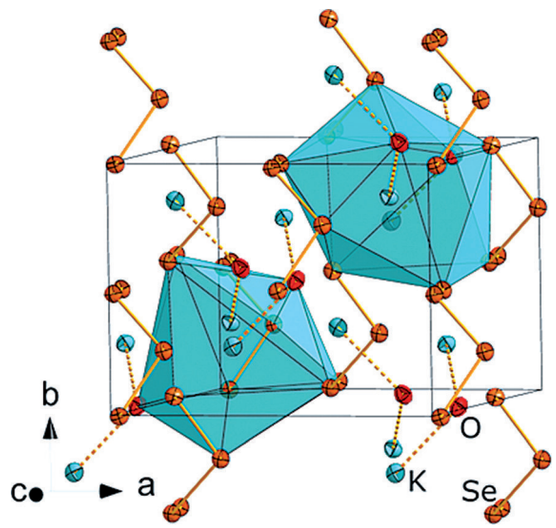

Figure 18. Crystal structure of **19** and coordination polyhedron for potassium cations. Thermal ellipsoids are drawn at 50 % probability.

Dedicated Cluster

2.3567(14) Å (Se3–Se4); Se–Se–Se angles are 105.64(6) and 106.25(5)°, and the Se–Se–Se–Se torsion angle amounts to 99.64 (6)°.

[K$_2$(H$_2$O)$_2$](Se$_4$) (20)

The compound differs from **19** by an additional water ligand. Potassium cations are coordinated with c.n. 10. The first coordination environment results from η^1 coordination by three water molecules [K···O 2.728(8), 3.240(9), 3.259(9) Å], one η^1 coordination by one of the inner selenium atoms of an tetraselenide anion, one η^1 coordination by a terminal selenium atom of another anion, one η^2-(1,2) coordination and one η^3-(1,2,4) coordination by two further anions. K···Se distances are 3.341(3)–3.547(3) Å (Figure 19). The other coordination environment is realized by three oxygen atoms [K···O 2.709(7), 3.106(9), 3.148 (9) Å], one η^1 coordination by a terminal selenium atom, one η^3-(1,2,3) coordination and one η^3-(1,2,4) coordination. K···Se distances are 3.321(2)–4.293(3) Å. The tetraselenide anions possess Se–Se bond lengths of 2.3599(14) Å (Se1–Se2), 2.3611(14) Å (Se2–Se3), and 2.3450(16) Å (Se3–Se4), with Se–Se–Se angles of 104.04(6) and 106.80(5)°, and a Se–Se–Se–Se torsion angle of 76.51(6)°.

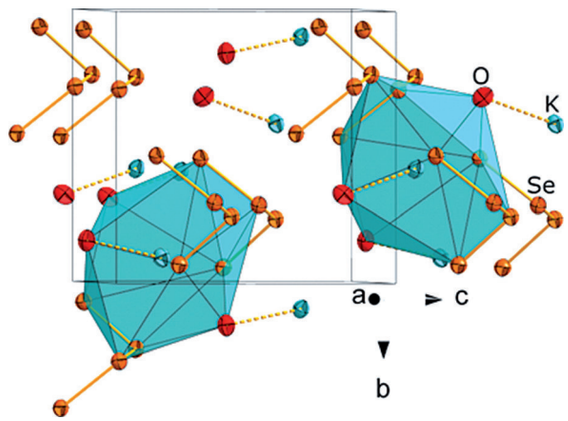

Figure 19. Crystal structure of **20**, highlighting the coordination polyhedra around the potassium cations. Thermal ellipsoids are drawn at 50 % probability.

[K$_2$(NH$_3$)](Se$_4$) (21)

Compound **21** crystallizes isotypically to **19** with Se–Se distances 2.368(3) Å (Se1–Se2), 2.361(3) Å (Se2–Se3), and 2.358(3) Å (Se3–Se4), Se–Se–Se angles of 106.19(8) and 105.70(8)°, and a torsion angle of 99.72(9)°.

[K([2.2.2]crypt)]$_2$(Se$_4$) (22)

Potassium cations are encapsulated by [2.2.2]*crypt* molecules, thus coordinated by six oxygen and two nitrogen atoms. The tetraselenide anions possess C_{2h} symmetry and are centered around the center of the unit cell edges parallel to the [100] axis [Se1–Se2 2.3239(11) Å, Se2–Se2′ 2.4058(15), Se–Se–Se 101.50(4)°, Figure 20].

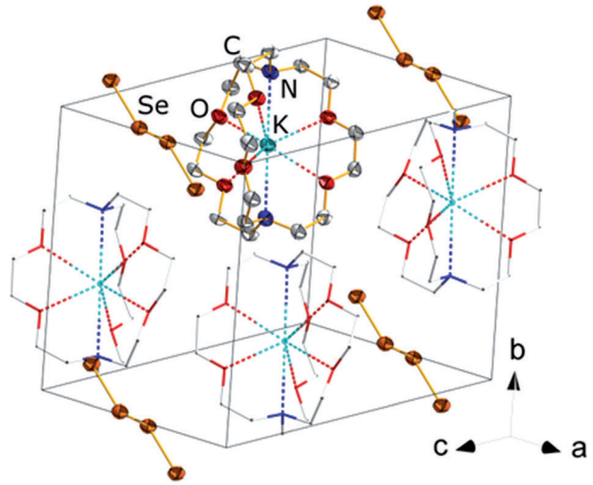

Figure 20. Crystal structure of **22**. Thermal ellipsoids are drawn at 50 % probability, three [K([2.2.2]*crypt*)]$^+$ fragments are drawn in wire/stick modus and hydrogen atoms are omitted for clarity.

[Ba(H$_2$O)$_6$](Se$_4$) (23)

Barium cations are coordinated by nine oxygen atoms from water molecules, forming a nearly regular delta-tetrakisdecaeder with nine apices. Each of these share three edges with adjacent polyhedra, thereby forming a honeycomb-like network (slightly compressed in [460] direction) parallel to (002) [Ba···O 2.697(6)–2.862(6) Å, Figure 21]. The tetraselenide anions (C_{2h} symmetry) are centered around the center of the unit cell edges parallel to [010] [Se1–Se2 2.3456(1) Å, Se2–Se2′ 2.392(2) Å; Se–Se–Se 98.88(6)°]. They are arranged in layers that are located between the cation complex layers; $(Se_4)^{2-}$ anions and $[Ba(OH_2)_9]^{2+}$ cations interact with each other by hydrogen bonds [Se···O 3.420(7)–3.585(8) Å].

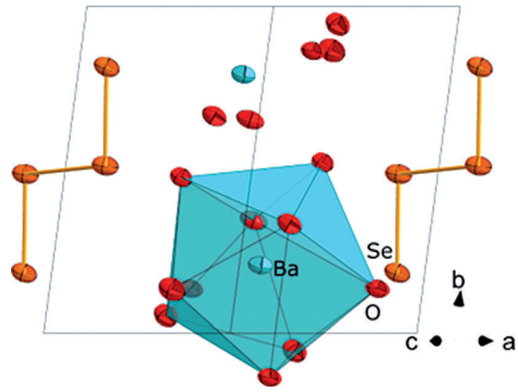

Figure 21. Crystal structure of **23** with barium coordination polyhedron. Thermal ellipsoids are drawn at 50 % probability.

[K(18-crown-6)]$_2$(Se$_6$)·(18-crown-6)·H$_2$O (24)

Potassium cations possess coordination number eight, by six oxygen from the crown ether molecules and by 1,2-type coordination of the $(Se_6)^{2-}$ fragment [K···Se 3.2750(8),

Dedicated Cluster

Zeitschrift für anorganische und allgemeine Chemie ZAAC Journal of Inorganic and General Chemistry

3.5242(9) Å]. The hexaselenide anion is disordered over two positions, with s.o.f. of approximately 0.95 vs. 0.05, and act as μ-η^2:η^2-bridge between two [K(18-*crown*-6)]$^+$ complexes. The resulting, neutral and centrosymmetric [K(18-*crown*-6)(μ-η^2:η^2-Se_6)K(18-*crown*-6)] units are aligned along [1$\bar{1}$0]. One additional 18-*crown*-6 molecule and one non-coordinating water molecule are situated between these *pseudo*-1D strands (Figure 22). Se–Se bond lengths are 2.3185(5) Å [Se1–Se2], 2.3239(6) Å (Se2–Se3), 2.3562(8) Å (Se3–Se3′). Se–Se–Se angles are 109.50(2)° (Se1–Se2–Se3), 108.92(2)° (Se2–Se3–Se3′). Torsion angles are 81.94(3)° (Se1–Se2–Se3–Se3′) and 65.10(3)° (Se2–Se3–Se3′–Se2′).

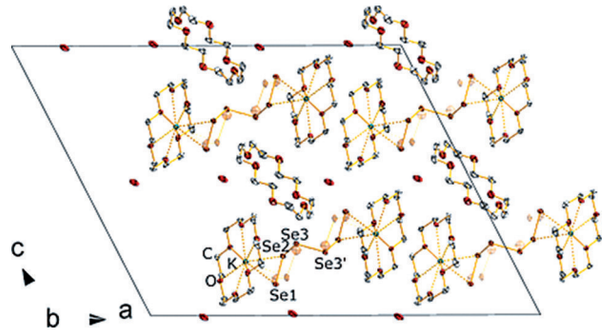

Figure 22. Crystal structure of **24.** Thermal ellipsoids are drawn at 50 % probability. The minor split positions of the atoms of the disordered hexaselenide unit is drawn in transparent mode; hydrogen atoms are omitted for clarity. The labelling scheme accords with the C_2 axis running through the barycenter of Se3–Se3′ bond.

[K(18-crown-6)]$_2$(Se$_6$)·(18-crown-6)·2NH$_3$ (25)

Compound **25** crystallizes isotypically with **24**. While the disorder of the hexaselenide fragment could not be crystallographically resolved (< 5 %), a second solvent molecule was located instead that can also be refined in **24** upon neglecting the disorder of the hexaselenide units.

(enH)$_2$(Se$_6$) (26)

All selenium atoms within one hexaselenide chain in **26** are crystallographically independent with Se···Se bond lengths of 2.346(2), 2.330(2), 2.352(2), 2.329(2), and 2.355(2) Å from head to tail. Terminal selenium atoms of neighboring hexaselenide anions are in close contact [Se–Se 3.182(2) Å], thereby forming a pseudo infinity anionic strand along [001] (see Figure 23). Se–Se–Se angles are ranging from 103.55(8) to 107.99(8)°, torsion angles from 71.19(10) to 81.70(10)°.

Optoelectronic Properties of Compounds with Triselenide Anions

A special feature of all triselenide compounds that were obtained during our study is the phenomenon of dichroism. In general, pleochroism describes the exhibition of different colors depending on the absolute orientation of single crystals

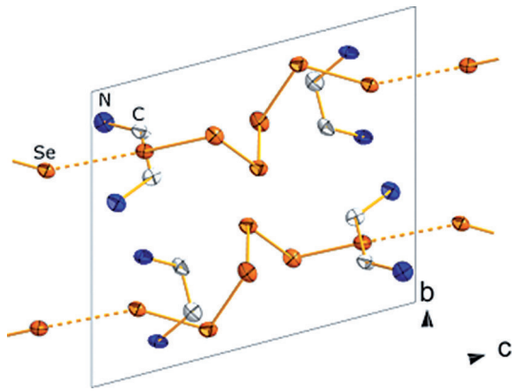

Figure 23. Crystal structure of **26**. Thermal ellipsoids are drawn at 50 % probability. Hydrogen atoms are omitted for clarity.

anent the plane of polarization of visible light. Whereas the description of pleochroic substances is quite common in mineralogy, this unique property so far has only scarcely been reported within the chemistry community.[80] Neither has such a property been mentioned within earlier discussion on triselenide containing substances.

The assumption that the optical activity is due to the chirality of the [$M(en)_3$]$^{2+}$ cation (M = Fe, Cd) in **17** and **18**, is easily frustrated by the fact that those salts crystallize in non-chiral space groups (e.g. in Laue class *mmm*), thus including both the Λ and the Δ isomer in varying relative arrangements along [110], [010], or [001], respectively. We synthesized a variety of further [$M(en)_3$]X_2 salts (X = NO_3, Cl, for instance) to validate this assumption. Indeed, almost all of them show distinct extinction upon rotation under a polarized-light microscope, yet no change in color could be observed, clearly ruling out the cation complex as the optically active chromophore.

We therefore focused on the triselenide anion as the source of pleochroism in the title compounds. Indeed, both **14** and **16** show different colors, depending on the very crystal orientation relative to the plane of polarized light. Ranging from green to red, we now tried quantification via both, simple UV/Vis spectroscopy of crystals suspended in nujol oil, and an angle-dependent measurement on a single crystal. While the latter suffered from too small crystal sizes and did not yield significant signals, the UV/Vis spectra of single-crystal suspensions showed two distinct absorption bands with E_{onset} of 1.6 and 2.4 eV (Figure 24).

Quantum chemical calculation of first singlet excitations using time-dependent density functional theory (TDDFT) methods on the crystal anion geometry exhibits four possible excitation energies for the C_{2v} symmetric anion: 1.796 eV (690 nm, b_2), 2.849 eV (435 nm, b_1), 2.365 eV (537 nm, a_2), and 3.085 eV (402 nm, a_1). Our previous investigations confirmed a general applicability of TDDFT values for interpretation of UV/Vis spectra of polychalcogenides;[78] therefore two of the excitations would be in the range of visible light and would explain (a) the measured UV/Vis spectra and (b) the observed change in color upon rotation under polarized light, thus the orthogonal excitation. The latter is in agreement with the clearly anisotropic anion packing (*vide supra*).

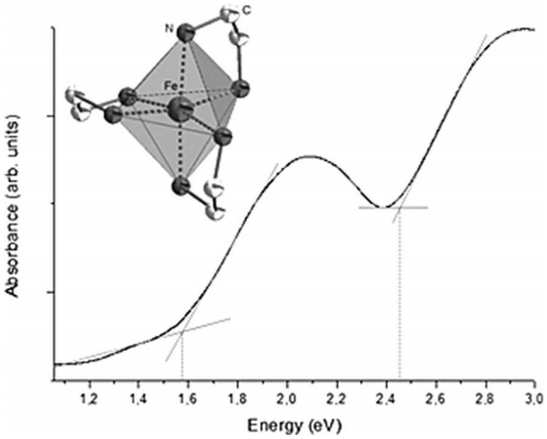

Figure 24. UV/Vis spectrum of (**14**), and structure of the Δ-[Fe(*en*)$_3$]$^{2+}$ enantiomer that is present beside the Λ-[Fe(*en*)$_3$]$^{2+}$ enantiomer in **17**. Hydrogen atoms are omitted for clarity.

The UV/Vis spectrum of **9** (E_{onset} = 1.82 eV, 681 nm; Figure 25) is shown as an example for the optical absorption behavior of diselenides in the solid state, which have not been reported to date. An experimental verification of the angular dependence of the UV/Vis absorbance is precluded due to the obtained crystal sizes. The presented data therefore remains qualitative. For absorption energies of compounds with longer polyselenide chains and monoselenide anions, see Refs. [71,20], for instance.

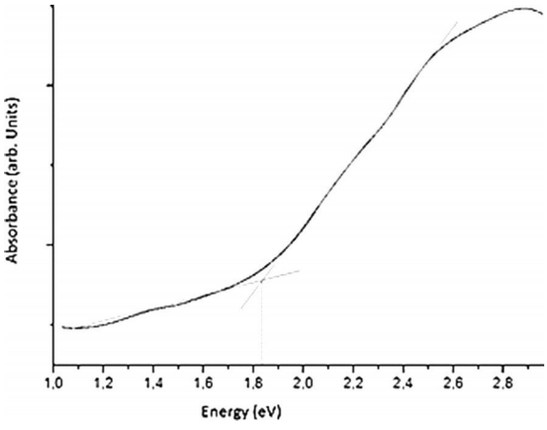

Figure 25. UV/Vis spectrum of **9** recorded on a suspension of crushed single crystals in Paratone^{TM} oil. E_{onset} = 1.8 eV (689 nm).

Conformational Isomerism within $(Se_x)^{2-}$ Anions with $x \geq 4$

As can be deduced in detail from Tables S9–S13 (Supporting Information), the dihedral angles within the structurally reported polyselenides cover a broad range from 49.5° in [Sr(15-*crown*-5)$_2$](Se$_9$)[58] (including secondary intramolecular interactions) to 180° in [Sr$_2$Sn(OH)$_6$(H$_2$O)$_6$](Se$_4$).[34] Since no *syn-periplanar* (∠ = 0°) conformation has been reported so far, this geometry seems to be energetically disfavored. In contrast, *syn-clinal* (∠ = 60°), *anti-clinal* (∠ = 120°) and *anti-periplanar* (∠ = 180°) arrangements, as well as angles in between appear to be primarily dependent of the coordination and packing within the crystal structure. We therefore performed density functional theory (DFT) calculations using the program system TURBOMOLE[83–86] on a tetraselenide anion, as an example, to elucidate the energy differences of different conformers characterized by different dihedral angles.

Indeed, the energy difference of *syn-periplanar* and *trans-periplanar* conformation is only 7.0 kJ·mol^{-1} (in favor of the *trans* isomer). As expected, the *syn-clinal* and *anti-clinal* isomers are energetically indistinguishable. However, an isomer with a dihedral angle of 60° is favored over the *trans* isomer. The optimum dihedral angle with lowest energy was found at 84.3°, with an energy difference of 16.8 kJ·mol^{-1} with respect to the *trans* isomer. Alongside the stabilization, a distinct contraction of the central Se–Se bond and a minor shortening of the terminal Se–Se bonds are observed, along with a change of the dihedral angle from 180° to 84.3° (see Figure 26, top). Regarding the molecular orbital diagrams of both isomers, the energy difference can easily be assigned to the repulsive interactions between the p orbitals of the central and the terminal Se atoms in both HOMO and HOMO-1, and between the p orbitals of the two central Se atoms in HOMO. Within the *trans* isomer, parallel orientation of the respective p orbitals enhances this repulsion, while tilting of the chain reduces the repulsion, especially along the central Se–Se bond (see Figure 26, right). Further orbitals are widely unaffected by the rotation.

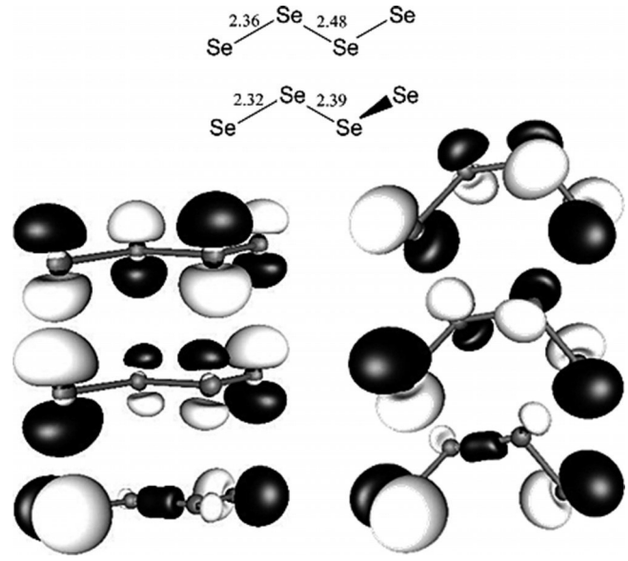

Figure 26. Calculated bond lengths in Å for the *trans* isomer (top, upper representation) and the isomer with a dihedral angle of 84.3° (top, lower representation). Representation of molecular orbitals with dihedral angles of 180° (bottom, left) and 84.3° (bottom, right); from top to bottom: HOMO, HOMO-1, HOMO-2. Amplitudes are plotted at +/– 0.05 a.u.

Nevertheless, even with a total energy difference of 23.7 kJ·mol^{-1} between the *syn-periplanar* isomer and the global minimum structure (with ∠ = 84.3°), the packing ef-

Zeitschrift für anorganische und allgemeine Chemie ZAAC Journal of Inorganic and General Chemistry

fects are likely to compensate these rather small energy differences. Therefore, *syn-periplanar* polyselenides are expected to be found with suitable counterions that allow for an according stabilization by the packing of the ions within the crystal.

Conclusions

By this report on 26 new (poly-)selenides with organic or metal complex cations, we have approximately doubled the number of respective compounds. We have provided a survey over syntheses and crystal structures along with some selected further properties that show the diversity of these salts. A classification according to *Ibers'* work on related polytellurides was made, and both the new and the known compounds were assigned to these classes.

Experimental Section

General Remarks on the Syntheses: All manipulations and reactions were performed in an argon atmosphere using standard *Schlenk* or glovebox techniques. The ternary parent phases "$A_xM_ySe_z$" were prepared by fusion of the elements if not stated otherwise, with an oxygen/methane burner for at least 15 min until homogeneity was achieved. In case of the presence of a metallic by-product phase, this was manually removed. The ternary product was pestled and further worked-up as described below. Solvent *en* was freshly distilled from CaH_2, THF, toluene and Et_2O from Na/K, and EtOH from Mg. All solvents were stored in an argon atmosphere prior to use. Deionized water was degassed at least 3 times to a final pressure $<1 \times 10^{-3}$ mbar and saturated with an argon atmosphere. The synthetic procedures are outlined in the following for all new compounds.

In the case of solvothermal reaction conditions, the bulk phase always contained amorphous (side-)products that were not further investigated. In the presence of K^+ ions, K_2Se_2, and K_2Se_3 could always be identified by single crystal diffraction. Binary selenides M_yCh_z are most likely side-products from extractions of the $A_xM_yCh_z$ alloys. Corresponding colors of side-product powder were observed. No metallic precipitate was observed. As a consequence, the provision of yields is afflicted with high uncertainty and is therefore omitted for all of the solvothermal reactions.

Energy dispersive X-ray spectroscopy has been performed for all samples to verify the absence of further metal atoms. All yields are given with respect to Se.

$[Li_2(H_2O)_7]Se$ (1): A binary solid of the nominal composition "$PbSe_2$" (1 g, 2.74 mmol) was suspended in liquid NH_3 (150 mL) at –35 °C and elemental lithium (40 mg, 5.75 mmol) was added within 2 h. The resulting suspension was stirred for 12 h. The reaction mixture was brought to room temperature and NH_3 evaporated. The resulting gray powder was extracted with H_2O (50 mL). 10 mL of the resulting solution was carefully layered with THF (15 mL). **1** crystallized after 1 week as colorless blocks in approx. 20 % yield.

$[K(H_2O)_4]_2Se$ (2): A ternary solid of the nominal composition "$K_2Hg_2Se_3$" (250 mg, 0.35 mmol), yielded from fusions of K_2Se (10g, 63.63 mmol) and the elements (9.13 g, 127.26 mmol Hg; 3.59 g, 127.26 mmol Se) were stirred for 2 h in H_2O (25 mL). The resulting solution was filtered and the solvent slowly evaporated to dryness. **2** crystallized as colorless blocks in approx. 15 % yield.

$[K_4(H_2O)_{10}](Se_2)Se$ (3): An alloy of the nominal composition "K_4PbSe_4" (250 mg, 0.37 mmol) was stirred for 2 h in H_2O (50 mL). The reaction mixture was filtered and 10 mL of the resulting solution were layered with an NMe_4Cl saturated THF solution (15 mL). **3** crystallized after 3 d as orange-red sticks in approx. 5 % yield.

$[Ba(H_2O)_x]_3[Ba(OH)_2(H_2O)_{x-2}](Se)_3$ (4): An alloy with the nominal composition "$PbSe_2$" (5 g, 13.69 mmol) and elemental Ba (2.43 g, 17.69 mmol) were stirred in *en* (50 mL). The reaction mixture was evaporated to dryness and 250 mg of the resulting powder was stirred for 12 h in H_2O (25 mL), filtered and layered with Et_2O (15 mL). **4** crystallized after 3 weeks as colorless sticks in approx. 20 % yield.

$(enH)_2(Se_2)$ (5): An alloy with the nominal composition "K_2TiSe_2" (0.5 g, 1.76 mmol) was stirred for 2 d in *en* (20 mL), filtered and carefully layered with toluene (15 mL). After 4 weeks the resulting solution was filtered and slowly evaporated to dryness. **5** was obtained as red sticks in approx. 10 % yield.

$[Li(en)_3]_2(Se_2)$ (6): Same procedure as for **4** but with elemental Li (198 mg, 28.57 mmol) instead of Ba. **6** crystallized after slow evaporation of *en* as red blocks in approx. 5 % yield.

$[K_2(H_2O)](Se_2)$ (7): An alloy of nominal composition of "K_2PbSe_2" (500 mg, 1.13 mmol) was heated for 7 d at 150 °C in a Teflon steel autoclave with *en* (2 mL) and H_2O (50 μL). After turning off the heating, the autoclave was left for 2 d to slowly cool to room temperature. Red plates of **7** were picked from the reaction mixture.

$[K_2(NH_3)](Se_2)$ (8): An alloy of the nominal composition "K_2PbSe_2" (5 g, 11.28 mmol) obtained by fusion of the elements (882.1 mg, 22.56 mmol K; 2.34 g, 11.28 mmol Pb; 1.78 g, 22.56 mmol Se) was soxhlet-extracted with NH_3 (350 mL) and refluxed for 4 h. The solution was slowly allowed to warm to room temperature and NH_3 to evaporate within 1 week. **8** crystallized as red needles in approx. 30 % yield.

$[K(18\text{-}crown\text{-}6)]_2(Se_2)\cdot en$ (9): An alloy of the nominal composition "$PbSe_2$" (0.5 g, 1.37 mmol) and 18-*crown*-6 (1.3 g, 4.92 mmol) were suspended in *en* (20 mL) and elemental potassium (0.15 g, 3.84 mmol) was added, stirred for 12 h, filtered and layered with toluene (20 mL). **9** crystallized after 4 weeks as red-orange plates in approx. 5 % yield.

$^1_\infty[\{K(18\text{-}crown\text{-}6)\}\{K(NH_3)\}(Se_2)]$ (10): Same procedure as for **8**, yet the resulting solution (15 mL) and 18-*crown*-6 (493 mg, 1.87 mmol) were stirred for 2 d prior to evaporation of solvent over 1 week. **10** crystallized as red blocks in approx. 25 % yield.

$Cs_4(Se_2)(Se_3)\cdot en$ (11): An alloy of the nominal composition "$CsPb_{0.26}Se$" (0.73 g, 2.75 mmol) and *en* (2 mL) were heated for 5 d at 200 °C in a Teflon steel autoclave. After turning off the heating, the autoclave was left another 2 d stand to cool to room temperature. **11** was picked manually as red plates.

$(NMe_4)_2(Se_2)$ (12): Same procedure as for **3**, yet using an NMe_4Cl saturated EtOH solution (15 mL) for layering. **12** crystallized after 2 d as red blocks in approx. 15 % yield.

$[K(18\text{-}crown\text{-}6)]_2(Se_3)\cdot H_2O$ (13): A solution of $[K(18\text{-crown-}6)]_2[Pb_2Se_3]$[81] (10 mL) was carefully layered with a saturated THF – that was not dried prior use – solution of $[Rh(PPh_3)_3Cl]$ (10 mL) and left for 4 weeks. The resulting reaction mixture was filtered and the solvents evaporated to dryness. **13** crystallized as orange blocks in approx. 5 % yield.

Dedicated Cluster

[K(18-*crown*-6)]$_2$(Se$_3$)·H$_2$O (14): An alloy of nominal composition "K_4PbSe_4" (0.5 g, 0.74 mmol), 18-*crown*-6 (400 mg, 1.51 mmol), and *trien* (2 mL) were heated in a Teflon steel autoclave that was only lightly closed – enabling certain air/moisture exposition – for 7 d at 150 °C. After cooling to room temperature for 2 d **14** was manually picked as red/green pleochroic plates.

[{K(18-*crown*-6)}$_2$(H$_2$O)$_3$](Se$_3$)·2H$_2$O (15): An alloy of the nominal composition "K_6HgSe_4" (3.28 g, 4.37 mmol), 18-*crown*-6 (6.98 g, 26.41 mmol) and H_2O (125 mL) were stirred for 12 h and filtered. 25 mL of the resulting solution were added to $Pb(NO_3)_2$ (292 mg, 0.88 mmol) and stirred for 2 h. The reaction mixture was filtered and the solvent volume decreased to ca. 10 mL and left standing for 3 months. **15** crystallized as red sticks in approx. 5 % yield.

[K([2.2.2]*crypt*)]$_2$(Se$_3$)·H$_2$O (16): Same procedure as for **15**, yet using [2.2.2]*crypt* (568.5 mg, 1.51 mmol) instead of 18-*crown*-6. **16** crystallized as red/green pleochroic plates.

[*M*(*en*)$_3$](Se$_3$) [*M* = Fe, Cd] (17, 18): An alloy of the nominal composition "K_2PbSe_2" (500 mg, 1.13 mmol), $FeCl_2$ (300 mg, 2.37 mmol) or $CdSO_4$ (400 mg, 1.92 mmol) and *en* (2 mL) were heated for 7 d at 150 °C in a Teflon steel autoclave. **17** and **18** crystallized as red/green pleochroic sticks.

[K$_2$(H$_2$O)](Se$_4$) (19): An alloy of the nominal composition "K_2PbSe_2" (500 mg, 1.13 mmol), $VO(acac)_2$ (300 mg, 1.13 mmol) and H_2O (2 mL) were heated for 7 d at 190 °C in a Teflon steel autoclave. **19** was manually picked as black sticks.

[K$_2$(H$_2$O)$_2$](Se$_4$) (20): An alloy of the nominal composition "$K_2Pb_2Se_6$" (250 mg, 0.26 mmol) was stirred with H_2O (25 mL) for 12 h and filtered. Upon removal of solvent, **20** crystallized as black sticks in approx. 15 % yield.

[K$_2$(NH$_3$)](Se$_4$) (21): Same procedure as for **8**, yet 11 mL of the resulting reaction solution was added to frozen *en* (7.5 mL). Upon evaporation of NH_3 and slow removal of *en* over 12 h **21** crystallized as red needles in approx. 15 % yield.

[K([2.2.2]*crypt*)]$_2$(Se$_4$) (22): An alloy of the nominal composition "K_2TiSe_2" (500 mg, 1.76 mmol), [2.2.2]*crypt* (729 mg, 1.94 mmol) and *en* (25 mL) were stirred for 2 d, filtered and the solvents evaporated to dryness. **22** crystallized as transparent-yellow blocks in approx. 30 % yield.

[Ba(H$_2$O)$_6$](Se$_4$) (23): Same procedure as for **4** yet layering with THF (15 mL) instead of Et_2O. **23** crystallized as transparent-yellow sticks in approx. 40 %.

[K(18-*crown*-6)]$_2$(Se$_6$)·(18-*crown*-6)·H$_2$O (24): Same procedure as **20**, yet in the presence of an excess of 18-*crown*-6 (343 mg, 1.3 mmol). **24** crystallized as red sticks in approx. 25 % yield.

[K(18-*crown*-6)]$_2$(Se$_6$)·(18-*crown*-6)·2NH$_3$ (25): Same procedure as for **8**, yet 100 mL of the resulting reaction solution was added to 18-*crown*-6 (350 mg, 1.33 mmol) and stirred for 2h. Upon evaporation of NH_3 over 1 week **25** crystallized as pale green blocks in approx. 20 % yield.

(*en*H)$_2$(Se$_6$) (26): An alloy of the nominal composition "$K_2Hg_2Se_3$" (0.5 g, 0.69 mmol) and $MnSO_4$ (300 mg, 1.98 mmol) were placed in a Teflon steel autoclave with a 1:1 mixture of *en*/*tmeda* (2 mL) and heated for 5 d to 150 °C. After turning off the heating, the autoclave was left another 2 d stand to cool to room temperature. **26** was picked manually as red sticks.

Single-Crystal X-ray Crystallography: All measurements were performed with a Stoe IPDS-II or a Stoe IPDS-II/T diffractometer at 100 K except measurements of **4**, **6**, **17** with a Stoe IPDS I at 193 K and **24**, **25** with a Bruker Quest at 100 K. All devices applied Mo-K_α radiation (λ = 0.71073 Å) and a graphite monochromator. Upon numerical absorption correction (for **24**, **25** semi-empirical SADABS correction), the structure solution was performed by direct methods, followed by full-matrix-least-squares refinement against F^2, using SHELXS-97, SHELXL-97, and OLEX2 software.[82] A summary of crystallographic and refinement details are given in the Supporting Information (Tables S1–S7).

Further details of the crystal structure investigations for compounds **1–4**, **7–8**, **19–21**, **23** may be obtained from the Fachinformationszentrum Karlsruhe, 76344 Eggenstein-Leopoldshafen, Germany (Fax: +49-7247-808-666; E-Mail: crysdata@fiz-karlsruhe.de, http://www.fiz-karlsruhe.de/request for deposited data.html) on quoting the depository number CSD-428547.

Crystallographic data (excluding structure factors) for the structures **5**, **6**, **9–18**, **22**, **24–26** in this paper have been deposited with the Cambridge Crystallographic Data Centre, CCDC, 12 Union Road, Cambridge CB21EZ, UK. Copies of the data can be obtained free of charge on quoting the depository numbers CCDC-1027047, CCDC-1027048, CCDC-1027049, CCDC-1027050, CCDC-1027051, CCDC-1027052, CCDC-1027053, CCDC-1027054, CCDC-1027055, CCDC-1027056, CCDC-1027057, CCDC-1027058, CCDC-1027059, CCDC-1027060, CCDC-1027061, and CCDC-1027062 (Fax: +44-1223-336-033; E-Mail: deposit@ccdc.cam.ac.uk, http://www.ccdc.cam.ac.uk).

UV/Vis Spectroscopy: Optical absorption spectra were recorded with a Varian Cary 5000 spectrometer. Single-crystalline samples were pulverized in nujol oil between two quartz plates.

Methods of the Quantum Chemical Inverstigations: All molecular electronic structure calculations were carried out with the TURBOMOLE program package V6.4.[83] The COSMO model was used for the compensation of negative charges.[84] Structure optimizations were undertaken by employment of the RIDFT program, using the BP86 functional[85] and def2-TZVP basis sets.[86] For the TD-DFT calculations, all geometries were optimized. Contour plots were generated with gOpenMole.[87]

Supporting Information (see footnote on the first page of this article): X-ray crystallographic data of **1**–**26** and selected structural parameters of all known organic cation and complex cation-stabilized (poly-)selenides, $[cation]_x(Se_y)_z$.

Acknowledgements

This work was financially supported by the Friedrich-Ebert-Stiftung (PhD grant for G.T.) and the Deutsche Forschungsgemeinschaft (DFG) within the framework of SPP 1415. Preparative assistance by *M. Müller*, *S. Krisch* and crystallographic support by *R. Riedel* and *Prof. Dr. W. Massa* is greatly appreciated.

References

[1] a) S. Wagner, J. L. Shay, P. Migliorato, H. M. Kasper, *Appl. Phys. Lett.* **1974**, *25*, 434–435; b) M. G. Panthani, V. Akhavan, B. Goodfellow, J. P. Schmidtke, L. Dunn, A. Dobabalapur, P. F. Barbara, B. A. Korgel, *J. Am. Chem. Soc.* **1998**, *120*, 16770–16777.
[2] F. Lips, S. Dehnen, *Inorg. Chem.* **2008**, *47*, 5561–5563.

Dedicated Cluster

[3] General review see, for example: a) W. S. Sheldrick in *Handbook of Chalcogen Chemistry*, (Ed.: F. Devillanova), The Royal Society of Chemistry, London, **2007**, ch 9.2; b) W. S. Sheldrick, M. Wachhold, *Angew. Chem. Int. Ed. Engl.* **1997**, *36*, 206–224; c) M. G. Kanatzidis, S.-P. Huang, *Coord. Chem. Rev.* **1994**, *130*, 509–621; d) M. A. Ansari, J. A. Ibers, *Coord. Chem. Rev.* **1990**, *100*, 223–266; Solid state (poly-)selenides: e) C. Graf, A. Assoud, O. Mayasree, H. Kleinke, *Molecules* **2009**, *14*, 3115–3131; f) H. Schäfer, B. Eisenmann, W. Müller, *Angew. Chem.* **1973**, *85*, 742–760; *Angew. Chem. Int. Ed. Engl.* **1973**, *12*, 694–712; Selenium-rich selenides: g) W. S. Sheldrick, *Z. Anorg. Allg. Chem.* **2012**, *638*, 2401–2424; h) P. Böttcher, T. Doert, *Phosphorus Sulfur Silicon Relat. Elem.* **1998**, *136–138*, 255–282; Selenidometalates: i) O. Mayasree, C. R. Sankar, K. M. Kleinke, H. Kleinke, *Coord. Chem. Rev.* **2012**, *256*, 1377–1383; j) J. Zhou, J. Dai, G.-Q. Bian, C.-Y. Li, *Coord. Chem. Rev.* **2009**, *253*, 1221–1247; k) S. Dehnen, M. Melullis, *Coord. Chem. Rev.* **2007**, *251*, 1259–1280; l) M. W. DeGroot, J. F. Corrigan, *Comprehensive Coordination Chemistry*, Pergamon, Oxford, **2003**, Chapter 7.2; m) J. Li, Z. Chen, R.-J. Wang, D. M. Proserpio, *Coord. Chem. Rev.* **1999**, *190–192*, 707–735; n) J. W. Kolis, *Coord. Chem. Rev.* **1990**, *105*, 195–219; o) M. G. Kanatzidis, *Commun. Inorg. Chem.* **1990**, *10*, 161–195.

[4] D. B. Mitzi, *Solution Processing of Inorganic Materials*, John Wiley & Sons, Hoboken, **2008**, Chapter 3.

[5] S. Dev, E. Ramli, T. B. Rauchfuss, C. L. Stern, *J. Am. Chem. Soc.* **1990**, *112*, 6385–6386.

[6] U. Müller, *Phosphorus Sulfur Silicon Relat. Elem.* **1997**, *124–125*, 395–400.

[7] S. Licht, *Sol. Energy Mater. Sol. Cells* **1995**, *38*, 305–319.

[8] D. M. Smith, J. A. Ibers, *Coord. Chem. Rev.* **2000**, *200–202*, 187–205.

[9] W. Teichert, W. Klemm, *Z. Anorg. Allg. Chem.* **1939**, *243*, 86–98.

[10] One needs to keep in mind, however, that selenium is a semimetal and no metal; this holds also for respective tellurium compounds, although the term "metalate" is used in several cases.

[11] B. Krebs, E. Lührs, R. Willmer, F.-P. Ahlers, *Z. Anorg. Allg. Chem.* **1991**, *592*, 17–34; M. G. Kanatzidis, S.-P. Huang, *Inorg. Chem.* **1989**, *28*, 4667–4669.

[12] P. Sekar, J. A. Ibers, *Inorg. Chem.* **2004**, *43*, 5436–5441.

[13] For recent reviews concerning organoselenium chemistry see, for example: a) L. Jain, V. K. Jain, N. Kushwah, M. K. Pal, A. P. Wadawale, V. I. Bregadze, S. A. Glazun, *Coord. Chem. Rev.* **2014**, *258–259*, 72–118; b) G. Kedarnath, V. K. Jain, *Coord. Chem. Rev.* **2013**, *257*, 1409–1435; c) A. J. Mukherjee, S. S. Zade, H. B. Singh, R. B. Sunoj, *Chem. Rev.* **2010**, *110*, 4357–4416; d) A. Ahrika, J. Robert, M. Anouti, J. Paris, *New J. Chem.* **2001**, *25*, 741–746.

[14] J. Beck, *Coord. Chem. Rev.* **1997**, *163*, 55–70.

[15] See, for example a) M. Panthöfer, D. Shopova, M. Jansen, *Z. Anorg. Allg. Chem.* **2005**, *631*, 1387–1390; b) V. V. Poborchii, *J. Chem. Phys.* **2001**, *114*, 2707–2717; and references cited therein; c) R. A. Stevens, C. C. Raymond, P. K. Dorhout, *Angew. Chem. Int. Ed. Engl.* **1995**, *34*, 2509–2511.

[16] A. Goldbach, F. Fayon, T. Vosegaard, M. Wachhold, M. G. Kanatzidis, D. Massiot, M.-L. Sabougi, *Inorg. Chem.* **2003**, *42*, 6996–7000.

[17] A. Kromm, W. S. Sheldrick, *Z. Anorg. Allg. Chem.* **2006**, *632*, 191–194.

[18] J.-F. Chen, Q.-Y. Jin, Y.-L. Pan, Y. Zhang, D.-X. Jia, *Chem. Commun.* **2009**, 7212–7214.

[19] R. M. H. Banda, J. Cusick, M. L. Scudder, D. C. Craig, I. G. Dance, *Polyhedron* **1989**, *8*, 1995–1998.

[20] A. Goldbach, J. Johnson, D. Meisel, L. A. Curtiss, M.-L. Saboungi, *J. Am. Chem. Soc.* **1999**, *121*, 4461–4467.

[21] M. Björgvinsson, G. J. Schrobilgen, *Inorg. Chem.* **1991**, *30*, 2540–2547.

[22] For different synthetic approaches see Refs. [20,67] and references cited therein.

[23] F. Weller, J. Adel, K. Dehnicke, *Z. Anorg. Allg. Chem.* **1987**, *548*, 125–132.

[24] B. Gautheron, G. Tainturier, C. Degrand, *J. Am. Chem. Soc.* **1985**, *107*, 5579–5581.

[25] A. Goldbach, M.-L. Saboungi, J. A. Johnson, A. R. Cook, D. Meisel, *J. Phys. Chem. A* **2000**, *104*, 4011–4016.

[26] T. Chivers, D. D. Doxsee, M. Parvez, *Inorg. Chem.* **1993**, *32*, 2238–2242.

[27] F. Wendland, C. Näther, W. Bensch, *Z. Naturforsch.* **2004**, *59b*, 629–634.

[28] T. Chivers, D. D. Doxsee, J. F. Fait, M. Parvez, *Inorg. Chem.* **1993**, *32*, 2243.

[29] E. Ruzin, E. Zent, E. Matern, W. Massa, S. Dehnen, *Chem. Eur. J.* **2009**, *15*, 5230–5244.

[30] R. J. Batchelor, F. W. B. Einstein, I. D. Gay, C. H. W. Jones, R. D. Sharma, *Inorg. Chem.* **1993**, *32*, 4378–4383.

[31] D. Bedlivy, A. Preisinger, *Z. Kristallogr.* **1965**, *121*, 131–144.

[32] D. Bedlivy, A. Preisinger, *Z. Kristallogr.* **1965**, *121*, 114–130.

[33] R. D. Shannon, *Acta Crystallogr., Sect. A* **1976**, *32*, 751–926.

[34] T. Chivers, M. Krahn, G. Schatte, M. Parvez, *Inorg. Chem.* **2003**, *42*, 3994–4005.

[35] C. G. Pernin, J. A. Ibers, *Inorg. Chem.* **1997**, *36*, 3802–3803.

[36] X. Wang, H. H. Wang, B. Makarenko, A. J. Jacobson, *Z. Anorg. Allg. Chem.* **2012**, *638*, 2538–2541.

[37] O. Kysliak, J. Beck, *Inorg. Chem. Commun.* **2013**, *38*, 146–151.

[38] X.-M. Lin, J. Zhou, N. Cheng, X.-X. Chen, Y. Zhang, J. Dai, *Huaxue Jinzhan* **2008**, *20*, 719.

[39] F. Wendland, C. Näther, W. Bensch, *Z. Naturforsch.* **2000**, *55b*, 871.

[40] T. Hanauer, F. Kraus, N. Korber, *Monatsh. Chem.* **2005**, *136*, 119–125.

[41] D. C. Green, B. W. Eichhorn, S. G. Bott, *J. Solid State Chem.* **1995**, *120*, 12–16.

[42] T. König, B. Eisenmann, H. Schäfer, *Z. Anorg. Allg. Chem.* **1983**, *498*, 99–104.

[43] T. König, B. Eisenmann, H. Schäfer, *Z. Naturforsch.* **1982**, *37b*, 1245–1249.

[44] P. W. Menezes, T. F. Fässler, *Z. Anorg. Allg. Chem.* **2012**, *638*, 1109–1113.

[45] O. Foss, V. Janicks, *J. Chem. Soc., Dalton Trans.* **1980**, 620–623.

[46] N. E. Brese, C. R. Randall, J. A. Ibers, *Inorg. Chem.* **1988**, *27*, 940–943.

[47] T. A. J. Worden, D. S. Wright, A. Steiner, *Polyhedron* **1998**, *17*, 4011–4014.

[48] V. Müller, A. Ahle, G. Frenzen, B. Neumüller, K. Dehnicke, D. Fenske, *Z. Anorg. Allg. Chem.* **1993**, *619*, 1247–1256.

[49] J. Dietz, U. Müller, V. Müller, K. Dehnicke, *Z. Naturforsch.* **1991**, *46b*, 1293–1299.

[50] C.-N. Chau, R. W. M. Wardle, J. A. Ibers, *Acta Crystallogr., Sect. C* **1988**, *44*, 883–885; G. Kräuter, K. Dehnicke, D. Fenske, *Chem.-Ztg.* **1990**, *114*, 7.

[51] P. J. Barrie, R. J. H. Clark, D.-Y. Chung, D. Chakrabarty, M. G. Kanatzidis, *Inorg. Chem.* **1995**, *34*, 4299–4304. Further details on solid state NMR see references herein.

[52] V. Müller, G. Frenzen, K. Dehnicke, D. Fenske, *Z. Naturforsch.* **1992**, *47b*, 205–210.

[53] O. Kysliak, J. Daniels, G. Schnakenburg, J. Beck, *Z. Anorg. Allg. Chem.* **2012**, *638*, 129–135.

[54] K. Tatsumi, H. Kawaguchi, K. Inoue, K. Tani, R. E. Cramer, *Inorg. Chem.* **1993**, *32*, 4317–4323.

[55] D. Fenske, C. Kraus, K. Dehnicke, *Z. Anorg. Allg. Chem.* **1992**, *607*, 109–112.

[56] R. G. Teller, L. J. Krause, R. C. Haushalter, *Inorg. Chem.* **1983**, *22*, 1809–1812.

[57] R. Sathyamurthy, J. L. Brumaghim, D. G. VanDerveer, *J. Chem. Crystallogr.* **2007**, *37*, 109–117.

[58] V. Müller, C. Grebe, U. Müller, K. Dehnicke, *Z. Anorg. Allg. Chem.* **1993**, *619*, 416–420.

[59] $[Ph_3PNPPh_3]_2[Se_2(Se_4)_2]\cdot DMF$ was originally described as $[Ph_3PNPPh_3]_2[Se_{10}]\cdot DMF$, yet in accordance with our interpret-

ation regarding a central $[Se_2]^{2+}$ fragment: D. Fenske, G. Kräuter, K. Dehnicke, *Angew. Chem.* **1990**, *102*, 420–421; *Angew. Chem. Int. Ed. Engl.* **1990**, *29*, 390–391.
[60] V. Müller, K. Dehnicke, D. Fenske, G. Baum, *Z. Naturforsch.* **1991**, *46b*, 63–67.
[61] R. Staffel, U. Müller, A. Ahle, D. Dehnicke, *Z. Naturforsch.* **1991**, *46b*, 1287–1292.
[62] O. Kysliak, J. Beck, *Eur. J. Inorg. Chem.* **2013**, 124–133.
[63] Y. Lin, X. Jin, J. Wu, G. Xu, Beijing Dax. Xue., Zir. Kex. (Chin.) (Acta Sci. Nat. Univ. Pek.) **1987**, 8–2.
[64] M. Björgvinsson, J. F. Sawyer, G. J. Schrobilgen, *Inorg. Chem.* **1991**, *30*, 4238–4245.
[65] E. Zintl, J. Goubeau, W. Dullenkopf, *Z. Phys. Chem. A* **1931**, *154*, 1–46.
[66] L. E. Lyons, T. L. Young, *Aust. J. Chem.* **1986**, *39*, 511–527.
[67] A. Ahrika, J. Paris, *New J. Chem.* **1999**, *23*, 1177–1180.
[68] Y. Cui, A. Abouimrane, J. Lu, T. Bolin, Y. Ren, W. Weng, C. Sun, V. A. Maroni, S. M. Heald, K. Amine, *J. Am. Chem. Soc.* **2013**, *135*, 8047–8056.
[69] C. Hugot, *Ann. Chim. Phys.* **1900**, *21*, 72.
[70] K. W. Sharp, W. H. Koehler, *Inorg. Chem.* **1977**, *16*, 2258–2265.
[71] S. Licht, F. Forouzan, *J. Electrochem. Soc.* **1995**, *142*, 1546–1551.
[72] A. Goldbach, M. Grimsditch, L. Iton, M.-L. Saboungi, *J. Phys. Chem. B* **1997**, *101*, 303–334 and references cited therein.
[73] A. Goldbach, L. E. Iton, M. Grimsditch, M.-L. Saboungi, *Chem. Mater.* **2004**, *16*, 5107–5113.
[74] C. C. Raymond, D. L. Dick, P. K. Dorhout, *Inorg. Chem.* **1997**, *36*, 2678–2681.
[75] J. Cusick, I. Dance, *Polyhedron* **1991**, *10*, 2629–2640.
[76] C. A. Bayse, *J. Chem. Theory Comput.* **2005**, *1*, 1119–1127.
[77] W. Nakanishi, S. Hayashi, Y. Katsura, M. Hada, *J. Phys. Chem. A* **2011**, *115*, 8721–8730.
[78] G. Thiele, N. Lichtenberger, R. Tonner, S. Dehnen, *Z. Anorg. Allg. Chem.* **2013**, *639*, 2809–2815.
[79] Determination with program package *TOPOS*: V. A. Blatov, *Struct. Chem.* **2012**, *23*, 955–963.
[80] See for example: a) H. T. Evans, J. S. Showell, *J. Am. Chem. Soc.* **1969**, *91*, 6881–6882; b) R. F. Ziolo, R. H. Stanford, G. R. Rossmann, H. B. Gray, *J. Am. Chem. Soc.* **1974**, *96*, 7910–7915.
[81] G. Thiele, L. Vondung, S. Dehnen, *unpublished results*.
[82] a) G. M. Sheldrick, *SHELXL97*, Program for the Refinement of Crystal Structures, Universität Göttingen, **1997**; b) O. V. Dolomanov, L. J. Bourhis, R. J. Gildea, J. A. K. Howard, H. Puschmann, *J. Appl. Crystallogr.* **2009**, *42*, 339.
[83] *TURBOMOLE Version 6.4*, © TURBOMOLE GmbH, **2012**. TURBOMOLE is a development of University of Karlsruhe and Forschungszentrum Karlsruhe 1989–2007, TURBOMOLE GmbH since 2007.
[84] A. Klamt, G. Schürmann, *J. Chem. Soc. Perkin Trans. 2* **1993**, 799.
[85] A. D. Becke, *Phys. Rev. A* **1988**, *38*, 3098–3100; J. P. Perdew, *Phys. Rev. B* **1996**, *33*, 8822–8824.
[86] F. Weigend, R. Ahlrichs, *Phys. Chem. Chem. Phys.* **2005**, *7*, 3297–3305; F. Weigend, *Phys. Chem. Chem. Phys.* **2006**, *8*, 1057–1065.
[87] *gOpenMol*, L. Laaksonen, Center for Scientific Computing, Espoo, Finland, Version 3.0, **2005**: D. L. Bergman, L. Laaksonen, A. Laaksonen, *J. Mol. Graph. Model.* **1997**, *15*, 301–306.

Received: September 30, 2014
Published Online: November 11, 2014

Organic Cation and Complex Cation-Stabilized (Poly-)Selenides, $[Cation]_x(Se_y)_z$: Diversity in Structures and Properties

Günther Thiele, Lisa Vondung, Carsten Donsbach, Susanne Pulz, and Stefanie Dehnen.*

Fachbereich Chemie and Wissenschaftliches Zentrum für Materialwissenschaften, Hans-Meerwein-Straße, 35043 Marburg, Germany.

S U P P O R T I N G I N F O R M A T I O N

Contents:

1) **Tables S1-S7** summarizing the crystallographic data of compounds **1** – **26**

2) **Tables S8-S13** summarizing selected structural parameters of known compounds with organic cation and complex cation-stabilized (poly-)selenides, $[cation]_x(Se_y)_z$

Table S1. Crystallographic data and refinement details for **1** – **4**.

Compound	**$[Li_2(H_2O)_7](Se)$ (1)**	**$[K(H_2O)_4]_2(Se)$ (2)**	**$[K_4(H_2O)_{10}](Se_2)(Se)$ (3)**	**$[Ba(H_2O)_x]_3[Ba(OH)_2(H_2O)_{x-2}](Se)_3$ (4; x ≈ 13)**
Empirical formula	$H_{14}Li_2O_7Se_1$	K_2O_8Se	$K_4O_{10}Se_3$	$Ba_4O_{25}Se_3$
Formula weight /g·mol^{-1}	204.84	285.16	553.28	1186.24
Crystal color and shape	Colorless stick	Colorless stick	Red stick	Colorless stick
Crystal size /mm	0.30·0.14·0.05	1.04·0.53·0.27	0.20·0.18·0.15	0.28·0.22·0.15
Crystal system	Orthorhombic	Orthorhombic	Monoclinic	Monoclinic
Space group	*Pnna*	*Fddd*	*C*2/*c*	*C*2/*m*
a/Å	7.6379(8)	9.3054(10)	12.5107(8)	31.288(4)
b/Å	14.0668(16)	12.7071(17)	13.1863(7)	7.6703(8)
c/Å	8.0972(9)	17.717(2)	11.6291(8)	14.6801(17)
β/°			114.062(5)	
V/Å^3	869.97(17)	2095.0(4)	1751.75(19)	113.544(13)
Z	4	8	4	
ρ_{calc}/g·cm^{-3}	1.564	1.808	2.098	3229.8(6)
$\mu(Mo_{K\alpha})$ /mm^{-1}	4.295	4.380	7.274	8.266
2Θ range/°	5.80-53.38	5.90-53.34	4.72-53.40	4.70-50.92
Abs. corr. T_{min}/T_{max}	0.4587/0.8178	0.1213/0.3305	0.2660/0.4373	0.1623/ 0.3279
Reflections measured	4631	3939	8374	22059
Independent reflections	923	561	1849	3213
R(int)	0.0623	0.0447	0.0728	0.0351
Indep. Reflections (I>2σ(I))	646	542	1186	2793
Parameters	47	27	78	262
R_1(I>2σ(I))	0.0408	0.0434	0.0421	0.0305
*wR*2 (all data)	0.1210	0.1316	0.0935	0.0815
Goof (all data)	0.933	1.523	0.831	1.058
Max. peak/hole /e$^-$·10^{-6}pm^{-3}	0.009/0.001	0.775/-1.757	0.977/-0.629	3.314/ -2.445

Table S2. Crystallographic data and refinement details for **5** – **8**.

Compound	**(*enH*)$_2$(Se$_2$) (5)**	**[Li(*en*)$_3$]$_2$(Se$_2$) (6)**	**[K$_2$(H$_2$O)](Se$_2$) (7)**	**[K$_2$(NH$_3$)](Se$_2$), (8)**
Empirical formula	$C_2H_9N_2Se$	$C_6H_{24}Li_2N_6Se_2$	K_2OSe_2	K_2NSe_2
Formula weight /g·mol^{-1}	140.07	352.11	252.12	250.13
Crystal color and shape	Red stick	Red block	Red plate	Red plate
Crystal size max·mid·min /mm	0.24·0.14·0.08	0.29·0.23·0.16	0.55·0.40·0.15	0.20·0.14·0.01
Crystal system	Monoclinic	Triclinic	Monoclinic	Monoclinic
Space group	*C*2/*c*	$P\bar{1}$	*C*2/*c*	*C*2/*c*
a/Å	14.4952(12)	7.1012(15)	10.8692(10)	10.7512(13)
b/Å	7.7804(4)	7.1296(15)	6.3450(4)	6.3432(14)
c/Å	9.3126(8)	7.4995(17)	8.6290(8)	8.7865(11)
α/°		73.046(17)		
β/°	94.634(7)	87.460(18)	104.442(8)	104.097(10)
γ/°		89.204(17)		
V/Å^3	1046.83(14)	362.83(14)	576.29(8)	581.17(16)
Z	8	1	4	4
ρ_{calc}/g·cm^{-3}	1.778	1.611	2.906	2.859
$\mu(Mo_{K\alpha})$ /mm^{-1}	7.014	5.078	14.126	13.999
2Θ range/°	5.64-53.32	5.68-50.78	7.60-53.40	7.52-53.40
Abs. corr. T_{min}/T_{max}	0.2325/ 0.7504	0.3394/ 0.4777	0.003/ 0.0283	0.1162/ 0.8012
Reflections measured	6342	4439	567	3217
Independent reflections	1108	1242	567	606
R(int)	0.0319	0.0271	0.0657	0.1244
Indep. Reflections (I>2σ(I))	995	1179	486	389
Parameters	54	85	25	24
R_1(I>2σ(I))	0.0267	0.0236	0.0624	0.1081
*wR*2 (all data)	0.0658	0.0798	0.1464	0.2647
Goof (all data)	1.039	1.241	1.078	0.952
Max. peak/hole /e$^-$·10^{-6}pm^{-3}	0.492/ -0.648	0.612/ -0.817	1.793/ -0.985	

Table S3. Crystallographic data and refinement details for **9** – **12**.

Compound	**[K(*18-crown-6*)]$_2$(Se$_2$)·*en*, (9)**	**$^1_\infty$[{K(*18-crown-6*)}{K(NH$_3$)}(Se$_2$)], (10)**	**Cs$_4$(Se$_2$)(Se$_3$)·*en*, (11)**	**(NMe$_4$)$_2$(Se$_2$) (12)**
Empirical formula	$C_{13}H_{28}KNO_6Se$	$C_{12}H_{27}K_2NO_6Se_2$	$C_{0.5}H_{1.25}Cs_3N_{0.5}Se_{3.5}$	$C_8H_{24}N_2Se_2$
Formula weight /g·mol^{-1}	412.42	517.47	689.36	306.21
Crystal color and shape	Red plate	Red block	Red plate	Red block
Crystal size /mm	0.41·0.26·0.09	0.20·0.18·0.16	0.09·0.06·0.03	0.22·0.15·0.11
Crystal system	Triclinic	Orthorhombic	Monoclinic	Cubic
Space group	$P\bar{1}$	$Cmc2_1$	$P2_1$	$Pa\bar{3}$
a/Å	8.6160(3)	14.4995(10)	6.9084(14)	10.8172(2)
b/Å	8.7423(3)	13.1544(9)	31.537(6)	
c/Å	13.4725(5)	10.7928(10)	10.280(2)	
α/°	107.706(3)			
β/°	101.769(3)		102.74(3)	
γ/°	100.667(3)			
V/Å^3	912.57(6)	2058.5(3)	2184.6(8)	1265.74(4)
Z	2	4	8	4
ρ_{calc}/g·cm^{-3}	1.501	1.670	4.192	1.607
$\mu(Mo_{K\alpha})$ /mm^{-1}	2.310	4.020	21.547	5.804
2Θ range/°	3.30-53.44	5.64-53.40	2.58-53.48	7.54-53.40
Abs. corr. T_{min}/T_{max}	0.4775/ 0.7789	0.16225/ 0.33115	0.1349/ 0.6859	0.3265/ 0.5637
Reflections measured	14131	5901	13973	16705
Independent reflections	3851	2085	7849	453
R(int)	0.0328	0.0299	0.0660	0.0496
Indep. Reflections (I>2σ(I))	3599	1886	6136	448
Parameters	199	121	273	22
R_1(I>2σ(I))	0.0306	0.0264	0.0475	0.0492
*wR*2 (all data)	0.0812	0.0610	0.0955	0.0870
Goof (all data)	1.079	0.962	0.920	1.291
Max. peak/hole /e$^-$·10^{-6}pm^{-3}	0.700/- 0.733	0.515/ -0.488	1.729/ -1.711	1.699/ -0.602

Table S4. Crystallographic data and refinement details for **13** – **16**.

Compound	**[K(18-*crown*-6)]$_2$(Se$_3$) (13)**	**[K(*18-crown-6*)]$_2$(Se$_3$)·H$_2$O (14)**	**[{K(*18-crown-6*)}$_2$(H$_2$O)$_3$](Se$_3$)·2H$_2$O (15)**	**[K([2.2.2]*crypt*)]$_2$(Se$_3$)· H$_2$O (16)**
Empirical formula	$C_{24}H_{48}K_2O_{12}Se_3$	$C_{24}H_{48}K_2O_{13}Se_3$	$C_{24}H_{56}K_2O_{17}Se_3$	$C_{36}H_{72}K_2N_4O_{13}Se_3$
Formula weight /g·mol^{-1}	843.70	859.70	931.77	1084.06
Crystal color and shape	Orange block	Green plate	Red stick	Green block
Crystal size max·mid·min /mm	0.21·0.15·0.12	0.18·0.13·0.05	0.21·0.08·0.02	0.32·0.20·0.14
Crystal system	Monoclinic	Monoclinic	Monoclinic	Monoclinic
Space group	$P2_1/n$	$P2_1/n$	$P2_1/c$	$C2/c$
a/Å	12.0912(4)	10.1135(8)	20.2174(12)	24.4495(15)
b/Å	18.5757(7)	9.6626(5)	10.0682(4)	10.1073(6)
c/Å	16.5732(6)	18.5016(14)	19.4531(13)	21.547(2)
α/°				
β/°	107.822(3)	96.658(6)	97.144(5)	113.082(4)
γ/°				
V/Å^3	3543.8(2)	1795.8(2)	3929.0(4)	4898.4(6)
Z	4	2	4	4
ρ_{calc}/g·cm^{-3}	1.581	1.590	1.575	1.470
$\mu(Mo_{K\alpha})$ /mm^{-1}	3.40	3.359	3.084	2.482
2Θ range/°	3.38-53.48	4.38-53.44	4. 06-53.50	3.62-53.60
Abs. corr. T_{min}/T_{max}	0.4995/0.7392	0.5663/ 0.8488	0.14002/ 0.19400	0.5136/ 0.8219
Reflections measured	37990	7641	26852	19247
Independent reflections	7495	3752	8312	5158
R(int)	0.063	0.0754	0.0943	0.0726
Indep. Reflections (I>2σ(I))	5673	2829	4671	3535
Parameters	379	296	424	271
R_1(I>2σ(I))	0.038	0.0534	0.0387	0.0418
*wR*2 (all data)	0.0938	0.1505	0.0798	0.1061
Goof (all data)	0.985	1.082	0.808	0.926
Max. peak/hole /e$^-$·10^{-6}pm^{-3}	2.471/-0.679	0.731/ -2.619	0.685/ -0.640	3.369/ -0.324

Table S5. Crystallographic data and refinement details for **17** – **19**.

Compound	**[Fe(*en*)$_3$](Se$_3$) (17)**	**[Cd(*en*)$_3$](Se$_3$) (18)**	**[K$_2$(H$_2$O)](Se$_4$) (19)**
Empirical formula	$Se_3Fe_1N_6C_6H_{24}$	$C_6CdN_6Se_3$	K_2OSe_4
Formula weight /g·mol^{-1}	473.04	505.40	410.04
Crystal color and shape	Red/Green pleochroic sticks	Red/Green pleochroic block	Black stick
Crystal size max·mid·min /mm	0.08·0.15·0.29	0.22·0.09·0.01	0.53·0.21·0.04
Crystal system	Orthorhombic	Monoclinic	Monoclinic
Space group	*Pbcn*	*C*2/*c*	*Cc*
a/Å	11.4708(15)	11.4922(16)	9.8572(8)
b/Å	14.955(3)	15.0483(16)	7.4443(5)
c/Å	9.3093(11)	9.3041(13)	11.3089(8)
β/°		90.005(12)	91.257(6)
V/Å^3	1597.0(4)	1609.0(4)	829.65(11)
Z	4	4	4
ρ_{calc}/g·cm^{-3}	1.967	2.086	3.283
$\mu(Mo_{K\alpha})$ /mm^{-1}	7.770	8.128	18.597
2Θ range/°	4.3 – 51.84	4.46-53.46	6.86-53.40
Abs. corr. T_{min}/T_{max}	0.3707 / 0.6005	0.3692/ 0.8771	0.0676/ 0.4658
Reflections measured	12603	5199	4606
Independent reflections	1465	1700	1754
R(int)	0.0328	0.0950	0.0526
Indep. Reflections (I>2σ(I))	1019	1067	1726
Parameters	122	101	64
R_1(I>2σ(I))	0.0521	0.0562	0.0472
*wR*2 (all data)	0.0640	0.1410	0.1446
Goof (all data)	0.985	0.886	1.082
Max. peak/hole /e$^-$·10^{-6}pm^{-3}	0.487 / -0.554	0.808/-2.619	0.991/ -1.690

Table S6. Crystallographic data and refinement details for **20** – **23**.

Compound	**$[K_2(H_2O)_2](Se_4)$ (20)**	**$[K_2(NH_3)](Se_4)$ (21)**	**$[K([2.2.2]crypt)]_2(Se_4)$ (22)**	**$[Ba(H_2O)_6](Se_4)$ (23)**
Empirical formula	$K_2O_2Se_4$	K_2NSe_4	$C_{18}H_{35}KN_2O_6Se_2$	BaO_6Se_2
Formula weight /g·mol^{-1}	426.04	408.05	572.50	391.26
Crystal color and shape	Black stick	Red needle	Black block	Black plate
Crystal size /mm	0.17·0.10·0.04	0.13·0.06·0.02	0.11·0.10·0.09	0.22·0.13·0.04
Crystal system	Monoclinic	Monoclinic	Triclinic	Triclinic
Space group	*Pc*	*Cc*	$P\bar{1}$	$P\bar{1}$
a/Å	6.1993(4)	9.8742(11)	9.6908(11)	6.0229(8)
b/Å	8.5714(5)	7.4438(6)	11.5286(12)	8.2660(11)
c/Å	8.8464(6)	11.3130(14)	12.8184(15)	9.8175(12)
α/°			106.954(9)	75.730(10)
β/°	106.750(5)	91.124(9)	107.773(9)	73.694(10)
γ/°			102.176(9)	71.301(10)
V/Å^3	450.12(5)	831.36(15)	1231.7(2)	437.71(10)
Z	2	4	2	2
ρ_{calc}/g·cm^{-3}	3.143	3.260	1.544	2.969
$\mu(Mo_{K\alpha})$ /mm^{-1}	17.153	18.552	3.204	12.823
2Θ range/°	4.76-53.50	6.86-53.50	3.62-53.56	5.28-53.32
Abs. corr. T_{min}/T_{max}	0.0156/ 0.0578	0.05821/ 0.11498	0.6938/ 0.8054	0.1524/ 0.5686
Reflections measured	8425	4268	14203	3467
Independent reflections	1890	1708	5204	1813
R(int)	0.0460	0.0635	0.1115	0.0579
Indep. Reflections (I>2σ(I))	1839	1326	3206	1552
Parameters	73	65	262	83
R_1(I>2σ(I))	0.0441	0.0502	0.0786	0.0528
*wR*2 (all data)	0.1367	0.1219	0.2115	0.1456
Goof (all data)	1.110	0.921	0.921	1.044
Max. Peak/hole /e$^-$·10^{-6}pm^{-3}	0.896/ -1.379	1.002/ -1.630	1.299/ -1.296	1.916/ -2.805

Table S7. Crystallographic data and refinement details for **24** – **26**.

Compound	**[K(*18-crown-6*)]$_2$(Se$_6$)·(*18-crown-6*)·H$_2$O (24)**	**[K(*18-crown-6*)]$_2$(Se$_6$)·(*18-crown-6*)·2NH$_3$ (25)**	**(*en*H)$_2$(Se$_6$) (26)**
Empirical formula	$C_{18}H_{38}KO_{10}Se_3$	$C_9H_{18}K_{0.5}N_{0.5}O_{4.5}Se_{1.5}$	$C_4H_8N_4Se_6$
Formula weight /g·mol^{-1}	690.46	343.23	585.9
Crystal color and shape	Red needles	Red needles	Red block
Crystal size /mm	0.27·0.05·0.03	0.24·0.09·0.05	0.12·0.10·0.09
Crystal system	Monoclinic	Monoclinic	Triclinic
Space group	*C*2/*c*	*C*2/*c*	$P\bar{1}$
a/Å	30.6376(17)	30.5584(12)	7.7678(9)
b/Å	8.4835(4)	8.4904(3)	9.4184(11)
c/Å	23.6637(12)	23.6592(10)	10.8079(14)
α/°			74.518(10)
β/°	117.410(2)	117.3690(10)	79.116(9)
γ/°			84.789(9)
V/Å^3	5460.0(5)	5451.3(4)	747.63(16)
Z	8	16	2
ρ_{calc}/g·cm^{-3}	1.680	1.673	2.603
$\mu(Mo_{K\alpha})$ /mm^{-1}	4.240	4.244	14.657
2Θ range/°	5.02-54.40	5.02-55.88	3.97-53.41
Abs. corr. T_{min}/T_{max}	0.41/ 0.52	0.4290/ 0.8158	0.0583/ 0.1643
Reflections measured	31985	68052	8877
Independent reflections	6036	6530	3099
R(int)	0.0870	0.0698	0.1116
Indep. Reflections (I>2σ(I))	4006	4967	2065
Parameters	315	289	127
R_1(I>2σ(I))	0.0398	0.0435	0.0754
*wR*2 (all data)	0.0735	0.1096	0.2033
Goof (all data)	1.013	1.043	1.029
Max. Peak/hole /e$^-$·10^{-6}pm^{-3}	0.969/ -0.541	3.701/ -0.987	2.109/-1.166

Table S8. Selected structural parameters of known monoselenide and diselenide compounds.

Compound	Anion	d(Se–Se_t) [Å]	d(Se–Se_b) [Å]	∢(Se–Se–Se) [°]	∢(Se–Se–Se–Se) [°]	d_{min} Se…cat/solv [Å]
$[(Me_2NH_2P)_2N]_2Se$[1]	Se^{2-}					3.302(6) (Se...(H)N)
$[Mn(cyen)_3]_2[H_2cyen](Se_2Te)_2Se$[2]	Se^{2-}, $(Se_2Te)^{2-}$	2.478(1) (Te–Se)		106.44(3) (Se-Te-Se)		3.376(5) (Se...(H)N)
$[Ph_2P(NH_2)_2]_2Se$[3]	Se^{2-}					3.226(5) (Se…N)
$K_{10}[Zn_4Sn_4Se_{13}Te_4]\cdot 4K_2Se$[4]	Se^{2-}					2.454(2) (Se...Zn)
$(NMe_4)(HSe)$[5]	HSe^-					3.8465(20) (Se...(H)C)
$Na_2Se\cdot 5H_2O$[6]	Se^{2-}					3.0123 (Se…Na)
$Na_2Se\cdot 9H_2O$[7]	Se^{2-}					3.3065 (Se…(H)O)
$[Li_2(H_2O)_7]Se$ (**1**)	Se^{2-}					3.303(3) (Se...(H)O)
$[K(H_2O)_4]_2Se$ (**2**)	Se^{2-}					3.391(2) (Se...(H)O)
$[K_4(H_2O)_{10}](Se_2)Se$ (**3**)	Se^{2-}, $(Se_2)^{2-}$	2.447(1) (Se2–Se2)				3.277(4) (Se...(H)O)
$[Ba(H_2O)_x]_3[Ba(OH)_2(H_2O)_{x-2}]Se_3$ (**4**; x ≈ 13)	Se^{2-}					3.260(7) (Se…O)
$(enH)_2(Se_2)$ (**5**)	$(Se_2)^{2-}$	2.3917(5)				3.3417(19) (Se...(H)N)
$[Li(en)_3]_2(Se_2)$ (**6**)	$(Se_2)^{2-}$	2.3911(7)				2.648(6) (Se...Li)
$[K_2(H_2O)](Se_2)$ (**7**)	$(Se_2)^{2-}$	2.405(1)				3.305(2) (Se...K)
$[K_2(NH_3)](Se_2)$ (**8**)	$(Se_2)^{2-}$	2.405(2)				3.294(4) (Se…K)
$[K(18\text{-}crown\text{-}6)]_2(Se_2)\cdot en$ (**9**)	$(Se_2)^{2-}$	2.4063(3)				3.1867(5) (Se...K)
$^1_\infty[\{K(18\text{-}crown\text{-}6)\}\{K(NH_3)\}(Se_2)]$ (**10**)	$(Se_2)^{2-}$	2.4182(4)				3.2828(11) (Se...K)
$Cs_4(Se_2)(Se_3)\cdot en$ (**11**)	$(Se_2)^{2-}$	2.358(3)-2.404(3)				3.522(3) (Se...Cs)
$(NMe_4)_2(Se_2)$ (**12**)	$(Se_2)^{2-}$	2.3888(3)				3.9113(25) (Se…(H)C)

Table S9. Selected structural parameters of known triselenide and tetraselenide compounds.

Compound	Anion	d(Se–Se_t) [Å]	d(Se–Se_b) [Å]	∢(Se–Se–Se) [°]	∢(Se–Se–Se–Se) [°]	d_{min} Se…cat/solv [Å]
$Cs_4(Se_2)(Se_3)$·*en* (**12**)	$(Se_3)^{2-}$	2.305(4)-2.349(3)		107.85(13)-108.28(15)		3.522(3) (Se...Cs)
[K(18-*crown*-6)]$_2(Se_3)$ (**13**)	$(Se_3)^{2-}$	2.2485(10)-2.4891(11)		105.72(4)-106.55(4)		3.2969(14) (Se…K)
$[Sr_2Sn(OH)_6(H_2O)_5](Se_3)·H_2O$[8]	$(Se_3)^{2-}$	2.360(2)-2.377(2)		106.07(7)-106.34(7)		not given
$[Mn(NH_3)_6](Se_3)$[9]	$(Se_3)^{2-}$	2.3658(6)-2.3669(4)		110.41(2)		3.420(3) (Se...(H)N)
[Ni(*tren*)$_2$](Se_3)[10]	$(Se_3)^{2-}$	not given		not given		not given
[Mn(*en*)$_3$](Se_3)[11]	$(Se_3)^{2-}$	2.3395(5)		104.65(2)		3.572(2) (Se...(H)N)
$Li(NH_3)_4Rb(Se_3)$[12]	$(Se_3)^{2-}$	2.3611(7)-2.3627(8)		104.05(3)		3.4764(7) (Se...Rb)
$Na(NH_3)_5Rb(Se_3)_3$[12]	$(Se_3)^{2-}$	2.3634(3)		107.63(2)		3.605(3) (Se...(H)N)
[K(18-*crown*-6)]$_2(Se_3)·H_2O$ (**14**)	$(Se_3)^{2-}$	2.2928(11)-2.6111(12)		74.81(4)		1.419(7) (Se...(H)O)
[{K(18-*crown*-6)}$_2(H_2O)_3$]$(Se_3)·2H_2O$ (**15**)	$(Se_3)^{2-}$	2.3611(6)-2.3686(8)		110.62(2)		3.286(3) (Se...(H)O)
[K([2.2.2]*crypt*)]$_2(Se_3)·H_2O$ (**16**)	$(Se_3)^{2-}$	2.3474(9)-2.4225(9)		68.41(3)		1.369(6) (Se...(H)O)
[Fe(*en*)$_3$](Se_3) (**17**)	$(Se_3)^{2-}$	2.3489(8)		103.63(3)		3.548(5) (Se...(H)N)
[Cd(*en*)$_3$](Se_3) (**18**)	$(Se_3)^{2-}$	2.3412(15)		104.70(7)		3.357(16) (Se...(H)N)
$[Sr_2Sn(OH)_6(H_2O)_6](Se_4)$[8]	$(Se_4)^{2-}$	2.330(1)	2.399(1)	98.28(2)	180.00(3)	3.388(2) (Se...(H)O)
[Ba([2.2.2]*crypt*)](Se_4)·*en* [13]	$(Se_4)^{2-}$	2.3290-2.3293	2.3485	110.7(1)-113.9(1)	76.0(1)	3.4281 (Se...O)
$[Ba_2(OH)_2(H_2O)_{10}]_2(Se)_4$[14]	$(Se_4)^{2-}$	2.3382(8)	2.3934(9)	99.11(3)	180	3.443(4) (Se...(H)O)
[Ba(*en*)$_4$](Se_4)·*en*[15]	$(Se_4)^{2-}$	2.3291	2.3408	112.12	95.49	>4
[Ca(*en*)$_4$](Se_4)[16]	$(Se_4)^{2-}$	2.3300(5)	2.3445(7)	not given	110.70(1)	not given
$[Ph_3PNPPh_3]_2(Se_4)·4MeCN$[17]	$(Se_4)^{2-}$	2.312 (3)	2.397 (4)	103.4 (1)	180	3.611(19) (Se...(H)C);
$[Mn(MeNH_2)_6](Se_4)$[9]	$(Se_4)^{2-}$	2.3389(4)	2.3366(4)	111.47(1)	88.22(2)	3.514(2) (Se...(H)N)
$[K_2(H_2O)](Se_4)$ (**19**)	$(Se_4)^{2-}$	2.3567(15)-2.3618(14)	2.3622(15)	105.64(5)-106.25(5)	99.64(6)	3.287(2) (Se...K)
$[K_2(H_2O)_2](Se_4)$ (**20**)	$(Se_4)^{2-}$	2.3450(15)-2.3600(14)	2.3613(18)	104.04(6)-106.80(6)	76.51(6)	3.322(3) (Se...K)
$[K_2(NH_3)](Se_4)$ (**21**)	$(Se_4)^{2-}$	2.359(2)-2.367(2)	2.364(2)	105.70(8)-106.19(8)	99.72(9)	3.287(4) (Se...K)
[K([2.2.2]*crypt*)]$_2(Se_4)$ (**22**)	$(Se_4)^{2-}$	2.3239(12)	2.4057(10)	101.50(4)	180.00(4)	3.554(9) (Se...(H)C)
$[Ba(H_2O)_6](Se_4)$ (**23**)	$(Se_4)^{2-}$	2.3456(12)	2.3959(17)	98.88(5)	180	3.420(7) (Se...(H)O)

Table S10. Selected structural parameters of known pentaselenide compounds.

Compound	Anion	d(Se–Se_t) [Å]	d(Se–Se_b) [Å]	∢(Se–Se–Se) [°]	∢(Se–Se–Se–Se) [°]	d_{min} Se…cat/solv [Å]
$[Cs(18\text{-}crown\text{-}6)]_2(Se_5)\cdot DMF$[18]	$(Se_5)^{2-}$	2.295(5)	2.345(4)	109.4(2) (Se1-Se2-Se3); 106.5(2) (Se2-Se1-Se2A)	95.3(2)	3.743(4) (Se...Cs)
$[Cs(18\text{-}crown\text{-}6)]_2(Se_5)\cdot MeCN$[17]	$(Se_5)^{2-}$	2.316(3)	2.343(3)	106.6(2)-106.6(2)	96.3(1)	3.730(3) (Se...Cs)
$(NEt_4)_2(Se_5)\cdot(Se_7)\cdot(Se_6)$[19]	$(Se_5)^{2-}$	2.309(6)-2.312(6)	2.330(7)-2.348(7)	107.2(3)-109.5(3)	85.3(3); 88.6(3);	3.737(15) (Se...(H)C)
$(PPh_4)_2(Se_5)$[20]	$(Se_5)^{2-}$	2.314(2)-2.316(2)	2.355(2)-2.366(2)	108.83(6)-110.59(7)	77.33(7); 89.16(8)	3.354(12) (Se...(H)C)
$(NMe_4)_2(Se_5)$[21]	$(Se_5)^{2-}$	2.301(8)-2.305(8)	2.331(9)-2.348(7)	109.3(3)-112.5(3)	67.5(4); 75.2(4)	3.60(2)(Se...(H)C)
$[Na(15\text{-}crown\text{-}5)]_2(Se_5)$[22]	$(Se_5)^{2-}$	2.310(6)-2.330(7)	2.308(7)-2.377(7)	104.9(3)-111.8(2)	96.5(3); 108.3(3)	3.48(3) (Se...(H)O)
$[Mn(NH_2CH_3)_6](Se_5)$[24]	$(Se_5)^{2-}$	2.3274(4)	2.3426(4)	106.70(1)-109.11(3)	94.00(3)	2.774(13) (Se…(H)C)

Table S11: Selected structural parameters of known hexaselenide compounds.

Compound	Anion	d(Se–Se_t) [Å]	d(Se–Se_b) [Å]	∢(Se–Se–Se) [°]	∢(Se–Se–Se–Se) [°]	d_{min} Se…cat/solv [Å]
$(PPh_4)_2(Se_6)$[23]	$(Se_6)^{2-}$	2.268(2)-2.293(2)	2.2546(19)-2.355(2)	104.54(7)-110.15(7)	71.91(8); 75.54(8); 79.66(7);	3.543(9) (Se...(H)C)
[Ba(15-*crown*-5)$_2$](Se_6)·DMF[18]	$(Se_6)^{2-}$	2.300(3)-2.302(3)	2.333(3)-2.365(3)	108.5(1)-110.8(1)	87.1(1); 96.2(1)	3.72(2) (Se...(H)C)
[Rb([2.2.2]crypt)]$_2(Se_6)$[18]	$(Se_6)^{2-}$	2.299(2)-2.305(2)	2.339(2)-2.362(2)	109.56(7)-112.99(7)	82.36(8); 98.73(8)	3.551(9) (Se….(H)C)
$[NMe_4]_2(Se_6)$[21]	$(Se_6)^{2-}$	2.304(4)	2.317(4)-2.383(6)	105.1(1)-109.5(1)	59.0(3); 92.9(2)	3.63(2) (Se...(H)C)
$(NBu_4)_2(Se_6)$[24]	$(Se_6)^{2-}$	2.295(2)	2.337(2)-2.362(3)	106.75(7)-108.57(7)	94,54; 94.73;	3.7475 (Se...(H)C)
[Me_3N(*Td*)]$_2(Se_6)$[23]	$(Se_6)^{2-}$	2.274(4)	2.268(5)-2.352(9)	105.5(6)-110.6(2)	63.3(3); 93.3(2);	3.49(6) (Se...(H)C)
[Mn$(NH_3)_6$](Se_6)[9]	$(Se_6)^{2-}$	2.24(2)-2.35(2)	2.3155(17)-2.3647(13)	104.5(12)-110.83(5)	87.73(6); 59.32(6); 82.46(6)	3.15(2) (Se...(H)N)
[Fe$(NH_3)_6$](Se_6)[9]	$(Se_6)^{2-}$	2.28(5)-2.37(4)	2.20(6)-2.43(6)	104(2)-110.72(5)	87.59(6); 59.10(7); 82.24(7)	3.36(4) (Se...(H)N)
[Mn(*cyen*)$_3$](Se_6)[2]	$(Se_6)^{2-}$	2.3129(5)	2.3403(6)-2.3602(8)	106.08(2)-108.32(2)	88.34(2); 81.10(2)	3.484(2) (Se...(H)N)
[$Mg_6(\mu^4$-OH$)_2(\mu^3$-MeO$)_4$(MeO$)_4$(MeOH$)_{12}$](Se_6)·2MeOH[25]	$(Se_6)^{2-}$	2.3168(8)	2.3113(7)-2.3657(9)	105.66(3)-110.07(3)	86.30(3); 54.61(4)	3.264(2) (Se...(H)O)
[K(18-*crown*-6)]$_2(Se_6)$·(18-*crown*-6)·H_2O **(24)**	$(Se_6)^{2-}$	2.3240(7)	2.3185(6)-2.3563(8)	108.92(2)-109.50(2)	81.94(3)	3.2750(8) (Se...K)
[K(18-*crown*-6)]$_2(Se_6)$·(18-*crown*-6)·2NH_3 **(25)**	$(Se_6)^{2-}$	2.3146(6)	2.3188(6)-2.3564(8)	108.81(2)-109.56(2)	82.08(3); 64.63(3)	3.2764(9) (Se...K)
(*en*H$)_2(Se_6)$ **(26)**	$(Se_6)^{2-}$	2.346(2)-2.355(2)	2.329(2)-2.351(2)	103.56(8)-107.98(9)	73.35(10); 71.19(10); 81.70(10)	3.395(14) (Se...(H)N)

Table S12: Selected structural parameters of known heptaselenide and nonaselenide compounds.

Compound	Anion	d(Se–Se_t) [Å]	d(Se–Se_b) [Å]	∢(Se–Se–Se) [°]	∢(Se–Se–Se–Se) [°]	d_{min} Se…cat/solv [Å]
$[Na(12\text{-}crown\text{-}4)_2]_2(Se_7)$[18]	$(Se_7)^{2-}$	2.296(2)-2.297(1)	2.332(2)-2.354(1)	108.39(4)-113.19(4)	58.44(5); 97.41(4); 99.95(4); 111.28(4);	3.453(5) (Se...(H)C)
$[K([2.2.2]crypt)]_2(Se_7)\cdot H_2O$[26]	$(Se_7)^{2-}$	2.273(4)-2.286(4)	2.326(3)-2.342(4)	104.12(14)-110.64(15)	65.55(16); 72.39(15); 81.87(15); 83.61(15); 83.61(15)	3.479(15) (Se...O)
$[Sr(15\text{-}crown\text{-}5)_2](Se_9)$[27]	$(Se_9)^{2-}$	2.283(4)-2.27.2(4)	2.309(4)-2.473(4)	93.0(1)-109.7(1)	49.5(2); 56.3(2); 83.7(2); 91.9(2); 95.6(2); 132.0(1);	3.35(7) (Se...(H)C)

Table S13: Selected structural parameters of known mixed polychalcogenide compounds.

Compound	Anion	d(Se–Se_t) [Å]	d(Se–Se_b) [Å]	∢(Se–Se–Se) [°]	∢(Se–Se–Se–Se) [°]	d_{min} Se…cat/solv [Å]
$[Mn(MeNH_2)_6(S_5)_{0.15}(S_{1.57}Se_{2.43})_{0.85}$[9]	$(S_{1.57}Se_{2.43})^{2-}$	2.2476(8)	2.2631(11)	110.47(4)	86.38 (5)	3.433(3) (Se...(H)N)
$[Mn(NH_3)_6](S_{2.71}Se_{2.29})$[9]	$(S_{2.71}Se_{2.29})^{2-}$	2.2062(19)-2.2511(16)	2.1988(19)-2.2486(18)	107.95(7)-111.59(8)	64.88 (9); 75.632(89)	3.514(6) (Se...(H)N)
$[Mn(en)_3](Se_2Te)$[11]	$(Se_2Te)^{2-}$	2.5025(7) (Se–Te)		102.50(2) (Se–Te–Se)		3.568(4) (Se...(H)N)
$(NBu_4)_2(Se_3SSe_2)$[28]	$(Se_3SSe_2)^{2-}$	2.275(7)	2.287(7)-2.289(7)	108.4(2)-109.1(2)	92.4(3); 94.0(3)	3.79(3) (Se...(H)C)
$[K([2.2.2]crypt)]_2[SeTeSe]\cdot en$[29]	$(SeTeSe)^{2-}$	2.5018-2.5038 (Se–Te)		111.32 (Se–Te–Se)		3.49(2) (Se...(H)N)

REFERENCES FOR THE SUPPORTING INFORMATION

[1] T. Chivers, D. D. Doxsee, M. Parvez, *Inorg. Chem.* **1993**, *32*, 2238-2242.

[2] F. Wendland, C. Näther, W. Bensch, *Z. Naturforsch., B: Chem. Sci.* **2004**, *59*, 629-634.

[3] T. Chivers, D. D. Doxsee, J. F. Fait, M. Parvez, *Inorg. Chem.* **1993**, *32*, 2243.

[4] E. Ruzin, E. Zent, E. Matern, W. Massa, S. Dehnen, *Chem.-Eur. J.* **2009**, *15*, 5230-5244.

[5] R. J. Batchelor, F. W. B. Einstein, I. D. Gay, C. H. W. Jones, R. D. Sharma, *Inorg. Chem*. **1993**, *32*, 4378-4383.

[6] D. Bedlivy, A. Preisinger, *Z. Kristallogr.* **1965**, *121*, 131-144.

[7] D. Bedlivy, A. Preisinger, *Z. Kristallogr.* **1965**, *121*, 114-130.[8] X. Wang, H. H. Wang, B. Makarenko, A. J. Jacobson, *Z. Anorg. Allg. Chem.* **2012**, *638*, 2538-2541.

[9] O. Kysliak, J. Beck, *Inorg. Chem. Commun*. **2013**, *38*, 146-151.

[10] X.-M. Lin, J. Zhou, N. Cheng, X.-X. Chen, Y. Zhang, J. Dai, *(Huaxue Yanjiu Yu Yingyong) Chin. Chem. Res. Appl*. **2008**, *20*, 719.

[11] F. Wendland, C. Nather, W. Bensch, *Z. Naturforsch., B: Chem. Sci.* **2000**, *55*, 871.

[12] T. Hanauer, F. Kraus, N. Korber, *Monatsh. Chem.* **2005**, *136*, 119-125.

[13] T. König, B. Eisenmann, H. Schäfer, *Z. Anorg. Allg. Chem.* **1983**, *498*, 99-104.

[14] D. C. Green, B. W. Eichhorn, S. G. Bott, *J. Solid State Chem.* **1995**, *120*, 12-16.

[15] T. König, B. Eisenmann, H. Schäfer, *Z. Naturforsch., B: Chem. Sci.* **1982**, *37*, 1245-1249.

[16] P. W. Menezes, T. F. Fässler, *Z. Anorg. Allg. Chem*. **2012**, *638*, 1109-1113.

[17] N. E. Brese, C. R. Randall, J. A. Ibers, *Inorg. Chem.* **1988**, *27*, 940-943.

[18] V. Müller. A. Ahle, G. Frenzen, B. Neumüller, K. Dehnicke, D. Fenske, *Z. Anorg. Allg. Chem.* **1993**, *619*, 1247-1256.

[19] J. Dietz, U. Müller, V. Müller, K. Dehnicke, *Z. Naturforsch., B: Chem. Sci.* **1991**, *46*, 1293-1299.

[20] C.-N. Chau, R. W. M. Wardle, J. A. Ibers, *Acta Crystallogr.* **1988**, *C44*, 883-885; G. Kräuter, K. Dehnicke, D. Fenske, *Chemiker-Zeitung*, **1990**, *114*, 7.

[21] P. J. Barrie, R. J. H. Clark, D.-Y. Chung, D. Chakrabarty, M. G. Kanatzidis, *Inorg. Chem*. **1995**, *34*, 4299-4304. Further details on solid state NMR see references herein.

[22] V. Müller, G. Frenzen, K. Dehnicke, D. Fenske, *Z. Naturforsch*., B: Chem. Sci. **1992**, *47*, 205-210.

[23] D. Fenske. C. Kraus, K. Dehnicke, *Z. Anorg. Allg. Chem.* **1992**, *607*, 109-112.

[24] R. G. Teller, L. J. Krause, R. C. Haushalter, *Inorg. Chem.* **1983**, *22*, 1809-1812.

[25] R. Sathyamurthy, J. L. Brumaghim, D. G. VanDerveer, *J. Chem. Cryst.* **2007**, *37*, 109-117.

[27] V. Müller, C. Grebe, U. Müller, K. Dehnicke, *Z. Anorg. Allg. Chem.* **1993**, *619*, 416-420.

[26] V. Müller, K. Dehnicke, D. Fenske, G. Baum, *Z. Naturforsch., B: Chem. Sci.* **1991**, *46*, 63-67.

[28] Y. Lin, X. Jin, J. Wu, G. Xu, *Beijing Dax. Xue., Zir. Kex. (Chin.)(Acta Sci. Nat. Univ. Pek)* **1987**, 8-2.

[29] M. Björgvinsson, J. F. Sawyer, G. J. Schrobilgen, *Inorg. Chem*. **1991**, *30*, 4238-4245.

VI

$K_4[PbSe_4]\cdot en\cdot NH_3$ – A Non-Oxide, Non-Halide Inorganic Lead(IV) Compound

Günther Thiele, Thomas Krüger, Stefanie Dehnen, *Angew. Chem*. **2014**, *126*, 4792-4797;
Angew. Chem. Int. Ed. **2014**, *53*, 4699-4703.

The first inorganic lead(IV) compound without oxygen, nitrogen or halogen ligands attached to the lead atom was obtained as the potassium salt of the tetraselenidoplumbate(IV) anion $[Pb^{IV}Se_4]^{4-}$. It is stable under inert conditions which may enable the transfer of the chemistry of chalcogenidogermanate(IV) or chalcogenidostannate(IV) materials, to the lead homologues.

Themenkomplex Solvothermalesynthese von Plumbaten und Merkuraten

Inhalt: Es wird auf aktuelle Fragestellungen der Bleichemie verwiesen. Die Stabilitäten von Verbindungen unterschiedlicher formaler Oxidationsstufen an den Bleiatomen werden benannt und die wenigen bekannten anorganischen Blei(IV)-Verbindungen berichtet.

Die Synthese von $K_4[PbSe_4]\cdot en\cdot NH_3$ durch solvothermale Extraktion einer „K_2PbSe_2"-Phase in Ethylendiamin bei 150°C und die Kristallstruktur werden beschrieben, sowie der Nachweis der elementaren Zusammensetzung. Die optischen Absorptionseigenschaften werden angegeben und mithilfe quantenchemischer Rechnungen mit den teilweise bekannten oder hypothetischen Chalkogenidotetrelat-Anionen verglichen.

Mithilfe von Populationsanalysen und Molekülorbitalschemata wird die Stabilität der verwandten Anionen diskutiert und die Existenz eines $[PbS_4]^{4-}$ vorhergesagt.

Eigener Anteil: Alle Experimente wurden von mir konzipiert. Die Aufnahme und Auswertung der analytischen Daten wurde von mir durchgeführt. Die quantenchemischen Untersuchungen wurden von mir durchgeführt und zusammen mit Stefanie Dehnen ausgewertet. Thomas Krüger führte die Experimente unter meiner Anleitung durch. Stefanie Dehnen und ich schrieben das Manuskript gemeinsam.

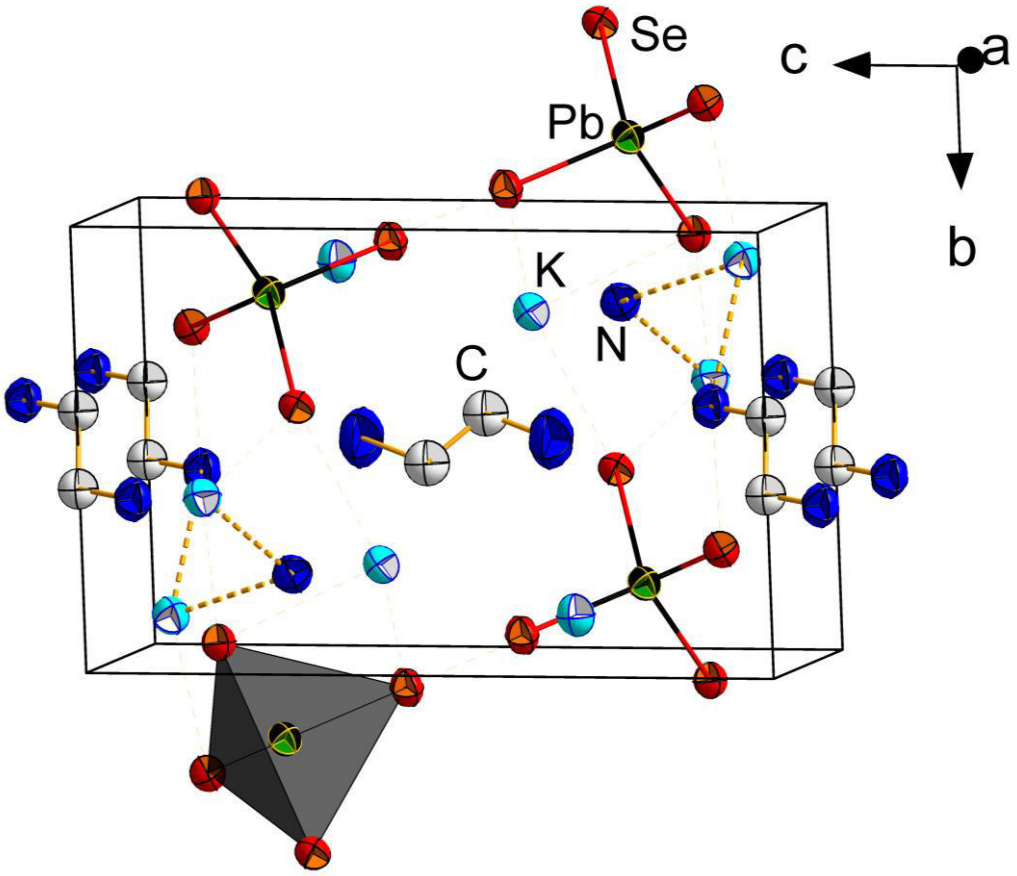

Abbildung 26. Ausschnitt aus der Kristallstruktur von $K_4[PbSe_4]\cdot en\cdot NH_3$.

Inorganic Lead(IV) Compound

DOI: 10.1002/anie.201310455

$K_4[PbSe_4]\cdot en\cdot NH_3$: A Non-Oxide, Non-Halide Inorganic Lead(IV) Compound**

*Günther Thiele, Thomas Krüger, and Stefanie Dehnen**

Dedicated to Professor Walter Thiel on the occasion of his 65th birthday

Abstract: *The first inorganic lead(IV) compound without oxygen, nitrogen or halogen ligands attached to the lead atom was obtained as the potassium salt of the tetraselenidoplumbate(IV) anion $[Pb^{IV}Se_4]^{4-}$. It is stable under inert conditions which may enable the transfer of the chemistry of chalcogenidogermanate(IV) or chalcogenidostannate(IV) materials, to the lead homologues.*

The chemistry of lead is both very traditional, going back to the late 7th millennium B.C. and ancient metallurgy,[1] and also highly topical, for instance in the synthesis of low-valence organometallic lead compounds,[2] chalcogenide or pnictogenide clusters,[3] or the use of Zintl polyanions of lead as precursors to form intermetalloid clusters.[4]

However, most academic as well as technical developments are correlated with formal oxidation states of the Pb atoms from −I to +II. Of course, this is a well-established feature, and textbooks attribute this situation to the relativistic effect that strongly stabilizes the 6s atomic orbital (AO), thus making it fairly unavailable to chemistry; exceptions are limited to salts with extremely high electronegativity nonmetal partners provided suitable crystal lattices exist which can overcompensate the high ionization energy through the corresponding lattice energies, and to lead(IV) organic compounds, such as $PbEt_4$ that was used in petrol.

By ab initio calculations on the series R_xPbX_{4-x} (R = H, Me; X = F, Cl; x = 0–4) and R_xPbX_{4-x} (x = 0–2), the concept of stable "organic Pb^{IV}" compounds, in addition to stable "inorganic Pb^{II}" compounds has been illustrated. According to these studies, an increase of the metal charge caused by more electronegative ligands leads to the 6p AO becoming unfavorable for covalent bonding.[5a] These results are in excellent agreement with the empirically found decrease of stability in the order $R_4Pb > R_3PbX > R_2PbX_2 \gg RPbX_3 > PbX_4$.[5b]

Thus, the only known "inorganic Pb^{IV}" compounds can be listed in a few lines:[6] PbO_2, as the minerals scrutinyite and plattnerite,[7] or as the prominent anode material in car batteries as well as several binary oxides, such as Pb_2O_3 and Pb_3O_4, various oxoplumbates, as first described by Zintl and co-works,[8] $Pb(OAc)_4$, an oxidizing agent for organic syntheses,[9] Pb^{IV} salts with anions of high symmetry, such as $[HAsO_4]^{2-}$, $[HPO_4]^{2-}$, $[SeO_3]^{2-}$, plumbate anions with substituents of high group electronegativity, $(AsPh_4)_2[Pb(N_3)_6]$,[10] $K_2[Pb(OH)_6]$,[11] and the corresponding acid $Pb(OH)_4$, characterized by infrared spectroscopy in solid argon.[12] For the halides, only PbX_4 (X = F, Cl)[13] and salts of the $[PbX_6]^{2-}$ ions with X = F, Cl, (IO_6) have been crystallographically determined.[14] In conclusion, no (isolable) chalcogenides PbE_2 (E = S, Se, Te) and no tetrahedral Pb^{IV}/E aggregates are known to date.

It thus is quite unexpected to find a tetrahedral unit in the first chalcogenidoplumbate(IV), $K_4[PbSe_4]\cdot en\cdot NH_3$ (**1**, Figure 1; en = ethane-1,2-diamine), which was obtained by solvothermal extraction of a homogeneous phase with the nominal composition "K_2PbSe_2". The reaction was performed

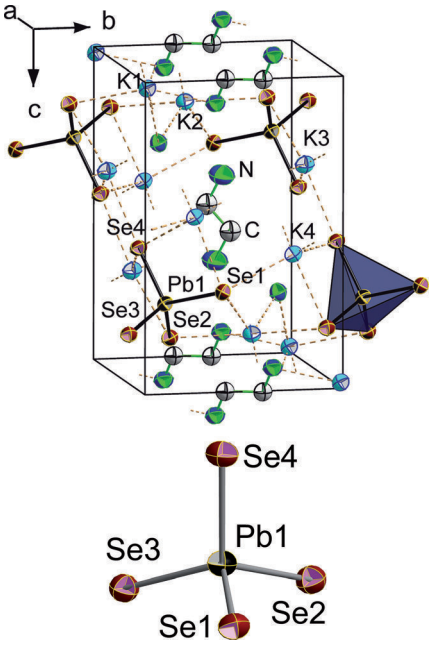

Figure 1. Fragment of the crystal structure (top) and thermal ellipsoid plot (ellipsoids set at 50% probability) of the $[Pb^{IV}Se_4]^{4-}$ ion (bottom) in **1**. Selected structure parameters: Pb-Se 2.600(2)–2.610(1) Å; Se-Pb-Se 107.71(6)-110.79(6)°.

[*] Dipl.-Chem. G. Thiele, T. Krüger, Prof. Dr. S. Dehnen
Fachbereich Chemie und Wissenschaftliches Zentrum für Materialwissenschaften, Philipps-Universität Marburg
Hans-Meerwein-Strasse, 35032 Marburg (Germany)
E-mail: dehnen@chemie.uni-marburg.de
Homepage: http://www.uni-marburg.de/fb15/ag-dehnen

[**] This work was supported by the Deutsche Forschungsgemeinschaft (SPP 1415) and the Friedrich Ebert Stiftung. We thank Dr. Johanna Heine, N. Mohri and Prof. Dr. W. Tremel for fruitful discussion, and Dr. K. Harms and R. Riedel for their help with X-ray measurements. en = ethane-1,2-diamine.

Supporting information for this article is available on the WWW under http://dx.doi.org/10.1002/anie.201310455.

based on our expertise on the chemistry of chalcogenidotetrelates(IV),[15] and on the extraction of ternary phases A/T/E (A = alkali metals, T = Group 13–14 (semi-)metal, E = pnictogen, chalcogen) by means of basic solvents.[16]

The title compound was obtained as deep red crystals (Figure 2). The crystal structure (triclinic space group $P\bar{1}$) contains near tetrahedral $[PbSe_4]^{4-}$ ions that are embedded

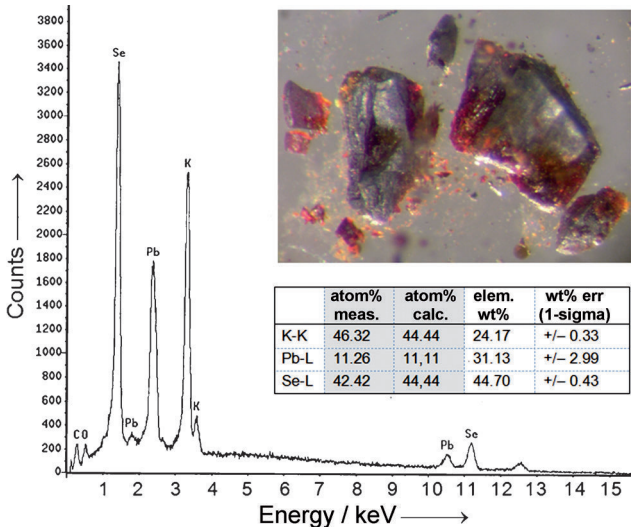

Figure 2. EDX spectrum of **1** along with the analysis data; the inset shows a photograph of partially crushed crystals of **1**, as used for the structural and elemental analyses.

between four K^+ counterions (K···Se 3.282–3.412 Å) and two solvent molecules (NH_3 and en; Se···(H)N 3.346–3.969 Å) per formula unit. The atomic K:Pb:Se ratio of **1** was confirmed by means of EDX analyses of the crystals (Figure 2). The formal +IV oxidation state at the Pb atom was rationalized by quantum chemical calculations using Møller–Plesset 2nd order perturbation theory (MP2) methods[17] implemented in the program system TURBOMOLE,[18] which show unreasonable elongations of the Pb–Se bonds for a hypothetic "$[Pb^{II}Se_4]^{6-}$" ion (Supporting Information, Table S3).

Single-crystals of the title compound are rapidly covered by a metallic film upon contact with air, but are stable under inert conditions for months. They are stable enough to be kept as a suspension in nujol oil between two quartz plates for several hours; over more than 12 h, the solid-state UV/Vis spectrum (Figure 3) remained the same. Neither room temperature, nor illumination by visible light changed the situation. Only upon exposure of the suspension to air, the sample color turned black and the absorption signal diminished, indicating decomposition of the compound. In agreement with the visible color (Figure 2), the measured optical excitation energy, given as onset of absorption, amounts to $E_{onset} = 2.0$ eV.

Quantum chemical calculations using time-dependent DFT methods (TDDFT, singlet excitations)[19] also implemented in the program system TURBOMOLE[18] were performed to rationalize the measured excitation energy, and to compare it to the E_{onset} values of the entire $[TE_4]^{4-}$ series with T = Si–Pb and E = O–Te (Figure S1). The calculations show a con-

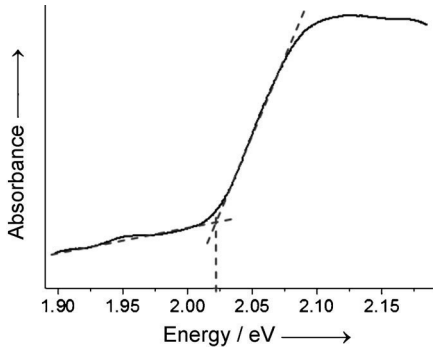

Figure 3. Solid state UV/Vis spectrum of **1**, recorded from a suspension of pulverized crystals in nujol oil.

tinuous development of E_{onset} along the tetrel family and, for a given tetrel element, along the chalcogen family.[20] As expected from the color of the deep red crystals, $[PbSe_4]^{4-}$ and $[SnTe_4]^{4-}$ [20a–c] have the same absorption energy. In both cases, the calculated values (1.9 eV) differ by only 0.1 eV from the measured ones (2.0 eV).

More detailed information about the electronic situation was gained by further MP2 calculations and consecutive inspection of the molecular orbitals (MOs) of all possible $[TE_4]^{4-}$ combinations (T = Si–Pb; E = O–Te) by means of Mulliken population analysis.[21] The highest occupied MOs (HOMO, HOMO−1, HOMO−2) and the lowest energy valence MO (HOMO−5) have distinct lone-pair character at the terminal chalcogenide ligands, whereas HOMO−3 and HOMO−4 are T–E bonding in nature. Most developments of MO energies are steady along the T or E series (Figure S2), indicating slight destabilization of the HOMO along Pb→Si, nearly no change for HOMO−1 and HOMO−2, and a slight stabilization for HOMO−3, however, the HOMO−4 energies reflect the distinct stabilization of the 6s and 6p AO at Pb. As an example, we compare the MOs for $[PbSe_4]^{4-}$ and $[SnSe_4]^{4-}$ (Figure 4) into detail.

In $[PbSe_4]^{4-}$, HOMO and HOMO−1 (t_2, t_1) are nearly the same energy, HOMO−2 (e) is lower by 0.7 eV. The higher-energy Pb–Se bonding orbital (HOMO−3, t_2) is below the "lone pairs" by another 1.2 eV. As expected, a very stable, Pb–Se bonding MO (HOMO−4, a_1) with a significant Pb 6s contribution is found another 5 eV lower, that is, 7 eV below the HOMO energy level; according to population analyses, the contributions to this MO are 23.3% Pb 6s and 23.3% Pb 6p, along with 40.8% Se 4s, and 12.6% Se 4p (all four Se atoms in total). Apart from the energetic order of the highest t_2 and t_1 MOs (t_2 is higher in energy than t_1 by 0.002 eV for $[PbSe_4]^{4-}$), both the energy differences and AO contributions found for HOMO, HOMO−1, HOMO−2, and HOMO−3 are very similar for $[PbSe_4]^{4-}$ and $[SnSe_4]^{4-}$. In contrast, the situation for HOMO−4 differs significantly: for the Sn/Se combination, not only the orbital contributions of the central atom are lower (19.0% Sn 5s and 19.0% Sn 5p along with 50.5% Se 4s and 11.5% Se 4p), but this MO is also by only 4 eV lower in energy than HOMO-3, and by only 6 eV below the HOMO level in $[SnSe_4]^{4-}$. Both the energies of the T–E bonding MOs HOMO−3 and HOMO−4, and the electron-

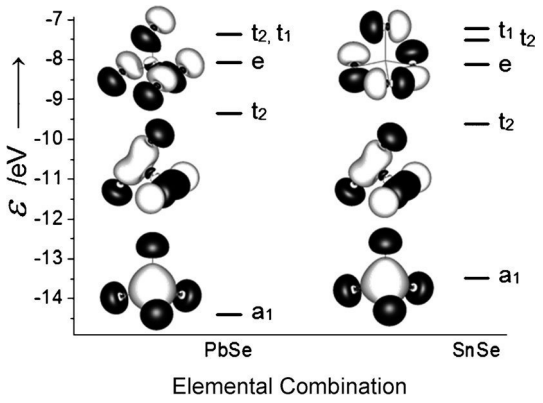

Figure 4. MO schemes along with the visualization of representative occupied orbitals in $[PbSe_4]^{4-}$ (left) and $[SnSe_4]^{4-}$ (right). MO plots from top: HOMO ($[PbSe_4]^{4-}$: t_2, $[SnSe_4]^{4-}$: t_1), HOMO−3 (t_2), HOMO−4 (a_1). Amplitudes are drawn at ±0.033 a.u.; note that only one of the degenerate MOs is shown for all examples. The lowest energy valence orbitals (HOMO−5) that represent the 5s AOs from Se atoms in both cases are not shown.

density distribution in HOMO−3 may be made responsible for the observed stability. In the particular case of $[PbSe_4]^{4-}$, although the higher energy bonding MO (t_2, HOMO−3) is slightly destabilized (with respect to the situation in $[SnSe_4]^{4-}$), the plumbate(IV) anion is not that reactive as a consequence of the high stability of the lower energy bonding MO (a_1, HOMO−4), which is indeed the lowest energy HOMO−4 in the entire $[TE_4]^{4-}$ series (Figure S2). By inspection of the relative energies, our recent observation that a preparation of $[PbTe_4]^{4-}$ is not possible using the described method can be explained, whereas the synthesis of $[PbS_4]^{4-}$ should, in general, be possible. Our efforts so far have failed because no homogenous parent phase (such as "K_2PbS_2") could be obtained. In addition to these molecular effects, we assume a considerable influence of the lattice energy of the solid **1**. This assumption is supported by the observation that **1** precipitates from the mother liquor during the solvothermal treatment and does not re-dissolve in en, which can be understood in terms of suitable molecular measures: the Pb–Se bond lengths in **1** (2.600(2)–2.610(1) Å) are right within the Sn–E bond lengths observed in *ortho*-selenidostannate (2.50–2.54 Å) and *ortho*-telluridostannate anions (2.72–2.80 Å),[15] the potassium salts (hydrates) of which are known,[20a,22] hence rationalizing the stability of the corresponding crystal lattice for **1**.

To further elucidate the stability or reactivity of *ortho*-chalcogenidotetrelate anions, including the anion in **1**, we calculated reaction energies E_r (Table 1) for all possible permutations of elements in reactions of the following type [Eq. (1)].

$$[T^1E_4]^{4-} + T^2 \rightarrow [T^2E_4]^{4-} + T^1 \qquad \Delta E = E_r \tag{1}$$

For a given chalcogen E, all reactions forming a lighter $[T^2E_4]^{4-}$ homologue are exoenergetic; for given tetrel atoms T^1 and T^2, the reactions become more exoenergetic as the chalcogen E is replaced by a lighter congener; as expected, a maximum step in E_r is observed when changing from E = S to E = O, in accordance with the extraordinary stability of oxotetrelates compared to all of their heavier homologues. In contrast, the E_r values differ only marginally between $[TE_4]^{4-}$ species comprising the heavier elemental combinations, such as $[PbSe_4]^{4-}$ versus $[SnSe_4]^{4-}$ (5.2 kJ mol^{-1}), suggesting similar stabilities and reactivities of the respective anions.

In summary, it was possible to prepare and unambiguously characterize the first non-oxide, non-halide inorganic Pb^{IV} compound. The potassium salt of the tetraselenidoplumbate(IV) anion can be kept under inert conditions (inert gas or oil) without change to date. This stability should enable the previously unexpected transfer of the chemistry of chalcogenidogermanate(IV) or chalcogenidostannate(IV) materials, which has been comprehensively investigated in recent times, to the homologues of the heaviest tetrel congener, with accordingly varied photophysical, photochemical, and redox behavior of the resulting compounds.

Experimental Section

General: All manipulations and reactions were performed under an Ar atmosphere using standard Schlenk or glove box techniques. The ternary parent phase "K_2PbSe_2" was prepared by fusion of potassium and lead in a 2:1 molar ratio, subsequent addition of granular selenium (2 equiv), and heating with an oxygen/methane burner for 15 min, which yielded an amorphous black powder upon grinding. Ethane-1,2-diamine (en) was freshly distilled and stored under Ar prior to use.

1: "K_2PbSe_2" (500 mg) and en (2 mL) were placed in a glass vial within a Teflon-lined autoclave; the autoclave was tightly closed and heated for 7 days at 150 °C. After turning off the heating, the autoclave was left for another 2 days to slowly cool down to room temperature. Compound **1** appeared as deep red crystals along with orange polyselenide by-products.

Single-crystal X-ray diffraction: Data collection was performed using a Stoe IPDSI diffractometer at 193 K with $Mo_{K\alpha}$ radiation and graphite monochromatization ($\lambda = 0.71073$). Structure solution was realized by direct methods, refinement with full-matrix-least-squares against F^2 using SHELXS-97, SHELXL-97, and Olex2 software.[24] Crystal data for $C_2H_{11}K_4N_3PbSe_4$ (**1**, $M_W = 756.6$ g mol^{-1}): $a = 8.055(2)$, $b = 8.292(2)$, $c = 12.790(3)$ Å, $\alpha = 92.64(2)$, $\beta = 103.69(2)$, $\gamma = 92.45(2)$°. CCDC 970129 contains the supplementary crystallographic data for this paper. These data can be obtained free of charge from The Cambridge Crystallographic Data Centre via www.ccdc.cam.ac.uk/data_request/cif.

Quantum chemical methods: DFT calculations were performed with the program system TURBOMOLE[18] using the RIDFT program[25] and employing the Becke–Perdew 86 (BP86) functional[26] with def2-TZVP bases[27] and respective fitting bases[28] for the evaluation of the

Table 1: Reaction energies E_r [kJ mol^{-1}] for the reactions given in Equation (1).[a]

T^1	Pb	Pb	Pb	Pb	Pb	Pb	Pb	Pb	Pb	Pb	Pb	Pb
T^2	Si	Ge	Sn	Si	Ge	Sn	Si	Ge	Sn	Si	Ge	Sn
E	O	O	O	S	S	S	Se	Se	Se	Te	Te	Te
E_r	−32.8	−15.4	−10.2	−13.9	−8.8	−6.3	−11.3	−7.4	−5.2	−7.8	−5.5	−3.9

[a] Values for all further permutations with T^1 = Sn, Ge, or Si, respectively, or with $T^1 = T^2$ for different types of E can be calculated according to Born–Haber cycles[23] from the given numbers.

Coulomb matrix. MP2 calculations were undertaken with the program RIMP2,[29] using def2-TZVP bases[27] and the corresponding fitting bases.[30] Effective core potentials (ECPs) were used for Sn, Te, and Pb atoms (ECP-28, ECP-28, and ECP-60, respectively).[31] Counterions were modeled by application of COSMO with default parameters.[32] Mulliken population analyses[21] served to evaluate atomic orbital contributions to the molecular orbitals. MO plots were generated using the visualization tool gOpenMol.[33]

Received: December 2, 2013
Published online: March 20, 2014

Keywords: DFT calculations · lead · MP2 calculations · plumbates · structure elucidation

[1] D. L. Heskel, *Curr. Anthropol.* **1983**, *24*, 362 – 366.
[2] Reviews: a) R. C. Fischer, P. P. Power, *Chem. Rev.* **2010**, *110*, 3877 – 3923; b) M. Weidenbruch, *J. Organomet. Chem.* **2002**, *646*, 39 – 52; c) M. Driess, H. Grützmacher, *Angew. Chem.* **1996**, *108*, 900 – 929; *Angew. Chem. Int. Ed. Engl.* **1996**, *35*, 828 – 856. Selected examples: d) A. Jana, S. P. Sarish, H. W. Roesky, D. Leusser, I. Objartel, D. Stalke, *Chem. Commun.* **2011**, *47*, 5434 – 5436; e) C. Förster, K. W. Klinkhammer, B. Tumanskii, H.-J. Krüger, H. Kelm, *Angew. Chem.* **2007**, *119*, 1174 – 1177; *Angew. Chem. Int. Ed.* **2007**, *46*, 1156 – 1159; f) A. Murso, M. Straka, M. Kaupp, R. Bertermann, D. Stalke, *Organometallics* **2005**, *24*, 3576 – 3578; g) K. Jurkschat, K. Peveling, M. Schürmann, *Eur. J. Inorg. Chem.* **2003**, 3563 – 3571; h) F. Stabenow, W. Saak, H. Marsmann, M. Weidenbruch, *J. Am. Chem. Soc.* **2003**, *125*, 10172 – 10173; i) L. Pu, B. Twamley, P. P. Power, *J. Am. Chem. Soc.* **2000**, *122*, 3524 – 3525; j) S. Wingerter, H. Gornitzka, R. Bertermann, S. K. Pandey, J. Rocha, D. Stalke, *Organometallics* **2000**, *19*, 3890 – 3894.
[3] a) S. Traut, C. v. Hänisch, *Chem. Commun.* **2010**, *46*, 1538 – 1540.
[4] a) J. B. Friauf, *J. Am. Chem. Soc.* **1926**, *48*, 1906 – 1909; b) P. A. Edwards, J. D. Corbett, *Inorg. Chem.* **1977**, *16*, 903 – 907; c) S. Scharfe, F. Kraus, S. Stegmaier, A. Schier, T. F. Fässler, *Angew. Chem.* **2011**, *123*, 3712 – 3754; *Angew. Chem. Int. Ed.* **2011**, *50*, 3630 – 3670.
[5] a) M. Kaupp, P. v. R. Schleyer, *J. Am. Chem. Soc.* **1993**, *115*, 1061 – 1073; b) P. G. Harrison in *Comprehensive Organometallic Chemistry II*, *Vol. 2* (Eds.: E. W. Abel, F. G. A. Stone, G. Wilkinson), Pergamon, Oxford, **1995**, Chap. 12.
[6] Note that the term "inorganic" addresses Pb compounds without any Pb–C or Pb–H bonds. For organometallic Pb^{IV} compounds, see recent Reviews: a) M. C. Kuchta, G. Parkin, *Coord. Chem. Rev.* **1998**, *176*, 323 – 372; b) M. G. Moloney, *Science of Syntheses*, *Vol. 5* (Eds.: D. Bellus, G. F. Herrmann), Georg Thieme, Stuttgart, **2003**, pp. 619 – 626. For Pb_xH_y see for example c) X. Wang, L. Andrews, *J. Am. Chem. Soc.* **2003**, *125*, 6581 – 6587.
[7] a) J. E. Taggart, E. E. Foord, A. Rosenzweig, T. Hanson, *Can. Mineral.* **1988**, *26*, 905 – 910; b) E. Kinch, *J. Chem. Soc. Abstr.* **1887**, *52*, 451 – 456.
[8] K_4PbO_4: a) E. Zintl, W. Morawietz, *Z. Anorg. Allg. Chem.* **1938**, *236*, 372 – 410. For more-recent reports on further oxoplumbates(IV), see for example: b) K. Yoshii, M. Mizumaki, K. Kato, T. Uruga, H. Abe, A. Nakamura, Y. Shimojo, Y. Ishii, Y. Morii, *J. Solid State Chem.* **2007**, *180*, 377 – 381; c) E. Ksepko, A. Winiarski, A. Ratuszna, *Phase Transitions* **2004**, *77*, 335 – 344.
[9] a) R. Criegee in *Oxidation in Organic Chemistry*, *Vol. A* (Ed.: K. B. Wiberg), Academic Press London, London, **1965**, Chap. V; b) O. Dimroth, R. Schweizer, *Ber. Dt. Chem. Ges.* **1923**, *56B*, 1375 – 1385.
[10] a) E. R. Losilla, M. A. Salvado, M. A. G. Aranda, A. Cabeza, P. Pertierra, S. G. Granda, S. Bruque, *J. Mol. Struct.* **1998**, *470*, 93 – 104; b) S. Bruque, K. A. G. Aranda, E. R. Losilla, P. Olivera-Pastor, P. Maireles-Torres, *Inorg. Chem.* **1995**, *34*, 893 – 899; c) G. Steinhauser, C. Luef, M. Wildner, G. Giester, *J. Alloys Compd.* **2006**, *419*, 45 – 49; d) K. Polborn, E. Leidl, W. Beck, *Z. Naturforsch. B* **1988**, *43*, 1206 – 1208.
[11] H. Jacobs, R. Stahl, *Z. Anorg. Allg. Chem.* **2000**, *626*, 1863 – 1866.
[12] X. Wang, L. Andrews, *J. Phys. Chem. A* **2005**, *109*, 9013 – 9020.
[13] a) I. J. Maley, S. Parsons, C. R. Pulham, *Acta Crystallogr. Sect. E* **2002**, *58*, 79 – 81; b) R. Hoppe, W. Dähne, *Naturwissenschaften* **1962**, *49*, 254 – 255.
[14] a) P. Charpin, H. Marquet-Ellis, N. Nguyen, P. Plurien, *C. R. Hebd. Seances Acad. Sci. Ser. C* **1972**, *275*, 1503 – 1506; b) G. Engel, *Naturwissenschaften* **1933**, *21*, 704; c) D. B. Currie, W. Levason, R. D. Oldroyd, M. T. Weller, *J. Mater. Chem.* **1993**, *3*, 447 – 451.
[15] a) S. Dehnen, M. Melullis, *Coord. Chem. Rev.* **2007**, *251*, 1259 – 1280; b) J. Heine, S. Dehnen, *Z. Anorg. Allg. Chem.* **2012**, *638*, 2425 – 2440.
[16] a) B. Weinert, A. R. Eulenstein, R. Ababei, S. Dehnen, *Angew. Chem.* **2014**, *126*, DOI: 10.1002/ange.201310456; *Angew. Chem. Int. Ed.* **2014**, *53*, DOI: 10.102/anie.201310456; b) R. Ababei, W. Massa, K. Harms, X. Xie, F. Weigend, S. Dehnen, *Angew. Chem.* **2013**, *125*, 13786; *Angew. Chem. Int. Ed.* **2013**, *52*, 13544; c) B. Weinert, F. Weigend, S. Dehnen, *Chem. Eur. J.* **2012**, *18*, 13589 – 13595; d) F. Lips, M. Holynska, R. Clerac, U. Linne, I. Schellenberg, R. Pöttgen, F. Weigend, S. Dehnen, *J. Am. Chem. Soc.* **2012**, *134*, 1181 – 1191; e) R. Ababei, J. Heine, M. Hołyńska, G. Thiele, B. Weinert, X. Xie, F. Weigend, S. Dehnen, *Chem. Commun.* **2012**, *48*, 11295 – 11297; f) F. Lips, R. Clérac, S. Dehnen, *J. Am. Chem. Soc.* **2011**, *133*, 14168 – 14171; g) F. Lips, R. Clérac, S. Dehnen, *Angew. Chem.* **2011**, *123*, 991 – 995; *Angew. Chem. Int. Ed.* **2011**, *50*, 960 – 964; h) F. Lips, S. Dehnen, *Angew. Chem.* **2011**, *123*, 986 – 990; *Angew. Chem. Int. Ed.* **2011**, *50*, 955 – 959; i) F. Lips, S. Dehnen, *Angew. Chem.* **2009**, *121*, 6557 – 6560; *Angew. Chem. Int. Ed.* **2009**, *48*, 6435 – 6438.
[17] C. Møller, S. Plesset, *Phys. Rev.* **1934**, *46*, 618 – 622.
[18] TURBOMOLE Version 6.4, TURBOMOLE GmbH 2012. TURBOMOLE is a development of University of Karlsruhe and Forschungszentrum Karlsruhe 1989–2007, TURBOMOLE GmbH since **2007**.
[19] a) F. Furche, D. Rappoport, *Theoretical and Computational Chemistry*, *Vol. 16* (Ed.: M. Olivucci), Elsevier, Amsterdam, **2005**, Chap. III; b) R. Bauernschmitt, M. Häser, O. Treutler, R. Ahlrichs, *Chem. Phys. Lett.* **1997**, *264*, 573 – 578; c) R. Bauernschmitt, R. Ahlrichs, *Chem. Phys. Lett.* **1996**, *256*, 454 – 464; R. Bauernschmitt, R. Ahlrichs, *J. Chem. Phys.* **1996**, *104*, 9047 – 9052.
[20] The only discontinuity within the electronic excitation energies of the $[TE_4]^{4-}$ series was observed for $[GeO_4]^{4-}$, as a result of its particular position as a post-transition element. Experimental values of $[SnE_4]^{4-}$ are found in: a) E. Ruzin, A. Kracke, S. Dehnen, *Z. Anorg. Allg. Chem.* **2006**, *632*, 1018 – 1026; b) T. Kaib, *Diploma Thesis*, Marburg **2009**; c) M. Melullis, S. Dehnen, *Z. Anorg. Allg. Chem.* **2007**, *633*, 2159 – 2167.
[21] R. S. Mulliken, *J. Chem. Phys.* **1955**, *23*, 1833 – 1840.
[22] S. Dehnen, M. K. Brandmayer, *J. Am. Chem. Soc.* **2003**, *125*, 6618 – 6619.
[23] P. W. Atkins, *Physikalische Chemie*, *Vol. 3*, Wiley-VCH, Weinheim, **2001**, p. 81.
[24] a) G. W. Sheldrick, SHELXTL 5.1, Bruker AXS Inc. 6300 Enterprise Lane, Madison, WI 53719 – 1173, USA, **1997**; b) Absorption correction was applied with the program XPREP V5.1/NT 1997 Bruker Analytical X-ray Systems c) O. V. Dolomanov, L. J. Bourhis, R. J. Gildea, J. A. K. Howard, H. Puschmann, *J. Appl. Crystallogr.* **2009**, *42*, 339 – 341.
[25] a) K. Eichkorn, O. Treutler, H. Öhm, M. Häser, R. Ahlrichs, *Chem. Phys. Lett.* **1995**, *242*, 652 – 660; b) K. Eichkorn, F. Weigend, O. Treutler, R. Ahlrichs, *Theor. Chim. Acta* **1997**, *97*, 119 – 124.

[26] a) A. D. Becke, *Phys. Rev. A* **1988**, *38*, 3098 – 3109; b) S. H. Vosko, L. Wilk, M. Nusair, *Can. J. Phys.* **1980**, *58*, 1200 – 1205; c) J. P. Perdew, *Phys. Rev. B* **1986**, *33*, 8822 – 8837.
[27] F. Weigend, R. Ahlrichs, *Phys. Chem. Chem. Phys.* **2005**, *7*, 3297 – 3305.
[28] F. Weigend, *Phys. Chem. Chem. Phys.* **2006**, *8*, 1057 – 1065.
[29] F. Weigend, M. Häser, *Theor. Chem. Acc.* **1997**, *97*, 331 – 340.
[30] F. Weigend, M. Häser, H. Patzelt, R. Ahlrichs, *Chem. Phys. Lett.* **1998**, *294*, 143 – 152; A. Hellweg, C. Hättig, S. Höfener, W. Klopper, *Theor. Chem. Acc.* **2007**, *117*, 587 – 597.
[31] B. Metz, H. Stoll, M. Dolg, *J. Chem. Phys.* **2000**, *113*, 2563 – 2569.
[32] a) A. Klamt, G. Schürmann, *J. Chem. Soc. Perkin Trans.* **1993**, 799 – 805; b) A. Schäfer, A. Klamt, D. Sattel, J. C. W. Lohrenz, F. Eckert, *Phys. Chem. Chem. Phys.* **2000**, *2*, 2187 – 2193.
[33] gOpenMol, Leif Laaksonen, Center for Scientific Computing, Espoo, Finland, Version 3.0, **2005**: D. L. Bergman, L. Laaksonen, A. Laaksonen, *J. Mol. Graphics Modell.* **1997**, *15*, 301 – 306.

Angewandte Chemie
Eine Zeitschrift der Gesellschaft Deutscher Chemiker

Supporting Information

69451 Weinheim, Germany

$K_4[PbSe_4]\cdot en\cdot NH_3$: A Non-Oxide, Non-Halide Inorganic Lead(IV) Compound**

*Günther Thiele, Thomas Krüger, and Stefanie Dehnen**

anie_201310455_sm_miscellaneous_information.pdf

Contents:

1 Details of the Single-Crystal Data Collection, Structure Solution and Refinement

Data collection was performed using a Stoe IPDS diffractometer at 193 K with MoKα radiation and graphite monochromatization (λ = 0.71073). Structure solution was realized by direct methods, refinement with full-matrix-least-squares against F^2 using SHELXS-97, SHELXL-97 and Olex2 software.[1] Table S1 summarizes the relevant data.

Table S1. X-ray measurement, structure solution and refinement of **1**.

Compound	**1**
Empirical formula	$C_2K_4N_3PbSe_4$
Formula weight /g·mol^{-1}	745.48
Crystal color, shape	Red Block
Crystal size /mm^3	0.16 x 0.09 x 0.04
Crystal system	Triclinic
Space group	P-1
a /Å *b* /Å *c* /Å	8.0555 (16) Å 8.292 (2) Å 12.790 (3) Å
α /° β /° γ /°	92.643 (18)° 103.692 (16)° 92.445 (18)°
V /Å^3	827.8 (3)
Z	2
ρ_{calc} /g·cm^{-3}	2.991
$\mu(Mo_{K\alpha})$ /mm^{-1}	19.96
2Θ range /°	4.92–52.24
Reflections measured	7773
Independent reflections	2848
R(int)	0.076
Ind. reflections ($I > 2\sigma(I)$)	1864
Parameters	123
Restraints	0
R_1 ($I > 2\sigma(I)$)	0.052
wR_2 (all data)	0.127
GooF (all data)	0.92
Max. peak/hole /e$^-$·Å^{-3}	2.03
Absorption correction type	psi-scan
Min. /Max. transmission	0.012/0.052

2 Solid State UV-Visible Spectroscopy

UV-vis spectra were recorded on a Perkin-Elmer Cary 5000 UV-vis-near-infrared spectrometer in the range of 800-200 nm employing a double-beam technique. The samples were prepared as suspensions in Nujol oil between two quartz plates.

3 Energy Dispersive X-ray (EDX) Spectroscopy Analyses

EDX analysis on **1** was performed using the EDX device Voyager 4.0 of Noran Instruments coupled with the electron microscope CamScan CS 4DV. Data aquisition was performed with an acceleration voltage of 20 kV and 100 s accumulation time. Results are summarized in Table S2.

Table S2. EDX analysis of **1** (K, Se, Pb).

Element-edge	k-ratio	ZAF	Atom %	Atomic ratio observed (calc)	Element wt %	wt % Err. (1-sigma)
K-K	0.1815	1.332	46.32	4.11 (4)	24.17	+/- 0.33
Se-L	0.3130	1.428	42.42	3.77 (4)	44.70	+/- 0.43
Pb-L	0.2539	1.226	11.26	1.00 (1)	31.13	+/- 2.99
Total			100	8.88 (9)	100	

4 Details of the Quantum Chemical Investigations

4.1 Computational Methods

DFT calculations were done with the program RIDFT[2] implemented in the program system TURBOMOLE[3] employing the Becke–Perdew 86 (BP86) functional[4] with def2-TZVP bases[5] and respective fitting bases[6] for the evaluation of the Coulomb matrix. MP2 calculations were undertaken with the program RIMP2,[7] using def2-TZVP bases and according fitting bases for the evaluation of the J matrix.[8] Effective core potentials (ECPs) were used for Sn, Te and Pb atoms (ECP-28 and ECP-60, respectively).[9] Counter ions were modeled by COSMO with default parameters.[10] Electronic excitation energies were calculated using the TDDFT module.[11] Mulliken Population analyses[12] served to evaluate atomic orbital contributions to the molecular orbitals. Contour plots were generated with gOpenMol.[13]

4.2 Structural parameters within $[PbSe_4]^{q-}$ (experimental and MP2-calcuations; q = 4, 6)

In Table S3, the experimentally found structure parameters within the $[PbSe_4]^{4-}$ anion are given along with parameters calculated by means of MP2 calculations for $[PbSe_4]^{4-}$ and for the hypothetic species "$[Pb^{II}Se_4]^{6-}$". All calculations were done in C_1 symmetry. However, for $[PbSe_4]^{4-}$, the calculation ran into perfect T_d symmetry. Distinct bond elongations expulse "$[PbSe_4]^{6-}$" from being reasonable.

Table S3. Structural parameters of $[PbSe_4]^{4-}$ (exp.), $[Pb^{IV}Se_4]^{4-}$ (MP2) and "$[Pb^{II}Se_4]^{6-}$" (MP2).

Species	$[PbSe_4]^{4-}$ (X-ray)	$[PbSe_4]^{4-}$ (MP2)	"$[PbSe_4]^{6-}$" (MP2)
Pb–Se /Å	2.600(2)-2.610(1)	2.571	2.975-3.033
Se–Pb–Se /°	107.71(6)-110.79(6)	109.5	107.1-111.2

4.3 Electronic Excitation Energies for the $[TE_4]^{4-}$ Series with T = Si…Pb and E = O…Te

Figure S1 shows calculated and experimentally reported electronic excitation energies for the $[TE_4]^{4-}$ series with T = Si…Pb and E = O…Te.

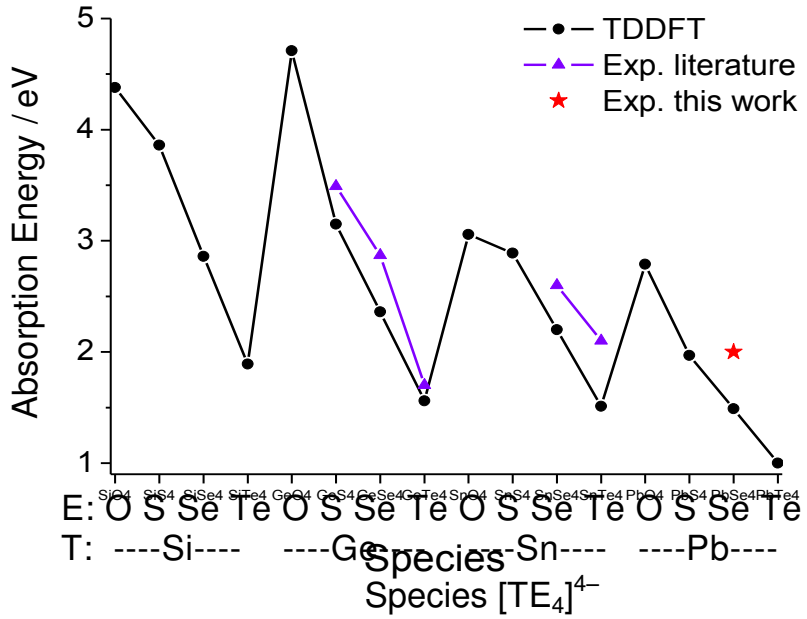

Figure S1. Calculated and measured optical absorption energies for the series $[TE_4]^{4-}$. Experimental values, except those of $[PbSe_4]^{4-}$, were taken from Ref. [14].

4.4 MO-Energies for the $[TE_4]^{4-}$ Series with T = Si…Pb and E = O…Te

Figure S2 shows the energies of the five highest occupied molecular orbitals for the $[TE_4]^{4-}$ series with T = Si…Pb and E = O…Te, as calculated by MP2 methods. Observable trends are summarized below.

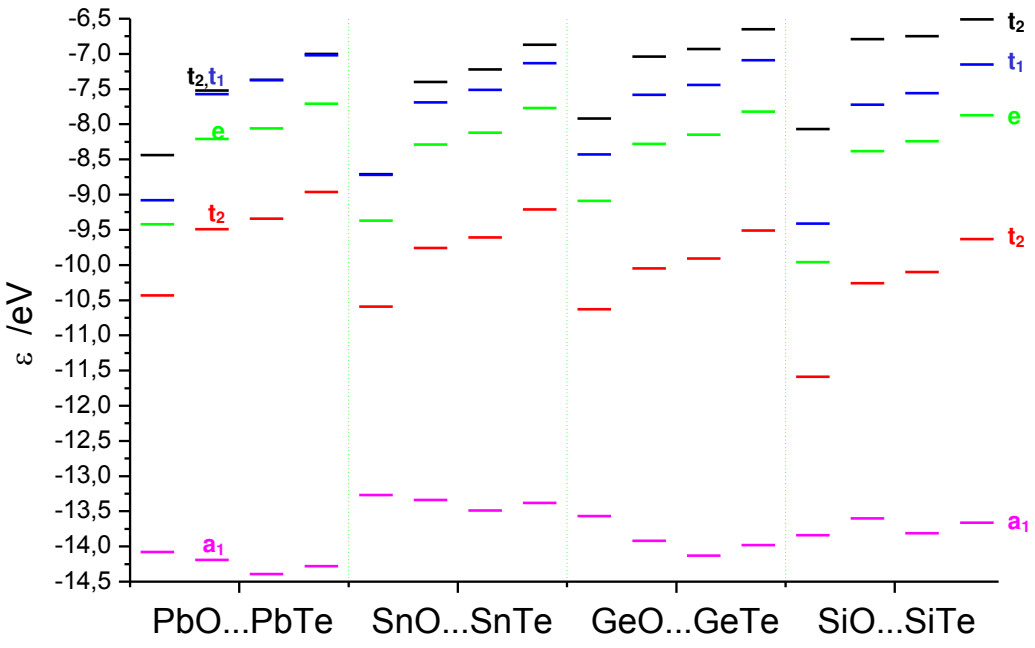

Figure S2. Energies of the five highest occupied molecular orbitals for the $[TE_4]^{4-}$ series with T = Si…Pb and E = O…Te as calculated by means of MP2 methods. Negative charges of the anions were compensated for by application of the COSMO program.

The following trends were observed when going from T = Pb to T = Si:

1) energy differences between HOMO, HOMO–1, HOMO–2, and HOMO–3 increase (*exception*: Pb/O → Sn/O; for Sn/O, energies of HOMO, HOMO–1 are nearly equal)
2) HOMO ($\mathbf{t_2}$) energies increase for given E
3) HOMO–1 ($\mathbf{t_1}$) energies decrease for given E (*exception:* unsteady for E = O)
4) HOMO–2 (**e**) energies decrease for given E (*exception:* unsteady for E = O)
5) HOMO–3 ($\mathbf{t_2}$) energies decrease for given E
6) HOMO–4 ($\mathbf{a_1}$) energies decrease for given E (*exception 1:* for T = Pb, HOMO–4 energies are *always significantly* lower (!); *exception 2:* Ge/S,Se,Te → Si/S,Se,Te)

The following trends were observed when going from E = O to E = Te:

1) MO energies increase (*exception:* for $\mathbf{a_1}$ (Pb, Sn, Ge): O>S>Se<Te, whereas for $\mathbf{a_1}$ (Si) O<S>Se<Te)

5 References for the Supporting Information

[1] a) G.W. Sheldrick, SHELXTL 5.1, Bruker AXS Inc. 6300 Enterprise Lane, Madison, WI 53719-1173, USA, **1997**; b) O.V. Dolomanov, L. J. Bourhis, R. J. Gildea, J. A. K. Howard, H. Puschmann, *J. Appl. Cryst.* **2009**, *42*, 339-341.

[2] K. Eichkorn, O. Treutler, H. Oehm, M. Haeser, R. Ahlrichs, *Chem. Phys. Lett.* **1995**, *242*, 652-660.

[3] TURBOMOLE Version 6.4, (c) TURBOMOLE GmbH 2012. TURBOMOLE is a development of University of Karlsruhe and Forschungszentrum Karlsruhe 1989-2007, TURBOMOLE GmbH since 2007.

[4] A. D. Becke, *Phys. Rev. A* **1988**, *38*, 3098-3100; J. P. Perdew, *Phys. Rev. B* **1996**, *33*, 8822-8824.

[5] F. Weigend, R. Ahlrichs, *Phys. Chem. Chem. Phys.* **2005**, *7*, 3297-3305.

[6] F. Weigend, *Phys. Chem. Chem. Phys.* **2006**, *8*, 1057–1065.

[7] F. Weigend, M. Häser, *Theor. Chem. Acc.* **1997** *97*, 331-340.

[8] F. Weigend, M. Häser, H. Patzelt, R Ahlrichs, *Chem. Phys. Lett.* **1998**, *294*, 143-152.

[9] B. Metz, H. Stoll, M. Dolg, *J. Chem. Phys.* **2000**, *113*, 2563-2569.

[10] A. Klamt; G. Schürmann *J. Chem. Soc. Perkin Trans.* **1993**, *2*, 799-805.

[11] a) R. Bauernschmitt, R. Ahlrichs, *Chem. Phys. Lett*. **1996**, *256*, 454-464; b) *J. Chem. Phys.* **1996**, *104*, 9047-9052.

[12] R. S. Mulliken, *J. Chem. Phys*. **1955**, *23*, 1833-1841.

[13] D. L. Bergman, L. Laaksonen, A. Laaksonen, *J. Mol. Graph. Model.* **1997**, *15*, 301-306.

[14] a) E. Ruzin, A. Kracke, S. Dehnen, *Z. Anorg. Allg. Chem*. **2006**, *632*, 1018-1026. b) T. Kaib, *Diploma Thesis*, Marburg **2009.** c) M. Melullis, S. Dehnen, *Z. Anorg. Allg. Chem*. **2007**, *633*, 2159-2167.

VII

Reactions In and With Acetonitrile

Günther Thiele, Stefanie Dehnen, *Manuskript in Vorbereitung*.

Solvothermal reactions and *in-situ*-reductions in acetonitrile yield a variety of new metal salts and organometallic compounds including	ligands of dimers and tetramers of acetonitrile upon oxidative C–C and/or C–N bond formation and its specific decomposition.

Themenkomplex Solvothermalsynthese von Plumbaten und Merkuraten

Inhalt: Es werden bekannte Synthesen ausgehend von Acetonitril zusammengefasst und exemplarisch beschrieben. Die wenigen solvothermalen Umsetzungen mit Acetonitril werden beschrieben und die typische Vorgehensweise für solvothermale Metallatsynthesen dargelegt.

Die Reaktion von „KPbTe“ mit $NiCl_2$ in Acetonitril unter solvothermalen Bedingungen mit dem dabei entstehenden $[(C_8H_{12}N_4)NiCl(\mu\text{-}Cl)]_2$ wird beschrieben. In Abwesenheit von „KPbTe“ wird bei sonst gleichen Reaktionsbedingungen die bekannte Perowskit-artige Verbindung $(NH_4)[NiCl_3]$ gefunden, wohingegen bei Zugabe von Base die Verbindung $[Ni(C_4N_3H_8)(C_4N_3H_9)]Cl$ entsteht. In Abwesenheit von Ni^{2+} wird bei der Reaktion von $PbCl_2$ unter gleichen Reaktionsbedigungen $[Pb(C_4H_8N_2)_2(\mu\text{-}Cl)_2]_n$ als Reaktionsprodukt beschrieben. Alle Verbindungen werden bezüglich ihres Oxidationszustandes und der Landungsverteilung anhand der Kristallstruktur und quantenchemischer Rechnungen diskutiert. Reaktionsschemata für die Oligomerisierung von Acetonitril werden präsentiert.

Zur *in-situ*-Reduktion zur Darstellung von Metallaten wird Cobaltocen getestet und eine Reaktion mit Acetonitril unter C–C Knüpfung vorgestellt.

Eigener Anteil: Alle Experimente wurden von mir konzipiert. Die Aufnahme und Auswertung der analytischen und quantenchemischen Daten wurde von mir durchgeführt. Experimentelle Arbeiten wurden teilweise von Thomas Krüger, Marcus Müller und Lukas Trombach im Rahmen einer Vertiefung unter meiner Anleitung durchgeführt. Das Manuskript wurde von Stefanie Dehnen und mir zusammen verfasst.

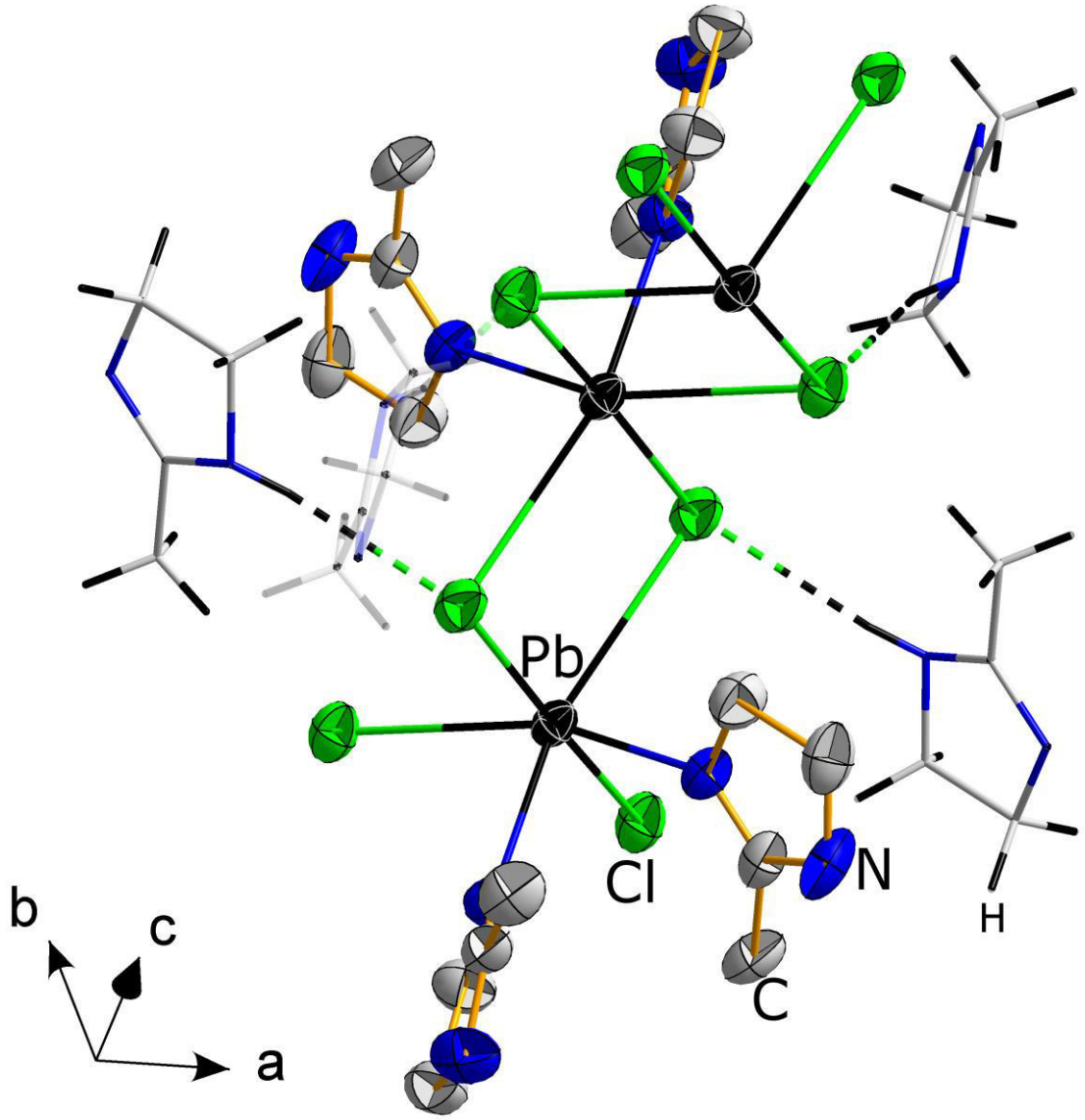

Abbildung 27. Ausschnitt aus der Kristallstruktur von $[Pb(C_4H_8N_2)_2(\mu\text{-}Cl)_2]_n$.

Journal Name

RSCPublishing

COMMUNICATION

Reactions In and With Acetonitrile

Cite this: DOI: 10.1039/xoxxoooooox

Günther Thiele and Stefanie Dehnen

Received ooth January 2012,
Accepted ooth January 2012

DOI: 10.1039/xoxxoooooox

www.rsc.org/

Solvothermal reactions and *in situ* reductions in acetonitrile yield a variety of new metal salts and organometallic compounds including ligands of dimers and tetramers of acetonitrile upon oxidative C–C and/or C–N bond formation and its specific decomposition.

Acetonitrile is an extensively used solvent both in common organic chemistry and inorganic chemistry, due to its favorable solvation parameters. Besides, it has also been investigated as synthon for hydrogenation of cyclization processes. Especially considering the hydration, various catalysts have been exploited, ranging from homogenous Os[1] or Ru[2] compounds to heterogeneous Au[3] or Pd[4] systems. Cyclization of acetonitrile into pyrimidine has been reported applying mesoporous carbon nitride[5] or SmI_2[6] as catalysts. In contrast, the usage of acetonitrile or more complex organic nitriles in solvothermal reactions, that is under elevated temperature and pressure, has been applied only rarely: in most cases, such reactions included the nitriles as ligands[7,8] or reactands towards carboxylic acids,[9] oxadiazole,[10] hydrazines,[11] azides or ammonia.[12] A dimerization towards imidazole or a corresponding tetramerization has not been reported to date.

Our current interests include the extraction of ternary phases of the general type $A_xM^{MG}_yCh_z$ (M^{MG} = main group (heavy) metal, Ch = S, Se, Te) in the presence of transition metal (M^{TM}) salts under solvothermal conditions, with the purpose to use these for the generation and further reactions of multinary, isolated or extended metalate anions.[13] For this, we are exploring the behavior of various solvents. In contrast to the syntheses and reactions of binary and multinary gallates, indates,[14] germanates and stannates,[15] these syntheses of metalates of the heavy main group elements cannot be performed in alcoholic solvents that are too reactive and only afford decomposition into undefined powders. Amines have extendedly been used,[16] but usually take place in sequestration reactions to form $[M^{TM}(amine)_x]^{q+}$ cations[17] or adducts of the latter with the binary metalate substructures. In order to explore the influence of another solvent on the course of the reactions and their product spectra in the supercritical treatment of chalcogenidometalates, we have been using acetonitrile in according solvothermal reactions – and obtained quite unexpected side products, which we would like to report about herein.

In a typical solvothermal synthesis, we apply 500 mg of a ternary phase such as “KPbTe”, 1 equivalent of a (transition) metal salt per main group metal atom, and 2 mL of the chosen

solvent. All is combined under inert gas conditions in a glass vial within a Teflon vessel, which is then placed in a stainless steel autoclave. The latter is tightly closed, heated for one week at 150°C, and then allowed to cool down to room temperature within one day.

Instead of the originally targeted multinary metalates, in a reaction of "KPbTe" with $NiCl_2$ we obtained the acetonitrile tetramer, as a ligand to the dinuclear Ni complex, $[(C_8H_{12}N_4)NiCl(\mu\text{-}Cl)]_2$ (**1**; Figure 1).

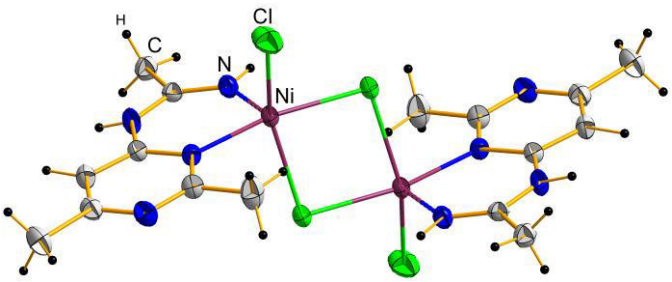

Figure 1. Molecular structure of the dinuclear complex in **1**. Ellipsoids are drawn at 50% probability, H atoms are omitted for clarity. Selected structural parameters [Å,°]: Ni–N 1.955(2)-2.052(2), Ni–Cl 2.2984(8), Ni–μ-Cl 2.4032(7)-2.4266(8), N—Ni—N 91.34(9), Ni—μ-Cl—Ni 97.31(2), Cl—Ni—μ-Cl 92.69(3).

In **1**, one tetrameric ligand each coordinates to a Ni ion (fomally Ni^{3+}) *via* one of the pyrimidine N atoms and one NH^{θ} group of the anionic $CH_3C(NH^{\theta})=N$ substituent, beside a terminal Cl^- ligand. Another Cl^- ligands per subunit acts as μ-bridge to form the dinuclear complex, which comprises five-coordinated Ni atoms. Similar dinuclear and five-coordinated Ni complexes have been discussed for their unusual coordination geometry[19] as well as for catalytic properties[20] and magnetism.[21] However, very small yields so far prevented further investigation into these directions in the case of **1**. Still, the product exhibits an excellent crystallinity, the new synthesis is straight forward and does not require high temperatures; nevertheless, the synthesis is still being optimized to overcome the quoted drawbacks.

The oligomerization reaction is atom-neutral; while one of the methyl groups was integrated as CH moiety into the pyrimidine cycle, two of its H atoms have been transferred to the NH_2 group of the $CH_3C(NH_2)=N$ group attached to the pyrimidine ring (Scheme 1).

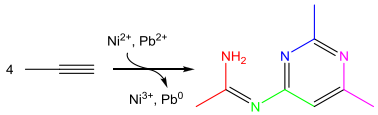

Scheme 1. Suggested reaction scheme for the tetramerization of acetonitrile in the presence of "KPbTe" during formation of compound **1**. The different CCN moieties from originally separate CH_3CN molecules are discriminated by different colors in the product.

We assume that oxidized lead atoms (formally Pb^{2+}) from the ternary phase "KPbTe" to have acted as sacrificial oxidant for the oxidation of Ni atoms under formation of elemental lead. Te^{2-} anions and in situ formed $(HTe)^-$ might have acted as base to care for the transfer of protons that did not reductively couple to form H_2. To confirm the necessity of the presence of "KPbTe", we performed corresponding solvothermal reaction of only $NiCl_2$ in CH_3CN, which almost quantitatively yielded, single crystalline $(NH_4)[NiCl_3]$ with perovskite structure, which has been obtained previously in a much more drastic conditions (400°C, 1 kbar).[22] Assumedly, the Ni complex has catalyzed the decomposition of acetonitrile to form the ammonium counterion.

To check the influence of the pH value on the reaction, we used $NiCl_2{\cdot}6H_2O$ without drying by (acidic) $SOCl_2$. However, this did not lead to the formation of crystalline products. We therefore added 1 equivalent of LiOH to the dried $NiCl_2$. Under these conditions, another product, $[Ni(C_4N_3H_8)(C_4N_3H_9)]Cl$ (**2**; Figure 2) was obtained in approx. 15% yield. Here, a dimerization of the solvent took place under inclusion of another N atom – again gained upon cleavage of acetonitrile, however not yielding $(NH_4)^+$ under these basic conditions (Scheme 2). Additionally, (partial) deprotonation was observed, producing the monoanionic ligand $HN=C(CH_3)–N=C(CH_3)=NH^{\theta}$, similar to a corresponding reaction involving Cr(III) at 200°C.[23]

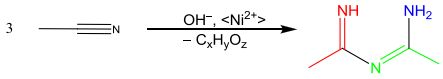

Scheme 2. Suggested reaction scheme for the formation of the $C_4N_3H_{10}$ ligand from acetonitrile in the presence of "KPbTe" during formation of compound **2**. The different CCN moieties from originally separate CH_3CN molecules are discriminated by different colors in the product. Before formation of the complex in **2**, the ligand underwent partial deprotonation. The identity of the organic byproduct could not be elucidated so far as is forms a solid, insoluble residue that points to the formation of a polymer.

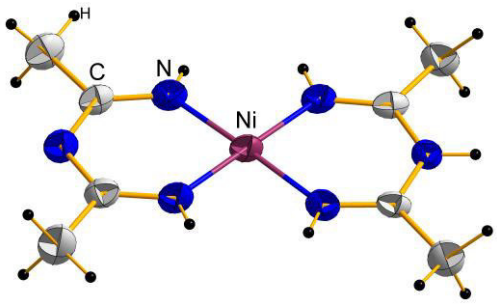

Figure 2. Molecular structure of the complex cation in **2**. Ellipsoids are drawn at 50% probability, H atoms are omitted for clarity. Selected structural parameters [Å,°]: Ni–N 1.832(4)-1.875(4), N—Ni—N 88.9(2)-90.4(2).

Again, Ni^{2+} ions beside a base (here $(OH)^-$) have caused oligomerization of acetonitrile. Within **2** an asymmetric protonation of the two ligands appears uncommon, yet quantum chemical calculation with and without partial protonation – and thereby comparing Ni^{II} versus Ni^{III} – only yields the asymmetry of the different bond lengths (see SI) that is found within the crystal structure for a Ni^{2+} compound. Corresponding bond lengths for Ni^{3+} are almost completely shorter than has been determined which – for DFT – supports our assumption of a wrong oxidation state. Furthermore, within the crystal structure only one H atom at the non-coordination N can be assigned via the electron density and a resulting hydrogen bond towards the Cl– counterion (H...Cl 2.37 Å) can only be formed on one side of the complex.

To get further insight in the potential role of Pb^{2+} ions during the original synthesis of **1**, we performed a similar reaction with only $PbCl_2$ instead of $NiCl_2$ that yielded the acetonitrile dimer imidazole, which coordinated to Pb^{2+} ions in the crystalline product of this reaction, $[Pb(C_4H_8N_2)_2(\mu\text{-}Cl)_2]_n$ (**3**; Figure 3) in approximately 40% yield. In **3**, the lead atoms achieve a distorted octahedral coordination environment through coordination by two imidazole molecules and four chloride ions each. The octahedra are edge-bridging *via* two chloride ions, thereby forming a coordination polymer along the crystallographic *c* axis.

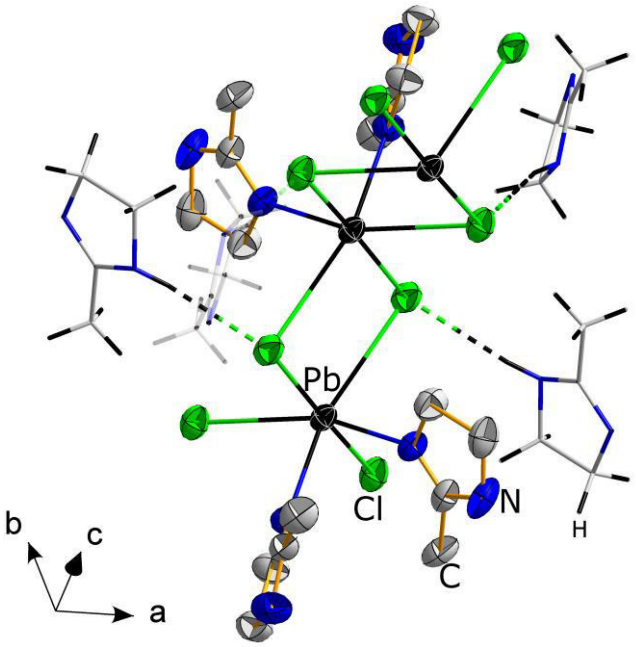

Figure 3. Fragment of one of the coordination polymer strands in **3**. Ellipsoids are drawn at 50% probability, H atoms on Pb-coordinating imidazole ligands are omitted for clarity. Imidazole molecules that are connected via H-bridges are drawn in wire/stick mode. Selected structural parameters [Å,°]: Pb—N 2.470(6), Pb—Cl 2.892(2), N—Pb—N 81.1(3), N—Pb—Cl 89.85(15)-94.78(15), Cl—Pb—Cl 173.91(7).

The formation of **3** suggests that the lead atoms do not only act as oxidatant to Ni ions, but also trigger the C–C and C–N bond formations that come along with the observed oligomerizations. Hence, Ni atoms are only welcome central atoms for the formation of relatively stable coordination compounds and do not seem to b necessary for the organic reactions themselves.

To finally elucidate the impact of chalcogenide anions on the original reaction to form **1**, we investigated the treatment of $NiCl_2$ in acetonitrile in the presence of A_2Ch (A = Li, Na, K; Ch = S, Se, Te) under the same solvothermal reactions. However, no crystalline product could be obtained upon corresponding reactions so far, again indicating the obvious necessity of the metalate phase.

Another attempt for generating metalates that we are currently developing is the *in situ*-reduction of binary metal chalcogenide/chalcogen

mixed phases, such as "PbTe·Te", with elemental alkali metals in room temperature amines. Again, we transferred the corresponding reaction strategy to acetonitrile to test the impact of using another solvent. Since the alkali metals caused immediate decomposition of the solvent, we utilized $CoCp_2$ as a more gentle reduction agent. Upon reflux for 2 days, $[CpCo(C_7H_7N)]$ (**4**; Figure 4) was obtained in approximately 35% yield.

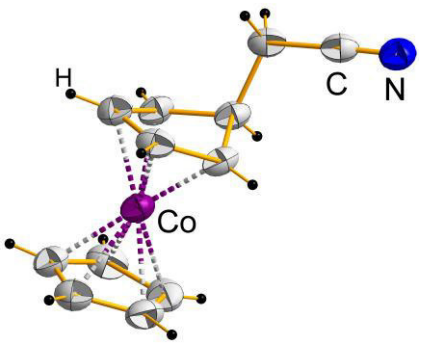

Figure 4. Molecular structure of **4**. Ellipsoids are drawn at 50% probability. Selected structural parameters [Å]: Co—C 1.970(4)-2.098(4), C—N 1.155(5).

Under the given conditions, an oxidative C–C coupling reaction was observed that led to a functionalization of one of the Cp rings under formation of a cyclopentadiene (C_5H_5R) derivative. Since H_2 generation was not observed during the reaction, we assume that the role of the "KPbTe" phase was to act as base under formation of $(HTe)^-$. According investigations are underway.

Conclusions

Solvothermal treatment of "KPbTe" with Ni^{2+} or Co^{2+} compounds in acetonitrile as both solvent and synthon yielded heterocyclic acetonitrile oligomers and derivatives that act as ligands to new coordination compounds **1**, **2**, **3**, and **4**. Apparently, the nature of the very metal cations, which undergo redox side reactions, and/or chalcogenide anions, as well as the presence of OH^- present during the reaction is proposed to be responsible for the very type of heterocycle formed under the given conditions. Additionally, the reactions afforded a simple method for preparing the perovskite-type $(NH_4)[NiCl_3]$ with high crystallinity and yields, and the synthesis of a nitrile functionalized cobaltocene complex.

Notes and references

Philipps-Universität Marburg, Fachbereich Chemie and Wissenschaftliches Zentrum für Materialwissenschaften (WZMW), Hans-Meerwein-Straße 1, 35043 Marburg.

Financial support from Deutsche Forschungsgemeinschaft (SPP 1415) and Friedrich-Ebert-Stiftung (FES) are gratefully acknowledged. We thank T. Krüger, M. Müller and L. Trombach for preparative support in preliminary studies.

† Crystal structure and refinement details: $[(C_8H_{12}N_4)_2Ni_2Cl_4]$ (**1**): $P2_1/c$, a = 8.3432(11) Å, b = 10.6886(16) Å, c = 13.128(2) Å, β = 101.468(11)°, V = 1147.3(3) Å³, final $R_1(I>3\sigma)$ = 0.036, wR_2(all) = 0.096, GooF = 1.068. $[Ni(C_4N_3H_8)(C_4N_3H_9)]Cl$ (**2**): P21/n, a = 8.8236(12) Å, b = 13.881(3) Å, c = 10.2611(16) Å, β = 91.900(12)°, V = 1256.1(4) Å³, final $R_1(I>3\sigma)$ = 0.048, wR_2(all) = 0.084, GooF = 0.943. $(C_4H_8N_2)_2PbCl_2$ (**3**): $C2/c$, a = 13.246(2) Å, b = 12.119(2) Å, c = 8.1684(13) Å, V = 1295.7(4) Å³, final $R_1(I>3\sigma)$ = 0.033, wR_2(all) = 0.079, GooF = 1.046. $C_{12}H_{12}CoN$ (**4**): $P2_1/c$, a = 12.6373(13) Å, b = 7.4477(7) Å, c = 11.0658(10) Å, β = 106.189(8)°, V = 1000.20(17) Å³, final $R_1(I>3\sigma)$ = 0.041, wR_2(all) = 0.0957, GooF = 0.846.

Electronic Supplementary Information (ESI) available: Crystal structure refinement, results from energy dispersive X-ray spectroscopy and details on syntheses and all experimental methods. See DOI: 10.1039/c000000x/

1 M. L. Buil, V. Cadierno, M. A. Esteruelas, J. Gimeno, G. Herrero, S. Izquierdo, E. Oñate, *Organometallics*, 2012, **31**, 6861.
2 R. García-Álvarez, M. Zablocka, P. Crochet, C. Duhayon, J.-P. Majoral, V. Cadierno, *Green Chem*., 2013, **15**, 2447.
3 Y.-M. Liu, L. He, M.M. Wang, Y. Cao, H.-Y. He, K.-N. Fan, *ChemSusChem*, 2012, **5**, 1392.
4 K.-i. Shimizu, T. Kubo, A. Satsuma, T. Kamachi, K. Yoshizawa, *ACS Catal.*, 2012, **2**, 2467.
5 F. Goettmann, A. Fischer, M. Antonietti, A. Thomas, *New. J. Chem*., 2007, **31**, 1455.
6 F. Xu, J.-H. Sun, H.-B. Yan, Q. Shen, *Syn. Commun*., 2000, **30**, 1017.
7 C. D.Molek, J. A. Halfen, J. C Loe, R. W. McGaff, *Chem. Commun.*, 2001, **24**, 2644.
8 M. R. Razali, A. Urbatsch, G. B. Deacon, S. R. Batten, *Polyhedron,* 2013, **64**, 352.
9 K. M. L: Rai, M. S. Babu, K. Byrappa, *Asian J. Chem.*, 2012, **24**, 1395.
10 Y. Djebli, S. Mosbah, S. Boufas, L. Bencharif, T. Roisnel, *Acta Crystallogr., Sect. E*, 2010, **66**, m410.
11 L. Cheng, W.-X. Zhang, B.-H. Ye, J.-B. Lin, X.-M. Chen, *Inorg. Chem*. 2007, **46**, 1135.
12 X.-M. Chen, M.-L. Tong, *Acc. Chem. Res.* 2007, **40**, 162.
13 Z. H. Fard, R. Clérac, S. Dehnen, *Chem. Eur. J.,* 2010, **16**, 2050.
14 indate, gallate (Johanna?)
15 germanate, stannate…
16 W. S. Sheldrick, M. Wachhold, *Angew. Chem. Int. Ed. Engl.* 1997, **36**, 206; G. Thiele, T. Krüger, S. Dehnen, *Angew. Chem. Int. Ed.* 2014, **53**, 4699.
17 G. Thiele, S. Santner, C. Donsbach, M. Assmann, M. Müller, S. Dehnen, *Z. Kristallogr*. 2014, in the print; G. Thiele, L. Vondung, C. Donsbach, S. Krisch, S. Pulz, S. Dehnen, *manuscript in preparation*.
18 J. Pietikäinen, A. Maaninen, R. S. Laitinen, R. Oilunkaniemi, J. Valkonen*, Polyhedron*, 2002, **21**, 1089.

19 G. J. Long, E. O. Schlemper, *Inorg. Chem.* 1974, **13**, 279.
20 A. O. Eseola, M. Zhang, J.-F. Xiang, W. Zuo, Y. Li, J. A. O. Woods, W.-H. Sun, *Inorg. Chim. Acta*, 2010, **363**, 1970; R. Gao, L. Xiao, X. Hao, W.-H. Sun, F. Wang, *Dalton Trans*., 2008, 5645.
21 G. A. v. Albada, J. J. A. Kolnaar, W. J. J. Smeets, A. L. Spek, J. Reedijk, *Eur. J. Inorg. Chem*. 1998, 1337.
22 H. T. Witteveen, J. A. R. v. Veen, *J. Phys. Chem. Solids*, 1974, **35**, 337.
23 L. J. Batchelor, M. Sander, F. Tuna, M. Helliwell, F. Moro, J. v. Slageren, E. Burzurí, O. Montero, M. Evangelisti, F. Luis, E. J. L. McInnes, *Dalton Tran*. 2011, **40**, 5278.

Journal Name

RSCPublishing

COMMUNICATION

Reactions In and With Acetonitrile

Günther Thiele and Stefanie Dehnen

Fachbereich Chemie, Wissenschaftliches Zentrum für Materialwissenschaften, Philipps-Universität Marburg, Hans-Meerwein-Straße, D-35043 Marburg, Germany, email: dehnen@chemie.uni-marburg.de

SUPPLEMENTARY INFORMATION

Contents:

Synthesis details

General: All synthesis steps were performed with strict exclusion of air and moisture. Acetonitrile was dried with CaH_2 and freshly distilled prior to use. "KPbTe" and "PbTe·Te" was generated by fusion of the elements in a 1:1:1 and 1:2 ratio in a quartz ampule using an oxygen/butane. $NiCl_2$ was generated from $NiCl_2 \cdot 6H_2O$ in excess $SOCl_2$ reflux for 5 h, subsequent filtration and dynamic vacuum for 12 h at $p < 1 \cdot 10^{-6}$ bar. All other salts were dried at a dynamic vacuum for 12 h at $p < 1 \cdot 10^{-6}$ bar and subsequent store in a Ar operating glovebox.

Standard procedure for solvothermal treatment will place all reagents in a glass within a Teflon vessel, which is then placed in a stainless steel autoclave. The latter is tightly closed, heated for one week at 150°C, and then allowed to cool down to room temperature within one day. Products can manually be picked.

Synthesis of $[(C_8H_{12}N_4)_2Ni_2Cl_4]$ (1):

0.5 g (1.37 mmol, 1 eq) of "KPbTe", 175 mg (1.38 mmol, 1.1 eq) of $NiCl_2$ and 2 mL of acetonitrile were treated according to the solvothermal method, yielding orange-green blocks.

Synthesis of $[Ni(C_4N_3H_8)(C_4N_3H_9)]Cl$ (2):

500 mg (3.85 mmol) of $NiCl_2$, 150 mg (6.27 mmol) of LiOH and 2 mL of acetonitrile were treated according to the solvothermal method, yielding yellow blocks in ~ 15% yield.

Synthesis of $(C_4H_8N_2)_2PbCl_2$ (3):

500 mg (1.80 mmol) of $PbCl_2$ and 2 mL of acetonitrile were treated according to the solvothermal method, yielding colorless blocks in ~ 40% yield.

Synthesis of $[(C_5H_5)(C_7H_7N)Co]$ (4):

500 mg (1.08 mmol, 1 eq) of "PbTe·Te", 410 mg (2.17 mmol, 2 eq) of $CoCp_2$ and 100 mL of acetonitrile were heated at reflux for 5 h. The resulting reaction mixture was filtered and slowly evaporated until only a small residue of approx.. 5 mL solvent was still present. 4 crystallizes as brown sticks in ~ 35% yield.

Single crystal X-ray diffraction

General: Data of the X-ray structure analysis: T = 293 K (**1-3**) or 293 K (**4**), graphite monochromator, imaging plate detector Stoe IPDS (**1-3**) or IPDS2 (**4**). All structures were solves by direct methods in WinGX[1] and OLEX2[2] refined by fullfull-matrix least-squares refinement against F2 in SHELXL-2013.[3] Absorption correction were performed numerically including shape optimization with STOE X-AREA.[4] Table S1 summarizes the crystallographic data of all crystalline compounds. CCDC XXX - XXX contain the supplementary crystallographic data for this paper. These data can be obtained free of charge from The Cambridge Crystallographic Data Centre via www.ccdc.cam.ac.uk/data_request/cif.

Tabel S1: Crystallographic and refinement details for Compounds **1** – **4**.

Compound	**$[(C_8H_{12}N_4)_2Ni_2Cl_4]$ (1)**	**$[Ni(C_4N_3H_8)(C_4N_3H_9)]Cl$ (2)**	**$(C_4H_8N_2)_2PbCl_2$ (3)**	**$[(C_5H_5)(C_7H_7N)Co]$ (4)**
Empirical formula	$C_{16}H_{24}C_{l4}N_8Ni_2$	$C_8H_{17}ClN_6Ni$	$C_8H_{16}C_{l2}N_4Pb$	$C_{12}H_{12}CoN$
Formula weight /g·mol^{-1}	587.65	291.43	446.34	229.16
Crystal color and shape	Orange-green block	Yellow block	Colorless block	Brown stick
Crystal size /mm	0.25·0.22·0.19	0.12·0.11·0.08	0.32·0.25·0.21	0.20·0.13·0.09
Crystal system	Monoclinic	Monoclinic	Monoclinic	Monoclinic
Space group	$P2_1/c$	$P2_1/n$	$C2/c$	$P2_1/c$
a/Å	8.3432(11)	8.8236(12)	13.246(2)	12.6373(13)
b/Å	10.6886(16)	13.881(3)	12.119(2)	7.4477(7)
c/Å	13.128(2)	10.2611(16)	8.1684(13)	11.0658(10)
β/°	101.468(11)	91.900(12)	98.831(13)	106.189(8)
V/Å^3	1147.3(3)	1256.1(4)	1295.7(4)	1000.20(17)
Z	2	4	4	4
ρ_{calc}/g·cm^{-3}	1.701	1.541	2.278	1.522
μ($Mo_{K\alpha}$) /mm^{-1}	2.128	1.741	13.409	1.67
2Θ range/°	4.9-50.8	4.9-50.9	4.6-50.8	3.3-53.4
Abs. corr. T_{min}/T_{max}	0.6637 / 0.7831	0.6683 / 0.8130	0.0141 / 0.0660	0.6368 / 0.8903
Reflections measured	10427	11678	5686	5148
Independent reflections	2104	2238	1127	2099
R(int)	0.0407	0.0838	0.035	0.0694
Indep. Reflections (I>2σ(I))	1884	1458	1064	1378
Parameters	160	165	74	175
R_1(I>2σ(I))	0.0358	0.0478	0.0329	0.0405
*wR*2 (all data)	0.0958	0.0749	0.0787	0.0957
Goof (all data)	1.068	0.943	1.046	0.846
Max. peak/hole /e$^-$·10^{-6}pm^{-3}	0.103 / -0.876	0.071 / -0.261	1.182 / -1.275	0.071 / -0.397

Energy dispersive X-Ray spectroscopy

EDX analyses were carried out using an EDX-device Voyager 4.0 of Noran Instruments coupled with an electron microscope CamScan CS 4DV. Data acquisition was performed with an acceleration voltage of 20 kV and 100 s accumulation time. Differences in observed and calculated atomic composition is caused by inhomogenous decomposition of applied single crystals due to contact with air and moisture during sample preparation.

Table xx. EDX results for 2.

Element	k-ratio (calc.)	ZAF	Atom %	Element Wt %	Wt % Err. (1-Sigma)
Cl-K	0.6060	1.138	78.62	68.95	+/- 0.96
Ni-K	0.2876	1.080	21.38	31.05	+/- 1.64
Total			100	100	

Quantum chemical calculations

General: DFT calculations were done with the program RIDFT[5] implemented in the program system TURBOMOLE[6] employing the Becke–Perdew 86 (BP86) functional[7] with def2-TZVP bases[8] and respective fitting bases[9] for the evaluation of the Coulomb matrix. Counter ions were modelled by COSMO with default parameters.[10]

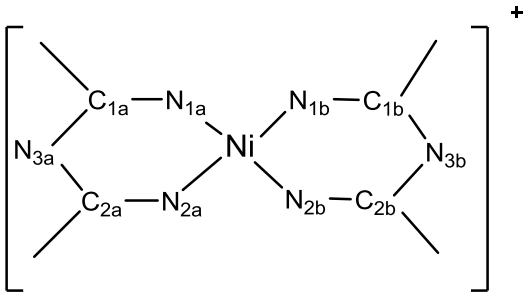

Fig. S2: Labelling scheme for optimizes compounds. N3b has one H atom attached (protonated) or no H atom (deprotonated).

Starting from the crystal structure as determined experimentally the monocation in 2 (see Fig. S2) has been optimized to minimize external forces, resulting in a minimum structure. While one calculation has been done with two symmetric ligands that are both deprotonated at N3 (therefore Ni3+) a cooresponding calculated started from an asymmetric deprotonation of the ligands (N(3a) deprotonated, N(3b) protonated, therefore Ni^{2+}). The resulting bond length and those from X-ray diffraction results are summarized in table S3. Applied symmetry: C_1.

Table S3: Comparision of calculated and determined bond length in the cation in 2. All values in Å.

	X-ray results		Protonated N(3b)		Deprotonated	
	a	b	a	b	a	b
Ni…N1	1.843(4)	1.875(4)	1.850	1.871	1.838	1.839
Ni…N2	1.843(4)	1.857(4)	1.850	1.871	1.839	1.838
N3—C1	1.349(5)	1.361(5)	1.347	1.374	1.345	1.345
N3—C2	1.338(5)	1.370(5)	1.347	1.374	1.345	1.345

References

[1] Louis J. Farrugia, *WinGX for MS-Windows V2013-3*, University of Glasgow, United Kingdom, **2013**.

[2] O. V. Dolomanov, L. J. Bourhis, R. J. Gildea, J. A. K. Howard, H. Puschmann*, Appl. Cryst.* 2009, **42**, 339.

[3] G. M. Sheldrick, *SHELXL-2013*, University of Göttingen, Germany, **2013**.

[4] *X-AREA version 1.56*, Stoe & Cie GmbH, Darmstadt, Germany, **2011**.

[5] K. Eichkorn, O. Treutler, H. Oehm, M. Haeser, R. Ahlrichs, *Chem. Phys. Lett.* 1995, ***242***, 652.

[6] *TURBOMOLE Version 6.4*, (c) TURBOMOLE GmbH 2012. TURBOMOLE is a development of University of Karlsruhe and Forschungszentrum Karlsruhe 1989-2007, TURBOMOLE GmbH since 2007.

[7] A. D. Becke, *Phys. Rev. A* 1988, **38**, 3098; J. P. Perdew, *Phys. Rev. B*, 1996, **33**, 8822.

[8] F. Weigend, R. Ahlrichs, *Phys. Chem. Chem. Phys.* 2005, ***7***, 3297.

[9] F. Weigend, *Phys. Chem. Chem. Phys.* 2006, **8,** 1057.

[10] A. Klamt; G. Schürmann *J. Chem. Soc. Perkin Trans.* 1993, **2**, 799.

VIII

$K_2Hg_2Se_3$: A Novel Selenidomercurate(II) for Photothermoelectric Applications

Günther Thiele, Sina Lippert, Philipp Bron, Felix Fahrenbauer, Maik Assmann, Phil Rosenow, Ralf Tonner, Oliver Oeckler, Arash Rahimi-Iman, Martin Koch, Bernhard Roling, Stefanie Dehnen, *Manuskript in Vorbereitung.*

$K_2Hg_2Se_3$ has been obtained in quantitative yields by means of solvothermal extraction of the corresponding parental alloy and analyzed for its photoelectric, electrochemical and thermoelectric properties.

Themenkomplex Solvothermalsynthese von Plumbaten und Merkuraten

Inhalt: Die Synthese von $K_2Hg_2Se_3$ durch solvothermale Behandlung einer festen Mischung gleicher Zusammensetzung wird zusammen mit der Kristallstruktur des Produktes beschrieben. Impedanzspektroskopische Messungen werden bezüglich ionischer und elektrischer Leitfähigkeit diskutiert, die Photoleitfähigkeiten bei Raumtemperatur und erhöhter Temperatur angegeben und auf Basis der berechneten Bandstruktur erörtert.

Eigener Anteil: Alle Experimente zur Synthese wurden von mir konzipiert. Die experimentellen Arbeiten wurden in Teilen von Maik Assmann, Marcus Müller und Thomas Krüger unter meiner Anleitung durchgeführt. Alle Einkristallstrukturdaten und UV-Vis-Spektren wurden von mir aufgenommen und ausgewertet. EDX-Spektren wurden unter meiner Anleitung von Thomas Krüger aufgenommen und von mir ausgewertet. Pulverdiffraktogramme wurden unter meiner Anleitung von Marcus Müller aufgenommen und von mir ausgewertet. Die thermogravimetrische Analyse wurde von Uwe Justus durchgeführt, impedanzspektroskopischen Untersuchungen wurden von Philipp Bron durchgeführt und zusammen mit Bernhard Roling ausgewertet. Die thermoelektrischen Messungen wurden von Felix Fahrenbauer durchgeführt und zusammen mit Oliver Oeckler ausgewertet. Alle Experimente zur Photoleitfähigkeit bei Raumtemperatur wurden von Sina Lippert durchgeführt und mit Arash Rahimi-Iman und Martin Koch ausgewertet. Die quantenchemischen Rechnungen wurden von mir unter Mithilfe von Phil Rosenow und Ralf Tonner durchgeführt und von Sina Lippert und Arash Rahimi-Iman ausgewertet. Das Manuskript wird derzeit von Sina Lippert, Philipp Bron, Bernhard Roling, Felix Fahrenbauer, Oliver Oeckler, Arash Rahimi-Iman, Stefanie Dehnen und mir zusammen verfasst.

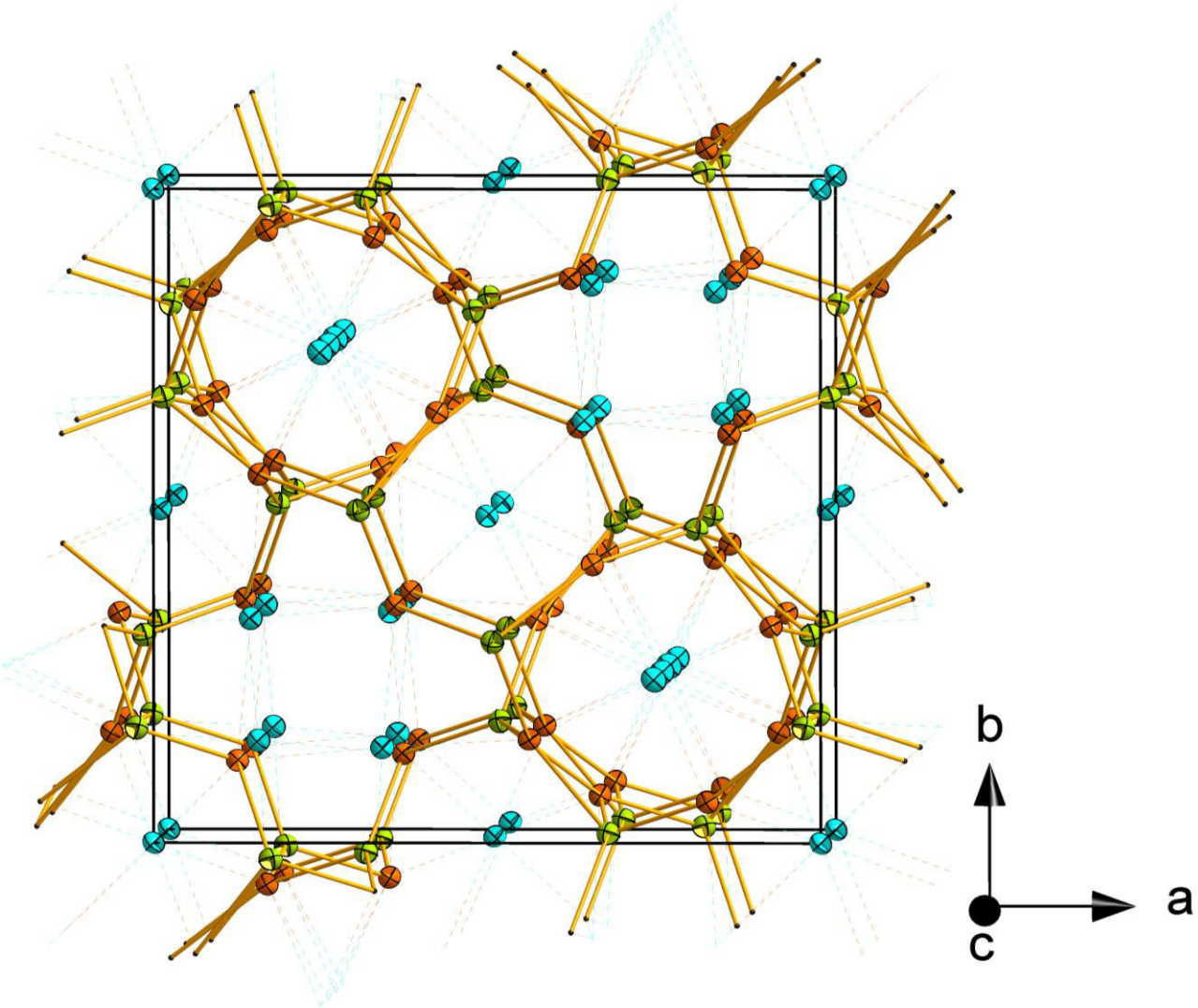

Abbildung 28. Ausschnitt aus der Kristallstruktur von $K_2Hg_2Se_3$.

$K_2Hg_2Se_3$: A novel Selenidomercurate(II) for Photothermoelectric Applications

GüntherThiele[a)], Sina Lippert[b)],FelixFahrnbauer[c)],Philipp Bron[a)], MaikAssmann[a)],Oliver Oeckler[c)], Arash Rahimi-Iman[b)], Martin Koch[b)],Bernhard Roling[a)]and Stefanie Dehnen[a)]*

a) Philipps-Universität Marburg, Fachbereich Chemie and Wissenschaftliches Zentrum für Materialwissenschaften, Hans-Meerwein-Straße, 35043 Marburg, Germany.

b) Philipps-Universität Marburg, Fachbereich Physik and Wissenschaftliches Zentrum für Materialwissenschaften, Renthof 5, 35032 Marburg, Germany.

c) Universität Leipzig, Fakultät für Chemie und Mineralogie, Scharnhorststraße 20, 04275 Leipzig, Germany.

Supporting Information Placeholder

ABSTRACT: $K_2Hg_2Se_3$ has been obtained in quantitative yields by means of solvothermal extraction of the corresponding parental alloy and analyzed for its photoelectric, electrochemical and thermoelectric properties.

The chemistry of mercury is fascinating due to its structural diversity and unique properties, yetneglected for its toxicity.[1,2] But whereas organic compounds of mercury often exhibit high vapor pressures and thus are easily inhaled or absorbed via the skin, most inorganic compounds – especially its salts – are fairly easy to handle if care is taken to avoid contamination of skin or inhalation of dusts. In addition, the combination of Hg and Se is known to be antagonistic at a toxicological significance.[3]

In terms of unique properties and application heavy metal chalcogenides and chalcogenidometallates are discussed for their thermoelectric properties,[4] defined by the figure of merit, $zT = S^2\sigma_{eon}T/\sigma_{th}$ (with the Seebeck coefficient S and the electrical and thermal conductivity σ_{eon} and $\sigma_{th)}$which is known to largely depend – besides structural composition – on particle size and composition for binary and multinary materials.[5]

Isolated binary *ortho*- and *meta*-mercurate anions $[HgCh_4]^{6-}$[6,7](Ch = chalcogen) and $[HgCh_3]^{4-}$[8]as well as linear $[HgCh_2]^{2-}$ and planar $[HgCh_3]^{4-}$ units within $[Hg_2Ch_4]^{4-}$[9]are long known yet most often only been discussed for their structural features.More complex mercurates such as one dimensional (1D) $[Hg_3Ch_4]^{2-}$,[10,11] 3D $[Hg_6Ch_7]^{2-}$ [11-13] and the 1D $[Hg_5Te_{13}]^{4-}$ [14] were reported as wide-band-gap semiconductors or discussed for band gap engineering respectively. However, within the divers structural library of mercurate anions, only multinarymercurates, such as $Tl_2HgGeTe_4$[7] have so far been examined considering their thermoelectric application.

Extending our previous studies on heavy chalcogenidometallates,[15] we examined solvothermal reaction conditions to the K-Hg-Se system. Upon aminothermal reaction of a parental alloy of the same composition $K_2Hg_2Se_3$ (**1**) can be obtained in quantitative yield.

In contrast to a sulfidocadmate with a corresponding stoichiometry $K_2Cd_2S_3$[16] that exhibits two dimensional (2D) layers of $[Cd_2S_3]^{2-}$that are interconnected by potassium ions, **1** exhibits a 3D structure incorporating channels with K^+ ions along the crystallographic*c*-axis (see figure 1).

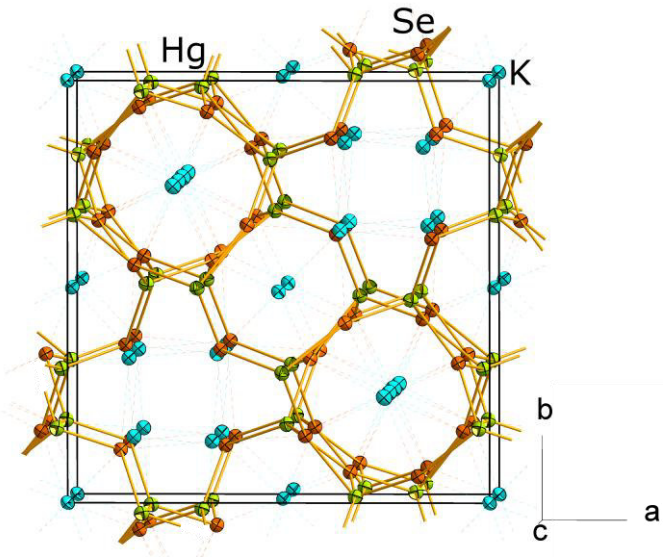

Figure 1: Crystal structure of **1** with representation of channels along the crystallographic *c* axis. Ellipsoids are drawn at 50% probability.

1 crystallizes in tetragonal space group $P4_2/ncm$ with cell constants a = 15.0690(4)Å, c = 7.1060(3)Å. The Hg atom obtains distorted tetrahedral coordination with three Se atoms in close proximity (2.5758(13)-2.6634(12)Å) and one Se atom with an extended Hg—Se bond length of 2.9595(12). Selenium atoms in turn interconnect the $[HgSe_4]$ tetrahedral units to an anionic uninodal net (6-c, 6/3/t30) of the topological type *whp*.[17] The corresponding vertex symbol for the Hg sublattic (point symbol) is {3^3.4^5.5^5.6.7}. Potassium ions are located within the three different anionic channels with distorted octahedral or square antiprismatic coordination by Se atoms (see fig. 2).

Thermogravimetric analysis and diffential scanning calometry suggest a thermal stability of **1** up to 387.4 °C without alteration of the structure. With an onset of 430 °C an overall mass change of -54.54% is observed (see SI1). UV-visible spectroscopy reveals the onset of absorption E_{onset} = 2.0 eV (see SI2).

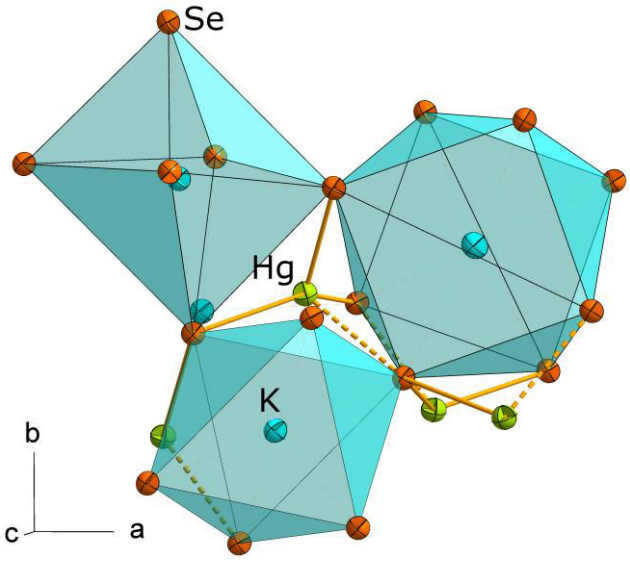

Figure 2: Coordinationpolyhedra of K^+ ions and tetrahedral [$HgSe_4$] unit with the elongated bond drawn with fragmentation. Ellipsoids are drawn at 50% probability.

Impedance spectroscopy

Charge transport in $K_2Hg_2Se_3$ may take place via electronic charge carriers and/or via mobile K^+ ions. Ion transport is generally not desirable for many semiconductor applications, since it can result in changes in the properties of junctions as well as influence the concentration of traps and other features of the semiconductor microstructure.

On the other hand, mixed conductors with very high ionic conductivity, such as cuprous and silver chalcogenides, exhibit a phonon-liquid electron-crystal (PLEC) behavior with excellent values of zT, as demonstrated for p-type $Cu_{2-x}Se$. This material reaches a value of zT = 1.6 at 1000 K, the highest value among all bulk TE materials.[P1] However, it was also stated, that the 'long-term effect of ionic mobility on the TE properties in these ion conductors should be addressed before commercialization'.[P1]

A simple method for determining electronic and ionic conductivities of mixed conductors is based on impedance spectroscopy using ionically-blocking electrodes. As shown by Jamnik et al., the Nyquist plot of a mixed conductor between ion-blocking electrodes exhibts a high frequency semi-circle followed by either a low-frequency semicircle or a finite-length Warburg impedance, depending on the electronic carrier density.[P2] The diameter of the high-frequency semicircle is identical to the parallel resistance R_{par} of ionic (ion) and electronic (eon) carriers $R_{par} = (R_{ion}^{-1} + R_{eon}^{-1})^{-1}$, whereas the resistance measured in the limit of low frequencies is the electronic resistance.

At high electronic charge carrier concentrations, a Warburg-like low frequency response is observed, which is governed by the electronic resistance and a chemical capacitance C_{chem}, the latter reflecting the storage of chemical energy in the sample due to stoichiometry changes. The chemical capacitance is proportional to the sample thickness L and hence the corresponding relaxation time of the Warburg impedance is proportional to L^2. [P2]

If, on the other hand, the electronic carrier concentration is several orders of magnitude lower than the ionic carrier concentration, the electrostatic energy stored in the ionic double layers is much larger than the chemical energy. In this case, a low-frequency semicircle determined by the electronic resistance and the ionic double layer capacitance is observed. The double layer capacitance C_{el} is independent of the sample thickness. Hence the relaxation time is proportional to L. [P2]

The latter was observed in our case and thus the pictured equivalent circuit on the left-hand side of figure P1 can be used for fitting the impedance spectra, with C_{diel} denoting the dielectric capacitance of the sample. The simplified equivalent circuit on the right-hand side allows to obtain the R_{par} values, if the low frequency semicircle is not completely resolved in the frequency window of the experiment.

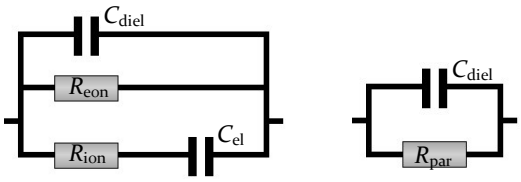

Figure P1: Left: Complete equivalent circuit for fitting the impedance spectra. Right: Simplified circuit for fitting the high-frequency semicircle at temperatures at which the low-frequency semicircle is not fully visible.

In the case of $K_2Hg_2Se_3$, the semicircle are suppressed, and therefore constant-phase elements (CPE) had to be used instead of capacitances. The impedance of a CPE is given by: $Z_{CPE} = Q^{-1} \cdot (i\omega)^{-n}$ with n ≤ 1. The capacitance values C_i were calculated from the parameters R_i, Q_i and n_i according to the Brug formula $C_i = \left(R_i^{1-n_i} \cdot Q_i\right)^{1/n_i}$.[P3] For both equivalent circuits exemplary Nyquist plots comparing the measured data points with the obtained fit values are shown in fig. P2.

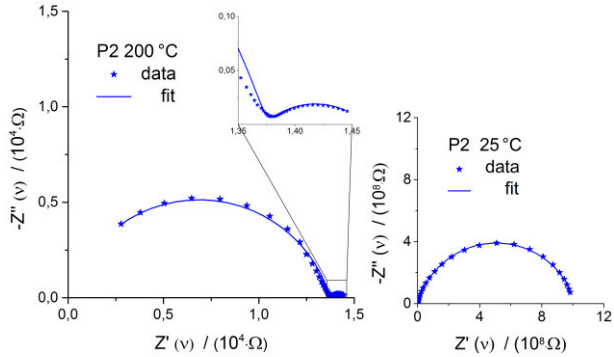

Figure P2: Representative Nyquist plots for pellet 2 at two different temperatures.

The strong dependence of the electronic conductivity on carrier concentration makes materials sensitive to impurities and dopant concentrations. Small inhomogeneities can result in large variations within a sample. Therefore measurements

on three different pellets P1-P3 were performed to determine the reproducibility. Figure P3 and P4 show that all pellets exhibit very similar conductivities. For the parallel conduction of both ions and electrons, the activation energies E_A is around 0.8 eV, and the parallel conductivities amount to 10-20 µS·cm^{-1} at 200 °C (see figure P3). As can be seen in figure P4 the parallel conduction is governed by the electronic conduction, and the ionic contribution is almost negligible. Up to 200 °C the electronic transference number $t_{eon} = R_{ion}/(R_{ion} + R_{eon})$ is well above 0.95. At temperatures above 210 °C, t_e drops slightly below 0.95. This temperature dependence is related to the higher activation energy of the ionic conduction process.

We expect that the tuning of the electron carrier concentration in this novel material class will result in a drastic increase of *zT*. Although the Seebeck coefficient will suffer from an increase in the carrier concentration, the resulting higher electronic conductivity should overcompensate by far the effect on *zT*. The most favorable carrier concentration is typically between 10^{19} and 10^{21} carriers per cm^3 and thus in the range of heavily doped semiconductors. [P4] The shape of the low-frequency semicircle in our impedance spectra reveals that the electronic carrier concentration $K_2Hg_2Se_3$ is several orders of magnitude lower.

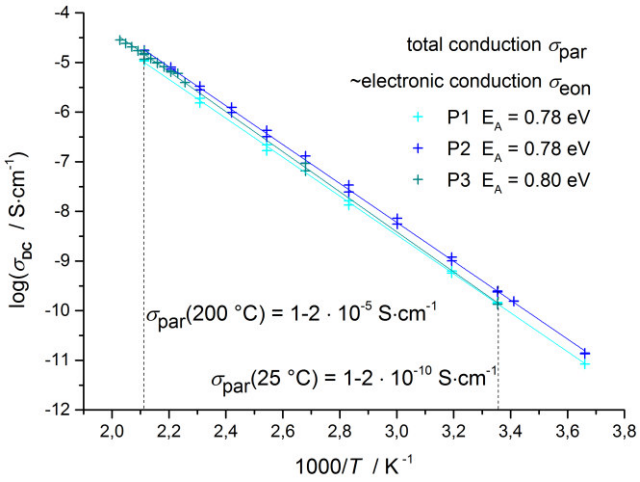

Figure P3: Arrhenius plot of the parallel conductivity σ_{par}.

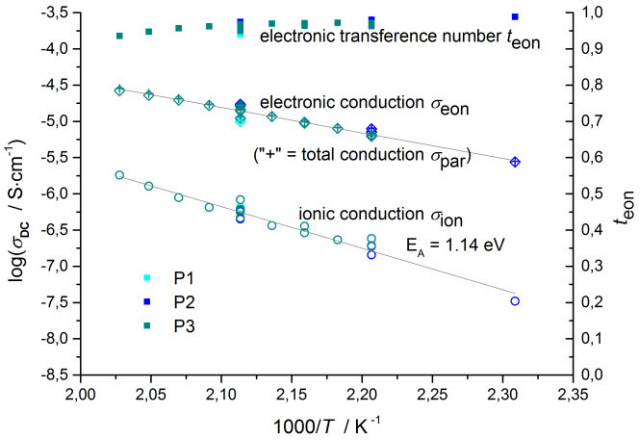

Figure P4: Arrhenius plot for the ionic and electronic conductivity of different pellets as well as the temperature dependence of the electronic transference number.

Wärmeleitung/Seebeckkoeffizienten

Photoleitfähigkeit

In this section, we present photocurrent spectroscopy measurements which allow for the characterization of the photoexcitation wavelength. The setup employed for this experiment is placed in a nitrogen-filled box. The sample is contacted via Tungsten needles with a tip diameter of 5 µm. The detection sensitivity limit lies at 50 fA. Light is shed on the sample from a white-light source via a monochromator (model/type: stanford research SR 850) and the photocurrent scan is performed with a maximum wavelength resolution of 3nm. We detected the current with a lock-in after amplification by a femto-current amplifier (Modell:DLCPA-100).

The measurements were performed at an external voltage of 10 V with a wavelength scan in steps of 10 nm. Two different samples of the investigated structure were probed in order to rule out a sample specific response. The recorded spectrum presented in Fig. xy clearly shows a dominant peak at 890 nm which we attribute to pronounced absorption and a rise in the electrical conductivity induced by photoexcitation. A representative absorption spectrum is presented as inset in Fig. 3. The absorption spectrum clearly shows an edge corresponding to the 'band-gap' energy. Remarkably, the experimental data well agrees with theoretical modeling of the sample's band structure from which the photoexcitation energy can be derived.

Next, we provide current-voltage (I-V) characteristics of $K_2Hg_2Se_3$ in order to compare their electrical properties to semiconductors. As prominent material with direct band gap, GaAs is chosen to provide a representative photo-induced current curve of semiconductor material. The current is measured for both materials, K2Hg2Se3(solid line) and GaAs (dashed line), in a dark environment (dark color line) and under white-light exposure (bright color line), applying maximum voltages of +/-10 V. Thereby, a similar performance of both materials is revealed which is attributed to the semiconductor-like properties of K2Hg2Se3. All curves show a clear Schottky behavior for positive and negative bias voltage. In a dark environment, the conductivity is little, while under light exposure, a significant rise is obtained, as can be seen in Fig. xy. Additionally, light of 890 nm is shed on our novel material system (red thick curve in Fig. xy) which reveals a pronounced modification of the electrical conductivity in the sample compared to an ordinary white-light excitation. In this case, a particularly high amount of charge carriers seems to be injected by resonant excitation. This leads to a situation where K2Hg2Se3 even overcomes the performance of GaAs.

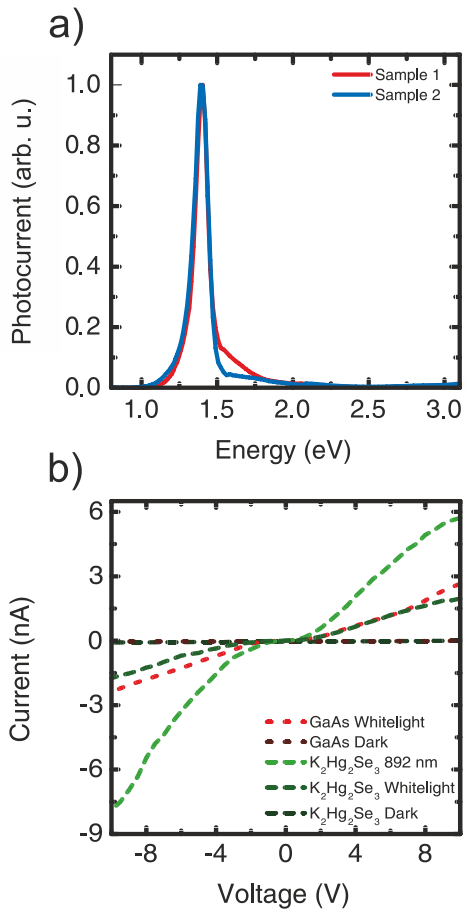

Figure 3. a) Photocurrent spectrum for two different samples of the investigated structure. The spectrum shows a dominant peak at 1.39 eV. b) Current-Voltage characteristic of $K_2Hg_2Se_3$ (red) and GaAs (green). Both materials are measured in a dark environment and under whitelight exposure. Additional, $K_2Hg_2Se_3$ is measured with light of 892 nm.

We attribute the small asymmetry observed in the measur#ed *I-V*-curves to the individual contacts established between the sample and the contact needles: Since these contacts are of Schottky type, a minor difference in the contact quality at each junction leads to a change in the current with respect to its direction.

Experimental Section

All experimental steps were performed with strong exclusion of air and moisture. Ethan-1,2-diamine was dried and freshly destilled prior to use. Elements were purchased from Sigma Aldrich (>98%) and used as received. K_2Se was synthezised from the elements in liquid ammonia, HgSe from fusion of the elements.

A parental alloy of the nominal composition "$K_2Hg_2Se_3$" was obtained from fusion of K_2Se and HgSe in a 1:2 ratio with a oxygen/methane burner. The resulting block was pestled and transferred into a glass vial with 2 mL ethane-1,2-diamine. The vial was placed in a Teflon Inlay within a stainless steel autoclave. The autoclave is tightly closed and heated to 150°C for 2 days and allowed to cool to room temperature for 1 day. Black sticks of **1**, suitable for single crystal diffraction or photoelectric measurements can manually be picked from the reaction mixture.

Larger quantities of powder samples of **1**can be obtained by subsequent separation of reaction solution and solid product. **1** was washed with ethane-1,2-diamine until no further colored components were dissolved. The reaction can be scaled from 0.5 g to 50 g (which is the limiting volume of the glass vial), yielding up to 94%.

ASSOCIATED CONTENT

Supporting Information

Details on crystallographic data and refinement, energy dispersive X-Ray and thermogravimetric results, impedance, photoelectronic and thermoelectric plots are supplied as Supporting Information. This material is available free of charge via the Internet at http://pubs.acs.org.

AUTHOR INFORMATION

CorrespondingAuthor

Stefanie Dehnen, Philipps-Universität Marburg, Fachbereich Chemie and Wissenschaftliches Zentrum für Materialwissenschaften, Hans-Meerwein-Straße, 35043 Marburg, Germany.

PresentAddresses

b) Philipps-Universität Marburg, Fachbereich Physik and Wissenschaftliches Zentrum für Materialwissenschaften, Renthof 5, 35032 Marburg, Germany.

c) Universität Leipzig, Scharnhorststraße 20, 04275 Leipzig, Germany.

Author Contributions

All authors contributed equally.

Notes

The authors declare no competing financial interests.

ACKNOWLEDGMENT

GT thanks the Friedrich Ebert Stiftung (FES) and the DFG (SPP1415) for financial support.

REFERENCES

[1] For chemical review see e.g. E. C. Constable, *Coord. Chem. Rev.***1984**, *58*, 53-85. M. Melnik, *Cent. Eur. J. Chem.***2010**, *8*, 469-485; M. P. Coles, *Annu. Rep. Prog. Chem., Sect. A***2009**, *105*, 269-275.

[2] For toxicity and pollution review see e.g. E. Steinnes: Heavy Metals in Soilsin*Environmental Pollution*, 3rd Ed. Springer, **2013**, *22*, 411-428.

[3] M. A. K. Khan, F. Wang, *Environ. Toxicol. Chem.***2009**, *28*, 1567-1577.

[4] C. Lee, J. Hong, M.-H. Whangbo, J. H. Shim, *Chem. Mater.***2013**, *25*, 3745-3752;T. Rosenthal, M. Döblinger, P. Wagatha, C. Gold, E.-W. Scheidt, W. Scherer, O. Oeckler, *Z. Anorg. Allg. Chem.***2011**, *637*, 2239-2245; M. A. McGuire, T. K. Reynolds, F. J. DiSalvo, *Chem. Mater.***2005**, *17*, 2875-2884. G. J. Snyder, T. Caillat, J.-P.Fleurial, *Mat. Res. Innovat.***2001**, *5*, 67-73. S. K. Dalafave, *Mat. Lett.***1998**, *37*, 177-181; X. Chem, Y. Wang, T. Cui, Y. Ma, G. Zou, T. Iitaka, *J. Chem. Phys.***2008**, *128*, 194713;

C. R. Sankar, S. Bangarigadu-Sanasy, A. Assoud, H. Kleinke, *J. Mater. Chem.***2010**, *20*, 7485-7490

[5] J. Androulakis, C.-H. Lin, H.-J. Kong, C. Uher, C.-I Wu, T. Hogan, B. A. Cook, T. Caillat, K. M. Paraskevopoulos, M. G. Kanatzidis, *J. Am. Chem. Soc.***2007**, *129*, 9780-9788; J. R. Sootsman, H. Kong, C. Uher, J. J. D'Angelo, C.-I Wu, T. P. Hogan, T. Caillat, M. G. Kanatzidis, *Angew. Chem. Int. Ed.***2008**, *47*, 8618-8622.

[6] H. Sommer, R. Hoppe, *Z. Anorg. Allg. Chem*. **1978**, *443*, 201-211.

[7] M. A. McGuire, T. J. Scheidemantel, J. V. Badding, F. J. DiSalvo, *Chem. Mater.***2005**, *17*, 6186-6191.

[8] H. D. Rad, R. Hoppe, *Z. Anorg. Allg. Chem.***1981**, *483*, 7-17.

[9] H. D. Rad, R. Hoppe, *Z. Anorg, Allg. Chem.***1981**, *483*, 18-25.

[10] S. Johnsen, S. C. Peter, S. L Nguyen, J.-H. Song, H. Jin, A. J. Freemann, M. G. Kanatzidis, *Chem. Mater*. **2011**, *23*, 4375-4383.

[11] E. A. Axtell III, Y. Park, K. Chondroudis, M. G. Kanatzidis, *J. Am. Chem. Soc.***1998**, *120*, 124-136.

[12] M. G. Kanatzidis, Y. Park, *Chem. Mater.***1990**, *2*, 99-101.

[13]D. E. Bugaris, J. I. Ibers, *ActaCrystallogr. Sec. E***2008**, *64*, i55-i56.

[14]X. Chen, X. Huang, J. Li, *Inorg. Chem.***2001**, *40*, 1341-1346.

[15] G. Thiele, K. Krüger, S. Dehnen, *Angew. Chem. Int. Ed.***2014**, *53*, 4699-4703.

[16] E. A. Axtell III, J.-H. Liao, Z. Pikramenou, M. G. Kanatzidis, *Chem. Eur. J.***1996**, *2*, 656-666.

[17]Determination with TOPOS program: V.A. Blatov, *Struct. Chem.***2012**, *23*, 955-963.

[P1] H. Liu, X. Shi, F. Xu, L. Zhang, W. Zhang, L, Chen, Q. Li, C. Uher, T. Day, G. J. Snyder, *Nat. Mater.* **2012**, *11*, 422-425.

[P2] J. Jamnik, J. Maier, S. Pejovnik, *Electrochim. Acta* **1999**, *44*, 4139-4145.

[P3] G. J. Brug, A. L. G. van den Eeden, M. Sluyters-Rehbach, J. H. J. Sluyters, *Electroanal. Chem.* **1984**, *176*, 275-295.

[P4] G. J. Snyder, E. S. Toberer, *Nat. Mater.* **2008**, *7*, 105-114.

Supporting Information

1. Complete X-Ray refinement details for **1**

Crystal Data for $Hg_8K_8Se_{12}$ (M =2865.04): tetragonal, space group $P4_2/ncm$ (no. 138), a = 15.0690(4) Å, c = 7.1060(3) Å, V = 1613.59(11) Å^3, Z = 2, T = 100(2) K, μ(MoKα) = 52.469 mm^{-1}, *Dcalc* = 5.897 g/mm^3, 11068 reflections measured (3.822 ≤ 2Θ ≤ 53.352), 904 unique (R_{int} = 0.1432) which were used in all calculations. The final R_1 was 0.0505 (I >2σ(I)) and wR_2 was 0.1262 (all data).

Table SI1 Crystal data and structure refinement for **1**.

Empirical formula	$Hg_8K_8Se_{12}$
Formula weight	2865.04
Temperature/K	100(2)
Crystal system	tetragonal
Space group	$P4_2/ncm$
a/Å	15.0690(4)
b/Å	15.0690(4)
c/Å	7.1060(3)
α/°	90
β/°	90
γ/°	90
Volume/Å^3	1613.59(11)
Z	2
ρ_{calc}mg/mm^3	5.897
m/mm^{-1}	52.469
F(000)	2400.0
Crystal size/mm^3	0.15 × 0.07 × 0.03
Radiation	MoK_α (λ = 0.71073)
2Θ range for data collection	3.822 to 53.352°
Index ranges	-19 ≤ h ≤ 19, -19 ≤ k ≤ 18, -8 ≤ l ≤ 9
Reflections collected	11068
Independent reflections	904 [R_{int} = 0.1432]
Data/restraints/parameters	904/0/38
Goodness-of-fit on F^2	1.180
Final R indexes [I>=2σ (I)]	R_1 = 0.0505, wR_2 = 0.1250
Final R indexes [all data]	R_1 = 0.0514, wR_2 = 0.1262
Largest diff. peak/hole / e Å^{-3}	1.66/-3.55

Table 2 Fractional Atomic Coordinates (×10^4) and Equivalent Isotropic Displacement Parameters (Å^2×10^3) for Compound 1. U_{eq} is defined as 1/3 of of the trace of the orthogonalised U_{IJ} tensor.

Atom	x	y	z	U(eq)

Hg1	169.5(3)	6841.3(3)	1076.1(7)	31.7(3)
Se2	-1312.2(8)	6312.2(8)	2593(2)	29.0(4)
Se3	1639.5(8)	5686.3(8)	2352.5(17)	28.6(3)
K1	0	5000	5000	29.4(10)
K2	-1515.0(16)	8485.0(16)	2512(6)	32.0(8)
K3	2500	7500	0	33.7(11)

Table 3 Anisotropic Displacement Parameters ($Å^2 \times 10^3$) for Compound 1. The Anisotropic displacement factor exponent takes the form: $-2\pi^2[h^2a^{*2}U_{11}+2hka^*b^*U_{12}+...]$.

Atom	U_{11}	U_{22}	U_{33}	U_{23}	U_{13}	U_{12}
Hg1	29.1(3)	30.9(3)	35.2(4)	-1.37(16)	2.03(16)	-1.01(17)
Se2	26.4(5)	26.4(5)	34.2(9)	-0.8(4)	0.8(4)	0.4(6)
Se3	25.8(6)	27.1(6)	33.0(6)	0.3(4)	-0.5(4)	1.3(4)
K1	27.3(14)	27.3(14)	34(2)	2.0(14)	-2.0(14)	1.3(18)
K2	28.2(11)	28.2(11)	40(2)	-0.9(10)	-0.9(10)	-0.5(14)
K3	33.0(15)	33.0(15)	35(2)	0	0	-3(2)

Table 4 Bond Lengths for Compound 1.

Atom	Atom	Length/Å	Atom	Atom	Length/Å
Hg1	Se2	2.6046(11)	K1	$Se3^8$	3.2731(12)
Hg1	$Se3^1$	2.6634(12)	K1	$Se3^4$	3.2731(12)
Hg1	$Se3^2$	2.5758(13)	K1	$K2^5$	3.689(4)
Hg1	Se3	2.9595(12)	K1	$K2^7$	3.689(4)
Hg1	K1	3.9419(5)	K2	$Hg1^{10}$	3.6905(12)
Hg1	$K2^3$	3.619(3)	K2	$Hg1^{11}$	3.619(3)
Hg1	K2	3.6905(12)	K2	$Hg1^{12}$	3.619(3)
Hg1	K3	3.7286(5)	K2	$Se2^{13}$	3.522(4)
Se2	$Hg1^4$	2.6045(11)	K2	$Se2^{12}$	3.637(4)
Se2	K1	3.2779(17)	K2	$Se2^6$	3.289(3)
Se2	$K2^5$	3.522(4)	K2	$Se3^1$	3.324(3)
Se2	$K2^6$	3.289(3)	K2	$Se3^{14}$	3.324(3)
Se2	K2	3.289(3)	K2	$K1^{13}$	3.689(4)
Se2	$K2^3$	3.637(4)	K2	$K2^6$	4.198(7)
Se3	$Hg1^2$	2.5758(13)	K3	$Hg1^2$	3.7286(5)
Se3	$Hg1^7$	2.6635(12)	K3	$Se3^{15}$	3.4561(12)
Se3	K1	3.2731(12)	K3	$Se3^7$	3.5623(12)
Se3	$K2^7$	3.324(3)	K3	$Se3^{16}$	3.5623(12)
Se3	K3	3.4562(12)	K3	$Se3^{17}$	3.5623(12)
Se3	$K3^1$	3.5623(12)	K3	$Se3^2$	3.4561(12)
K1	$Hg1^8$	3.9419(5)	K3	$Se3^1$	3.5623(12)
K1	$Hg1^4$	3.9419(5)	K3	$Se3^{18}$	3.4561(12)
K1	$Hg1^9$	3.9419(5)	K3	$K3^1$	3.55300(15)

2. TGA/DSC results

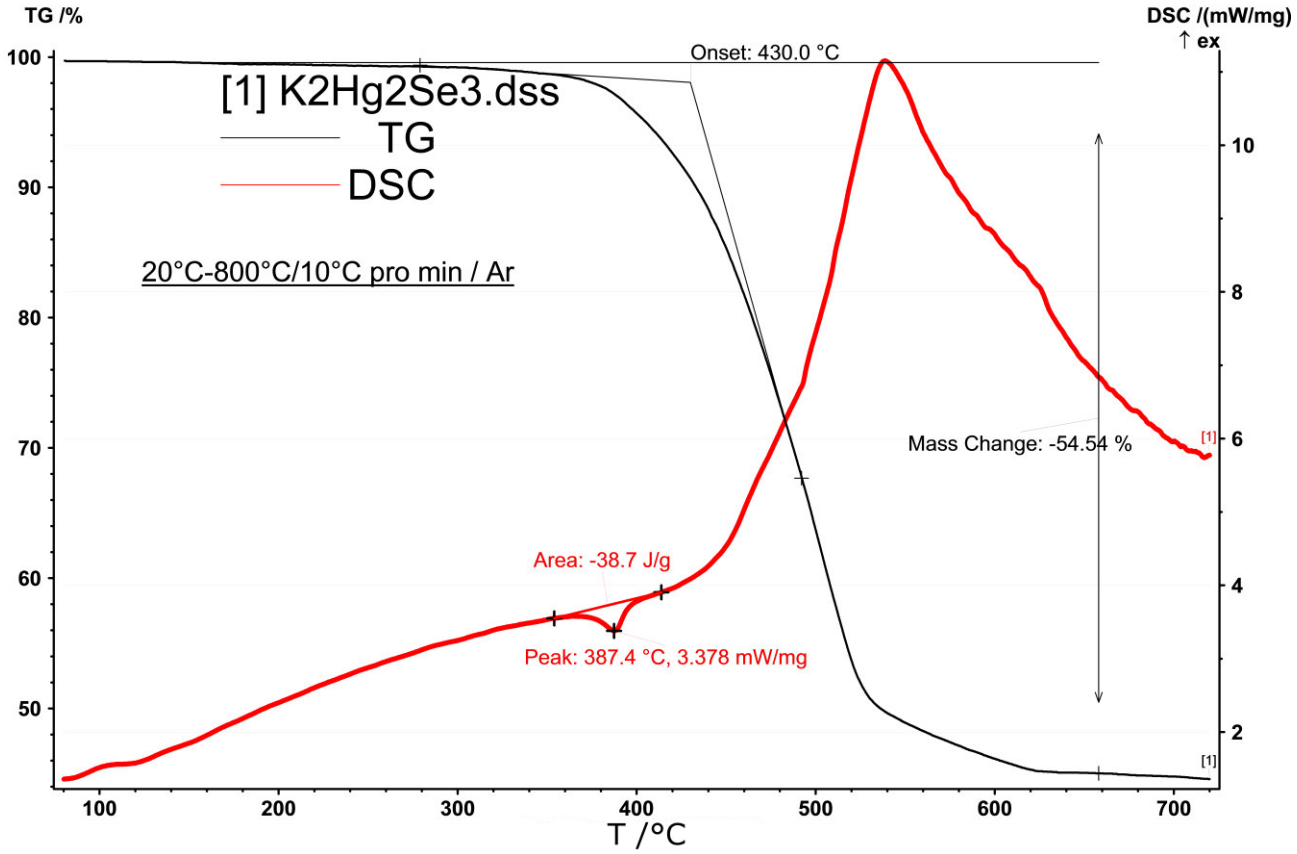

Figure SI1: Thermogravimetric Analysis and Differential Scanning Calorimetry Results of .

3. UV-Vis results

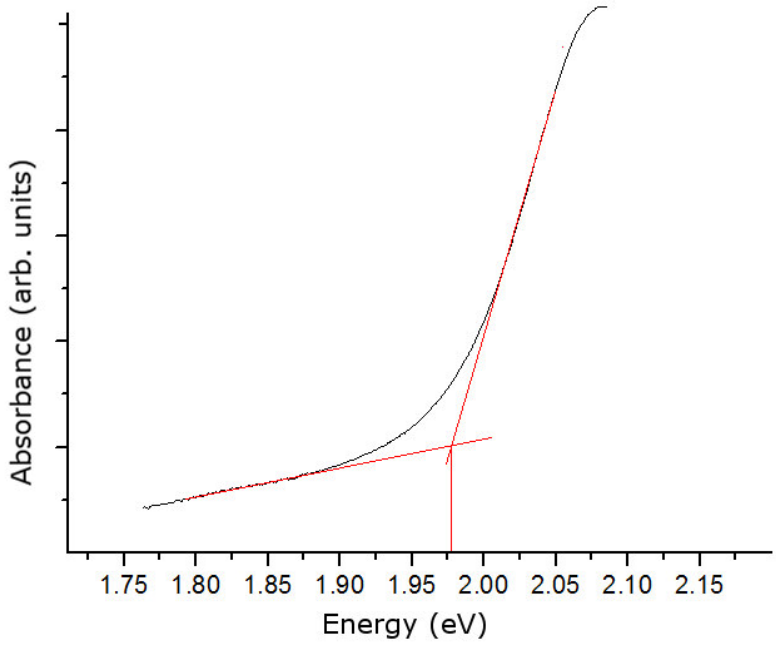

Figure SI2: UV-visible spectra of **1**with extrapolation towards onset of absorption E_{onset}.

IX

Solvothermal and Ionothermal Syntheses and Structures Of Amine- and/or (Poly-) Chalcogenide Coordinated Metal Complexes

Günther Thiele, Silke Santner, Carsten Donsbach, Maik Assmann, Marcus Müller, Stefanie Dehnen, *Z. Kristallogr*. **2014**, *229*, 489–495 (*Titelbild*).

A series of five compounds, namely $[Ba(trien)_2]_3[SbSe_4]_2 \cdot trien$ **(1)** (*trien* = diethylenetriamine), $[(Se_3)Cr(en)_2(Se_2)Cr(en)_2(Se_3)]_2$ **(2)** (*en* = ethylenediamine), $[(pren)_3Eu(Te_3)_2Eu(pren)_3]$ **(3)** (*pren* = 1,3-diaminopropane), $[(en)_4Ba(pren)Ba(en)_4](Te_3)_2$ **(4)** and $[enH]_4[Sn_2Se_6]$ **(5)**, which illustrate the transition of classical polychalcogenides to metalates, are presented, where mixed amine/(poly-)chalcogenide interaction with metal centers are in the focus of interest. A conventional aminothermal synthesis is discussed in comparison with ionothermal approaches. The compounds are considered useful precursors to study *in-situ* interconversion of selenido- and telluridometalates under ionothermal conditions.

Themenkomplex Ionothermale Umsetzungen

Inhalt: Die Synthesemethoden der solvothermalen und ionothermalen Reaktionen werden vorgestellt und bezüglich ihrer Temperatur-, Druck- und Löslichkeitsbedingungen diskutiert. Bisherige Synthesen in ionischen Flüssigkeiten werden vorgestellt mit den verschiedenen zugrundeliegenden Prinzipien.

Es werden allgemein beobachtete Nebenreaktionen und die Notwendigkeit des Zusatzes von Auxiliaren diskutiert und Voraussetzungen für eine optimierte Durchflusssynthese von Metallaten vorgestellt. Eine Zusammenfassung bekannter heteroleptischer Metallkomplexe mit Polychalkogenidliganden und Aminen im Kristallverband wird gegeben.

Die Strukturen und Synthesen von $[Ba(trien)_2]_3[SbSe_4]_2 \cdot trien$, $[(Se_3)Cr(en)_2(Se_2)Cr(en)_2(Se_3)]_2$, $[(pren)_3Eu(Te_3)_2Eu(pren)_3]$, $[(en)_4Ba(pren)Ba(en)_4](Te_3)_2$ und $[enH]_4[Sn_2Se_6]$ werden vorgestellt und als Synthone für ionothermale Reaktionen vorgeschlagen.

Eigener Anteil: Alle Experimente wurden vom mir konzipiert. Alle analytischen Untersuchungen wurden von mir durchgeführt und ausgewertet. Die Synthesen wurden zum Teil von Marcus Müller, Maik Assmann im Rahmen einer Vertiefung und Carsten Donsbach im Rahmen seiner Examensarbeit durchgeführt. Das Manuskript wurde gemeinsam von Stefanie Dehnen, Silke Santner und mir verfasst.

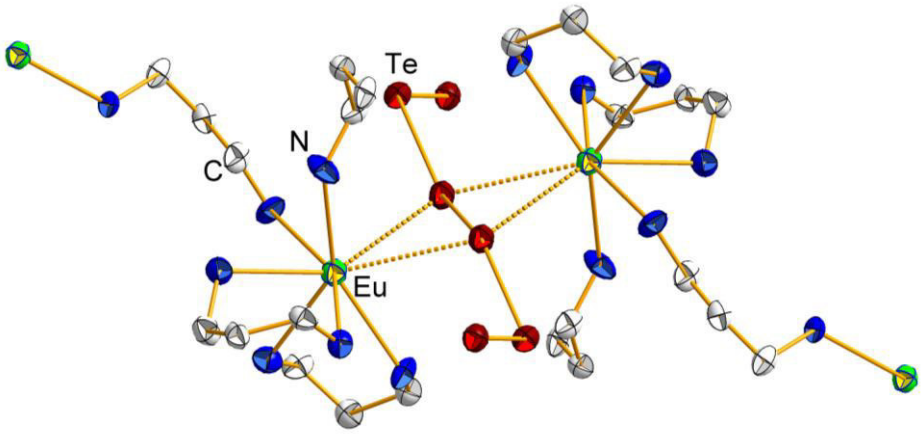

Abbildung 29. Ausschnitt der Kristallstruktur von $[(pren)_3Eu(Te_3)_2Eu(pren)_3]$.

Günther Thiele, Silke Santner, Carsten Donsbach, Maik Assmann, Marcus Müller and Stefanie Dehnen*

Solvothermal and ionothermal syntheses and structures of amine- and/or (poly-)chalcogenide coordinated metal complexes

Abstract: A series of five compounds, namely $[Ba(trien)_2]_3[SbSe_4]_2 \cdot trien$ **(1)** (*trien*=diethylenetriamine), $[(Se_3)Cr(en)_2(Se_2)Cr(en)_2(Se_3)]_2$ **(2)** (*en*=ethylenediamine), $[(pren)_3Eu(Te_3)_2Eu(pren)_3]$ **(3)** (*pren*=1,3-diaminopropane), $[(en)_4Ba(pren)Ba(en)_4](Te_3)_2$ **(4)** and $[enH]_4[Sn_2Se_6]$ **(5)**, which illustrate the transition of classical polychalcogenides to metalates, are presented, where mixed amine/(poly-)chalcogenide interaction with metal centers are in the focus of interest. A conventional aminothermal synthesis is discussed in comparison with ionothermal approaches. The compounds are considered useful precursors to study in situ interconversion of selenido- and telluridometalates under ionothermal conditions.

Keywords: chalcogenidometalates; ionothermal; mixed organic/inorganic compounds; polytellurides; solvothermal.

DOI 10.1515/zkri-2014-1746
Received March 2, 2014; accepted April 16, 2014; published online June 4, 2014

Introduction

Syntheses of new materials by smooth transformation of metastable compounds at relatively low temperatures is a highly desirable method for minimizing energetic costs. One methodology that has attracted considerable impact is the solvothermal synthesis under moderate temperatures (up to 200 °C) leading to a considerable pressure, which produces structural results that are not available by standard solvent chemistry, although temperatures are far below those applied in common solid state chemistry [1–3].

A new area that emerges in the same spirit employs ionic liquids (ILs) as solvent [4–7]. Due to an negligible vapor pressure of ILs, no pressure is generated during the reaction – in contrast to classical solvothermal approaches, yet anion and/or cation of the solvent can adopt templating properties or even be reagent at the same time.

Since a combination of temperature and pressure in classical solvothermal reactions affects the solvent's dielectric constant, therefore dramatically varying the solvent's properties, this method has been extensively employed for extraction of multinary phases or reaction of otherwise insoluable components, and has led to a variety of different M/Ch phases in our work (M=metal, Ch=chalcogen) [8–10]. In contrast, utilization of ILs is restricted to a variation of temperatures with approximately constant pressure unless further volatile auxiliaries are added.

Our current interest in the usage of ILs points at the syntheses of selenido- and telluridometalates and their in situ interconversion, where standard procedure starts from a chalcogenide source, a (main group) metal ion source, and an amine for tuning the pH value for appropriate synthesis conditions. Further investigations towards incorporation of transition metal ions are underway for controlling and fine tuning of optoelectronic properties. Reactions of the binary precursor $[Ge_4Se_{10}]^{4-}$ with tin salts in $[BM(M)Im][BF_4]$ (BM(M)Im=1-butyl-(2,)3-(di) methylimidazolium) in the presence of amines led to the formation of a variety of materials with different compositions including binary and ternary systems with topologies varying from discrete clusters, through 1D chains, 2D layered strutures to 3D extended frameworks [11, 12]. In contrast to this bottom-up strategy, a temperature-induced top-down approach caused the stepwise deconstruction of the 3D selenidostannate network in $K_2[Sn_2Se_5]$ [13] through a layered phase to infinite double-chain anions. In turn, synergistic effects of temperature and addition of

***Corresponding author: Stefanie Dehnen,** Fachbereich Chemie und Wissenschaftliches Zentrum für Materialwissenschaften, Philipps-Universität Marburg, Hans-Meerwein-Strasse, D-35043 Marburg, Germany, E-mail: dehnen@chemie.uni-marburg.de
Günther Thiele, Silke Santner, Carsten Donsbach, Maik Assmann and Marcus Müller: Fachbereich Chemie und Wissenschaftliches Zentrum für Materialwissenschaften, Philipps-Universität Marburg, Hans-Meerwein-Strasse, D-35043 Marburg, Germany

auxiliary amines lead to an inversion of the phase transformation direction under increase of the dimensionality back from the 1D chains into another 3D open-framework selenidostannate [14, 15].

However, so far we did not succeed in establishing atom economic reactions to facilitate either continuous flow or at least be able to recycle reaction media. Whereas $[BF_4]^-$ salts can be filtered off due to precipitation, especially halide containing byproducts form well soluable compounds that change solvent properties considerably and prevent reusage of the reaction medium.

We are therefore interested in the provision of compounds, that allow the introduction of metal and chalcogen atoms, as well as the auxiliary amine by the least possible number of synthons. Ensuring reaction would ideally accord to equations 1 or 2.

$$\left[TM\left(amine\right)_v\right]\left[M\left(Ch_w\right)_x\right]_y \rightarrow \left[TM\left(\mu^n\text{–}Ch_w\right)_z M_y\left(Ch_w\right)_{x\cdot y-z}\right]\cdot v\,amine \quad (1)$$

$$\left[TM\left(amine\right)_v M_y\left(Ch_w\right)_{x\cdot y}\right]\rightarrow \left[TM\left(\mu^n\text{–}Ch_w\right)_z M_y\left(Ch_w\right)_{x\cdot y-z}\right]\cdot v\,amine \quad (2)$$

Suitable compounds should thus

a. incorporate polychalcogenide anions or ligands for high reactivity and tendency to re-arrange into new (T)M–Ch–M aggregates,
b. as cations, include (partly) solvated metal and/or transition metal ions without (too strong and thus inreactive) (T)M–C or Ch–C bonds,
c. comprise amine solvent molecules or ligands that are restricted to a small to medium sterical demand, and that do not form a symmetric, dense coordination sphere around the metal ions,
d. if possible, exlude further, uncoordintated alkaline or alkaline earth metal cations or any kind of non-polychalcogenide anion, likely to be substituted by the IL counterpart and have to be removed after synthesis.

A group of compounds that comply with these requirements are solvated polychalcogenide metalates and polychalcogenides of the formulae $[TM(amine)_y][M'Ch_x]$ [1–3, 16] or $[TM(amine)_y][Ch_x]$ [17], respectively. However, most of these compounds include well-separated and fairly stable anions and cations that do not undergo the desired rearragements to larger aggregates. For instance, $[Mn(en)_3]^{2+}$ (*en*=1,2-diaminoethane) cations or $[SnSe_4]^{4-}$ anions remain intact, leading to simple ions exchange in ILs of ions such that treatment of $[Mn(en)_3]_2[SnSe_4]$ in $BMIm[BF_4]$ affords $[Mn(en)_3][BF_4]_2$ and $[BMIm]_4[SnSe_4]$. Therefore, we thought about introduction of heteroleptic metal complexes including polyselenide or polytelluride moieties beside amine ligands as synthons.

Only a small number of those alkali/alkaline earth ion-free compounds so far has been reported in the literature. Some of these compounds, such as $[\{(R^1)V(Se)\}_2(\mu^2\text{-}Se_2)]$ (R^1=2,6-(2,6-^{i}Pr$_2$-C$_6$H$_3$N=CPh)$_2$-C$_5$H$_3$N) [18] or $\{R^2Cr(\mu\text{-}\eta^2)(Ch_2)CrR^2\}$ (R^2=substituted terphenyle) [19], include amines that appear to be too bulky for further reactions.

In contrast, *Sheldrick*'s series of $[\{Mn_x(Se_y)(amine)\}_z]$, x=1, 2, y=4–6, z=1, 2 [20, 21], $[Mn_x(amine)_xAs_ySe_z]$ with x/y/z=3/2/8 or 2/2/6 [22], as well as $[M(en)_3][In_2Te_6]$ (M=Fe, Zn) or $[Mo_3(en)_3(\mu^2\text{-}Te_2)_3(\mu^3\text{-}Te)(\mu^3\text{-}O)][In_2Te_6]$ [23] appear suitable, with the Mo compound providing three metal ions at once. Further potential precursor complexes are $[(\mu\text{-}\eta^1\text{-}Te_2)(\mu\text{-}N^tBu)_2V_2Cp_2]$ [24], $[R^5Ni(\mu\text{-}\eta^2)(Se_2)NiR^5]$ (R^5=CH-(CMeN{2,6-^{i}Pr$_2$C$_6$H$_3$}$_2$)$_2$) [25], and $[ZnSe_4(N\text{-}MeIm)_2]$ (N-MeIm=N-methylimidazole), synthesized in an elegant way by in situ degeneration of N-MeIm and redox reaction of elemental Zn and Se [26]. As not all reactions within ILs that have been reported today require amine auxiliaries, further non-amine ligated precursors such as $\{M[Me_2SiCp_2]Se_5\}$ (M=Ti, Zr, Hf) [27], $[Cp^*Re(Se_3)(\mu\text{-}Se_2)]_8$ [28], $[Cp^*_2Mo(\eta^2\text{-}Se_4)]$ [29] would be also worth trying. Finally, further auxiliaries in ionothermal reactions still have to be exploited, expanding the field of possible synthons to phosphine coordinated compounds, such as $[(ppp)Ni(Te_2)Pt(PPh_3)_2]$ (*ppp*=bis(2-dipheny1phosphino-ethyl)phenylphosphane) [30], and amine/phosphine bifunctional auxiliaries releasing synthons like $[(N(CH_2CH_2PPh_2)_3)PdTe]_2$ [31].

Herein we report on several compounds that might have similar potential for further transformations in that they combine at least two of the aforementioned prerequisites.

Results and discussion

To contribute to the named class of synthons, we recently produced the following series of compounds: $[Ba(trien)_2]_3[SbSe_4]_2\cdot trien$ **(1)** (*trien*=diethylenetriamine), $[(Se_3)Cr(en)_2(Se_2)Cr(en)_2(Se_3)]_2$ **(2)**, $[(pren)_3Eu(Te_3)_2Eu(pren)_3]$ **(3)** (*pren*=1,3-diaminopropane), $[(en)_4Ba(pren)Ba(en)_4](Te_3)_2$ **(4)** and $[enH]_4[Sn_2Se_6]$ **(5)** that fulfill at least two of the criteria quoted above, yet might prove able to successively identify different kind of reactive sites and requirements for a profound understanding of ionothermal prospects.

Apart from **5**, all compounds have been obtained from solvothermal reactions from ternary alloys "AMCh" with A=K, Ba, Eu; M=Pb, Sb; Ch=Se, Te (in case of transition metal compounds under addition of one equivalent of $TM(SO_4)_x$ TM=Co, Cr), with the coordinating amines as solvent. In one case (**1**), also the main group metal of the ternary alloy was transferred into the product, whereas in the other cases, the main group metal was not part of the crystalline product. Here, the alloy served as transition metal (**2**, **3**) or barium (**4**) as well as (poly-)chalcogenide source (**2–4**). **5** was synthesized from $Li_4[Sn_2Se_6]$ [32] by means of ionothermal recrystallization from the above mentioned $[BMIm][BF_4]$ in the presence of *en*. All compounds were structurally characterized by means of single-crystal X-ray diffraction. The structures will be presented in the following.

$[Ba(trien)_2]_3[SbSe_4]_2 \cdot trien$ (1)

Compound **1** crystallizes in monoclinic space group $P2_1/c$ with four molecules in the unit cell. The two independent $[SbSe_4]^{3-}$ anions exhibit Sb–Se distances in the expected range (2.461(2)–2.477(2) Å) and coordinate to three adjacent $[Ba(trien)_2]^{2+}$ cations each. While one of the selenium ligands each (Se1, Se7) bridges two of the cations, the other three either coordinate to one complex fragment (Se2–Se5, Se8; Ba...Se 3.359(2)–3.665(2) Å), or do not coordinate the cationic complex (Se6). All Ba^{2+} ions possess coordination numbers (c.n.) 9 by two tridentate *trien* molecules and two adjacent antimonate anions that clearly disturb a pure hexa-coordination by N donors. The coordination by *trien* molecules differs by the ligands' constitutions, leading either to a half-sphere (Ba1, Ba2) or an equatorial coordination (Ba3). The entire assembly forms double strands along the crystallographic *a* axis (see Figure 1). An additional molecule of *trien* is incorporated within the structure as crystal solvent.

$[(Se_3)Cr(en)_2(Se_2)Cr(en)_2(Se_3)]_2$ (2)

Compound **2** crystallizes in monoclinic space group $C2/c$ with eight monomeric formula units per unit cell. These can be described as arrangement into dimers $[(Se_3)Cr(en)_2(Se_2)Cr(en)_2(Se_3)]_2$, thus as a dimeric arrangement of a dimer of $[Cr(en)_2]^{3+}$ units with two terminal $(Se_3)^{2-}$ and one bridging $(Se_2)^{2-}$ ligands (see Figure 2). Distances Se1–Se2 and Se7–Se8 are 2.3409(8) and 2.3540(10) Å, respectively, which are slightly smaller than Se2–Se3 and Se6–Se7 (2.3685(10) and 2.3583(8) Å, respectively), comprising coordination of an adjacent chromium ion each. The bridging $(Se_2)^{2-}$ ligand has a Se–Se distance of 2.3788(9) Å. Distances between two selenium atoms that coordinate one Cr^{3+} ions in *cis* fashion are much longer (3.2808(9) and 3.4698(9) Å for Se3...Se4 and Se5...Se6, respectively). Cr–Se distances are in the range 2.4896(10)–2.5226(12) Å, Cr...N distances amount to 2.080(5)–2.130(5) Å, causing distorted octahedral coordination of the chromium ion. Terminal selenium atoms Se1 and Se8 of the $(Se_3)^{2-}$ anions interact with hydrogen atoms from adjacent *en* molecules, and Se8' has a relatively short distance to Se3 in the neighboring $(Se_3)^{2-}$ fragment (Se8'...Se3 3.6758(9)Å).

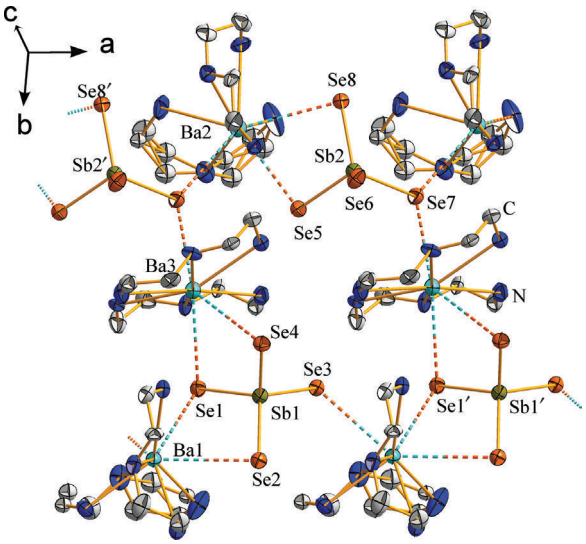

Fig. 1: Fragment of the crystal structure of **1**. Thermal ellipsoids are drawn at 50% possibility. Hydrogen atoms are omitted for clarity.

$[(pren)_3Eu(Te_3)_2Eu(pren)_3]$ (3)

Compound **3** crystallizes in orthorhombic space group *Pbca* with eight formula units per unit cell. The compound represents a dimeric complex $[(pren)_3Eu(Te_3)_2Eu(pren)_3]$ with the two $(Te_3)^{2-}$ fragments bridging two $[Eu(pren)_3]^{2+}$ counterions; the Te1–Te2 and Te2–Te3 distances (2.7544(12) and 2.7698(11) Å, respectively) are much shorter than that of Te3...Te3' with 3.3615(12) Å (see Figure 3), yet the difference between primary and secondary distances is not as large as in **2**. Eu–Te distances amount to 3.4761(10)–3.5165(9) Å. It should be noted that so far, structurally determined compounds that comprise Eu–Te bonds besides organic ligands can only be found in three further compounds: $\{Eu[TeSi(SiMe_3)_3]_2(dmpe)_2\}_2(\mu\text{-}dmpe)]$ [33] (*dmpe*=$Me_2PCH_2CH_2PMe_2$), $[(thf)_3Eu(TeC_6H_5)_2NaTePh]$, and $[(thf)_2Eu(TeC_6H_5)_2]$ [34] with Eu–Te distances in the range of 3.160–3.231Å, 3.335–3.359Å, and 3.324–3.426Å.

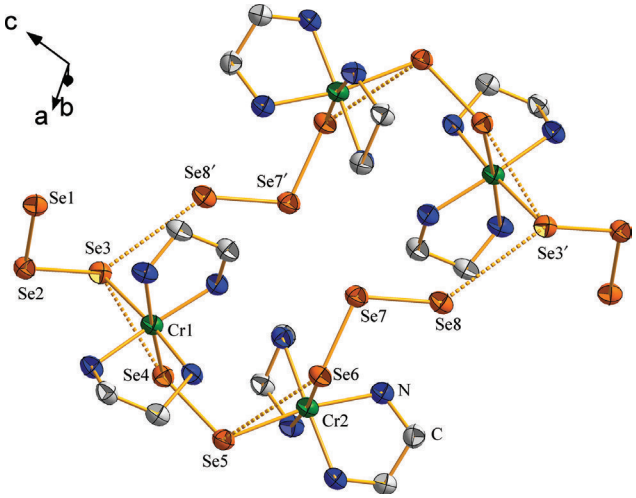

Fig. 2: Fragment of the crystal structure of **2**. Thermal ellipsoids are drawn at 50% possibility. Hydrogen atoms are omitted for clarity.

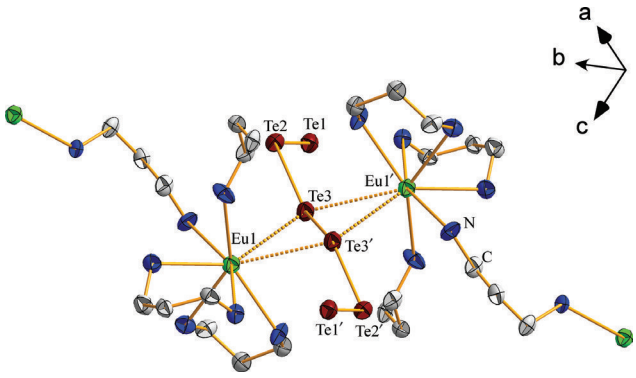

Fig. 3: Fragment of the crystal structure of **3**. Thermal ellipsoids are drawn at 50% possibility. Hydrogen atoms are omitted for clarity.

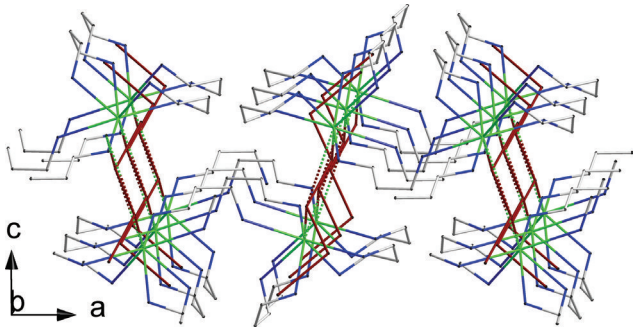

Fig. 4: 2D layers formed by coordination network in **2**. Atoms are drawn in wire/sticks model, hydrogen atoms are omitted for clarity.

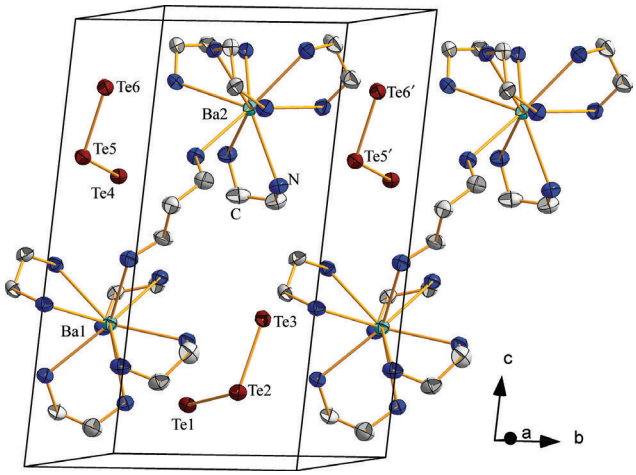

Fig. 5: Fragment of the crystal structure of **4**. Thermal ellipsoids are drawn at 50% possibility. Hydrogen atoms are omitted for clarity.

The europium ions obtain c.n. 8, by coordination of two of the Te atoms, two chelating *pren* molecules and two further *pren* molecules in end-on coordination mode. The latter act as bridges to two adjacent Eu^{2+} ions, thus generating a 2D coordination polymer that runs parallel to the crystallographic *ab*-plane (see Figure 4).

$[(en)_4Ba(pren)Ba(en)_4](Te_3)_2$ (4)

Compound **4** crystallizes in triclinic space group *P*1 with one molecule per unit cell and well-separated $[(en)_4Ba(pren)Ba(en)_4]^{2+}$ cations besides $(Te_3)^{2-}$ anions. Te–Te distances are in the range 2.7330(8)–2.7520(8) Å, Te–Te–Te angles amount to 109.01(3)–112.64(3)°. Ba^{2+} ions obtain c.n. 9 from four chelating *en* molecules and one *pren* molecule that bridges two adjacent $[Ba(en)_4]^{2+}$ fragments (Figure 5). The space group was rationalized by application of Platon software [35]; it is obvious that no inversion symmetry is present anywhere within or between the complexes.

$[enH]_4[Sn_2Se_6]$ (5)

Finally, a compound without any metallic counterion that still might provide an amine for coordination beside a main group chalcogenide moiety is compound **5**. It crystallizes upon ionothermal treatment of $Li_4[Sn_2Se_6]$ in $BMIm[BF_4]$ in triclinic spacegroup *P*1 with 2 formula units in the unit cell (Figure 6). It is a solvent isomer of the known salt $[enH]_4[Sn_2Se_6]\cdot en$ [36]. Hence, the synthesis accords with a simple cation exchange in IL in the presence of *en* and therefore much more convenient than as described in literature. It is worth noting that the IL cation

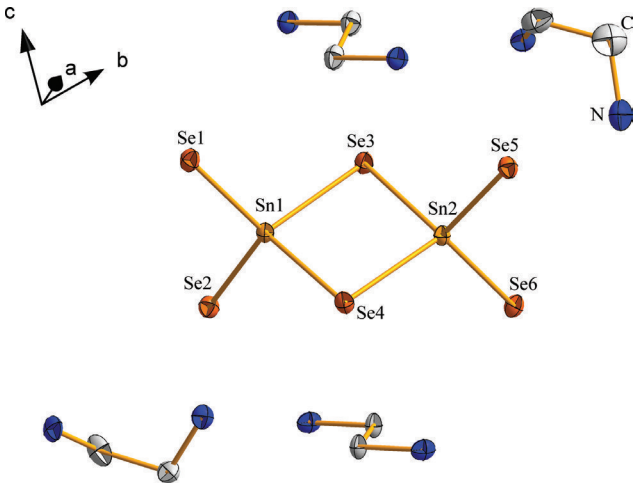

Fig. 6: Fragment of the crystal structure of **5** indicating the relative orientation of the anion and the *en*H counterions within one formula unit in the crystal. Thermal ellipsoids are drawn at 50% possibility. Hydrogen atoms are omitted for clarity.

had not been incorporated into the compound. All bond lengths and angles are similar to the reported ones.

Conclusion

Five potential synthons and their prerequisites for an efficient and continuous flow ionothermal synthesis have been presented, with compound **3** incorporating a rare Eu...Te interaction.

Experimental section

General

As all of the title compounds are highly sensitive to air and moisture, in that they would decompose into binary metal chalcogenides, (alkaline earth) metal oxides/hydroxides, higher polychalcogenides and/or elemental chalcogens, all manipulations and reactions were performed under an Ar atmosphere using standard Schlenk or glovebox techniques. All precursor materials for solvothermal reactions have been obtained by fusion of the elements in the respective equivalents. $BMIm[BF_4]$ has been degassed at $p<10^{-5}$ mbar for at least 12 h, all amines have been distilled from CaH_2 prior to use. Solvothermal reactions were performed in a glass vial that was placed within a Teflon cylinder that was tightly enclosed by a stainless steel autoclave. The autoclave was then heated to 150 °C for 7 days and allowed to cool to room temperature for 2 days. Products were manually picked under a light microscope. Due to the co-precipitation of differently-colored, inhomogeneous and usually amorphous by-products, the estimation of yields is difficult. Energy-dispersive X-ray spectroscopy of the single-crystalline products confirmed the given compositions of the heavy atoms in all cases.

Syntheses

$[Ba(trien)_2]_3[SbSe_4]_2 \cdot trien$ (**1**): 500 mg of an alloy of the nominal composition $K_2(Sb/Pb)Se_2$ and 2 mL of *trien* were reacted under solvothermal conditions as mentioned to yield **1** as yellow blocks.

$[(Se_3)Cr(en)_2(Se_2)Cr(en)_2(Se_3)]_2$ (**2**): 500 mg of an alloy of the nominal composition K_2PbSe_2, 300 mg $Cr_2[SO_4]_3 \cdot H_2O$ and 2 mL *en* were reacted under solvothermal conditions to yield **2** as black blocks.

$[(pren)_3Eu(Te_3)_2Eu(pren)_3]$ (**3**): 500 mg of an alloy of the nominal composition $EuPbSe_2$ and 2 mL *pren* were reacted under solvothermal conditions to yield **3** as black blocks.

$[(en)_4Ba(pren)Ba(en)_4](Te_3)_2$ (**4**): 500 mg of an alloy of the nominal composition BaPbTe and 2 mL of a 1:1 mixture of *en*/*pren* were reacted under solvothermal conditions to yield **4** as black blocks.

$[enH]_4[Sn_2Se_6]$ (**5**): 120 mg $Li_4[Sn_2Se_6]$, 20 µL *en* and 1 mL $BMIm[BF_4]$ were sealed under vacuum in a pyrex ampule and heated to 100 °C for 4 days. **5** can manually be picked as orange plates.

X-ray crystallography

Data collection was performed on a STOE IPDS-I (**5**) or IPDS-II (**1**–**4**) diffractometers with graphite-monochromated MoKα radiation (λ=0.71073 Å) at 193 K or 100 K. The structures were solved by direct methods and refined by full-matrix least-squares methods against F^2, using WinGX and OLEX2 software [37, 38]. Crystal data:

1 (M_w=1966.07 g·mol^{-1}): monoclinic, space group $P2_1/c$, a=8.2838(2), b=27.3069(9), c=26.9354(9) Å, β=90.889(2)°, V=6092.2(3) Å^3, Z=4, ρ_c=2.144 g·cm^{-3}, μ=7.605 mm^{-1}, 50,084 reflections measured (R(int)=0.14), 12,866 unique, 9514 with $I>2\sigma(I)$ and final R values $R1$=0.1123 ($I>2\sigma(I)$); $wR2$=0.2422 (all data). The compound suffers from poor crystal quality, hence the individual with best scattering properties that we could find (data given here) showed three-fold twinning. The respective domains contain 65.0%, 8.3%, and 5.8% of the peaks, respectively. The remaining 20.9% of peaks could not be assigned. We assume the twinning and an overlap of 19.9% during integration to be the main reason for the poor data quality besides heavy disorder of solvent and ligand molecules.

2 (M_w=966.01 g·mol^{-1}): monoclinic, space group $C2/c$, a=27.0402(10), b=8.1733(3), c=24.1854(12) Å, β=110.462(3)°, V=5007.9(4) Å^3, Z=8, ρ_c=2.563 g·cm^{-3}, μ=12.509 mm^{-1}, 32,820 reflections measured (R(int)=0.0618), 5314 unique, 4066 with $I>2\sigma(I)$ and final R values $R1$=0.0488 ($I>2\sigma(I)$); $wR2$=0.0987 (all data).

3 (M_w=745.05 g·mol^{-1}): orthorhombic, space group $Pbca$, a=15.6072(11), b=10.7546(5), c=23.6570(15) Å, V=3970.8(4) Å^3, Z=8, ρ_c=2.493 g·cm^{-3}, μ=7.477 mm^{-1}, 33,289 reflections measured (R(int)=0.1233), 4205 unique, 2238 with $I>2\sigma(I)$ and final R values $R1$=0.0458 ($I>2\sigma(I)$); $wR2$=0.1006 (all data).

4 (M_w=1591.21 g·mol^{-1}): triclinic, space group $P\bar{1}$, a=9.2783(10), b=9.7068(10), c=16.1630(16) Å, α=82.799(6), β=74.795(8), γ=61.45°, V=1233.9(2) Å^3, Z=1, ρ_c=2.141 g·cm^{-3}, μ=5.096 mm^{-1}, 18,738 reflections measured (R(int)=0.0285), 9211 unique, 8835 with $I>2\sigma(I)$ and final R values $R1$=0.0273 ($I>2\sigma(I)$); $wR2$=0.0664 (all data).

5 (M_w=879.36 g·mol^{-1}): triclinic, space group $P\bar{1}$, a=8.8572(13), b=11.0142(18), c=12.5583(18) Å, α=75.121(12), β=73.836(11), γ=89.939(13)°, V=1134.0(3) Å^3, Z=2, ρ_c=2.575 g·cm^{-3}, μ=11.83 mm^{-1}, 12,844 reflections measured (R(int)=0.0511), 3915 unique, 2647 with $I>2\sigma(I)$ and final R values R1=0.0286 ($I>2\sigma(I)$); $wR2$=0.0567 (all data).

The supplementary crystallographic data CCDC 989397–989401 for **1-5** can be obtained free of charge from The Cambridge Crystallographic Data Center via www.ccdc.cam.ac.uk.data_request.cif.

Acknowledgments: This work was supported by the Friedrich Ebert Stiftung (FES) and Deutsche Forschungsgemeinschaft (SPP 1415).

References

[1] J. Zhou, J. Dai, G.-Q. Bian, C.-Y. Li, Solvothermal synthesis of Group 13–15 chalcogenidometalates with chelating organic amines. *Coord. Chem. Rev.* **2009**, *253*, 1221.

[2] J. Li, Z. Chen, R.-J. Wang, D. M. Proserpio, Low temperature route towards new materials: solvothermal synthesis of metal chalcogenides in ethylenediamine. *Coord. Chem. Rev.* **1999**, *190–192*, 707.

[3] W. S. Sheldrick, M. Wachhold, Solventothermal synthesis of solid-state chalcogenidometalates. *Angew. Chem. Int. Ed. Engl.* **1997**, *36*, 206.

[4] A. Taubert, Z. Li, Inorganic materials from ionic liquids. *Dalton Trans.* **2007**, 723.

[5] E. Ahmed, M. Ruck, Chemistry of polynuclear transition-metal complexes in ionic liquids. *Dalton Trans.* **2011**, *40*, 9347.

[6] R. E. Morris, Ionothermal synthesis – ionic liquids as functional solvents in the preparation of crystalline materials. *Chem. Commun.* **2009**, 2990.

[7] E. R. Parnham, R. E. Morris, Ionothermal synthesis of zeolites, metal-organic frameworks, and inorganic-organic hybrids. *Acc. Chem. Res.* **2007**, *40*, 1005.

[8] J. Heine, S. Santner, S. Dehnen, Synthesis of complex polymeric telluridoindates from $KInTe_2$. *Inorg. Chem.* **2013**, *52*, 4424.

[9] G. Thiele, T. Krüger, S. Dehnen, K_4 [$PbSe_4$]·en·NH_3 – eine nichtoxidische, Halogenid-freie anorganische Blei(IV)-Verbindung". *Angew. Chem.* **2014**, *126*, 4787–4791.

[10] G. Thiele, T. Krüger, S. Dehnen, K_4 [$PbSe_4$]·en·NH_3 – eine nichtoxidische, Halogenid-freie anorganische Blei(IV)-Verbindung. *Angew. Chem. Int. Ed.* **2014**, *53*, 4699–4703.

[11] Y. Lin, W. Massa, S. Dehnen, "Zeoball" [Sn_{36} Ge_{24} Se_{132}]$^{24-}$: A molecular anion with zeolite-related composition and spherical shape. *J. Am. Chem. Soc.* **2012**, *134*, 4497.

[12] Y. Lin, W. Massa, S. Dehnen, Controlling the assembly of chalcogenide anions in Ionic liquids: From binary Ge/Se through ternary Ge/Sn/Se to binary Sn/Se frameworks. *Chem. Eur. J.* **2012**, *18*, 13427.

[13] K. O. Klepp, Preparation and crystal structure of $K_2Sn_2S_5$ and $K_2Sn_2Se_5$. *Z. Naturforsch. B* **1992**, *47*, 197.

[14] Y. Lin, D. Xie, W. Massa, L. Mayrhofer, S. Lippert, B. Ewers, A. Chernikov, M. Koch, S. Dehnen, Changes in the structural dimensionality of selenidostannates in ionic liquids: Formation, structures, stability, and photoconductivity. *Chem. Eur. J.* **2013**, *19*, 8806.

[15] Y. Lin, S. Dehnen, [BMIm]$_4$ [$Sn_{29}Se_{20}$]: Ionothermal synthesis of a selenidostannate with a 3D open-framework structure. *Inorg. Chem.* **2011**, *50*, 7913.

[16] S. Dehnen, M. Melullis, A coordination chemistry approach towards ternary M/14/16 anions. *Coord. Chem. Rev.* **2007**, *251*, 1259.

[17] W. S. Sheldrick in: Handbook of Chalcogen Chemistry, F. Devillanova, editor, The Royal Society of Chemistry, Cambridge, UK, Chapter 9.2. **2007**.

[18] C. Milsmann, Z. R. Turner, S. P. Semproni, P. J. Chirik, Azo N=N bond cleavage with a redox-active vanadium compound involving metal-ligand cooperativity. *Angew. Chem. Int. Ed* **2012**, *51*, 5386.

[19] E. S. Tamne, A. Noor, S. Qayyum, T. Bauer, R. Kempe, Quintuple bond reactivity toward Group 16 and 17 elements: addition vs insertion. *Inorg. Chem.* **2013**, *52*, 329.

[20] A. Kromm, W. S. Sheldrick, Solvothermal synthesis and structures of lamellar [$Mn(tren)_2$]Cl_2 and the dimeric and polymeric hexaselenidomanganese(II) complexes [{ $Mn(Se_6)$ (tren)}$_2$] and $^2_\infty$[{$Mn(Se_6)$(tren)}]. *Z. Anorg. Allg. Chem.* **2007**, *633*, 529.

[21] A. Kromm, Y. Geldmacher, W. S. Sheldrick, Polyamine and -imine manganese(II) complexes with tetra-, penta- and hexaselenide ligands: coligand and solvent influence on the polyselenide nuclearity and coordination mode. *Z. Anorg, Allg. Chem.* **2008**, *634*, 2191.

[22] A. Kromm, W. S. Sheldrick, Manganese(II) complexes with bridging selenidoarsenate(III) anions [$AsSe_2(Se_2)$]$^{3-}$ and [$(AsSe_2)_2(\mu\text{-}Se_2)$]$^{4-}$. *Z. Anorg. Allg. Chem.* **2009**, *635*, 205.

[23] J. Li, Z. Chen, T. J. Emge, D. M. Proserpio, New Type of polymeric indium tellurides: low-temperature synthesis and structure characterization of [$M(en)_3$]In_2 Te_6(M=Fe, Zn) and α- and β-[$Mo_3(en)_3(\mu_2\text{-}Te_2)_3(\mu_3\text{-}Te)(\mu_3\text{-}O)$]$In_2Te_6$. *Inorg. Chem.* **1997**, *36*, 1437.

[24] F. Preuss, M. Billen, F. Tabellion, G. Wolmershäuser, Darstellung und Kristallstruktur eines Ditelluridovanadium(IV)-komplexes:[$(\mu\text{-}\eta^1\text{-}Te_2)(\mu\text{-}N^tBu)_2V_2$ Cp_2]. *Z. Anorg. Allg. Chem.* **2000**, *626*, 2446.

[25] S. Yao, Y. Xiong, X. Zhang, M. Schlangen, H. Schwarz, C. Milsmann, M. Driess, Facile dissociation of [$(LNi^{II})_2E_2$] dichalcogenides:evidence for [$LNi^{II}E_2$] superselenides and supertellurides in solution. *Angew. Chem. Int. Ed.* **2009**, *48*, 4551.

[26] S. Dev, E. Ramli, T. B. Rauchfuss, C. L. Stern, Direct approaches to zinc polychalcogenide chemistry: ZnS_6(N-MeIm)$_2$ and $ZnSe_4$(N-MeIm)$_2$. *J. Am. Chem. Soc.* **1990**, *112*, 6385.

[27] N. Tzavellas, N. Klouras, C. P. Raptopoulou, Group 4 *ansa*-metallacyclohexaselenanes: synthesis, characterization, and properties. Crystal structure of {$Ti[Me_2Si(\eta^5\text{-}C_5H_4)_2]Se_5$}. *Z. Anorg. Allg. Chem.* **1997**, *623*, 384.

[28] G.-X. Jin, Y. Arikawa, K. Tatsumi, Spontaneous formation of a diamond-crown structure of Re_8 polyselenide and a cage structure of Re_3 Polytelluride. *J. Am. Chem. Soc.* **2001**, *123*, 735.

[29] J. H. Shin, D. G. Churchill, B. M. Bridgewater, K. Pang, G. Parkin, Hydride, halide, methyl, carbonyl, and chalcogenido derivatives of Permethylmolybdenocene. *Inorg. Chim. Acta* **2006**, *359*, 2942.

[30] M. D. Vaira, M. Peruzzini, P. Stoppioni, Synthesis and structure of compounds containing ditellurium side-on bonded to nickel complex fragments. *Angew. Chem. Int. Ed. Engl.* **1987**, *26*, 916.

[31] F. Cecconi, C. A. Ghilardi, S. Midollini, A. Orlandini, A novel phosphine Pd_2Te_2 dimer. synthesis and X-ray characterization of the complex [$(N(CH_2CH_2PPh_2)_3)PdTe]_2$. *Inorg. Chem. Commun.* **1999**, *2*, 275.

[32] T. Kaib, P. Bron, S. Haddadpour, L. Mayrhofer, L. Pastewka, T.T. Järvi, M. Moseler, B. Roling, S. Dehnen, Lithium chalcogenidotetrelates:LiChT – Synthesis and characterization

of New Li^+ ion conducting Li/Sn/Se compounds. *Chem. Mater.* **2013**, *25*, 2961.

[33] D. R. Cary, J. Arnold, Synthesis and characterization of divalent lanthanide selenolates and tellurolates. X-ray crystal structures of $Yb[SeSi(SiMe_3)_3]_2(TMEDA)_2$ and $\{Eu[TeSi(SiMe_3)_3]_2(DMPE)_2\}_2$ (μ-DMPE). *Inorg. Chem.* **1994**, *33*, 1791.

[34] D. V. Khasnis, M. Brewer, J. Lee, T. J. Emge, J. G. Brennan, Rare earth phenyltellurolates: 1D coordination polymers. *J. Am. Chem. Soc.* **1994**, *116*, 7129.

[35] A. L. Spek, PLATON, A Multipurpose Crystallographic Tool, Utrecht University, Utrecht, The Netherlands **2005**.

[36] S. Dehnen, C. Zimmermann, Syntheses, crystal structures and reactivity of $[enH]_4[Sn_2Se_6]\cdot en$, $[enH]_4[Sn_2Te_6]\cdot en$ and $[enH]_4[Sn_2S_6]$: known anions within novel coordination spheres obtained by novel synthesis routes. *Z. Anorg. Allg. Chem.* **2002**, *628*, 2463.

[37] L. J. Farrugia, WinGX and; ORTEP for Windows: an update, *J. Appl. Cryst.* **2012**, *45*, 849.

[38] O. V. Dolomanov, L. J. Bourhis, R. J. Gildea, J. A. K. Howard, H. Puschmann, OLEX2: a complete structure solution, refinement and analysis program. *J. Appl. Cryst.* **2009**, *42*, 339.

X

$K_2Hg_6Se_7$ – A new Mercurate from Ionothermal Synthesis: A Pseudo-Flux Reaction

Günther Thiele, Hendrik Borkowski, Lars Finger, Jörg Sundermeyer, Stefanie Dehnen,
Manuskript in Vorbereitung.

The new chalcogenidomercurate $K_2Hg_6Se_7$ has been prepared by ionothermal treatment of $K_2Hg_2Se_3$. The structure is closely related to its lighter congener $K_2Hg_6S_7$, however, it cannot be synthezised following classical pathways. Accordingly, the reaction conditions of the polychalcogenide flux are mimicked, though smoothened by application of a $(SH)^-$-based ionic liquid, hence by *pseudo*-flux conditions.

Themenkomplex Ionothermale Umsetzungen

Inhalt: Die Synthese von $K_2Hg_6Se_7$ aus $K_2Hg_2Se_3$ in Ethyl-Methyl-Imidazolium Hydrogensulfid bei 100-120°C und die Kristallstruktur der Titelverbindung werden vorgestellt. Die Verbindung und ihre Synthese wird im Vergleich zum bekannten Homologen $K_2Hg_6S_7$ diskutiert und verschiedene konventionelle Synthesemethoden diskutiert.

Eigener Anteil: Alle Experimente wurden von mir konzipiert. Alle analytischen Untersuchungen wurden von mir durchgeführt und ausgewertet. Hendrik Borkowski führte die Synthesen im Rahmen seiner Bachelorarbeit unter meiner Anleitung durch. Lars Finger und Jörg Sundermeyer synthetisierten die ionischen Flüssigkeiten und stellte sie uns zur Verfügung. Stefanie Dehnen und ich verfassten das Manuskript gemeinsam.

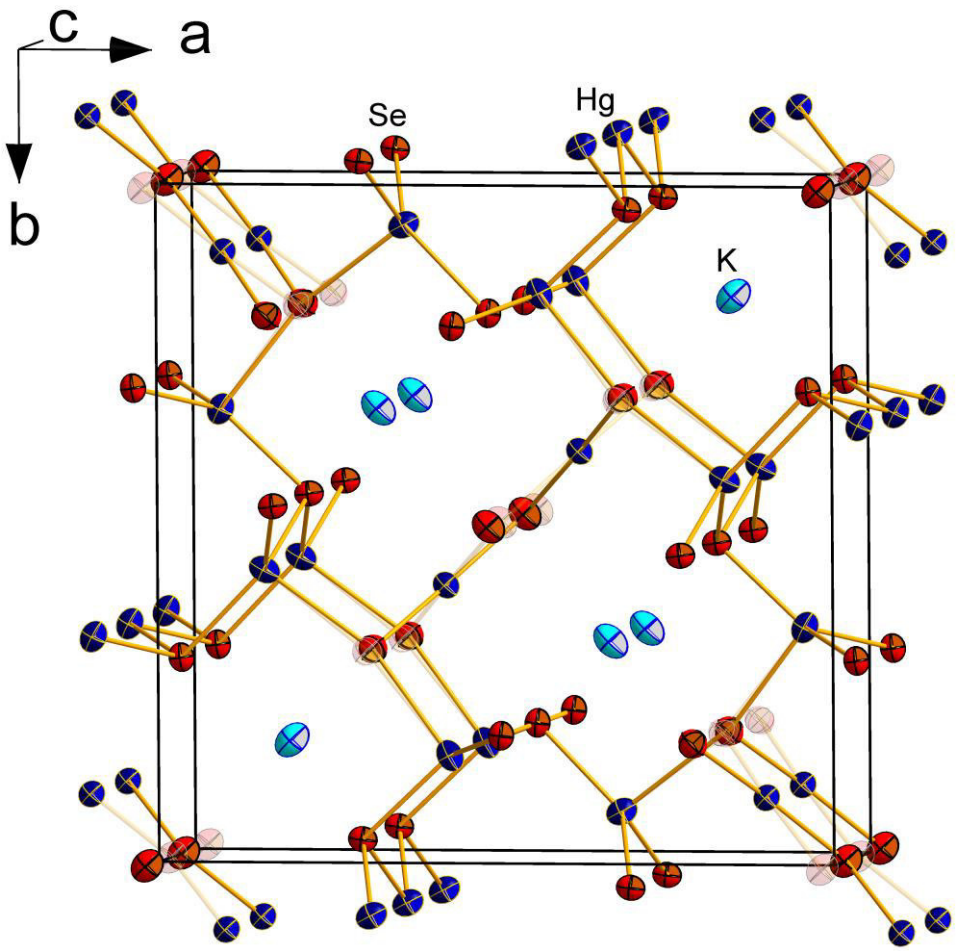

Abbildung 30. Ausschnitt aus der Kristallstruktur von $K_2Hg_6Se_7$.

Journal Name

RSCPublishing

COMMUNICATION

$K_2Hg_6Se_7$ – A new Mercurate from Ionothermal Synthesis: a *Pseudo*-Flux Reaction

Cite this: DOI: 10.1039/xoxxoooooox

G. Thiele, H. Borkowski, Lars Finger, Jörg Sundermeyer and S. Dehnen*

Received ooth January 2012,
Accepted ooth January 2012

DOI: 10.1039/xoxxoooooox

www.rsc.org/

Dedicated to W. Bensch and M. Ruck .

The new chalcogenidomercurate $K_2Hg_6Se_7$ has been prepared by ionothermal treatment of $K_2Hg_2Se_3$. The structure is closely related to its lighter congener $K_2Hg_6S_7$ though cannot be synthezised on classical pathways. Accordingly, the reaction conditions are mimicked, though smoothed by application of a $(SH)^-$ based ionic liquid, the *pseudo* flux.

Ionothermal reactions – that is syntheses in ionic liquids – have attracted considerable attention in recent times. Among the many advantages of this new technique are the reusability of solvent, low reaction temperatures and new structural motifs of product compounds.[1] We have been investigating the phase transitions of chalcogenidostannates in ionic liquids to gain a profund understanding of reaction pathways and equilibria in the still new area of low temperature inorganic synthesis,[2,3] and have now extended this work to chalcogenidomercurates. Those are promising materials for e.g. thermoelectric applications[4] or hard radiation detection.[5]

Common ionothermal reactions apply organic cations with halide anions or weakly coordinating halide containing anions. Our previous investigations[6] revealed the salt metathesis of educt metalates (MET) and ionic liquids (IL) to be a major side reaction, thereby reducing the efficiency of new reaction conditions (see equation 1-2). Thus the reusage of ionic liquid solvent is prevented.

$$(Cat_{MET})[An_{MET}] + (Cat_{IL})(An_{IL}) \rightarrow (Cat_{IL})[An_{MET}] + (Cat_{MET})[An_{IL}] \quad (1)$$

$$K_4[SnSe_4] + 4\ BMIM[BF_4] \rightarrow 4\ K[BF_4] + (BMIM)_4[SnSe_4] \quad (2)$$

Therefore we applied ionic liquids with chalcogenide containing anions, namely the hydrogensulfide, $(SH)^-$ and hydrogenselenide $(SeH)^-$,[7] to yield $K_2Hg_6Se_7$ (**1**) in 90% crystalline yield (see equation 3).

$$6\ K_2Hg_2Se_3 \text{ ----EMIM(SH)---> } 2\ K_2Hg_6Se_7 + 4\ K_2Se \quad (3)$$

1 posesses a close structural relationship to its lighter congener $K_2Hg_6S_7$[8] (see Fig. 1) yet with a disorder of two of the three crystallographically independent Se atoms (see Fig. 1) different tetragonal space groups $P4_2/mnm$ ($K_2Hg_6S_7$: $P\bar{4}2_1m$) with a = 14.2241(16) Å, c = 4.2075(5) Å ($K_2Hg_6S_7$: 13.805(8) Å, 4.080(3) Å). However, upon translation upon [0,½,¼] and neglection of disorder, both structures can be brought to congruence upon normalization of the unit cell.

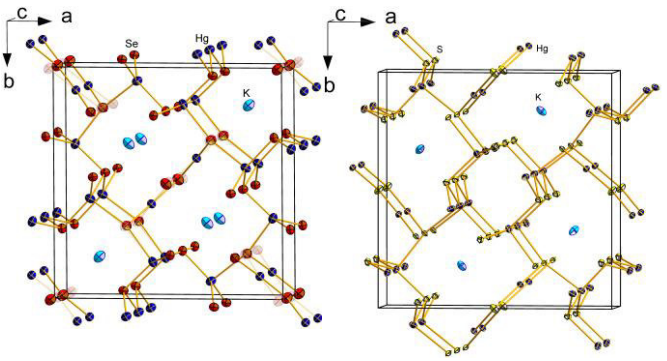

Figure 1. Crystal structure of **1** (left) and $K_2Hg_6S_7$ (right). Ellipsoids are drawn at 50% (left) or 90% (right) probability (see experimental section).

$K_2Hg_6S_7$, in contrast, has been prepared using flux reaction conditions at 380°C[9] and can also be recrystallized via solvothermal reactions.[10] The corresponding Se – **1** – analogue could not be prepared in the same manner via classical flux methods, which the authors allocate to the K^+ ions to be too small to support the enlarged tunnels.

Our own solvothermal attempts for any $A_2Hg_6Ch_7$ (A = alkali metal, Ch = chalcogen) failed, too, although we could obtain various selenidomercurates under aminothermal reactions, such as K_4HgSe_3[11] or $K_2Hg_2Se_3$.[3]

..::TGA Messung der Phase hier::..

We therefore conclude, that the unique chalcogen-flux conditions are necessary for the structural constitution of the corresponding $A_2Hg_6Ch_7$

structures, while the thermal instability at elevated temperatures of the compound prevents the respective reaction conditions. However, the present EMIM(SH) solvent mimics the salt melt while the temperatures are below those of product degradation and can thus be called *pseudo* flux.

This is supported by preceding attempts within common ionic liquids, such as EMIM- and BMIM salts with Cl^-, Br^- and $[BF_4]^-$ anions, that did not yield any crystalline samples, nor could the presence of **1** be elucidated from powder diffraction experiments. Reaction of $K_2Hg_6S_7$ within EMIM(SH) only resulted in recrystallization, while reactions in EMIM(SeH) did not yield homogenous and analysable product. Investigations are underway, whether AHgTe-compounds can, too, be obtained with typical AHgS structural motifs upon treatment under *pseudo* sulphur flux conditions.

Notes and references

[a] Address here.
[b] Address here.
[c] Address here.

† Footnotes should appear here. These might include comments relevant to but not central to the matter under discussion, limited experimental and spectral data, and crystallographic data.

Electronic Supplementary Information (ESI) available: [details of any supplementary information available should be included here]. See DOI: 10.1039/c000000x/

1 P. Wasserscheid, T. Welton, Ionic Liquids in Synthesis, 2nd Edition; Wiley-VCH, 2007, Weinheim.
2 Y. Lin, W. Massa, S. Dehnen, Chem. Eur. J. 2012, 18, 13427-13434.
3 G. Thiele, S. Lippert, F. Fahrnbauer, P. Bron, M. Assmann, O. Oeckler, A. Rahimi-Iman, M. Koch, B. Roling, S. Dehnen, Manuskript in preparation.
4 H. Li, J. A. Peters, Z. Liu, M. Sebastian, C. D. Malliakas, J. Androulakis, L. Zhao, I. Chung, S. L. Nguyen, S. Johnsen, B. W. Wessels, M. G. Kanatzidis, Cryst. Growth Des. 2012, 12, 3250.
5 G. Thiele, S. Santner, C. Donsbach, M. Assmann, M. Müller, S. Dehnen, Z. Kristallogr. 2014, 229, 489-495.
6 L. Finger, J. Sundermeyer, unpublished results.
7 Y. Park, M. G. Kanatzidis, Chem. Mater. 1990, 2, 99-101.
8 We have attempted the possible solvothermal reactions starting from mixtures of K_2Se and HgSe as well as crude "$K_2Hg_6Se_7$" in a variety of solvents and different temperatures ranging from 100°C to 200°C. Direct fusion of the elements and subsequent annealing does not result in the formation of the title compound as does not application of reactive flux techniques (see Ref. 7).
9 G. Thiele, C. Krug, R. Tonner, S. Dehnen, Manuscript in preparation.

5 Zusammenfassung

Die vorliegende Arbeit hatte das Ziel, einen optimierten Syntheseweg zur Darstellung bekannter und neuer binärer Chalkogenidometallatanionen der schwersten, nicht-radioaktiven Elemente zu finden. Die so erhaltenen Verbindungen sollten zu ternären Metallatanionen umgesetzt werden. Alle erhaltenen Verbindungen sollten bezüglich ihrer physikalischen Eigenschaften untersucht werden.

Es konnten zwei Synthesewege zur Darstellung von Chalkogenidoplumbaten erfolgreich etabliert werden. Einerseits konnte durch die *in-situ*-Reduktion von binären chalkogenreichen Bleichalkogeniden mit elementaren Alkalimetallen in Ethylendiamin in hoher Reinheit und Ausbeute das Trichalkogenidodiplumbat synthetisiert werden, andererseits konnte mithilfe solvothermaler Reaktionsbedingungen ein Tetraselenido-*ortho*-Plumbat(IV) als erste nicht-oxidische Blei(IV)-Chalkogenverbindung generiert werden.

Die Methode der *in-situ*-Darstellung konnte in analoger Weise zur Synthese von Verbindungen mit binären Anionen der Chalkogenidomerkurate, -thallate und -bismutate verwendet werden.

Umsetzungen von Lösungen der Trichalkogenidodiplumbate mit Edelmetallverbindungen ergaben molekulare Komplexe mit Edelmetall-Chalkogen-Bindungen, wobei das Plumbat einerseits als Oxidationsmittel und/oder Chalkogenid-Übertragungsreagenz fungiert, andererseits auch als Quelle für einen neuen {PbSe}-Liganden fungierte.

Unter solvothermalen Reaktionsbedingungen von ternären Phasen $A_xM_yCh_z$, die auf festkörperchemischem Wege erhalten wurden, konnte neben dem unerwarteten *ortho*-Plumbat(IV) eine Vielzahl neuer Chalkogenidomerkurate und -thallate synthetisiert und charakterisiert werden. Zudem wurde auch ein einfacher Zugang zu Bismutaten aufgedeckt. Hierbei war einerseits die Stöchiometrie $(A_2Ch):(M_xCh_y)$ entscheidend für die räumliche Ausdehnung der entstandenen Anionensubstrukturen, andererseits war die Wahl des Lösungsmittels – wahrscheinlich entsprechend der Lewis-Basizität der Reaktionslösung – für die Bildung der entsprechenden Anionen von entscheidender Bedeutung.

In Nebenreaktionen konnte die Bildung von Polychalkogeniden röntgenographisch und spektroskopisch nachgewiesen werden.

Bei Zugabe der elementaren Alkalimetalle Kalium, Rubidium oder Cäsium zu Ethylendiamin kommt es zur Oligomerisation dessen. Ähnliche Beobachtungen macht man für solvothermale Reaktionsbedingungen mit Acetonitril in Anwesenheit von Ni^{2+} oder Pb^{2+}, wobei der entsprechende pH-Wert den Grad der Oligomerisation vorzugeben scheint.

Mithilfe molekularer quantenchemischer Rechnungen konnte die Stabilität des *ortho*-Plumbates rationalisiert werden, die Analogie des PbSe Liganden zum bekannten CO Fragment verdeutlicht werden, die optischen und NMR-chemischen Daten von Polychalkogeniden erklärt sowie neue Konformationen für diese vorausgesagt werden.

Durch quantenchemische Rechnungen mit periodischen Randbedingungen konnte sowohl der Einfluss der Alkalimetallionen und deren Packung auf NMR-Verschiebungen von Polytelluriden, als auch der Verlauf der Bandlücken in ternären Chalkogenidomerkuraten bestimmt werden.

$K_2Hg_2Se_3$ wurde als Material mit hoher Photoleitfähigkeit und geringer thermischer Leitfähigkeiten identifiziert. Die Bestimmung des ZT-Wertes dieser Verbindung steht noch aus. Gleiches gilt für die Verbindungen $K_2Hg_2Te_3$, K_3BiSe_3, $K_2Hg_6Se_7$ und $K_6TlSe_4 \cdot H_2O$, die nicht alle in der vorliegenden Dissertation diskutiert werden.

Für die ionothermale Reaktionsführung scheint neben der Lewis-Basizität der Reaktionslösung die Ionenpaarbildung gemäß dem HSAB-Prinzip von übergeordneter Rolle.

Zusammenfassend konnte ein neuer Synthesezugang zu Chalkogenidometallaten in Lösung gefunden und eine Vielzahl neuer Metallatverbindungen synthetisiert und charakterisiert werden, wobei erstmalig sowohl ein *ortho*-Selenidoplumbat(IV) als auch ein Metallkomplex mit {PbSe}-Ligand dargestellt werden konnte.

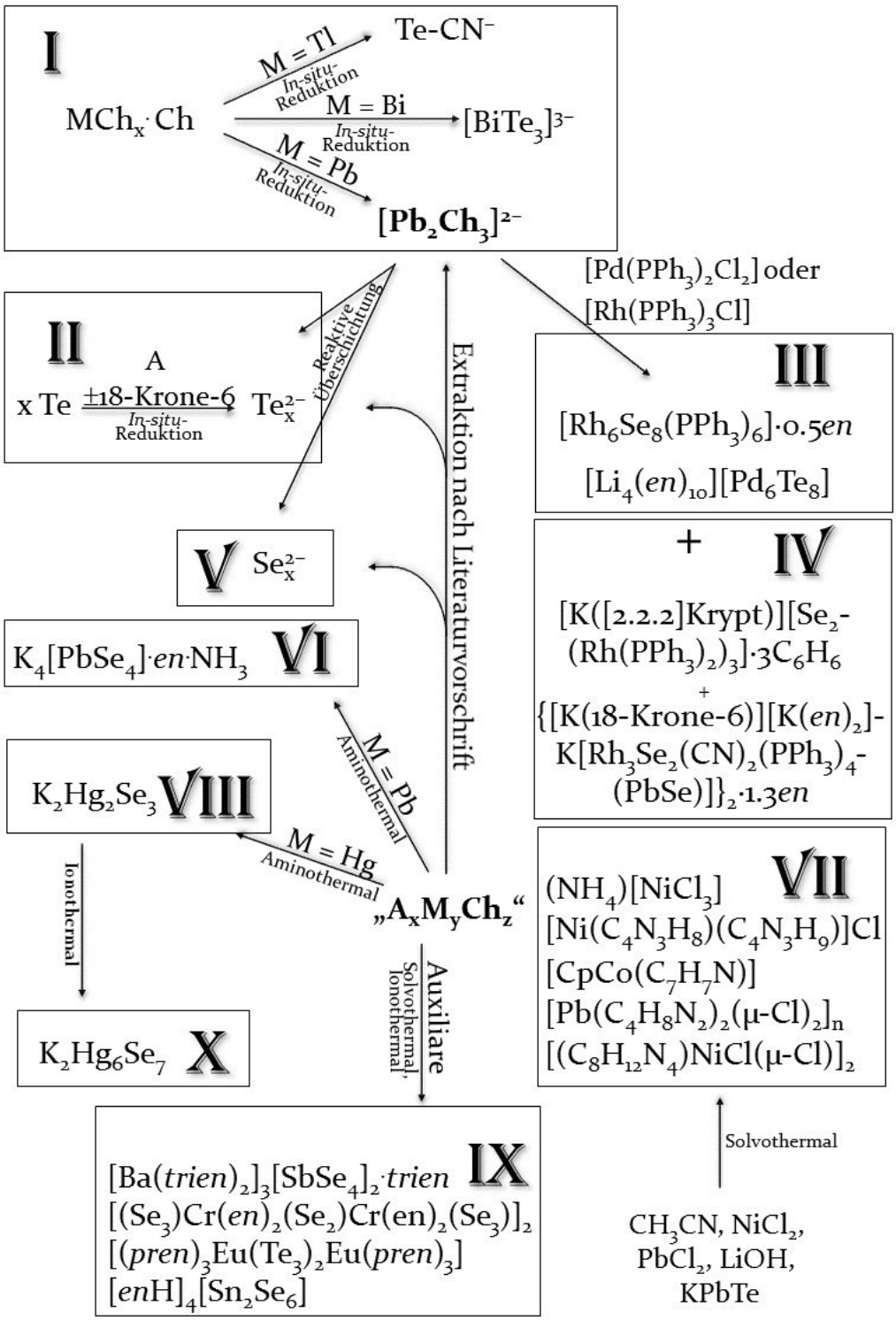

6 Summary

The aim of the present work has been the optimization of the synthesis of known and new binary chalcogenido metalate anions of the heaviest, non-radioactive elements. Those compounds were to be used for reactions towards ternary metalate anions. All obtained compounds were to be investigated towards their physical properties. Two synthetic routes towards chalcogenido plumbates were successfully identified. On the one hand via the *in-situ*-reduction of chalcogen-rich lead chalcogenides with elemental potassium in ethylene diamine to yield the trichalcogenido diplumbate in high yield and abundance. On the other hand the tetraselenido *ortho*-plumbate(IV), as the first non-oxidic lead(IV)-chalcogene compound, could be obtained under solvothermal reaction conditions.

The method of *in-situ*-reduction could be applied analogously for the synthesis of binary anions of the chalcogenido mercurates, thallates, and bismutates.

Solutions of the trichalcogenido diplumbates react with noble transition metal compounds towards molecular compounds with transition metal chalcogen bonds, while the plumbate serves as oxidizing agent and/or chalcogenide transferring agent on the one hand; on the other hand the selenido plumbate can also generate the new {PbSe} ligand.

Solvothermal extractions of $A_xM_yCh_z$, that was generated via solid-state high temperature methods, yields – besides the unexpected *ortho*-plumbate(IV) – a variety of new chalcogenido mercurates and thallates that were characterized in detail. Furthermore a simple access towards chalcogenido bismutates has been identified. The stoichiometry of $(A_2Ch):(M_xCh_y)$ purports the spacial extension of the anionic substructures, while the choice of solvent – probably due to the corresponding Lewis basicity – of the reaction solution is of importance for the generation of the corresponding anionic motifs.

In side reactions, polychalcogenides could crystallographically and spectroscopically be identified.

Ethylene diamine oligomerizes upon addition of alkali metals such as potassium or its heavier homologues. Acetonitrile oligomerizes in the presence of Ni^{2+}- or Pb^{2+}-ions under solvothermal reaction conditions, while the pH-value seems to determine the degree of oligomerization.

By means of molecular quantum chemical calculations the stability of the *ortho*-plumbate(IV) could be rationalized. Furthermore the analogy of the {PbSe} ligand to the known CO ligand could be illustrated and the optical and NMR-chemical data of polychalcogenides could be interpreted. New conformations of polychalcogenides could be predicted by comparison of absolute energies.

Via quantum chemical calculations with periodic boundary conditions the impact of alkali metal ions and the corresponding crystal packing effects on the NMR chemical shift of polytellurides was determined, as well as the development of band gaps within ternary chalcogenido mercurates.

$K_2Hg_2Se_3$ was identified as a material of high photo conductivity and low thermal conductivity. The determination of the ZT value for this compound, as those for $K_2Hg_2Te_3$, K_3BiSe_3, $K_2Hg_6Se_7$ and $K_6TlSe_4 \cdot H_2O$, that are not all discussed in detail within the present work, are still pending.

For ionothermal reaction conditions, the Lewis basicity of the reaction solution alongside the generation of ion pairs – according to the HSAB concept – seems to be of overriding importance.

In conclusion, a new synthetic access toward chalcogenido metalates in solution was found and a variety of new metalate compounds was synthesized and characterized. Alongside, the first *ortho*-selenido plumbate(IV) and a metal complex including a {PbSe}-ligand were obtained.

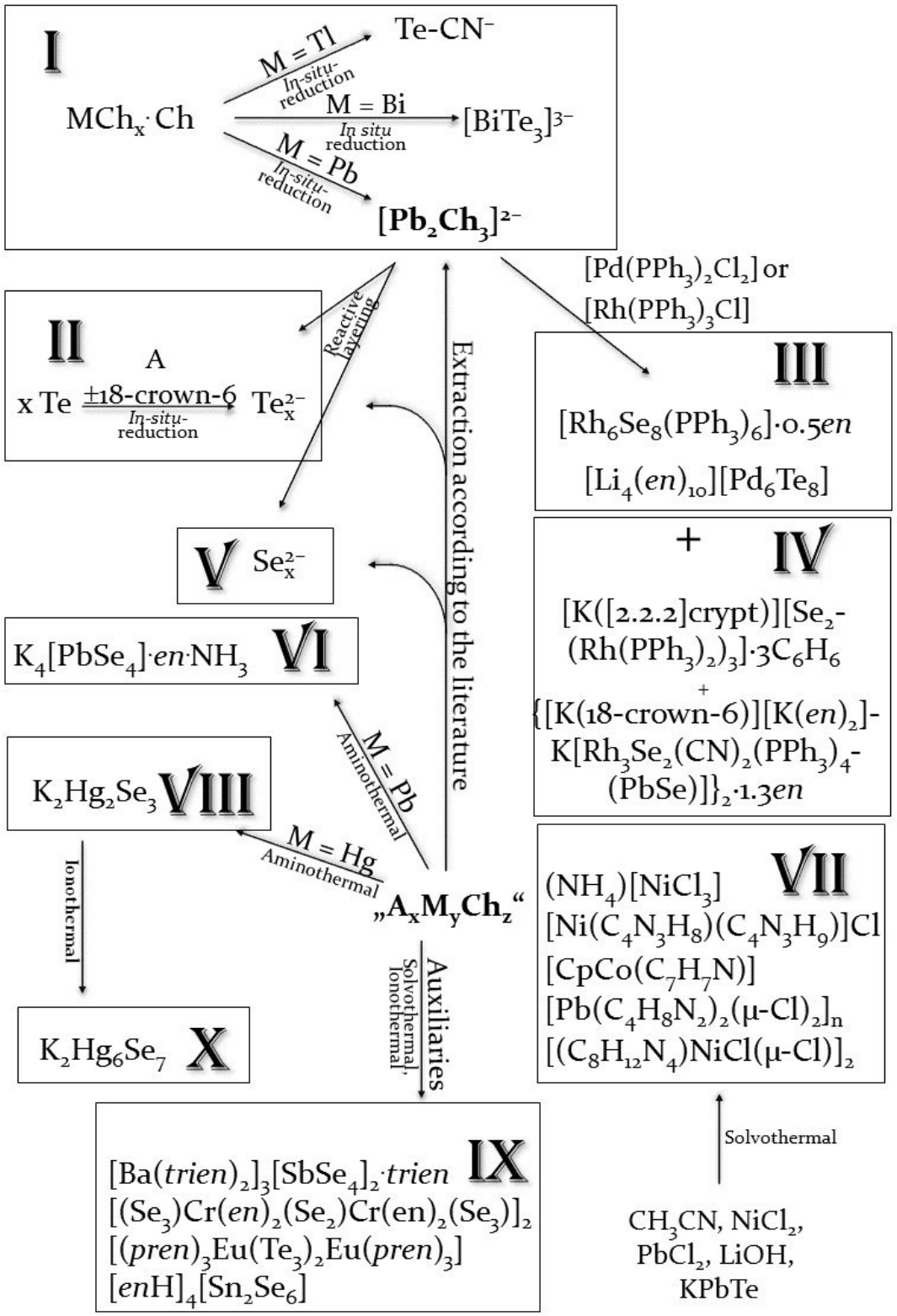

Lebenslauf

Name	Günther Thiele
Geburtsort	D-Potsdam
Geburtsdatum	21. Juni 1985
seit 12/2010	Doktorand an der Philipps-Universität Marburg
09/2008-03/2009	Auslandssemester, University of Sydney
10/2005-10/2010	Studium der Chemie an der Philipps-Universität Marburg
08/1997-06/2004	Hermann von Helmholtz Gymnasium Potsdam mit Abschluss Abitur

Vollständige Publikationsliste

(15*) "A Systematic Approach on Ternary Chalcogenidomercurates and their Solvates"
G. Thiele, C. Krug, M. Assmann, R. Tonner, S. Dehnen, *Manuskript in Vorbereitung.*

(14*) "$K_2Hg_6Se_7$ – A new Mercurate from Ionothermal Synthesis: A Pseudo-Flux Reaction"
G. Thiele, H. Borkowski, L. Finger, J. Sundermeyer, S. Dehnen, *Manuskript in Vorbereitung*.

(13*) "The Second Heaviest Ever Possible CO Homologue: {μ-PbSe}- An Unexpected Ligand"
G. Thiele, S. Dehnen, *Manuskript in Vorbereitung.*

(12*) "$K_2Hg_2Se_3$: A novel Selenidomercurate(II) for Photothermoelectric Applications"
G. Thiele, S. Lippert, F. Fahrenbauer, P. Bron, M. Assmann, O. Oeckler, A. Rahimi-Iman, M. Koch, B. Roling, S. Dehnen, *Manuskript in Vorbereitung.*

(11*) "Reactions In and With Acetonitrile"
G. Thiele, S. Dehnen, *Manuskript in Vorbereitung.*

(10*) "Molecular CHEVREL-like Clusters $[(RhPPh_3)_6Se_8]$ and $[Pd_6Te_8]^{4-}$"
G. Thiele, Z. You, S. Dehnen, *Inorg. Chem.* **2015**, *in Revision*.

(9*) "About the Syntheses of Chalcogenidometalates by in-situ Reduction with Elemental Alkali Metals"
G. Thiele, L. Vondung, S. Dehnen, *Z. Anorg. Allg. Chem.* **2015**, *im Druck*.

(8*) “Organic Cation and Complex Cation-Stabilized (Poly-)Selenides, $[Cation]_x(Se_y)_z$: Diversity in Structures and Properties”

G. Thiele, L. Vondung, C. Donsbach, S. Pulz, S. Dehnen, *Z. Anorg. Allg. Chem.* **2014**, *640*, 2684-2700.

(7) "Advanced NMR methods and DFT calculations on the Regioselective Deprotonation and Functionalization of 1,1’-Methylene-Bis-(3-methyl-imidazole-2-thione)"

M. Bauer, D. Premužić, G. Thiele, B. Neumüller, R. Tonner, I. Fernandez, I. Kuzu, 2014, *eingereicht*.

(6*) "Solvothermal and Ionothermal Syntheses and Structures Of Amine- and/or (Poly-) Chalcogenide Coordinated Metal Complexes"

G. Thiele, S. Santner, S. Dehnen, *Z. Kristallogr*. **2014**, *229*, 489–495 (*Titelbild*).

(5*) "$K_4[PbSe_4]\cdot en\cdot NH_3$ – A Non-Oxide, Non-Halide Inorganic Lead(IV) Compound"

G. Thiele, T. Krüger, S. Dehnen, *Angew. Chem*. **2014**, *126*, 4792-4797; *Angew. Chem. Int. Ed*. **2014**, *53*, 4699-4703.

(4*) "Syntheses, Structures and Electronic Properties of a New Series of Tellurides of the Type $[Sequestrated\ Cation]_2[Te_x]$ (x = 1-4)"

G. Thiele, N. Lichtenberger, R. Tonner, S. Dehnen, *Z. Anorg. Allg. Chem.* **2013**, *639*, 2809-2815 (*Titelbild*).

(3) "Crystalline beryllium carboxylate frameworks containing inorganic chains of BeO_4 tetrahedra"

M. Kang, D. Luo, Z. Lin, G. Thiele, S. Dehnen, *Cryst. Eng. Comm.* **2013**, *15*, 1845-1848.

(2) "Making practical use of the pseudo-element concept: an efficient way to ternary intermetalloid clusters by an isoelectronic Pb–/Bi combination"

R. Ababei, J. Heine, M. Hołyńska, G. Thiele, B. Weinert, X. Xie, F. Weigend, S. Dehnen, *Chem. Commun*. **2012**, *48*, 11295-11297.

(1) "Heterobimetallic Chalcogenidometallate Strands: Synthesis and Structure, Magnetism and Conductivity"

G. Thiele, S. Peter, M.C. Schwarzer, E. Ruzin, R. Clérac, H. Staesche, C. Rößer, B. Roling, S. Dehnen, *Inorg. Chem.* **2012**, *51*, 3349-3351.

Mit * gekennzeichnete Publikationen sind Teil dieser Dissertation.

AC-MPR-Vertiefungen: Claudio Krug, Mario Argentari, Maximilian Biermeier, Markus Balmer, Maximilian Fritz, Maik Assmann, Maximilian Jost, Susanne Pulz, Isabell Nußbruch, Lukas Trombach, Thomas Zimmermann, Fangyao Lin, Hui Wang, Alexander von Tesmar

AC-MPR-Projektarbeiten: Beata Wiekowsky, Michael Müller, Alexander Grevel, Benjamin Ringler, Susanne Pulz, Jasmin Heinzer

MatChem-MPR-Vertiefungen: Milan Mengel, Dominik Recktenwald

Bachelorarbeiten: Hendrik Borkowski, Stephan Krisch, Niels Lichtenberger

Masterarbeit: Lisa Vondung

Examensarbeit: Carsten Donsbach

Sonstige Praktikanten: Lovis Wagner, Torben Skrzypeh

Studentische Hilfskräfte: Steffen Emge, Maik Assmann

Auszubildende: Thomas Krüger, Marcus Müller

Kooperationen

Fachbereichsintern

AG Prof. Dr. Stefanie Dehnen: Zhiliang You, Silke Santner

AG Prof. Dr. Bernhard Roling: Philip Bron

AG Dr. Ralf Tonner: Phil Rosenow

AG Prof. Dr. Jörg Sundermeyer: Lars Finger

Abteilung Kristallstrukturanalyse: Michael Marsch, Klaus Harms

Fachbereichsextern

AG Prof. Dr. Martin Koch: Sina Lippert, Arash Rahimi-Iman, Philipps-Universität Marburg

AG Prof. Dr. Oliver Oeckler: Felix Fahrenbauer, Universität Leipzig

Abkürzungsverzeichnis

[2.2.2]Krypt	= [2.2.2]Kryptand = 4,7,13,16,21,24-Hexaoxa-1,10-diazabicyclo[8.8.8]hexacosan
18-Krone-6	= 1,4,7,10,13,16-Hexaoxacyclooctadecan
en	= Ethan-1,2-diamin
trien	= 3,6-Diazaoctan-1,8-diamin
pren	= Propan-1,3-diamin
EDX	= Energiedispersive Röntgenspektroskopie
NMR	= Nuklearmagnetische Resonanzspektroskopie
UV-Vis	= Ultraviolettes und sichtbares Licht
Ph	= Phenylgruppe
A	= Alkalimetallatom
Ch	= Chalkogenatom
Cp	= Cyclopentadien
Cp*	= Pentamethylcyclopentadien
M	= Metallatom
R	= Organischer Rest
T	= Tetrelatom
X	= Halogenidatom

Abbildungsverzeichnis

[1] R. Henning, *Chem. Zentralblatt* **1878**, 317.

[2] A. Kraft, *Nachr. Chemie* **2010**, *58*, 1124.

[3] P. Qin, S. Tanaka, S. Ito, N. Tetreault, K. Manabe, H. Nishino, M. K. Nazeeruddin, M. Graetzel, *Nature Commun*. **2014**, *5*, 3834.

[4] J. M. Marin-Beloqui, J. P. Hernandez, E. Palomares, *Chem. Commun.* **2014**, *50*, 14566.

[5] a) S. Roy, *Cryst. Eng. Comm.* **2014**, *16*, 4667; b) M. T. Pope, A. Mueller, *Angew. Chem. Int Ed.* **1991**, *30*, 34.

[6] N. Mizuno, *A.C.S. Div. Energy Fuels*, **2014**, *59*, 688.

[7] H. N. Miras, L. Vila-Nadal, L. Cronin, *Chem. Soc. Rev.* **2014**, *43*, 5679.

[8] C. Masquelier, L. Croquennec, *Chem. Rev*. **2013**, *113*, 6552.

[9] N. Pienack, W. Bensch, *Angew. Chem. Int. Ed.* **2011**, *50*, 2014.

[10] J. Heine, S. Dehnen, *Z. Anorg. Allg. Chem.* **2012**, *638*, 2425. S. Dehnen, M. Melullis, *Coord. Chem. Rev.* **2007**, *251*, 1259.

[11] Siehe z.B.: a) K. O. Klepp, *Z. Naturforsch.* **1992**, *B47*, 411; b) B. Eisenmann, J. Hansa, *Z. Kristallogr.* **1993**, *203*, 299; c) J. Li, H.-Y. Guo, D. M. Proserpio, A. Sironi, *J. Solid State Chem.* **1995**, *117*, 247; d) B. Krebs. *Angew. Chem. Int. Ed.* **1983**, *22*, 113; e) W. Schiwy, B. Krebs, *Angew. Chem. Int. Ed.* **1975**, *14*, 436; f) W. S. Sheldrick, M. Wachhold, *Angew. Chem. Int. Ed.* **1997**, *36*, 207.

[12] Seit 2012 gilt gemäß IUPAC auch Bismut als radioaktives Element, wird im weiteren Verlauf jedoch auch Teil der Untersuchungen sein.

[13] D. E. Bugaris, H.-C. zur Loye, *Angew. Chem. Int. Ed.* **2012**, *51*, 37080.

[14] M. G. Kanatzidis, R. Poettgen, W. Jeitschko, *Angew. Chem. Int. Ed.* **2005**, *44*, 6996.

[15] W. S. Sheldrick, M. Wachhold, *Angew. Chem. Int. Ed.* **1997**, *36*, 206.

[16] S. S. Dinghara, R. C. Haushalter, *Chem. Mater,* **1994**, *6*, 2376.

[17] G. A. Marking, J. A. Hanko, M. G. Kanatzidis, *Chem. Mater.* **1998**, *10*, 1191.

[18] M. Wu, W.-P. Su, N. Jasutkar, X.-Y. Huang, J. Li, *Mater. Res. Bull.* **2005**, *40*, 21.

[19] a) O. Palchik, R. G. Iyer, J. H. Liao, M. G. Kanatzidis, *Inorg. Chem.* **2003**, *42*, 5052; b) M. J. Manos, K. Chrissafis, M. G. Kanatzidis, *J. Am. Chem. Soc.* **2006**, *128*, 8875; c) O. Palchik, R. G. Iyer, C. G. Canlas, D. P. Weliky, M. G. Kanatzidis, *Z. Anorg. Allg. Chem.* **2004**, *630*, 2237.

[20] a) M. K. Brandmyer, R. Clérac, F. Weigend, S. Dehnen, *Chem. Eur. J.* **2004**, *10*, 5147; b) M. Melullis, C. Zimmermann, C. E. Anson, S. Dehnen, *Z. Anorg. Allg. Chem.* **2003**, *629*, 2325; c) S. Dehnen, M. K. Brandmayer, *J. Am. Chem. Soc.* **2003**, *125*, 6618; d) E. Ruzin, A. Fuchs, S. Dehnen, *Chem. Commun.* **2006**, 4796; e) E. Ruzin, C. Zimmermann, P. Hillebrecht, S. Dehnen, *Z. Anorg. Allg. Chem.* **2007**, *633*, 820; f) E. Ruzin, S. Jakobi, S. Dehnen, *Z. Anorg. Allg. Chem.* **2008**, *634*, 995; g) C. Zimmermann, C. E. Anson, F. Weigend, R. Clérac, S. Dehnen, *Chem. Commun.* **2005**, 6008.

[21] a) S. S. Dinghara, R. C. Haushalter, *Chem. Mater.* **1994**, *6*, 2376; b) N. Ding, D.-Y. Chung, M. G. Kanatzidis, *Chem. Commun.* **2004**, 1170; c) C. Zimmermann, S. Dehnen, *Z. Anorg. Allg. Chem*. **2003**, *629*, 1553.

[22] J. C. Schleicher, A. M. Scurto, *Green Chem.* **2009**, *11*, 694.

[23] R. E. Morris, *Chem. Commun.* **2009**, *21*, 2990.

[24] M. Wolff, A. Okrut, C. Feldmann, *Inorg. Chem.* **2011**, *50*, 11683.

[25] K. Biswas, Q. Zhang, I. Chung, J.-H. Song, J. Androulakis, A. J. Freeman, M. G. Kanatzidis, *J. Am. Chem. Soc.* **2010**, *132*, 14760.

[26] Y. Lin, W. Massa, S. Dehnen, *J. Am. Chem. Soc.* **2012**, *134*, 4497.

[27] Beispielhaft seien genannt: a) W. S. Sheldrick, M. Wachhold, *Coord. Chem. Rev.* **1998**, *176*, 211; b) J. Zhou, J. Dai, G.-Q. Bian, C.-Y. Li, *Coord. Chem. Rev.* 2009, 253, 1221; c) S. Dehnen, M. Melullis, *Coord. Chem. Rev.* **2007**, *251*, 1259; d) P. Feng, X. Bu, N. Zheng, *Acc. Chem. Res.* **2005**, *38*, 293.

[28] R. Hoppe, H. J. Röhrborn, *Naturwissenschaften* **1976**, *63*, 194.

[29] E. A. Axtell, Y. Park, K. Chondroudis, M. G. Kanatzidis, *J. Am. Chem. Soc.* **1998**, *120*, 124-136.

[30] H. Sommer, R. Hoppe, *Z. Anorg. Allg. Chem.* **1978**, *443*, 201-211.

[31] Y. Park, M. G. Kanatzidis, *Chem. Mater.* **1990**, *2*, 99-101.

[32] K. Chondroudis, M. G. Kanatzidis, *Chem. Commun*. **1997**, 401. X. Chen, X. Huang, J. Li, *Inorg. Chem.* **2001**, *40*, 1341-1346.

[33] Z.B. a) A. Muller, J. Schimanski, U. Schimanski, *Angew. Chem. Int. Ed.* **1984**, *23*, 159; b) R. C. Haushalter, *Angew. Chem. Int. Ed*. **1985**, *24*, 433; c) A. Ahle, K. Dehnicke, M. Maczek, D. Fenske, *Z. Anorg. Allg. Chem.* **1993**, *619*, 1699; d) J. Li, Z. Chen, J. L. Kelley, D. M. Proserpio, *Mat. Res. Swoc. Symp. Proc.* **1997**, *453*, 29; e) Y.-L. Wang, M.-L. Feng, K.-Y. Wang, J.-R. Li, Z.-P. Wang, G.-D. Zou, X.-Y. Huang, *Inorg. Chem. Commun.* **2013**, *33*, 10.

[34] S. G. Wang, Y. X. Qiu, E. Neumann, H. J. Deiseroth, W. H. E. Schwarz, *Z. Anorg. Allg. Chem.* **2003**, *629*, 1718.

[35] J. A. A. Ketelaar, W. H. T'Hart, M. Moerel, D. Polder, *Z. Kristallogr.* **1939**, *101*, 396.

[36] A. M. Pirani, H. P. A. Mercier, R. J. Suontamo, G. J. Schrobilgen, D. P. Santry, H. Borrmann, *Inorg. Chem.* **2005**, *44*, 8770.

[37] S. Dhingra, F. Liu, M. G. Kanatzidis, *Inorg. Chim. Acta*, **1993**, *210*, 237.

[38] S. S. Dhingra, M. G. Kanatzidis, *Inorg. Chem.* **1993**, *32*, 1350.

[39] H. Borrmann, J. Campbell, D. A. Dixon, H. P. A. Mercier, A. M. Pirani, G. J. Schrobilgen, *Inorg. Chem.* **1998**, *37*, 1929.

[40] R. C. Burns, J. D. Corbett, *J. Am. Chem. Soc.* **1981**, *103*, 2627.

[41] J. Campbell, H. P. A. Mercier, D. P. Santry, R. J. Suontamo, H. Borrmann, G. J. Schrobilgen, *Inorg. Chem*. **2001**, *40*, 233.

[42] S. S. Dhingra, M. G. Kanatzidis, *Inorg. Chem*. **1993**, *32*, 2298.

[43] H. Borrmann, J. Campbell, D. A. Dixon, H. P. A. Mercier, A. M. Pirani, G. J. Schrobilgen, *Inorg. Chem*. **1998**, *37*, 6656.

[44] C. D. W. Jones, F. J. DiSalvo, R. C. Haushalter, *Inorg. Chem.* **1998**, *37*, 821.

[45] a) H. Borrmann, J. Campbell, D. A. Dixon, H. P. A. Mercier, A. M. Pirani, G. J. Schrobilgen, *Inorg. Chem*. **1998**, *37*, 6656; b) M. Björgvinsson, J. F. Sawyer, G. J. Schrobilgen, *Inorg. Chem.* **1987**, *26*, 741; c) M. Björgvinsson, J. F. Sawyer, G. J. Schrobilgen, *Inorg. Chem.* **1991**, *30*, 2231; d) C.-W. Park, R. J. Salm, J. A. Ibers, *Can. J. Chem.* **1995**, *73*, 1148.

[46] R. M. H. Banda, J. Cusick, M. L. Scudder, D. C. Craig, I. G. Dance, *Polyhedron* **1989**, *8*, 1995.

[47] a) W. Bronger, A. Donike, D. Schmitz, *Z. Anorg. Allg. Chem.* **1996**, *622*, 1003; b) B. Eisenmann, R. Zagler, *Z. Kristallogr.* **1991**, *197*, 257.

[48] M. A. Pell, J. A. Ibers, *Inorg. Chem.* **1996**, *35*, 4559.

[49] T. J. McCarty, T. A. Tanzer, M. G. Kanatzidis, *J. Am. Chem. Soc.* **1995**, *117*, 1294.

[50] A. Müller, M. Zimmermann, H. Bögge, *Angew. Chem. Int. Ed.* **1986**, *25*, 272.

[51] a) M. A. Ansari, J. M. McConnachie, J. A. Ibers, *Acc. Chem. Res.* **1993**, *26*, 574; b) L. C. Roof, J. W. Kolis, *Chem. Rev.* **1993**, *93*, 1037; c) A. K. Singh, S. Sharma, *Coord. Chem. Rev.* **2000**, *209*, 49; d) W. S. Sheldrick in *Handbook of Chalcogen Chemistry* (Ed.: F. Devillanova), The Royal Society of Chemistry **2007**, 43; e) C. Graf, A. Assoud, O. Mayasree, H. Kleinke, *Molecules* **2009**, *14*, 3115; f) J. Beck, *Angew. Chem.* **1994**, *106*, 172.

[52] a) C. Hugot, Ann. Chim. Phys. 1900, 21, 72; b) K. W. Sharp, W. H. Koehler, *Inorg. Chem.* **1977**, *16*, 2258. c) S. Licht, F. Forouzan, *J. Electrochem. Soc.* **1995**, *142*, 1546; d) A. Goldbach, L. E. Iton, M. Grimsditch, M.-L. Saboungi, *Chem. Mater.* **2004**, *16*, 5107; e) M. Björgvinsson, G. J.

Schrobilgen, *Inorg. Chem*. **1991**, *30*, 2540; f) J. Cusick, I. Dance, *Polyhedron* **1991**, *10*, 2629; g) P. J. Barrie, R. J. H. Clark, D.-Y. Chung. D. Chakrabarty, M. G. Kanatzidis, *Inorg. Chem.* **1995**, *34*, 4299.

[53] C. C. Raymond, D. L. Dick, P. K. Dorhout, *Inorg. Chem.* **1997**, *36*, 2678.

[54] a) C. A. Bayse, *J. Chem. Theory Comput*. **2005**, *1*, 1119; b) W. Nakanishi, S. Hayashi, Y. Katsura, M. Hada, *J. Phys. Chem*. **2011**, *A115*, 8721.

[55] a) L. E. Lyons, T. L. Young, *Aust. J. Chem.* **1986**, *39*, 511; b) A. Ahrika, J. Paris, *New. J. Chem.* **1999**, *23*, 1177; c) Y. Cui, A. Abouimrane, J. Lu, T. Bolin, Y. Ren. W. Weng, C. Sun, V. A. Maroni, S. M. Heald, K. Amine, *J. Am. Chem. Soc.* **2013**, *135*, 8047.

[56] D. M. Smith, J. A. Ibers, *Coord. Chem. Rev.* **2000**, *200*, 187.

[57] C. Feldmann, A. Okrut, *Z. Anorg. Allg. Chem.* **2009**, *635*, 1807.

[58] Q. Zhang, C. D. Malliakas, M. G. Kanatzidis, *Inorg. Chem.* **2009**, *48*, 10910.

[59] a) A. Günther, A. Isaeva, A. I. Baranov, M. Ruck, *Chem. Eur. J.* **2011**, *17*, 6382; b) A. Panda, *Coord. Chem. Rev.* **2009**, *253*, 1947; c) E. R. Clark, R. L. Melen, J. M. Rawson, *Annu. Rep. Prog. Chem. Sect. A* **2010**, *106*, 119; d) C. D. Martin, P. J. Ragogna, *Annu. Rep. Prog. Chem. Sect. A* **2011**, *107*, 110.

[60] D. Y. Chung, L. Iordanidis, K. K. Rangan, P. W. Brazis, C. R. Kannewurf, M. G. Kanatzidis, *Chem. Mater.* **1999**, *11*, 1352.

[61] V. I. Vasil'ev, N. V. Pervukhina, S. V. Borisov, S. A. Magarill, *Geol. Ore Deposits* **2010**, *52*, 662.

[62] a) S. S. Dhingra, R. C. Haushalter, *Chem. Mater.* **1994**, *6*, 2376; b) J. Shreeve-Keyer, R. C. Haushalter, *Polyhedron* **1996**, *15*, 1213.

[63] a) M. G. Kanatzidis, A. C. Sutorik, *Prog. Inorg. Chem*. **1995**, *43*, 151; b) J.-H. Liao, *Dissertation*, Michigan State University, **1993**.

[64] G. Eulenberger, *Z. Naturforsch.* **1980**, *B35*, 335.

[65] J. H. Chou, M. G. Kanatzidis, *Inorg. Chem*. **1994**, *33*, 1001.

[66] C.-W. Park, M. A. Pell, J. A. Ibers, *Inorg. Chem.* **1996**, *35*, 4555.

[67] J. Campbell, D. P. DiCiommo, H. P. A. Mercíer, A. M. Pirani, G. J. Schrobilgen, M. Willuhn, *Inorg. Chem.* **1995**, *34*, 6265.

[68] a) O. M. Yaghi, Z. Sun, D. A. Richardson, T. L. Groy, *J. Am. Chem. Soc.* **1994**, *116*, 807; b) O. Achak, J. Y. Pivan, M. Maunage, M.Louër, D. Louër, *J. All. Compd*. **1995**, *219*, 111; c) O Achak, J. Y. Pivan, M. Maunage, M. Louër, D. Louër, *J. All. Compd*. **1996**, *221*, 473; d) C. L. Bowes, A. J. Lough, A. Malek, G. A. Ozin, S. Petrov, D. Young, *Chem. Ber.* **1996**, *129*, 283.

[69] C. L. Teske, *Z. Naturforsch*. **1980**, *35B*, 7.

[70] C. L. Teske, *Z. Anorg. Allg. Chem.* **1980**, *468*, 27.

[71] C. L. Teske, *Z. Anorg. Allg. Chem.* **1980**, *460*, 163.

[72] C. L. Teske, *Z. Naturforsch.* **1980**, *35B*, 509.

[73] C. L. Teske, *Z. Naturforsch.* **1979**, 34B, 386.

[74] C. L. Teske, *Z. Anorg. Allg. Chem.* **1976**, *419*, 67.

[75] C. L. Teske, O. Vetter, *Z. Anorg. Allg. Chem*. **1976**, *427*, 200.

[76] C. L. Teske, O. Vetter, *Z. Anorg. Allg. Chem.* **1976**, *426*, 281.

[77] C. L. Teske, *Z. Anorg. Allg. Chem.* **1985**, 522, 122.

[78] P. T. Wood, G. L. Schimek, J. W. Kolis, *Chem. Mater.* **1996**, *8*, 721.

[79] J.-H. Chou, M. G. Kanatzidis, *Chem. Mater.* **1995**, *7*, 5.

[80] a) P. Vaqueiro, *Dalton Trans.* **2010**, *39*, 5965; b) B. Seidlhofer, N. Pienack, W. Bensch, *Z. Naturforsch.* **2010**, *65B*, 937; c) J. Heine, S. Dehnen, *Z. Anorg. Allg. Chem.* **2012**, *15*, 2425.

[81] S. Methfessel, *Proc. Int. Conf.* **1971**, 619.

[82] K. G. Nikiforov, *Prog. Cryst. Growth Mat.* **2000**, *39*, 1.

[83] W. Bronger, *Pure Appl. Chem.* **1985**, *57*, 1363.

[84] G. Thiele, S. Peter, M.C. Schwarzer, E. Ruzin, R. Clérac, H. Staesche, C. Rößer, B. Roling, S. Dehnen, *Inorg. Chem.* **2012**, *51*, 3349.

[85] E. Ruzin, *Dissertation*, Philipps-Universität Marburg, **2007**.

[86] H. Li, J. A. Peters, Z. Liu, M. Sebastian, C. D. Malliakas, J. Androulakis, L. Zhao, I. Chung, S. L. Nguyen, S. Johnsen, B. W. Wessels, M. G. Kanatzidis, *Cryst. Growth Des.* **2012**, *12*, 3250

[87] Y. Lin, W. Massa, S. Dehnen, *J. Am. Chem. Soc.* **2012**, *134*, 4497.

[88] L.-D. Zhao, S.-H. Lo, Y. Zhang, H. Sun, G. Tan, C. Uher, C. Wolverton, V. P. Dravid, M. G. Kanatzidis, *Nature* **2014**, *508*, 373.

[89] GESTIS-Stoffdatenbank. Online aufgerufen am 10.12.2014.

[90] M. D. F. Gutiérrez, M. D. L. Leon, *N. Engl. J. Med.* **2000**, *342*, 1791.

[91] E. Trebin, *AHZ* **2012**, *257*, 19.

[92] G. Thiele, *Diplomarbeit*, Philipps-Universität Marburg **2010**.